# DESIGN AND SYNTHESIS OF CHELATING IONOPHORES AS CHEMOSENSORS BASED ON ANALYTICAL STUDIES

**Ph.D. THESIS**

*by*

**NEETU YADAV**

**DEPARTMENT OF CHEMISTRY**
**INDIAN INSTITUTE OF TECHNOLOGY ROORKEE**
**ROORKEE-247 667 (INDIA)**
**MARCH, 2019**

# DESIGN AND SYNTHESIS OF CHELATING IONOPHORES AS CHEMOSENSORS BASED ON ANALYTICAL STUDIES

**A THESIS**

***Submitted in partial fulfilment of the requirements for the award of the degree***

*of*

**DOCTOR OF PHILOSOPHY**

*in*

**CHEMISTRY**

*by*

**NEETU YADAV**


**DEPARTMENT OF CHEMISTRY**
**INDIAN INSTITUTE OF TECHNOLOGY ROORKEE**
**ROORKEE-247 667 (INDIA)**
**MARCH, 2019**

# INDIAN INSTITUTE OF TECHNOLOGY ROORKEE
# ROORKEE

## CANDIDATE'S DECLARATION

I hereby certify that the work which is being presented in the thesis entitled **"DESIGN AND SYNTHESIS OF CHELATING IONOPHORES AS CHEMOSENSORS BASED ON ANALYTICAL STUDIES"** in partial fulfilment of the requirements for the award of the Degree of Doctor of Philosophy and submitted in the Department of Chemistry of the Indian Institute of Technology Roorkee is an authentic record of my own work carried out during a period from January, 2014 to March, 2019 under the supervision of Dr. Ashok Kumar Singh, Emeritus Professor and Dr. M. R. Maurya, Professor, Department of Chemistry, Indian Institute of Technology Roorkee, Roorkee.

The matter presented in the thesis has not been submitted by me for the award of any other degree of this or any other Institution.

**(NEETU YADAV)**

This is to certify that the above statement made by the candidate is correct to the best of our knowledge.

(M. R. Maurya) (Ashok Kumar Singh)
**Supervisor** **Supervisor**

The Ph.D. Viva-Voce Examination of Ms. Neetu Yadav, Research Scholar, has been held on 7th June 2019.

**Chairperson, SRC** **Signature of External Examiner**

This is to certify that the student has made all the corrections in the thesis.

(M. R. Maurya) (Ashok Kumar Singh)
**Supervisor** **Supervisor** **Head of the Department**

**Dated: June 07, 2019**

# *ACKNOWLEDGEMENTS*

*First and foremost, my immense thanks from the bottom of heart to the almighty 'GOD' who provides this opportunity to me that I have completed my research work. I am thankful for the incessant source of divine blessings to move forward with his omens and love.*

*PhD is a project complimented of great endeavors writhes and support of number of associates. I hereby endure this moment to express my gratitude to all who have been supported and motivated throughout this journey.*

*Words are inadequate to express my deep sense of gratitude, indebtedness and heartiest respect to my supervisor* ***Prof. Ashok Kumar Singh*** *for his surveillance, meticulous guidance continuous support and enthusiastic interest throughout the duration of my research work. His mentorship was paramount in providing a well-rounded experience consistent my long-term career goal. Without his guidance and support I have not been thought to complete my research work. Further, I thanks to him for providing me all the facilities and keeping me free to do research up to the possible extent. He was very supportive since the day I had begin working in the lab and he taught me lot of things in the field of research. His appropriate thoughts and productive assessment not only promote my research methodology and qualities but also including to generate a positive research attitude in me. He encouraged me to not only grow as an experimentalist and a chemist but also as an instructor and an independent thinker. Though, I made various mistakes while pursuing my research program, he rectified me and place in a good path with lot of patience. He is a library to me where I have tried to learn many qualities in all aspects.*

*I am highly obliged and express gratitude to my co-supervisor* ***Prof. Mannar Ram Maurya****, Former Head, Department of Chemistry. He always support and help me in all situations during my research tenure. His support and guidance always encouraged me to complete my research work. He always promoted me to do work efficiently since the day when I joined up to now and he taught me lots of things. His valuable suggestions and comments during this time act as a treasure for me in developing a researcher*

*attitude. Both mentors encouraged me in all the way to finish this research work. I am highly thankful to both of you.*

*I am also thankful to* ***Prof. K. R. Justin Thomas,*** *Head, Department of Chemistry and all other faculty members of Chemistry Department for providing the basic requirements for completing this research work. I am also thankful to my SRC members,* ***Dr. R. K. Peddinti*** *(SRC Chairman),* ***Dr. M. Sankar*** *(Internal expert), Department of Chemistry,* ***Prof. K. L. Yadav*** *(External member), Department of Physics,* ***Prof. Shri Chand*** *(Former External member), Department of Chemical Engineering, IIT Roorkee, for their valuable suggestions to carry out this work. I am highly thankful to* ***Dr. Anuj Sharma*** *for his moral support when I was needed. I am also thankful to* ***Dr. Amit Pratap Singh*** *for teaching me lots of things in the field of research work.*

*I would like to thanks to* ***Dr. P. Gopinath*** *and his students* ***Mr. Shanid*** *and* ***Mr. Vinay,*** *Center of Nanotechnology for the biological studies.*

*I express my sincere thanks to* ***Mr. Madan Pal****,* ***Mr. D. C. Meena****,* ***Mr. Pankaj****,* ***Mr. Deepak, Mr. Ankur, Mr. Ashu*** *and other non-teaching staff members Department of Chemistry for their needful help.*

*The word thank is not enough to pay attention to my respected father,* ***Mr. Ramveer Singh Yadav*** *who always taught me not to accept defeat in any difficult situation by applying his own examples before me and my respected mother,* ***Mrs. Sarlesh Yadav****, who gave her amiable support whenever I needed during this period. I am very indebted to my parents because without the two of you I don't know where I would be. I like to express my heartiest love to my younger brothers* ***Mr. Amit Pratap Singh****,* ***Mr. Akanshu Yadav*** *and my sister in law* ***Mrs. Prateeksha*** *for their constant support in every up and down.*

*I would like to express my thanks to my best friends* ***Dr. Raj Kumar*** *and* ***Dr. Vijayesh Kumar*** *for their support and care in worst as well as good situations. They taught me lots of things to analyses the situations in this time.*

*I am also thankful my dearest senior* ***Dr. Tanpreet Kaur*** *for her support and suggestion. She always taught me lots of things related to my research work and clear all the confusions related to the work. She always treated me as a younger sister.*

*I would like to express my thanks to profound seniors, colleagues and juniors* ***Dr. Shubrajoytasana***, ***Dr. Neha Gupta***, ***Dr. Divya Singhal***, ***Dr. Debasmita saha***, ***Dr. Nivedita Chowdary***, ***Dr. Neetu Singh***, ***Dr. Bhawana Upretty***, ***Dr. Nirma Maurya***, ***Dr. Komal***, ***Mrs. Gurjinder***, ***Dr. Neha Taneja***, ***Dr. Waheed***, ***Mr. Ikrar***, ***Mr. Saurabh Bhagchi***, ***Ms. Mamta***, ***Ms. Reshu***, ***Mr. Khwaja***, *and* ***Ms. Krishna*** *for their support and help in this work.*

*At last I would like to thank and acknowledge my ever-increasing gratitude to all those who offered me most valuable suggestions, without inspiring profound guidance, sincere support, splendid chance to encouragement, deepest thinking, it would perhaps have been impossible for me to demonstrate this, in present form.*

**(NEETU YADAV)**

# *ABSTRACT*

Generally, chemical sensor comprises of a selective detection of molecule which is sensitive to stimuli by the analyte and a transduction material that develop an analytically advantageous signal whose significance is functionally contributing to the concentration of the analyte or substance. Based on working principal of chemosensors it can be categorized such as electrochemical, thermal sensor, mass sensors, magnetic sensor and optical sensors. The inexpensive optical sensors have vast applications in various area like medicine, environmental pollution and many others. It attracts the scientific community such as researcher, scientist and biologist due to highly sensitive and selective nature towards the various transition metal ions, other toxic metal ions and anions. Optical sensors depend on the optical changes observed upon the detection of targeted analyte with chemosensor. These are simple to use, portable, in-situ and miniature in size, these features are necessary for real-time on field measurements. The thesis is managed with some chemosensors and their analytical studies. For the convenience and clarity, the work in the thesis divided into six chapters and arranged as follows:

**Chapter 1** deals with "**Introduction**" of chemical sensor as well as classification of optical sensors. Chemosensors are generally based on chelating ligands such as Schiff bases, coumarin, bipyridine, indole, quinoline, calixrene, BODIPY, crown ether, porphyrin, rhodamine and nanoparticles. The theory behind the mechanism to sense the analyte has been described. The details of analytical (photoluminescence) processes is discussed in the different subsections. The optical chemosensors has been classified according to performance of the signal transmitted by the active unit and diverse possible mechanisms like PET, ICT, ET, CHEF/CHQF for signal transduction upon analyte binding to chemosensors and the term used in the fluorescence sensing have also been discussed in this chapter.

**Chapter 2**, entitled "**Thiosemicarbazide based chemosensor for Arsenite and cyanide ion**" described the synthesis and characterization of 2-((2-Hydroxynaphthalen-1-yl)methylene)hydrazinecarbothioamide (L1) and successfully applied for the detection of toxic anions arsenite and cyanide ion among other anions. L1 is utilized as a turn-on

sensor for arsenite and cyanide ions *via* deprotonation and hydrogen bonding mechanism upon interaction with both analytes in DMF: $H_2O$ (HEPES buffer, pH = 7.2, 9:1 v/v solution) medium. This L1 was characterized by different techniques including UV-vis, FT-IR, NMR and mass spectroscopy. This ligand shows 1:1 and 1:2 stoichiometry with arsenite and cyanide ions respectively *via* Job's plot. The binding constant of $AsO_2^-$ and $CN^-$ with L1 was calculated by using B-H (Benesi-Hilderbrand) plot and found as 3.1 $\times 10^5$ and 1.9 $\times$ $10^6$ for $AsO_2^-$ and $CN^-$ respectively and limit of detection of $AsO_2^-$ and $CN^-$ was 66 nM and 77 nM with ligand L1 respectively. Further the binding affinity of probe L1 with both anions was manifested using NMR, theoretical optimization, mass spectroscopy, optical studies and electrochemical studies and used in real time water analysis for the detection of both anions.

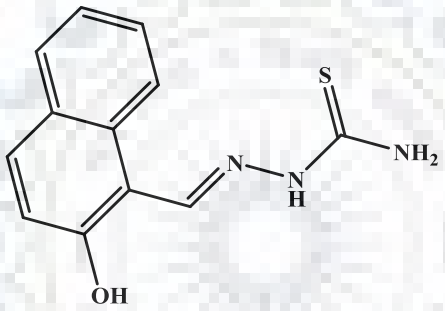


**L1**

**Chapter 3** entitled "**Pyridine dicarbohydrazide based chemosensor for the detection Copper and cyanide ions**" described the synthesis and characterization of bis-(4-hydroxy-3,5-dimethoxybenzylidene)pyridine-2,6-dicarbohydrazide (L2), bis(-(1H-pyrrol-2-yl)methylene)pyridine-2,6-dicarbohydrazide (L3), bis(-(2-hydroxynaphthalen-1-yl)methylene)pyridine-2,6-dicarbohydrazide (L4), bis(-anthracen-9-ylmethylene)pyridine-2,6-dicarbohydrazide (L5) by NMR, FT-IR, UV-vis spectroscopy, elemental analysis and mass spectroscopy, SC-XRD and emission spectra. These ligands were recognized copper ion among other metal ions and cyanide ion detection by copper complex *via* in-situ experiment with turn on-off-on behavior in MeOH: $H_2O$ (9:1, v/v solution) medium. The red shift was observed in absorption spectra and quenching behavior observed in emission spectra of these ligands with copper ions through PET mechanism and further copper complex was applied for $CN^-$ ion detection. The ligands

(L2-L5) were showed 1:2, 1:3, 1:2 and 1:2 stoichiometric ratios respectively, with copper ion *via* Job's plot based on UV-vis spectra. The S-V plot demonstrate the linear quenching of the ligands with copper ions. The formation constant of L2 to L5 was as 8.866, 17.645, 11.145 and 6.45 respectively. The limit of detection for copper ion with ligands (L2-L5) were calculated as 0.12, 0.10, 0.097, 0.098 μM respectively, using emission spectra. The binding affinity of copper ion with ligands was supported by FT-IR, mass spectroscopy, redox studies and optical studies. furthermore, cyanide detection was found by the copper complexes of ligands *via* in-situ experiment with displacement approach. Further, these ligands were applied for practical applications such as real water analysis and in logic gate behavior.

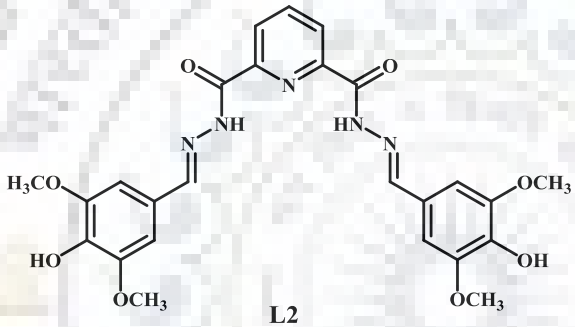


L2

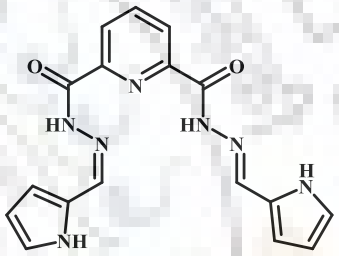


L3

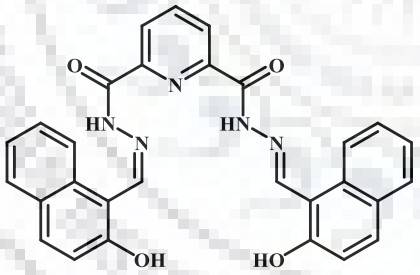


L4

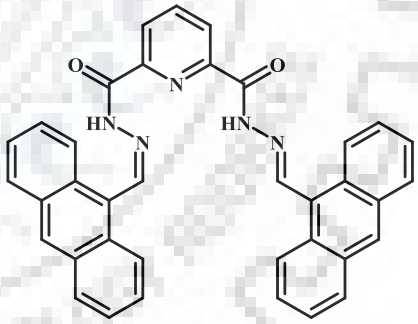


L5

**Chapter 4** entitled "**Pyrimidine based fluorescent sensor for aluminum ion detection**" illustrated the synthesis and characterization of 6-amino-5(((2-hydroxynaphthalen-1-yl)methylene)amino)-2-mercaptopyrimidin-4-ol (L6) and 6-amino-5((4-bromobenzylidene)amino)-2-mercaptopyrimidin-4-ol (L7) by different techniques (UV-vis, FT-IR, Mass spectroscopy and NMR and fluorescence spectroscopy) and found that L6 recognize the aluminum ion among other metal ion whereas L7 didn't show any

change in UV-vis and emission spectra with any metal ions. So further all studies have been performed only with L6 ligand. L6 was more selective towards aluminum ion with "OFF-ON type" behavior. The fluorescent sensor recommended 1:1 stoichiometry with aluminum ion by Job's plot in $CH_3CN$ medium. The high sensitivity of ligand L6 towards aluminum ion supports the high detection limit *viz.* 99 nM with $3.5 \times 10^4$ association constant ($K_a$). There was no interference was found by another metal ions. The binding was supported by NMR titration, Theoretical studies and cyclic voltammetry studies. Further, it was used in different practical applications such as bacterial cell imaging with E. coli DHα bacteria and logic gate applications that manifested the red and green fluorescent images in green and red channel with $Al^{3+}$ ion as well as in logic gate application it showed INHIBIT logic gate in switching behavior.

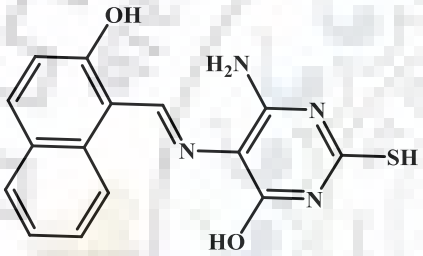


**L6**

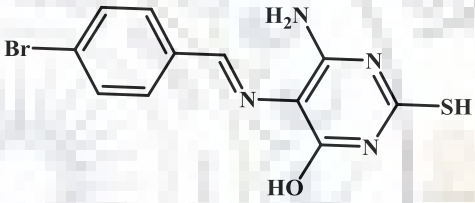


**L7**

**Chapter 5** entitled "**Oxalohdrazonamide based turn-off chemosensor for $Hg^{2+}$ and $Cu^{2+}$ and turn-on for $Cd^{2+}$ ion**" described the synthesis and characterization of Bis((indol-3-yl)methylene)oxalohydrazonamide (L8) *via* different spectroscopic techniques. It was found that ligand L8 was shown colorimetric and turn-off behavior with $Hg^{2+}$ and $Cu^{2+}$ ion among other metal ions through CHQF and PET mechanism whereas in fluorometric studies it shows turn-on demeanor for $Cd^{2+}$ ion with CHEF mechanism in aqueous medium. The binding constant of $Cu^{2+}$, $Hg^{2+}$ and $Cd^{2+}$ with ligands L8 *viz.* $7.35 \times 10^6$, $2.33 \times 10^6$ and 11.612 (log $\beta$) respectively. It has high sensitivity towards $Cu^{2+}$, $Hg^{2+}$ and $Cd^{2+}$ ions and LOD was *ca.* 0.16 μM, 0.33 μM and 0.11 μM respectively. The binding of these metal ions was supported by NMR titration, mass spectrometry, electrochemical studies and FT-IR spectra. Further, in situ

experiment for the detection of cyanide ion with ligand appended copper ion. The practical application such as logic gate and real water analysis was successfully applied.

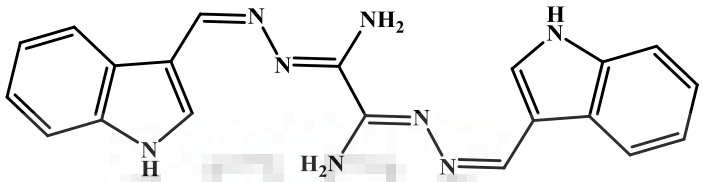

**L8**

**Chapter 6** entitled "**Carbohydrazide based chemosensors for magnesium, manganese and copper ion**" was determined the synthesis and characterization of ((6-nitro-4-oxo-4H-chromen-3-yl)methylene)furan-2-carbohydrazide (L9) and ((6-bromo-4-oxo-4H-chromen-3-yl)methylene)furan-2-carbohydrazide (L10) through various techniques such as NMR, FT-IR, UV-vis spectroscopy and fluorescence spectroscopy. Ligand L9 shown the detection of manganese and magnesium ion by UV-vis and emission spectra among other metal ions. However, L10 detected the $Cu^{2+}$ ion by UV-vis studies and $Mg^{2+}$ ion by emission studies. These ligands show good affinity towards these metal ions. The formation constant of $Mn^{2+}$ and $Mg^{2+}$ ion with L9, is $1.68 \times 10^5$ and $1.2 \times 10^5$, respectively. Similarly, the association constant of L10 with $Cu^{2+}$ and $Mg^{2+}$ ion as $1.99 \times 10^5$ and $5.25 \times 10^4$ respectively. The limit of detection of magnesium and manganese ion with L9 was as $2.56 \times 10^{-6}$ and $1.63 \times 10^{-7}$ respectively and LOD for $Cu^{2+}$ and $Mg^{2+}$ with L10 was $3.71 \times 10^{-7}$ and $1.28 \times 10^{-6}$ respectively. Binding of these metal ions is confirmed by NMR and cyclic voltammetry. Further these ligands and ligands with magnesium ion was used in different applications such as bioimaging.

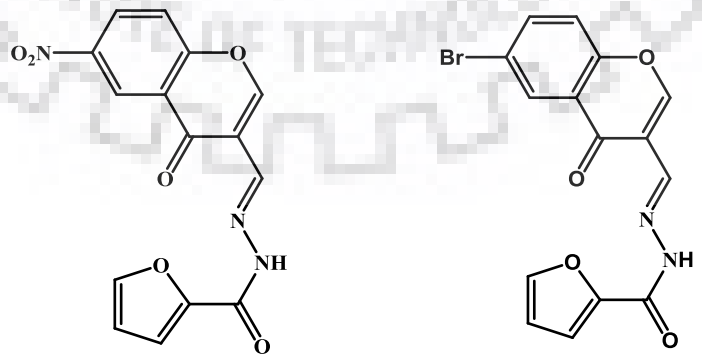

**L9** **L10**

# *LIST OF PUBLICATIONS*

1. **Neetu Yadav** and Ashok Kumar Singh, "Dual anion colorimetric and fluorometric sensing of arsenite and cyanide ions", RSC Adv., 6 (2016) 100136–100144.
2. **Neetu Yadav** and Ashok Kumar Singh, "Dicarbohydrazide based chemosensors for copper ion and Cyanide ion *via* displacement approach", New Journal of Chemistry 42 (2018) 6023-6033.
3. **Neetu Yadav** and Ashok Kumar Singh, "A turn-on ESIPT based fluorescent sensor for detection of aluminium ion with bacterial cell imaging and logic gate applications", Material science and Engineering: C, 90 (2018) 468-475.
4. **Neetu Yadav** and Ashok Kumar Singh, "Colorimetric and fluorometric detection of heavy metal ions in pure aqueous medium with logic gate application", J. Electrochem. Soc. 2019, 166 (6), B644-B653.
5. **Neetu Yadav** and Ashok Kumar Singh, "A fluorescent chemosensor for $Mg^{2+}$ ion and their different applications", (communicated).

# *PRESENTATION IN CONFERENCES*

1. Presented a poster on "Synthesis of Some New Compounds for Detection of Copper Ion" in ***"Contemporary Facets in Organic Synthesis 2017"*** held at IIT Roorkee.
2. Poster presentation on "Carbohydrazide based turn-off chemosensor for copper ion" in ***"Modern Trends in Inorganic Chemistry"*** in 17th biennial symposium held at CSIR-NCL, Pune and IISER Pune in 2017.
3. An oral presentation was presented on "A New Carbohydrazide Based Sensor for Cu(II) and Hg(II) Ions" in ***" International Conference on Nanotechnology: Ideas, Innovations and Initiatives-2017"*** held at IIT Roorkee, India.
4. An Oral presentation on "A Pyrimidine Based Fluorescent sensor for Aluminum Ion with Turn-on behaviour" was presented in ***"International Conference on Advances in Materials & Processing: Challenges & Opportunities (AMPCO'17)"*** held at IIT Roorkee, 2017.

5. Presented a poster on "A Pyrimidine Based Turn-on Fluorescent sensor for Aluminum Ion" in ***"21st CRSI National Symposium in Chemistry-2017"*** held at CSIR-Indian Institute of Chemical Technology, Hyderabad, India.
6. Presented a poster on "A naphthalene based trun-on fluorescent and colorimetric sensor for arsenite and cyanide ion" in ***"18th CRSI National Symposium in Chemistry"*** held in 2016 at Panjab university.
7. Presented A Poster in ***"ACS on Campus, IIT Roorkee"*** organised by American Chemical Society, at IIT Roorkee in 2018.

## *WORKSHOPS*

1. Attend ***One Day Workshop on "Nano Drug Delivery Systems (Industry-Academia Interaction)"*** organized by the Centre of Excellence: Nanotechnology, Indian Institute of Technology Roorkee, Roorkee on 10$^{th}$ January 2015.
2. Attended workshop on **"*Thin Film Solar Cells*"** organized by Department of Chemistry, Indian Institute of Technology, Roorkee, Apr. 16-17, 2018.

# *TABLE OF CONTENTS*

# *LIST OF SCHEMES*

# *LIST OF FIGURES*

# *LIST OF TABLES*

# *LIST OF ABBREVIATIONS*

| | |
|---|---|
| **A. U.** | Arbitrary Unit |
| **LOD** | Limit of Detection |
| **hr** | Hour |
| **nm** | Nanometer |
| **DNA** | Deoxyribonucleic acid |
| **µM** | Micromolar |
| **mM** | Millimolar |
| **gm** | Gram |
| **WHO** | World Health Organization |
| **ppb** | Parts per billion |
| **ppm** | Parts per million |
| **nM** | Nanomolar |
| **THF** | Tetrahydrofuran |
| **DMF** | Dimethylformamide |
| **DMSO** | Dimethylsulphoxide |
| **ACN** | Acetonitrile |
| **MeOH** | Methanol |
| **EtOH** | Ethanol |
| **˚C** | Degree Celsius |
| **δ** | Chemical Shift |
| **Φ** | Quantum Yield |
| **Conc.** | Concentration |
| **$CDCl_3$** | Deuterated Chloroform |
| **DMSO-$d_6$** | Deuterated Dimethylsulphoxide |
| **HEPES** | 4-(2-hydroxyethyl)-1-piperazineethanesulfonic acid |

# CHAPTER 1

## "INTRODUCTION"

# CHAPTER 1

## 1.1 INTRODUCTION

Now-a-days, there are many issues on ecological and public health interest due to infectious environment by the toxic ions. The hazardous effect of toxic metal ions and anions on environment extensively increased many health problems. The reason behind environment pollution is the major use of pesticides in agriculture, e-wastes, industries, mining, smelter, municipal waste, biomedical waste and fertilizers. Apart from this, some elements are useful biologically but beyond the certain limit they are also harmful. Environmental pollution and its cure are one of the main concerns for scientist or researchers. Accurate recognition and assessment of various toxicant is the early step to deal with this very serious problem and it is the stage where molecular sensors performed an essential role. The present work manages to identification of poisonous heavy metal ions and toxic anions.

## 1.2 TOXIC EFFECT OF ANIONS IN THE ENVIRONMENT

Anions are omnipresent in nature and in biological processes, they are also involved in many industrial processes like mining, smelting, extraction of gold and silver from ore, uses of pesticides, insecticides and fertilizers, electroplating, preservatives, enameling and anti-rust paints [1]. Due to the vital role of anions in the field of environment, catalysis and medicinal chemistry, it generates the attention of scientist or researcher. There are numerous anions such as cyanide, arsenite, acetate, chloride, nitrite, bromide, fluoride *etc.* that are pervasively present in the biological systems and affect the environment by their toxicity [2].

Chloride ion is an essential electrolyte in sustaining the potential across the cell membrane and the cause of cystic fibrosis is mis-regulation of chloride transport in the cell membrane through the chloride channels [3]. Prodigiosins transport chloride as HCl by biological lipid bilayer membranes which has been shown in uncouple lysosomal vacuolar-type ATPases [4]. Cyanide ion is also a very hazardous anion among other anions. It disturbs many functions of the body including visual, metabolic system, vascular, cardiac and endocrine. Whereas the best-known effect of cyanide is it binds with enzymatic proteins and disrupt the electron transfer chain in the mitochondria of cell

[5-9]. Similarly, the high concentration of acetate ion is also harmful for living organism whereas it plays an important role in the various metabolic processes such as acetyl coenzyme [10,11]. Some other anions that have some importance in biological systems $PO_4^{3-}$, $F^-$, $H_2PO_4^-$, $HPO_4^-$, $SO_4^{2-}$, $NO_3^-$ *etc*., these types of anions also permit for accurate assessment in numerous environmental systems [12-15]. In the treatment of osteoporosis $F^-$ ion plays an important role and preventing in tooth decay. But its high concentration leads fluorosis disease which is also known as fluoride disease [16-18]. Phosphorous is an essential nutrient for human body and it is also a key element for plants growth and animal that is absorb by daily diet such as milk product, vegetables, fish, meat and it is present in human body and other living system as phosphate ion [19]. it can be harmful and toxic if exist in very high level that causes damaging of tissues. The chronic kidney disease and higher existence of vascular calcification is associated to the higher retention of phosphate in the body [20,21].

## 1.3 BIOLOGICAL FUNCTIONS AND TOXIC EFFECT OF METAL IONS IN THE ENVIRONMENT

Heavy metals are commonly occurring in the nature by earth's crust, but pervasive human interference have intensely altered their biological balance and geological cycle [22]. The phrase that establish "heaviness" has been suggested based on atomic weight, density, atomic number and chemical properties. The common definition is "The metals whose density higher than 5 $g/cm^3$ are considered as heavy metals" [23]. Many researches have displayed that these metals play a major role in regulating of many physiological functions and bio-chemical in the living thing at convinced amount moreover excess above permissible amount inimically affect the system. Unluckily, the fact is heavy metals and anions are everywhere in the environment due to the extensive use of these ions in the modern society. The most common heavy metals are chromium (Cr), mercury (Hg), cadmium (Cd), silver (Ag), lead (Pb), copper (Cu), Iron (Fe), zinc (Zn), arsenic (As) and platinum group element. There are various sources of extraction of these metal ions in the environment like soil erosion, sewage parole, fossil fuel combustion, industrial waste, metal mining *etc*.

Alkali and alkaline earth metal ions perform an essential role in numerous biochemical activities because of their engrossment in various biological and environmental processes [24,25]. The reason behind the distribution of these metal ions into the climate is daily industrial turnover that leads negative effect on human being and biota. Recently, the structure of new potassium channel (*Streptomyces lividan*) has stimulated *via* construction of abiotic systems [26]. $Na^+/K^+$ plays an important role in blood circulatory system in the body to maintain blood pressure [27,28]. $Rb^+$ ion is mostly used in radiopharmaceutical analysis [29]. Nuclear fuel is essentially containing radioactive $Cs^+$ ion [30] and therefore its quantitative and qualitative assessment is demanding field of the many researchers. Magnesium ion is also an essential metal ion because it takes part in many enzymatic reactions as a cofactor, magnesium fulfills numerous intracellular physiological functions [31]. The imbalance magnesium status might generate unwanted neuromuscular, cardiac/neurons disorders [32,33] *etc.*

Same as, transition metal ions plays an important role in biomedical and natural processes. These metal ions such as $Zn^{2+}$, $Cu^{2+}$, $Mn^{2+}$ and $Fe^{2+}$ are indulged in various structural and catalytic aspects of the biological procedures [34]. In Alzheimer's disease, the transition metals $Cu^{2+}$, $Fe^{2+}$ and $Zn^{2+}$ have been bound to the peptides in the aggregation of β-amyloid peptides [35]. However, $Cu^{2+}$ ion is an essential element for human body and have importance in the field of biological processes. But its high concentration may cause many diseases, it is accumulated in kidney and liver that affects the gastrointestinal part of human body or may responsible for other diseases *viz.* Wilson's disease, infant liver damage, dyslexia and hypoglycemia [36]. Moreover, the most hazardous element $Ag^+$, $Hg^{2+}$, $Pb^{2+}$, $Cd^{2+}$ and Arsenic have the serious concern of their detection. Arsenic is the more toxic and carcinogenic metal among all heavy metals. In $19^{th}$ century, arsenic compounds arsphenamine (salvarsan), neoarsphenamine (neosalvarsan) *etc.* used as chemotherapeutic agents in the field of medicine [37,38]. It is present in the environment in two forms *viz.* organic and inorganic arsenic, its inorganic form (As(III) and As(V)) is highly toxic among both forms [39]. The main source of arsenic exposure is drinking water drawn from ground [40] that causes many diseases such as skin cancer, arterial disease, urothelial cancer, arsenic-induced skin lesion and hypertension [41,42]. The other more toxic metal ion is lead that can damage all the

organ and nervous system of the human body and causes many diseases such as kidney damage, muscular paralysis, memory loss, cardiovascular affect, mental retardation and anemia [43,44] *etc*. Similarly, mercury is also a very dangerous metal ion for living organism and environment [45]. It binds with sulfhydryl unit of tertiary and quaternary structure of proteins. Its adverse effect is mainly focusing the brain, it can also damage the nerve system, renal functions and immune system [46]. Cadmium ion is also a poisonous element that causes many disease [47]. Its small amount can bind with amino acids which affect the organs of the body. The sources of these heavy metal ion are aquatic, industrial, agricultural activity, nuclear waste and industrial waste. Therefore, the estimation and detection of these ions are very prominent area to scientist and researchers. The precise and accurate detection of anions and metal ion in the water, food, medical field as well as in environment is an important and challenging problem for the analytical chemist. For this, sensors are most suitable as fast and cost effective still it proposed high precision and sensitivity.

## 1.4 HISTORICAL SURVEY OF MOLECULAR SENSORS

The recent growth in the optical sensors arrays *i.e.* the substitute to electronic sensors has dance history as ocular indicators in the field of analytical chemistry. In recent years, Scientist and researchers are focusing on the advancement of the optical sensors arrays because of its high sensitivity and accessible recognition process. In early 23-79 AD, Elderpliny performed the papyrus test which was used in ancient Greece to detect the adulteration of copper ion from iron. Further, in $16^{th}$ century, Tachenius used this method for the detection of ferric ion in urine. Later, another Spanish botanist Nicolus Monardes was described the first recorded fluorescence by a strange blue grimmer from water confined in a specific wooden cup from Ligirium Nephiticiem. Further, Robert Boyle and Isaac Newton were widely explained this phenomenon in $17^{th}$ century. Than in 1865, the first crude fluorescence emission spectra were established by John Hershel for quinine. In 1852, Another famous scientist George Stokes was made good progress to understand of fluorescence process. He started the procedure of analyzing fluorescence by using two distinct filters, in which one for excitation wavelength and another for measuring emission wavelength. He found that the emission

wavelength was longer than excitation wavelength, and now this phenomenon of fluorescence known as "Stokes' Law". The first fluorescence dependent analysis was performed for the determination of Al(III) ion by producing morin chelate by F. Goeppelsrieder in late $19^{th}$ century [48]. In 1950, the fluorescent quinine was responsible for inspiring the development of first Spectro fluorometers.

## 1.5 CONVENTIONAL METHODS FOR DETECTION OF IONS

There are various inorganic techniques available for the detection of trace amount of metal ions. These techniques are Atomic Absorption Spectroscopy (AAS), Flame Atomic Absorption Spectrometry (FAAS), Graphite furnace Atomic Absorption Spectrometry (GAAS), Electrothermal Atomic Absorption spectrometry (EAAS) [49], Inductively Coupled Plasma (ICP), some hyphenated techniques are also available such as Inductively Coupled Plasma Mass Spectrometry (ICP-MS) [50], Inductively Coupled plasma optical Emission Spectrometry (ICP-OES) [51]. Several heavy metal ions such as Co, Cu, Cr, Cd, Ni, Pb, Sb, Hg and Zn are required to detect precisely and accurately on daily basis. These metal ions are present in the environment through industrial waste water. These instruments are used in the detection of various metal ions whereas these instruments are costly, time consuming and have large size therefore, the development of colorimetric and fluorometric chemosensors is the main concern for the effective and sensitive detection.

## 1.6 AIM OF THE THESIS

In the context of the importance and future-outlook of chemosensors based materials, the aim of the thesis is to design a chemosensor scheme that have capability to analyze the analyte accurately *via* selective detection procedure. For making the determination of analyte fast, simple and cost effective, the optical sensors are the better option than conventional methods because conventional methods instruments are sophisticated, highly expensive and complicated. Many of these analytes chemosensor is proposed for the specific planed purpose. The detailed overview of these is deliberated in the following sections. For the selective detection of analyte, these chemosensors performed *via* different techniques such as colorimetric, absorption and emission studies.

The goal of the thesis is to construct such optical sensors that are selective, sensitive and low-cost techniques for various toxic analytes. The thesis contains a number of chemosensors which is synthesized and having different heteroatom moieties (NH, OH, C=S and C=O) that can have high selectivity and sensitivity towards analytes.

## 1.7 MOLECULAR SENSOR

It is a device which collect the information through analyte and change into an appropriate signal that can be comfortably recordable and readable by an apparatus or observer. The recordable signal is countable on the interaction between the analyte and molecular sensors. Therefore, the molecular sensor is constructed based on response of the analyte on different phases [52]. Molecular sensors are made up of two basic functional units: a receptor part and a transducer part. The receptor part of the sensor is designed based on the functions of interaction towards analyte. The transducer unit is recorded the changes that generates on the interaction between the receptor part and analyte (figure 1.1).

The low- cost sensors have wide applications such as in environment pollution, mining, medicine, home safety and many others. A perfect chemosensor generally signifies to a molecular structure (organic or inorganic complex) that is used for sensing of an analyte to produce a detectable changes or signals. When analyte interact with the receptor (chemosensor) then its properties has been changed (i.e. color change, change in absorption, change in electrical potential at the surface of interaction and emission spectra) further, transducer transform the magnitude into essential analytical information.

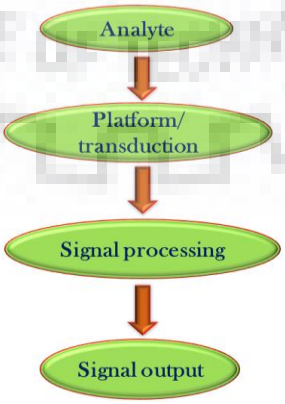


**Figure 1.1.** Schematic representation of a sensor.

### 1.7.1 MOLECULAR RECOGNITION

Molecular recognition is the procedure of non-covalent binding between organic molecule and a guest molecule. It also specifies as the process by which one or two molecules bind to each other in a specific geometry [53,54]. The source of molecular recognition is dependent on host-guest chemistry which is related to normal macrocyclic compounds that are capable to selective binding of alkali ions and supramolecular chemistry. The synthetic or natural receptors, known as carrier/ionophores recognize the ions. The molecule having hosting ability and suitable becomes sensitive and selective sensors for the guest analyte and ion. There are two ways for the recognition of guest by host which is presented in the figure 1.2. In this representation the molecular recongnition is performed, type (a) shows that the recognition unit and repoter are connected by a linker and when the anlyte is recognize by the molecule the reporter or receptor has some changes (in fluorescence), type (b) demontrate that there is only a recognition unit which is only recognize the analyte.

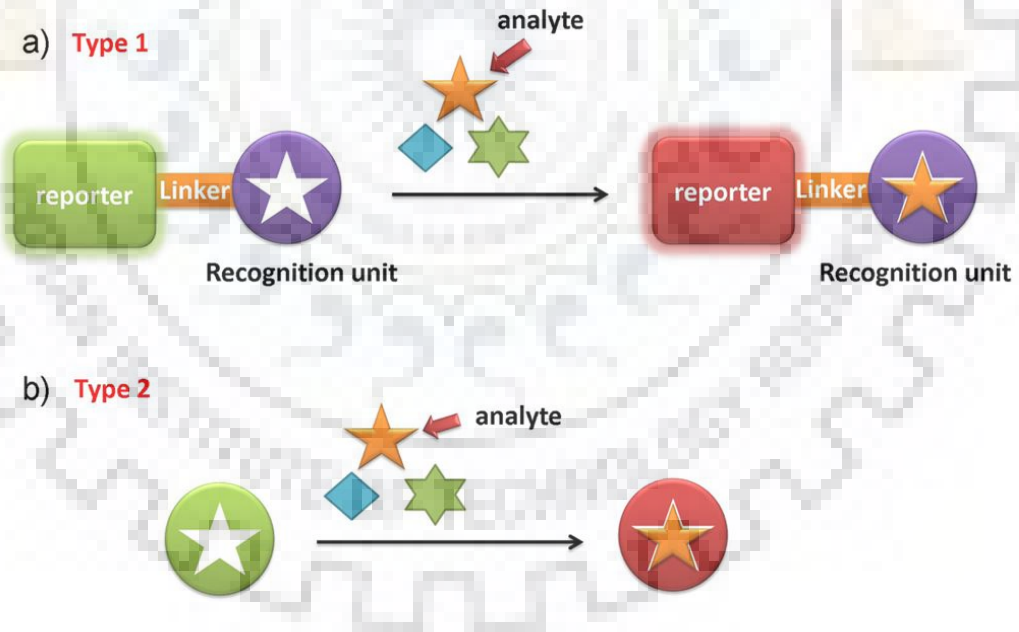


**Figure 1.2.** Two ways for the guest recognition.

#### 1.7.1.1 Cation Recognition

Since last decades scientists including environmentalists, clinical biochemists, chemists and biologists have great interest in “Cation Recognition” as a research area

[55,56]. In the alkali and alkaline earth metal ions $Na^+$, $K^+$, $Mg^{2+}$ and $Ca^{2+}$ ions are participating in many important biological functions such as required in different cellular mechanism, locomotion, DNA replication, transition of nerve impulse, enzyme catalysis, muscle contraction etc. and various metalloenzymes activities are found to operate by several metal ions [57,58]. In the favor of biological term, it is essential to restraint the level of $Li^+$ ion in the serum of patients under treatment of manic depression [59] and $K^+$ level should be controlled in high blood pressure [60,61]. According to the oceanography, the survival of micro-organisms under sea water depend upon some nutrients. Moreover, most of the nutrients contain chromium ($Cr^{3+}$), manganese ($Mn^{2+}$), iron ($Fe^{2+}$/$Fe^{3+}$), cobalt ($Co^{2+}$), copper ($Cu^{2+}$) and zinc ($Zn^{2+}$) that works as enzyme cofactors. In these metal ions aluminum toxicity has long been identified and Alzheimer's disease is a possible implication of its toxicity [62].

It is well-known that lanthanide ions are biologically and environmentally important due to their specific role in catalytic reactions and biological imagining processes [63]. Many of lanthanide metal ions are present in T-channel antagonist because of their +3 valency [64]. Other metal ions like $Pb^{2+}$, $Hg^{2+}$ and $Cd^{2+}$ are known as their toxic influence on living organisms as well as their biological significances [65]. Whereas, there are large number of analytical methods are available for the detection of metal ions such as flame photometry, electron microscope, atomic absorption spectroscopy, inductively coupled plasma *etc.* but all these instruments have high expenses, sophistication with very high expenditure for maintenance [66]. Moreover, these instrumental techniques are not well suited for *in-vivo* and *in-field* studies for detection of the metal ions. On the other hand, colorimetric and analytical techniques are present to be comparatively easier to handle with fast response time, high selectivity and sensitivity. Chromogenic sensors have an interesting quality that the visual detection of the ions, it permits the semiquantitative naked eye detection of selective analyte without establishment of any spectroscopic data. Similarly, fluorescent sensors are also important due to their simplicity, reliability and high sensitivity and used in different application such as bioimaging of living cell with high temporal and resolution.

Further, the luminescence response of the fluorophore is tune up by different photoinduced processes e.g. Charge Transfer (CT), Energy Transfer (eT), Electron Transfer (ET), Förster Resonance Energy Transfer (FRET). Figure 1.3 represents some chelating ionophores [67-71] that contain hetero atom group for ion sensing. In which compound 1 (7-nitrobenzo-2-oxa-1,3-diazolyl) shows turn-on behavior for $Hg^{2+}$ and $Ag^{+}$ ions, compound 2 (1 N-(9-Anthracenylmethyl)aza-18-crown-6)is recognized the alkali metal ions, compound 3 (derivative of terpyridine) is respond as a colorimetric sensor for $Hg^{2+}$ ion in aqueous media while compound 4 (quinoline-carbaldehyde) shows the naked eye detection for $Cu^{2+}$ and $Hg^{2+}$ ions and compound 5 (8-hydroxy-1,2,3,5,6,7-hexahydropyrido-[3,2,1-ij]quinoline-9-yl)methylene)benzohydra-zide) behave as a fluorescent chemosensor for $Al^{3+}$ ion.

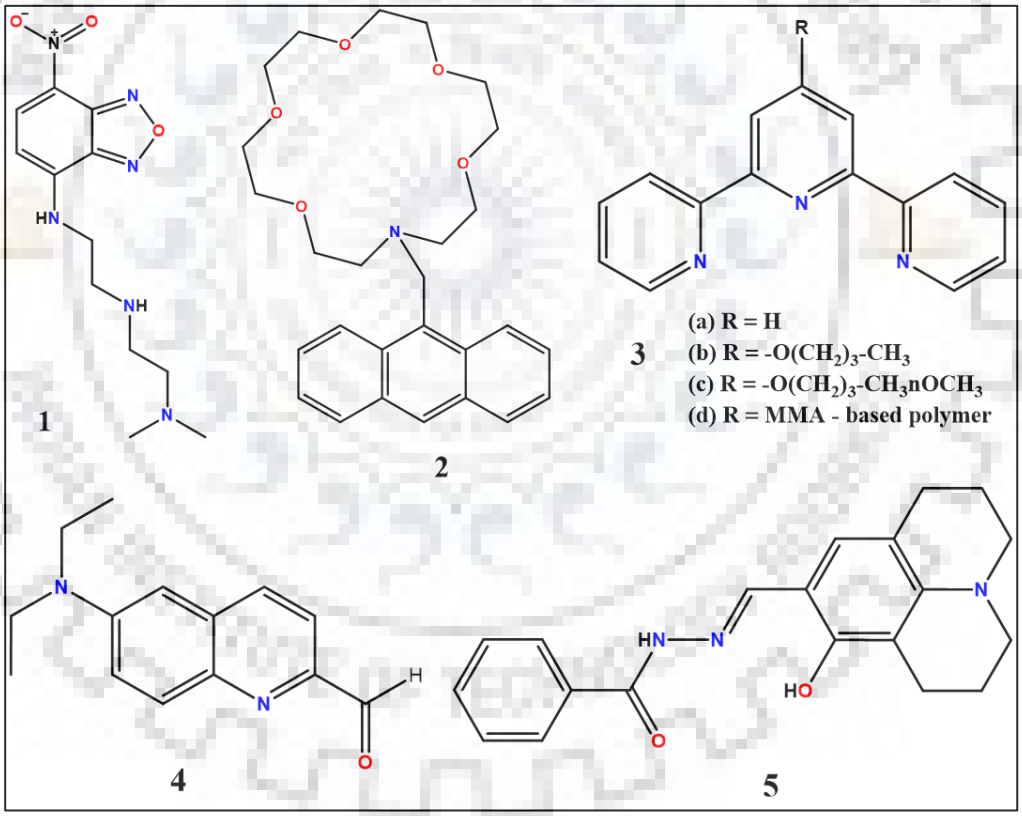


**Figure 1.3**. Different example of chelating ionophores for metal ions appropriate for optical chemosensor, compound 1 for $Hg^{2+}$ and $Ag^{+}$ ion, 2 for alkali metal ions, 3 for $Hg^{2+}$ ion, 4 for $Cu^{2+}$ and $Hg^{2+}$ ions and 5 for $Al^{3+}$ ion.

### 1.7.1.2 Anion Recognition

Anion are important for life, as various biological processes relay on the existence and transport of anions. Many of the chemical transformations and industrial processes are carried out by using anions. Rather than this these anions are generally found as injurious pollutants [72,73]. The anions binding with receptor realm in "Supramolecular Chemistry" and recognition [74] of the anions through different receptor molecules depend on the identification of the anions that can cause many changes like color, absorbance, emission and electrochemical studies which is advantageous in the recognition of anions as well as in real time concentration [75]. These studies are useful for the detection of toxic anions (e.g. $CN^-$, $AsO_2^-$, $F^-$, $NO_3^-$, $PO_4^{3-}$ *etc.*). Therefore, it is needed to develop the reliable and sensitive methods for detection of these anions in the favor of environment and human health. In this context, the most active area in research is optical anion sensors, in which the recognition of anions is occurred *via* receptor molecules with changes in color and spectral properties [76]. Figure 1.4 represents some chemosensors for anions [77-81] detection in which compound 6 (4-phenylsemicarbazide or 4-phenylthiosemicarbazide) shows urea and thiourea based compound for the detection of $F^-$ and $AcO^-$ ion. Compound 7 (1,3-Bis(4-nitrophenyl urea) is highly selective and efficient for $F^-$ ion. Compound 8 salicylaldehyde hydrazones based chemosensor is highly selective for $CN^-$ ion sensing, compound 9 (Dipyrrole carboxamide based) is highly sensitive towards $CN^-$ ion similarly, compound 10 is used for the sensing of $H_2PO_4^-$ anion among other anions.

### 1.7.2 TYPES OF SENSORS

Sensors can be classified as Physical sensors, Chemical sensors or Biosensors depending on the quantity they are measuring (figure 1.5). Physical sensors contain electrochemical sensors, magnetic sensors, thermal sensors *etc.*

- **Physical sensors:** These sensors have the capability to quantify the physical responses such as pressure, volume, force, magnetic field, temperature *etc.*
- **Biosensors:** Biological sensors measures biological properties such a cell or virus numbers. Biosensors can be physical, chemical or biological sensors, which

respond towards biomolecules such as amino acids, proteins, tissues and nucleotides [82-86].

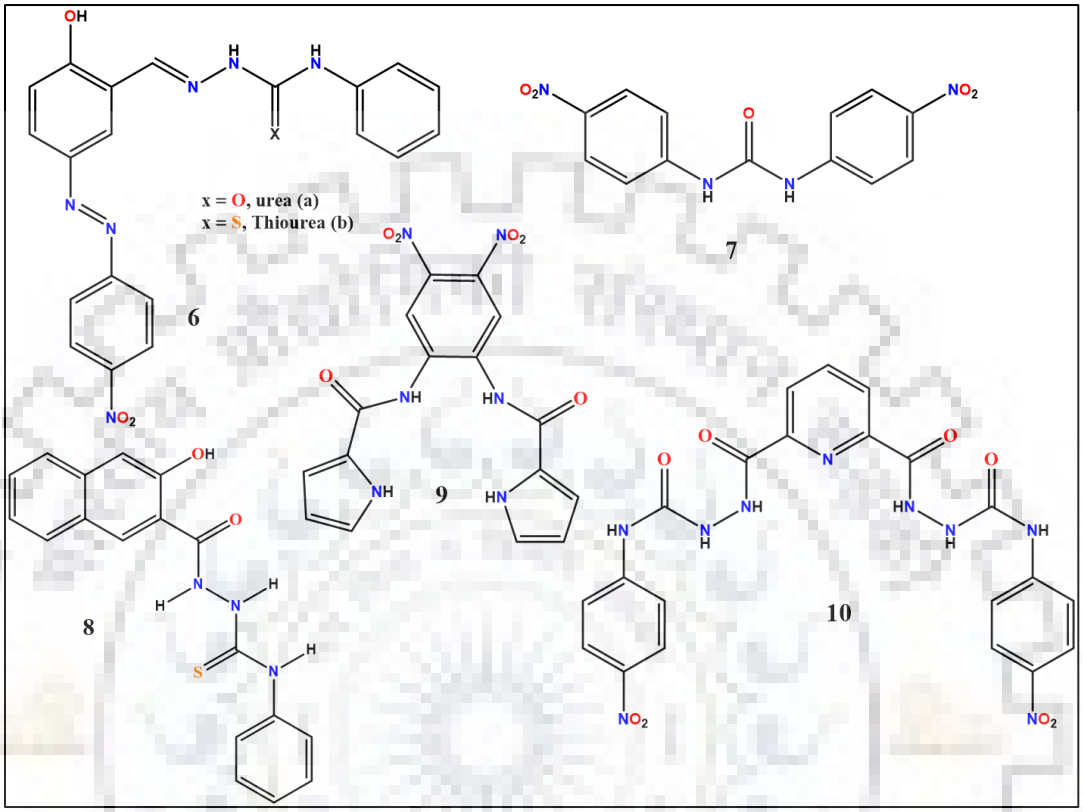


**Figure 1.4.** Various type of chemosensors for the detection of anions in which compound **6** $F^-$ and $AcO^-$ ion, **7** for $F^-$ ion detection, **8** for $CN^-$ ion, **9** for also for $CN^-$ detection and **10** for $H_2PO_4^-$.

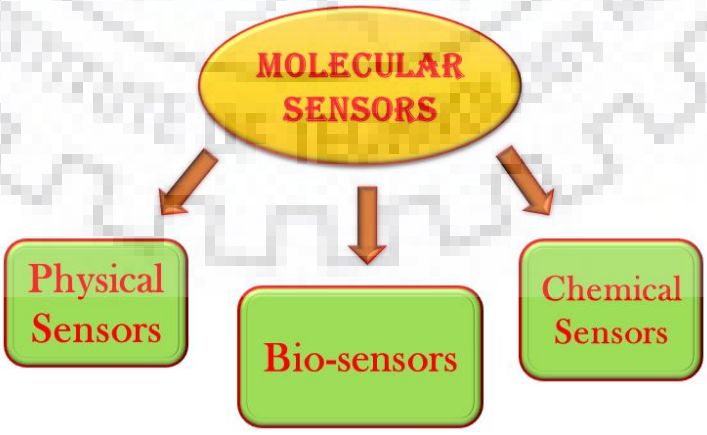


**Figure 1.5.** Types of Molecular sensors.

- **Chemical sensors:** Chemical sensors are the materials that transform chemical information to analytically useful signals. It distinguishes the molecule which is conscious towards stimuli yield by different chemical analytes and transduction part generate a signal whose magnitude is straightly proportional to concentration of analyte [87]. The suitable definition of a "chemical sensor" has been defined as "Cambridge definition", by which a "chemical sensor" is one that "a miniaturized device/ material, which passes real time and on-line information in the presence of specific ions in the complex". The phrase "chemosensor" had been described as a material of abiotic origin that indicate the existence of energy or matter [88]. Chemosensors can be divided by the nature of signals such as electrochemical, optical and colorimetric sensors *etc.* and further the electrochemical and optical sensors are briefly discussed.

### 1.7.2.1 Electrochemical sensors

Clinical chemistry has great interest in electrochemical sensors like potentiometric, amperometric and ion selective electrode because they propose fast response, relatively inexpensive and electroanalytical results [89,90]. The sensor membrane is an example of clinically useful sensor [91]. Membrane plays an essential role in ion-selective electrode/sensor where the chemical detection and other processes occurred. The necessity of the signal's quality and persistence of the sensor depend upon the membrane. Electrochemical sensors present electrochemical changes between the analyte and characteristic electrodes [92]. These devices convert the response of electrochemical interaction between analyte and electrode in to useful signals. Electrochemical sensors have following subgroups.

- Potentiometric sensors in which potential is measured for indicator electrode (e.g. metal/metal oxide, ion-selective electrode and redox electrode) *Vs* reference electrode.
- Next one is voltammetric sensors that include amperometric sensors. These sensors generally measured the direct current (d.c.) [93].

In various analytical techniques, the ISE (Ion-Selective electrode) sensor is found to simple and have wide range of benefits. Another way to sense the guest molecule by the receptor is electroanalytical techniques such as Cyclic Voltammetry (CV). Cyclic voltammetry measures the redox potential or properties of the receptor in the presence or absence of the guest molecule. This type of sensor has redox active groups and binding units. In this procedure, the binding processes must be connected to the redox reactions which is the necessity factor that means redox active center must be included with binding of guest molecule.

### 1.7.2.2 Optical Sensors

Generally, optical sensors are categorized into colorimetric sensors, fluorescent sensor, and electronic transfer path selective sensors [94,95]. Over the other method, fluorescent sensor has main concern due their high sensitivity, real time monitoring, high speed and safety. In the fluorescence, the substance emits the light on absorption of electromagnetic radiation, this emitted light always absorb at higher wavelength with lower energy than the absorb light. The main issue is sensitivity of fluorescence which is generated *via* difference between emission and excitation wavelength. Absorption measurement is described the concentration up to the range of micromolar whereas fluorescence measurement precisely determined the concentration in range of picomolar or femtomolar level. Therefore, fluorescent sensors have great interest, as they provide good output with very easy measurement of lower concentration. Further, it can be used in different biological system.

#### *1.7.2.2.1 Photoluminescence*

When a molecule absorbs the photons and emits the light from any form of molecules, this phenomenon is called photoluminescence [96]. Normally, this phenomenon is classified into two categories *i.e.* fluorescence and phosphorescence. In phosphorescence and fluorescence mechanism, the time interval between absorption and emission of light may vary from short femtosecond and millisecond respectively. Generally, fluorescence happens when the emission of the photons within the two energy levels of same spin multiplicity. The process is very vast, and an electron is in the excited

state has the lifetime is $10^{-5}$-$10^{-8}$ s. Phosphorescence mechanism takes place when a photon is transferred to the triplet excited state to singlet ground state, where the spin multiplicity is not same. The lifetime for phosphorescence is in the range $10^{-4}$-$10^{4}$ s. The photoluminescence method is divided into following sub-divisions (figure 1.6).

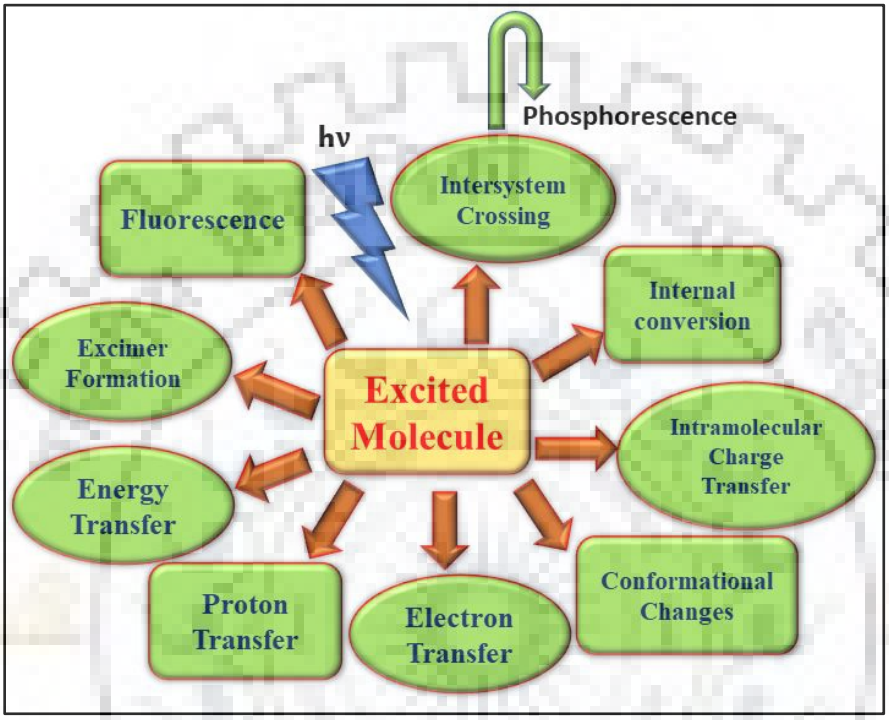


**Figure 1.6.** Possible pathways of excited molecule and various photoluminescence processes.

### *1.7.2.2.2 Absorption of light*

A molecule irradiates by electromagnetic radiation, it starts to absorb this radiation and becomes reactive in higher energy levels or excited state. Due to the reactivity of the molecule, the transition of the electrons occurred from highest occupied molecular orbital (HOMO, HOMO-1) to lowest unoccupied molecular orbital (LUMO, LUMO+1). For the transition between electronic energy level, the electromagnetic light must be of enough energy and these photons are found deceptive in UV-vis region. Because of this region, the visible range of electromagnetic radiation from 200-800 nm is called as “photochemical window”. The spam of the wavelength of spectrum and results of absorption are summarized in the table 1.1.

The optical UV-vis range are subdivided into ultraviolet, visible light and near-IR. When an extension in conjugation or mixed-valence system occurred, it is come under Near-IR absorption [97]. When electromagnetic radiation is irradiated any molecule or substance, the substance starts to absorb, scattered, transmitted or reflected the radiations. Substance absorbs the radiations only of exact frequency *i.e.* related to energy difference of two electronic levels.

**Table 1.1:** Ranges of the electromagnetic radiation and their significance on molecular structures

| **Radiation** | **Range of wavelength (λ)** | **Absorption Associated** |
|---|---|---|
| Gamma Rays | 0.1 nm | Nuclear Reactions |
| X-rays | 0.01-10 nm | Transitions of inner atomic electrons |
| UV | 10-400 nm | Transitions of outer atomic electrons |
| Visible | 400-750 nm | Transitions of outer atomic electrons |
| Infrared | 750 nm-15 μm | Molecular vibrations |
| Far Infrared | 15 μm-1mm | Molecular rotations |
| Radar | 1 mm-1m | Oscillation of movable electrons |

The molecule irradiated by light radiation, the excited state of the molecule is generated, and it has different chemical reactivity with its ground state. The intensity and shape of the absorption band or spectra are depending upon excitation between ground and excited state. The absorbance, concentration of absorber and path length is connected to each other by the Lambert-Beer Law [98].

$$A = \epsilon \times C \times l = log_{10} \frac{I_0}{I}$$

Where, A represents absorbance, ϵ for molar absorption coefficient, C represents conc. of the substance, l shows path length, $I_0$ represents incident radiation light and I show the transmitted light.

The absorption spectra of a substance can be achieved by using UV-vis spectrometer. The absorbance of a molecule at specific wavelength is dependent on the concentration of the species and its molar absorption coefficient. This coefficient is related to the electronic transition at specific wavelength. The analyzed value of this coefficient (through quantum chemical parameters) provides a proof of how allowed a transition is. The term "allowed" and "forbidden" are related to classical physics and meant as quantum chemical term. If the value of $\epsilon$ is greater than $10^5$ $dm^3$ $mol^{-1}$ $cm^{-1}$ for a transition, this transition is assigned as "fully allowed" and if the value of $\epsilon$ is below ~100 $dm^3$ $mol^{-1}$ $cm^{-1}$, this transition is act as "forbidden". The "forbidden" transition indicates that the molecule does not absorb the radiation well and transition is very low. The values of $\epsilon$ between ~$10^2$ and ~$10^4$, the transition is "partially allowed". The selection rule of transitions is based on two factors, "spin and symmetry" [99].

By the spin selection rule, the electronic transition is allowed, where the spin remains unchanged and "forbidden" transition occurred if there is difficulty in spin. This suggest that during transition spin changes from singlet to triplet. Whereas symmetry selection rule analyzes the symmetry of ground and excited state and it may be distorted by the environmental factor or presence of metal ion. Therefore, it is critical to know which transition is allowed and which is forbidden by the symmetry selection rule. To overcome this situation, the absorption coefficient is measured and found that if $\epsilon < 100$ than transition is symmetry allowed and spin-forbidden and if the transition is forbidden by the symmetry rule and allowed by the spin selection rule the value of $\epsilon$ is $10^2$~$10^4$ in the range due to the symmetry distortions [100].

The $\epsilon$ values, types of transitions and intensity defines the form of absorption spectra. The transitions are carried out by Franck-Condon principle, which declares that the electronic transitions in a molecule appeared very fast or in simple manner that transitions are vertical. Potential energy diagram reveals that each electronic orbital has their own vibrational levels for HOMO-LUMO transitions. During these transitions, the internuclear space remains unchanged. These transitions show very intense transition in absorption spectra. Generally, due to the large number of vibrational levels in electronic state, the organic system does not give fine and sharp transition in solution or solid

media. Comparatively, they represent the broad curves, such as a line drawn over the peak maxima of the specific transition. Moreover, the Franck-Condon principle is equally applicable to both absorption and florescence phenomenon [101]. In the fig 1.7 demonstrates the decay to the ground state through photon emission. Details of these processes and different types of relaxation will discussed in following section.

#### *1.7.2.2.3 Physical deactivation of excited state*

When a substance is exposed to light and it starts to form an excited state, which is chemically different substance to their corresponding ground state. This excited state of the molecule has been called "electronic isomers" which is moderately under assessment their relevance. Due to the instability of these excited states, they lose their excess energy instantly *via* deactivation processes. The Perrin-Jablonski diagram is suggested to visualize the most instinctive process in a simple way, which is usually occurs after absorption of photon and explains the properties of excited state and their relaxation processes. After absorption of light by the molecule, the vibrational energy levels in the excited state will be populous with electron, which have huge energy and starts to relax in lowest vibrational level of $S_1$ with in picosecond or less through vibrational relaxation and this process known as the **"Internal Conversion"** (non-radiative loss of energy). According to Kasha's rule, [102] the other photochemical processes like fluorescence, quenching *etc.* are occurs from $S_1$. This rule says that after excitation all the photochemical reactions will enduringly arises from $\nu = 0$ of $S_1$ due to the relaxation rate to the lowest vibrational level of $S_1$ is the fastest deactivation process. Now the excited electrons at $S_1$ level of excited molecule may go through either fluorescence by emission of photons or intersystem crossing to the triplet state or it may reduce to the ground singlet state $S_0$ through emission of energy by Internal conversion. In the idealized conditions, intersystem crossing for relaxation from singlet $S_1$ to triplet $T_1$ *via* spin alteration is forbidden transition process. Moreover, the relaxation from excited $T_1$ state to the ground state $S_0$ is a radiative process and it is called as "**phosphorescence**", it is also called a delay process. This process is lower energetic radiative, and it is also slower than the fluorescence processes due to the spin multiplicity. In this process, fluorescence is a spin-allowed radiative relaxation process because of same multiplicity of both states

excited $S_1$ and ground $S_0$. This process takes very short time period within the range of picoseconds to microseconds. According to the Jablonski's diagram (figure 1.7), during this process the emitted light has the higher wavelength (lower energetic) distinguished to absorbed light due to loss of limited energy by the molecules [103].

The difference between the $\lambda_{max}$ (spectral position) of absorption and emission is known as "Stokes Shift" (figure 1.8) [104]. The instant non-radiative decay to the lowest vibrational level of $S_1$ is the main reason of Stokes' shift. Furthermore, due to this effect, the fluorescent molecules show the stokes shift because of complex formation, solvent effect, energy transfer and excited-state reaction.

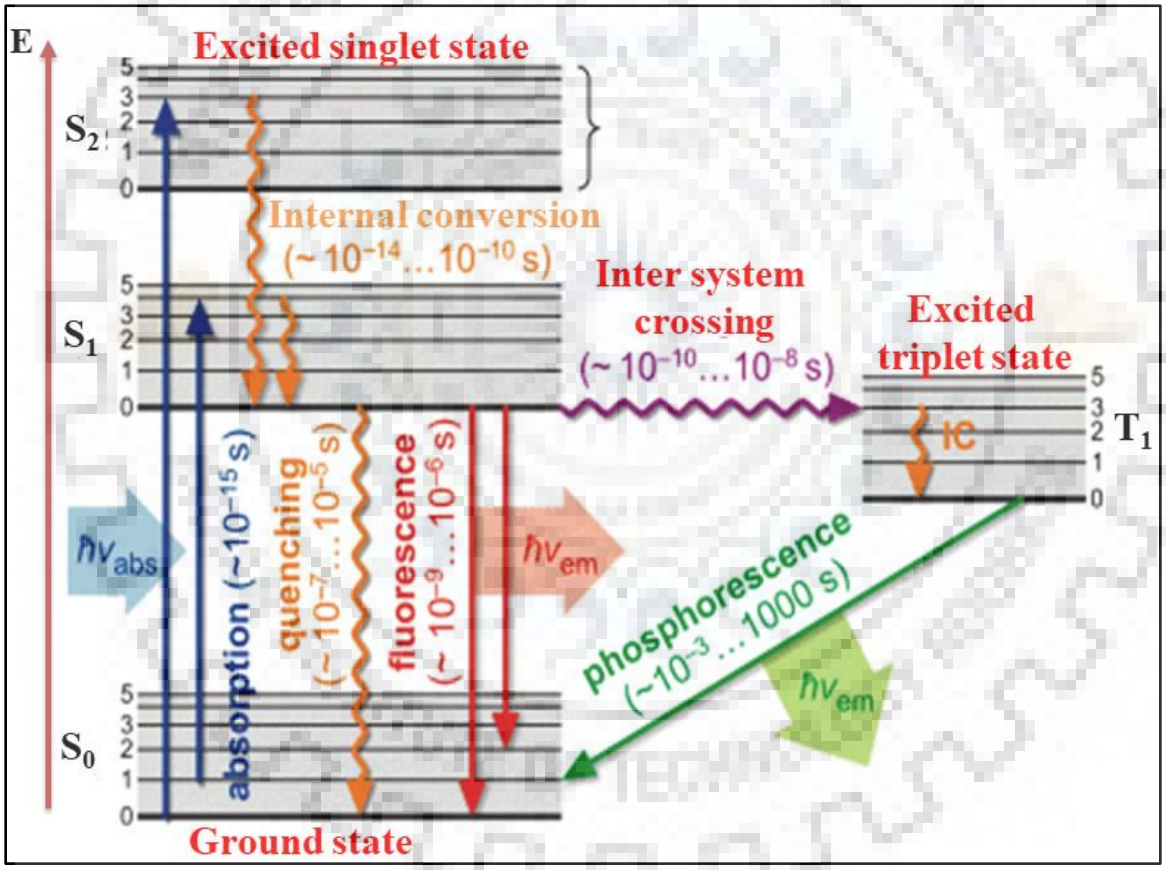


**Figure 1.7.** The Perrin-Jablonski diagram.

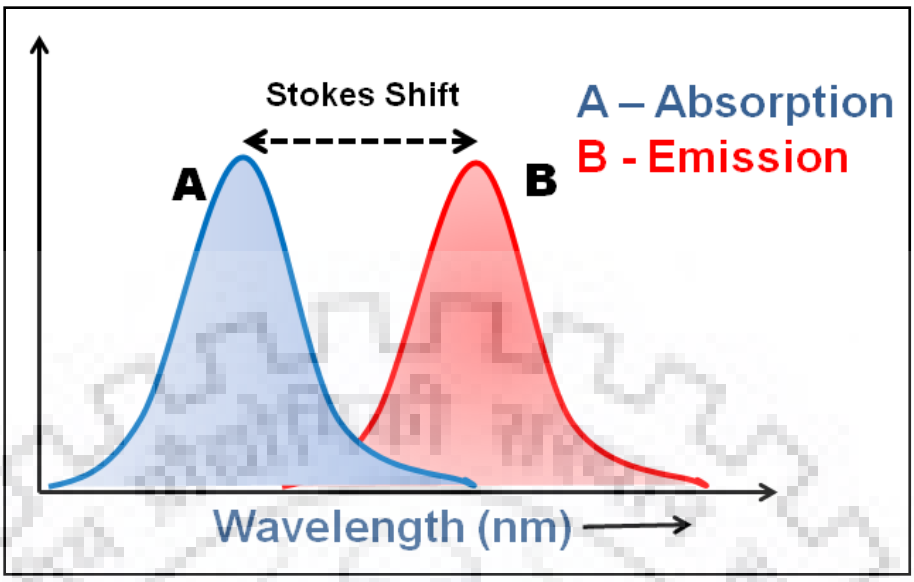


**Figure 1.8.** Demonstration of Stokes shift.

***1.7.2.2.4 Fluorescence Sensors***

Nowadays, fluorescence sensors are more fascinating for researchers due to their stability, reliability and luminescence behavior *via* different mechanism or photoinduced processes *viz.* charge transfer (CT), energy transfer (eT) and electron transfer (ET). The variations in the structure after host-guest binding leads *via* luminescence Reponses and these receptors shows both behavior (colorimetric and fluorometric) [105,106]. In favor to develop a competent artificial receptor for appropriate cationic or anionic analytes, multiple interaction between host and guest in a complementary fashion must be considered. The main factor for fluorescence sensing is fluorophore and it is responsible output signals.

***1.7.2.2.4.1 Mechanism of Signal Transduction***

Emission phenomenon takes place from excited state molecule due to the higher reactivity of the molecule in the excited state. The interaction between two molecules resulted the signal transduction and go through the intramolecular or intermolecular electron transfer, charge transfer, energy transfer and proton transfer. Different types of mechanism are further discussed.

### *1.7.2.2.4.2 Photoinduced electron transfer (PET)*

The photoinduced electron transfer chemosensors are an important part of the chemosensor family. Turn-on fluorescence by small molecule have been developed and examined based on PET mechanism. In the PET mechanism the indicators devices connected to an analyte recognition unit (called as chelating group, coordination site, ligand, receptor, host or probe) with a fluorophore. In PET chemosensors the receptor and fluorophore are separated by a spacer that electronically connected by the π-electrons of receptor with fluorophore. By the absorption of light, an electron hole pair or molecular ion pair is formed *via* excited of electrons. In these types of systems, generally receptors contain high-energy nonbonding electron pair. In the PET mechanism, the donor unit in the molecule can promote an electron to the empty low-level orbital of the receptor which is called as quencher. After excitation, an electron is transferred form highest occupied molecular orbital (HOMO) to lowest unoccupied molecular orbital (LUMO), which generates the fast-intramolecular electron transfer form HOMO of receptor to LUMO of excited fluorophore through radiative and non-radiative process [107,108].

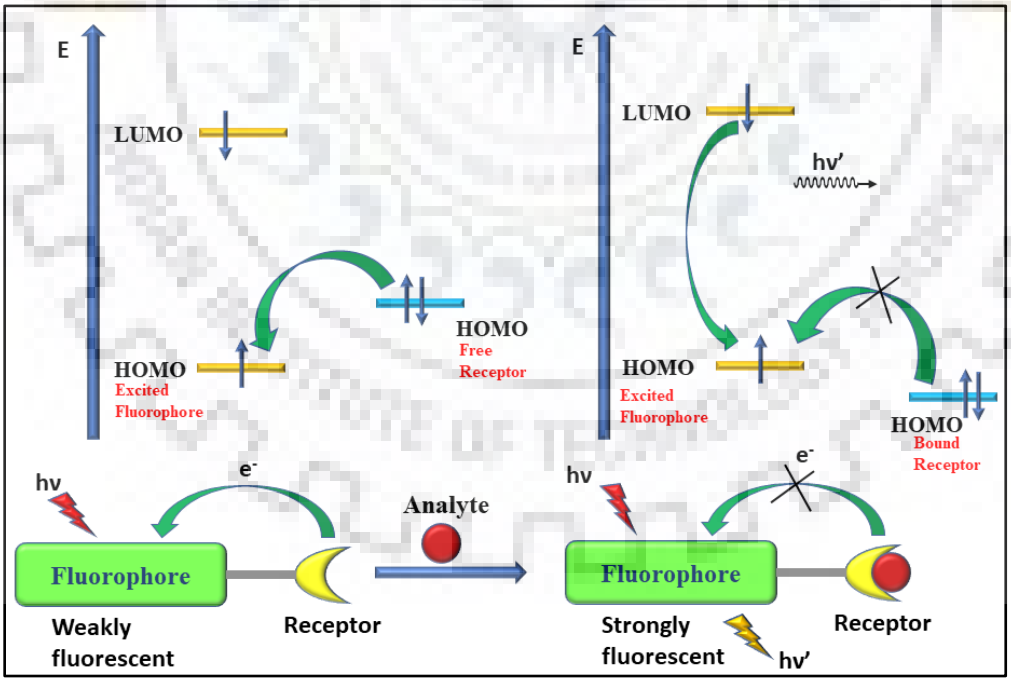


**Figure 1.9.** The graphically representation of "off-on" PET mechanism.

After absorption of light, the electron transfer occurred within the molecule that is called as photoinduced electron transfer. This type of chemosensor has both the units, receptor and fluorophore with in the same molecule which are linked by the non-conjugated bridges. Such a procedure produces a mechanism for nonradiative deactivation of the excited state of molecule, resulting a quenching effect of the fluorescence of the system. This system represents 'off-on' type chemosensor in which the fluorophore unit shows weak fluorescence on unbound condition, when receptor is coordinated to Lewis acid it shows strong fluorescence. Figure 1.9 demonstrated that when receptor is bound, the transfer of electron is not performed by the receptor, rather than this electron pair is transfer to Lewis acid or cation. In such cases the HOMO of the receptor is lowered than HOMO of the excited fluorophore, the redox potential of the receptor is hampered, and the PET process goes slow down, encouraging fluorescence emission; this can also be reversed [109]. This is also called as "Reductive PET" mechanism.

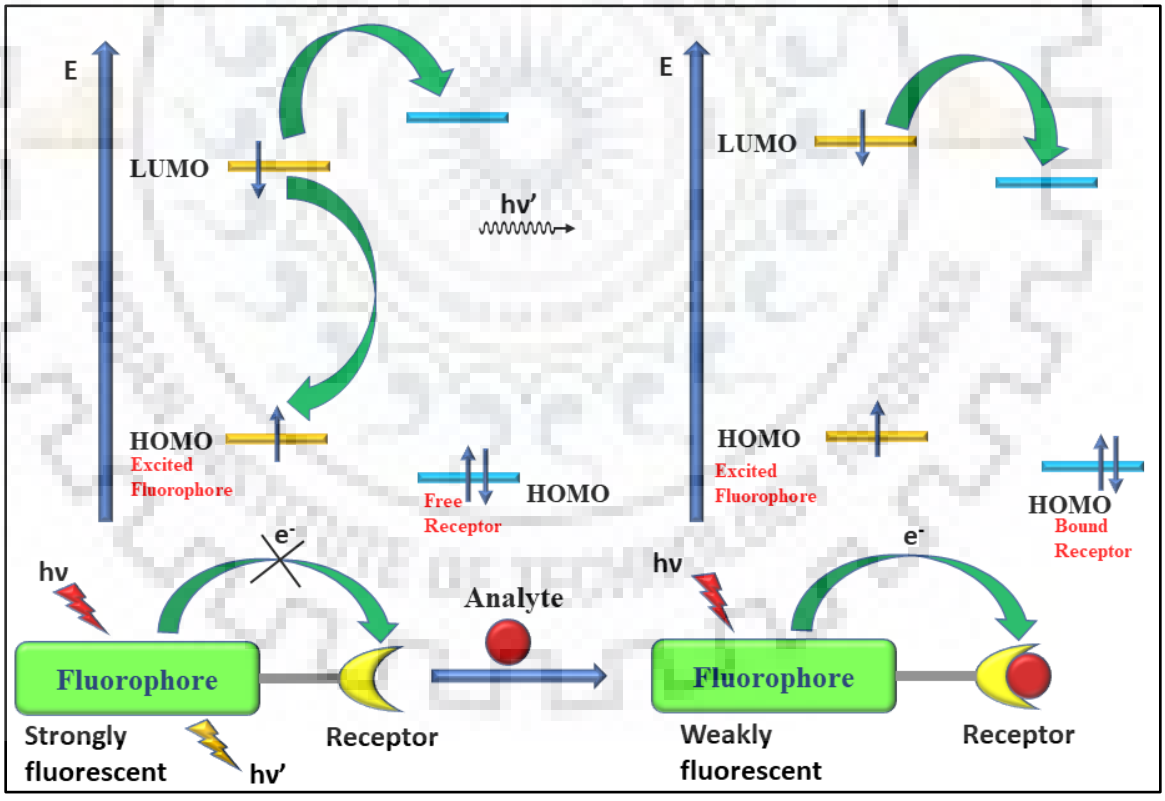


**Figure 1.10.** The graphically diagram of oxidative PET mechanism.

The oxidative photoinduced electron transfer mechanism between receptor and fluorophore is fully dependent on the redox potential of the both units. Apart from the reductive PET mechanism, oxidative PET chemosensor shows strong fluorescence from unbound molecule, whereas the fluorescence emission is quenched on bound species. This type of process called as 'on-off' System. The fluorescence intensity of such chemosensor is decreases as the amount of analyte increases. Figure 1.10 represents the molecular orbital diagrammed of oxidative PET process [110].

Liu et al. [111] synthesized 8-hydroxyquinoline based chemosensor HL (N-(quinoline-8-yl)-2-(quinoline-8-yloxy)acetamide) for $Cd^{2+}$ ion in ethanol *via* 'off-on' PET mechanism (Scheme 1.1). On the other hand, it also senses $Zn^{2+}$ ion simultaneously. In this study the composition between $Cd^{2+}$ ion and HL is 1:1 occurred based on emission and absorption titration. Scheme 1.1 represents the chemosensor for $Cd^{2+}$ and $Zn^{2+}$ ion.

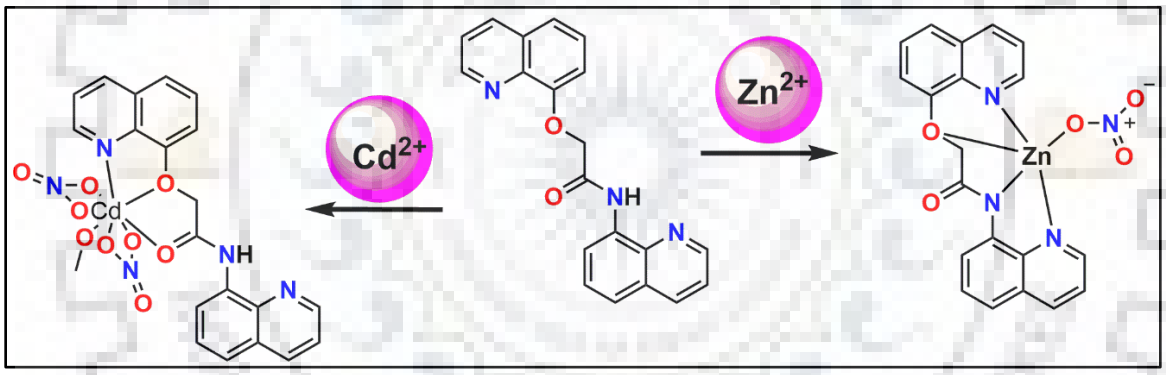


**Scheme 1.1.** PET based $Cd^{2+}$ and $Zn^{2+}$ ion selective chemosensor.

Lee et al. [112] has been reported a fluorescent sensor which is based on the pyrene unit (Scheme1.2). In this chemosensor the receptor and fluorophore unit both are present. This molecule has tryptophan unit as receptor and pyrene unit is as fluorophore unit for the detection of $Hg^{2+}$ and $Pb^{2+}$ ion in the aqueous medium (10 mM HEPES buffer of 7.4 pH) with 5% $CH_3CN$. This chemosensor viewing turn-on emission in case of $Pb^{2+}$ (380 nm) and in case of $Hg^{2+}$ ion (at 380 and 475 nm). Identification of $Pb^{2+}$ and $Hg^{2+}$ ion by the sensor hampered the PET mechanism from indole moiety to pyrene moiety in the molecule, that results enhancement in the emission. Whereas, in the sensing of $Hg^{2+}$ ion due to stacked dimerization of pyrene fluorophore, the absorption intensity is decreased.

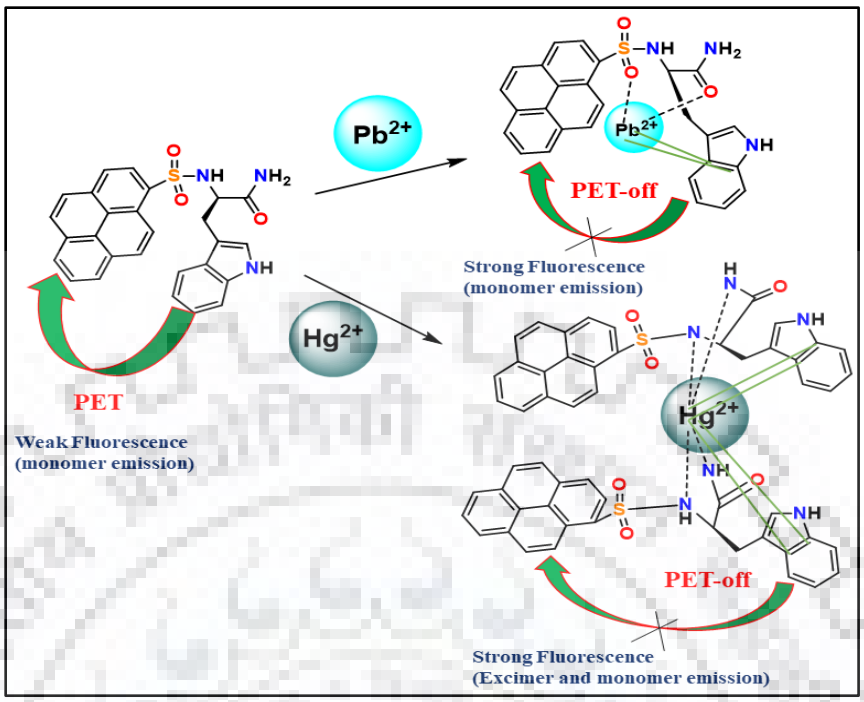


**Scheme 1.2.** $Pb^{2+}$ and $Hg^{2+}$ selective chemosensor based on oxidative PET process.

Saha et al. [113] worked on an azo based Schiff base ligand (E)-6,60 –((1E,10E)-(propane-1,3-diylbis(azanylylidene))bis(methanylylidene))bis(2-methoxy-4-((E)-phenyldiazenyl)phenol) $H_2L$ (Scheme 1.3) that exhibits highly selective towards $Al^{3+}$ ion with good selectivity in semi-aqueous medium.

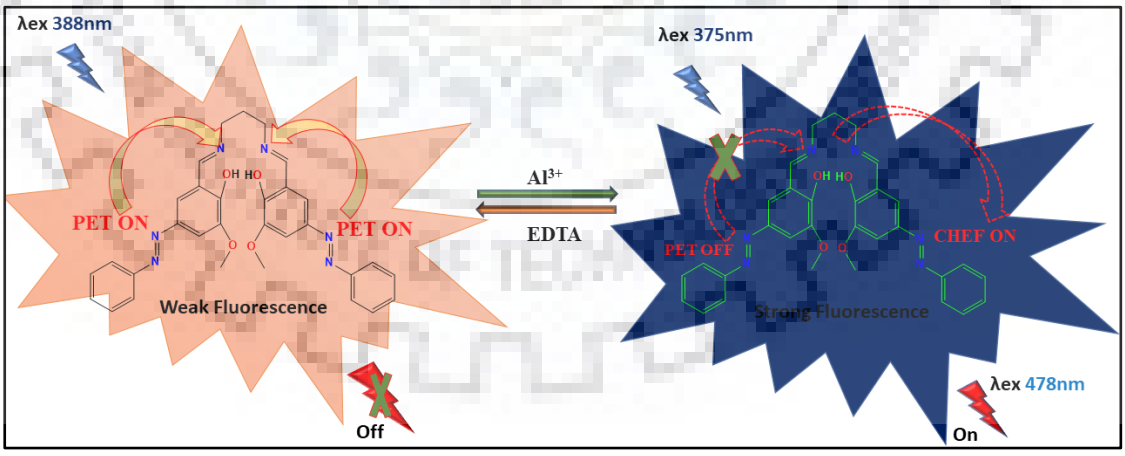


**Scheme 1.3.** Azo based PET chemosensor for aluminum ion.

The sensor represents the mechanism during sensing is chelation enhancement fluorescence (CHEF) through inhibition of PET mechanism. This chemosensor

demonstrate the 1:1 stoichiometry between the sensor and aluminum ion. it also shows reversibility behavior of the chemosensor.

Another PET chemosensor 1 based on anthracene with two imidazolium groups (Scheme 1.4) was developed by Yoon et al. [114] for recognition of anions *via* hydrogen bond formation. This Fluorescent PET based chemosensor demonstrate the sensing towards $H_2PO_4^-$ and three halides ($Cl^-$, $Br^-$ and $I^-$) anions through emission spectroscopy and $^1H$ NMR. Ab initio calculation predicted a unique tweezer-like binding of sensor with anions.

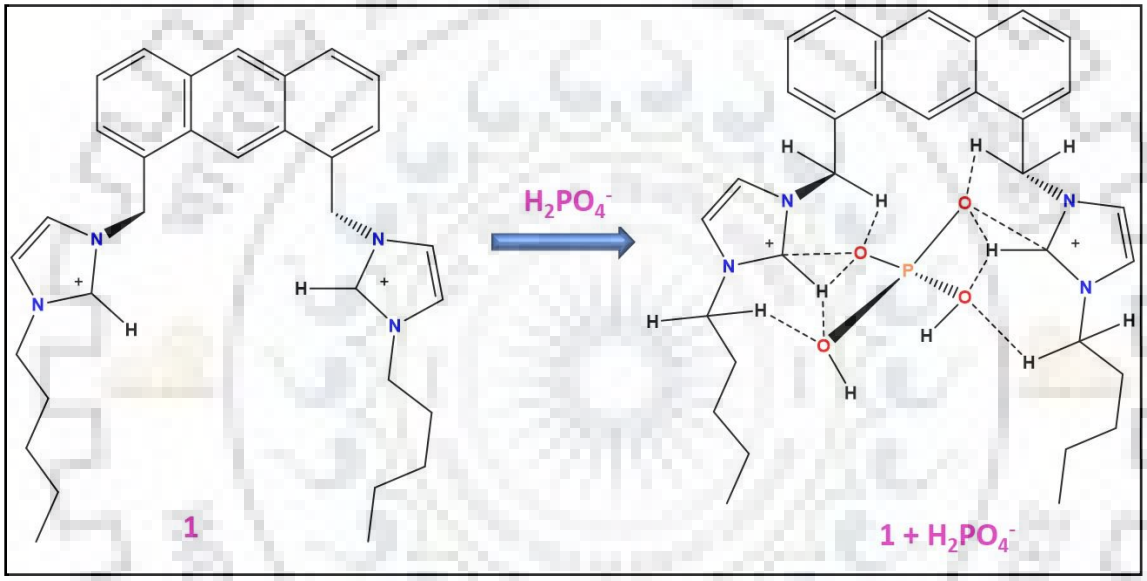


**Scheme 1.4.** Dihydrogen phosphate selective probe based on PET mechanism.

### *1.7.2.2.4.3 Intramolecular charge transfer (ICT)*

CT (charge transfer) mechanism is divided in to two categories. The promotion of charge from an electron-rich (Donor) moiety to an electron deficient (acceptor) moiety present in different molecules is known as intermolecular charge transfer method. However, the donor and acceptor both moieties are in the same molecule, this phenomenon known as intramolecular charge transfer process. The ICT process normally occurs in the excitation state of the molecule due to the absorption of light of proper wavelength. In the excited state of the molecule facilitate promotion of an electron from one segment of the molecule or ion to the other segment in the excited state, that generate

the charge distribution in the excited state is different from the ground state. In this type of molecule, the donor and acceptor are connected through a π-electron bridge not by the spacer [115, 116].

For this Pichumani et al. [117] synthesized a thiophene based sensor 4-methoxy-N-((thiophen-2-yl)methyl)benzenamine which is highly selective towards $Ag^+$ ion among other metal ions in methanol: water (1:1, v/v solution) medium with a detection limit as 5.0 μM (Scheme 1.5). A strong fluorescent enhancement is occurred on addition of $Ag^+$ ion that ascribed to an increase in intramolecular charge transfer.

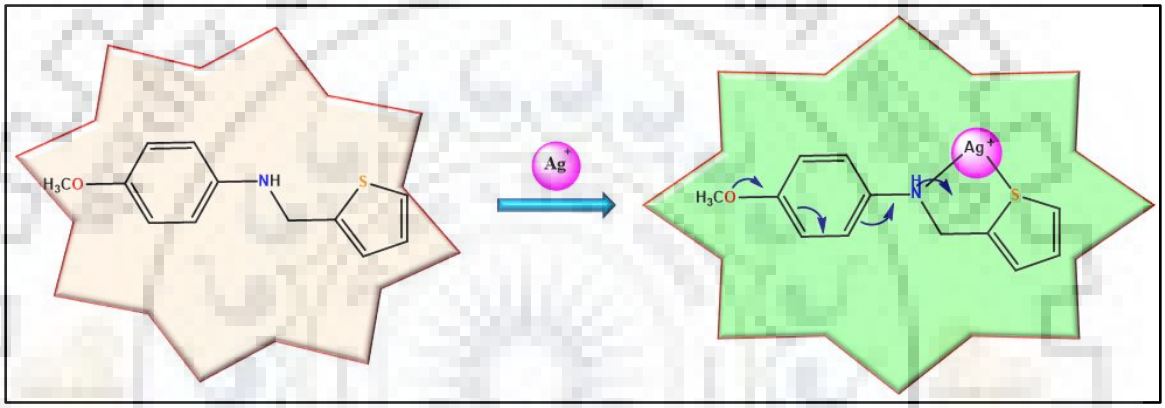


**Scheme 1.5.** Thiophene based $Ag^+$ selective probe with ICT mechanism.

A new fluorescent probe was developed by Misra et al. [118] that was further used in anion sensing. This tricyanoethylphenyl phenanthroimidazole (TCPPI) probe (Scheme 1.6) represents naked-eye "turn-on" detection for $F^-$ and $CN^-$ ion among other anions in acetonitrile ($CH_3CN$). The probe displays 1:1 stoichiometry with anions ($F^-$ and $CN^-$), shows good selectivity towards $F^-$ (0.98 μM, 18.68 ppb) and $CN^-$ (1.12 μM, 29.12 ppb). The other spectral analyses such as NMR titration represents the affinity towards both anions with acidic -NH fragment of imidazolyl unit *via* H-bonding interaction and deprotonation mechanism. Further, the anions activated probe shows the interaction for $CO_2$ with "On-Off-On" type fluorescence.

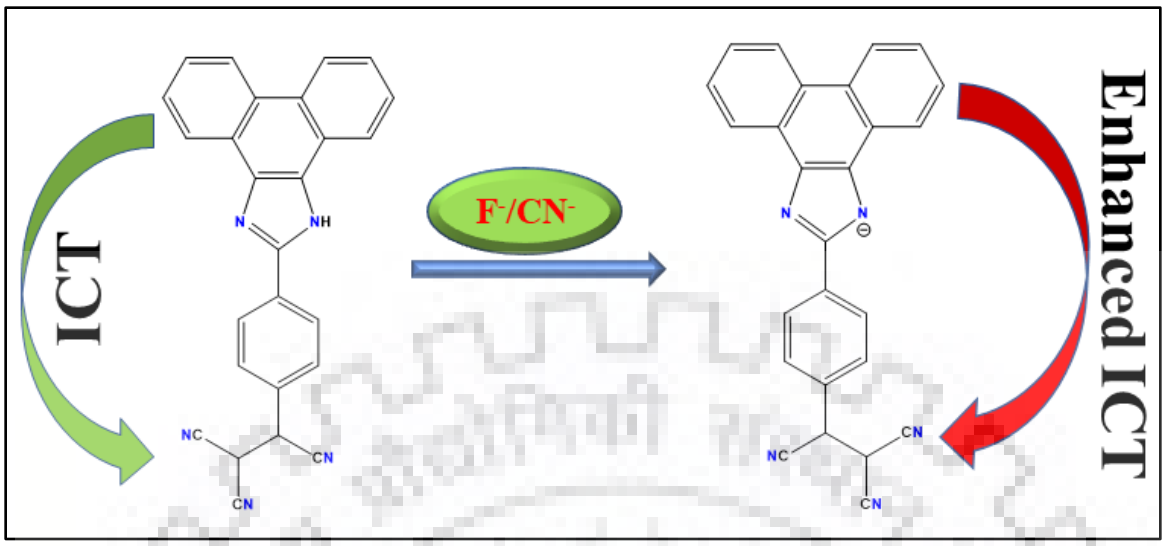


**Scheme 1.6.** $F^-$ and $CN^-$ selective probe based on intramolecular charge transfer mechanism.

***1.7.2.2.4.4 Energy transfer***

To understand optical sensing, energy transfer is an essential mechanism. This is classified as electronic energy transfer (EET) and fluorescence resonance energy transfer (FRET). Both mechanisms are relying upon distance between donor and acceptor groups in multi-chromophoric system [119]. In these types of systems, donor unit always absorb radiation at smaller wavelength and transferred this energy to acceptor unit that fluoresces at higher wavelength [120]. The fluorescence resonance energy transfer (FRET) is possible when the distance between donor and acceptor unit is in the range 10-100 Å *i.e.* known as Förster type energy transfer and similarly, electronic energy transfer (EET) is occurred when the distance remnant within 10 Å, this mechanism also known as Dexter electron transfer of energy transfer [121]. Figure 1.11 demonstrate the Forster and Dexter energy transfer.

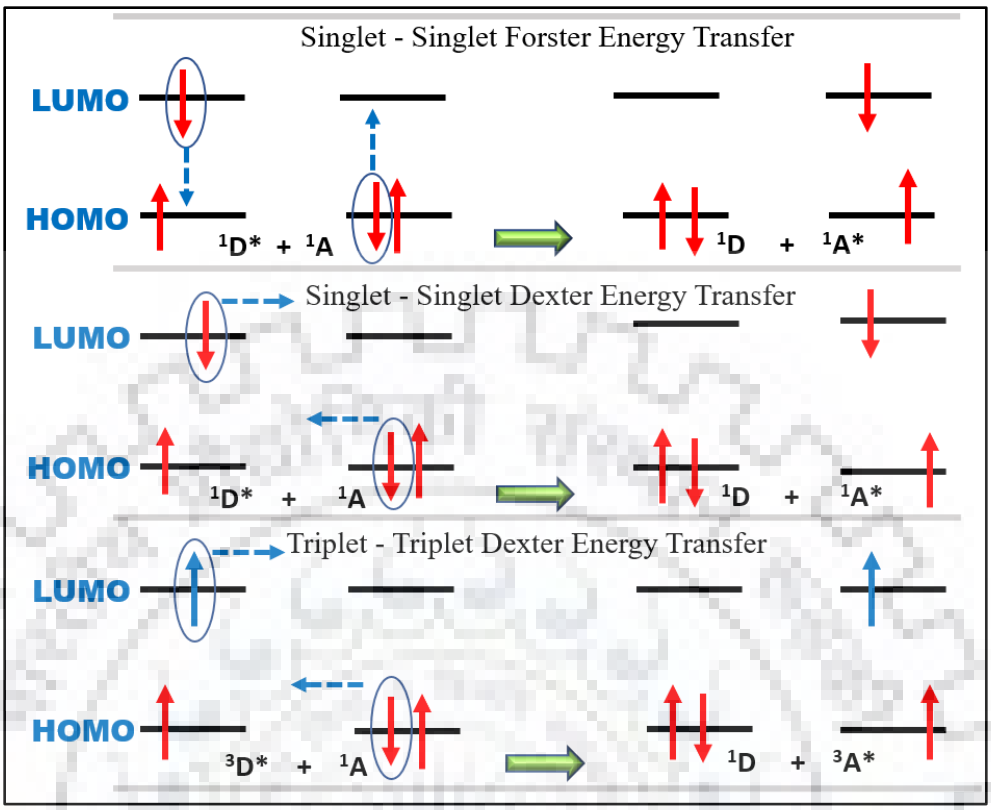


**Figure 1.11.** Energy transfer (Forster & Dexter type).

***(i) Forster energy transfer***

The Forster energy transfer or fluorescence resonance energy transfer is a nonradiative process, in this mechanism the energy transferred between a photoexcited donor (D) fluorophore which is in excited electronic state and an acceptor (A) chromophore molecule present in ground state *via* long range dipole-dipole interactions [122,123]. FRET based processes have two important advantages: one is emission band are well separated with comparable intensities, and second is the large spectral shift from emission to excitation, effects fluorescence detection [124]. This distinct mechanism is not applicable for simple fluorescent molecules because of their small stokes shift and emit fluorescence at different wavelength from excitation wavelength. In this mechanism, the acceptor molecule is present in ground state that absorb the energy from donor unit which is in excited state. Furthermore, this can be described that the energy released in electron relaxation process from LUMO to HOMO of donor unit is used for the excitation of electron in acceptor unit from HOMO to LUMO. Therefore, the overlapping must

appear in absorption and emission spectra. As FRET systems are distance dependent and its efficiency varies with metal ions that control the distance between two fluorophore units [125].

Kong et al. [126] designed and synthesized a naphthalimide rhodamine-based compound (Scheme 1.7). This chemosensor shows FRET based mechanism and OFF-ON type behavior with $Al^{3+}$ ion among other metal ions. This chemosensor represents a stable response with $Al^{3+}$ ion over a vast range of concentration from 5.0 x $10^{-7}$ to 1.0 ×$10^{-5}$ M. it shows a good detection limit as 1.0 × $10^{-7}$ M. it is pH independent in medium condition (pH 6.0 to 8.0). The other competitive studies show that the chemosensor is remarkably specific for $Al^{3+}$ except $Mn^{2+}$ ion in the presence of other metal ions. Further this chemosensor is used in practical application such as visualization of aluminum ion in living cells.

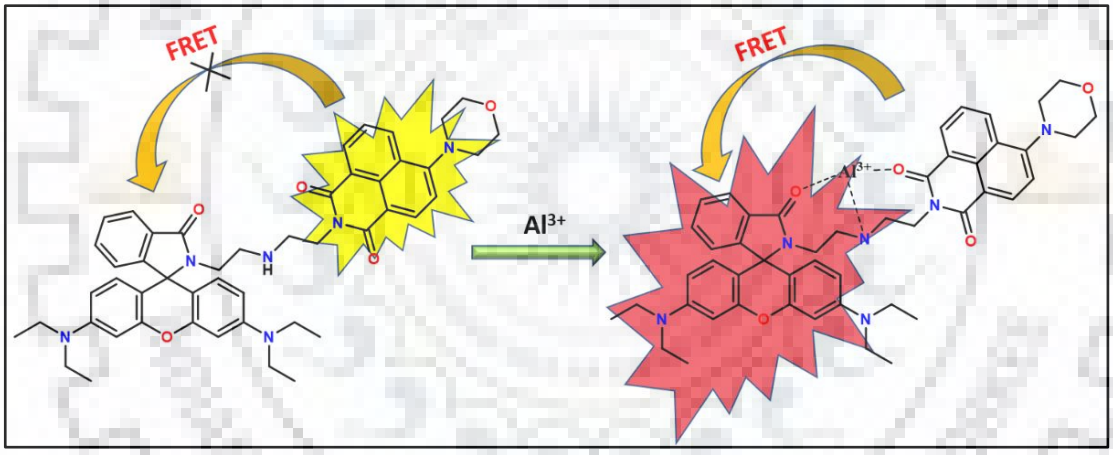


**Scheme 1.7.** FRET based aluminum ion sensor.

A FRET based cyclodextrin appended fluorescent probe has been reported by the co-worker of Wu et al. [127]. This cyclodextrin derived probe is selectively recognize the ferric ion in aqueous medium by the formation of supramolecular β-cyclodextrin complex or dye (Scheme 1.8). In this probe the dansyl moiety acts as donor unit and rhodamine B work as energy acceptor. The best phenomenon of this system is that the enough distance between donor and acceptor unit, that restrict any unwanted interactions (such as, π-π interaction) and settled inside or outside of the CD cavity.

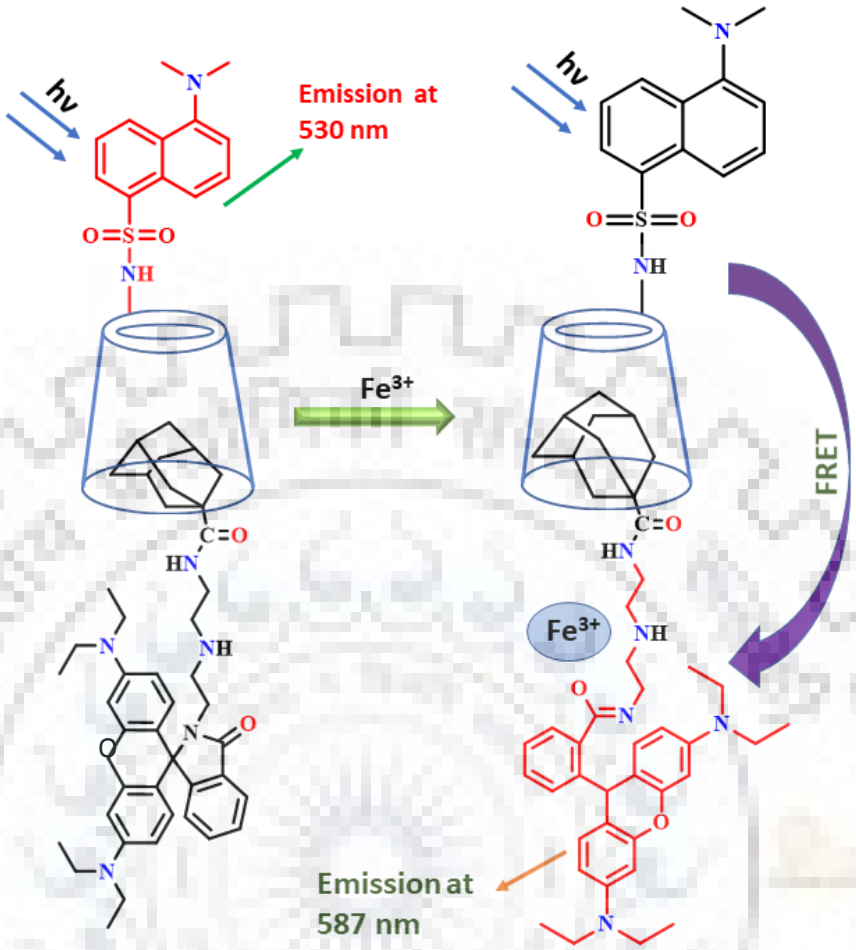


**Scheme 1.8.** Cyclodextrin derived fluorescent sensor with FRET mechanism.

***(ii) Dexter or Electronic Energy Transfer***

For the metal ion recognition, another process of energy transmission for fluorescence quenching is Dexter energy transfer or electron energy transfer [128-130]. This is also a nonradiative process and it can be performed *via* electron transfer, bond energy transfer and collision or exchange energy transfer. Both mechanisms are similar but varied only in distance scale. The needs of this mechanism are the proximity of metal ion or cation to fluorophore and another is direct overlapping of the orbitals. The electron transfer from donor to acceptor in a single molecule occurs within 10 Å distance spam [131-133]. Generally, it appeared where there is a linker between donor and acceptor group. Exchange of electron is relied upon Winger spin conversion rule, *i.e.*

1. Energy transfer in singlet-singlet

$$1D^* + 1A \rightarrow 1D + 1A^*$$

It is understanding that a singlet group is produces another excited singlet group.

2. Energy transfer in triplet-triplet:

$$3D^* + 1A \rightarrow 1D + 3A^*$$

By this, it also understood that a triplet group is produced another excited triplet group.

Singlet-singlet energy transfer involves the Coulombic interactions, whereas, the triplet-triplet energy transfer will free from the participation of Coulombic interactions because it violets the Wigner spin conservation law.

Mondal et al. [134] has been reported a chemosensor that is fluorescein-based Schiff base (FNSB), 1,4-bis(1-fluorescein)-2,3-diaza-1,3-butadiene (Scheme 1.9). This chemosensor shows efficient binding with $Cu^{2+}$ ion in water with 1:1 stoichiometry as copper-ligand complex. The complexation of $Cu^{2+}$ FNSB due to molecular interaction at longer wavelength in UV-vis absorption spectra. It also represents quenching behavior in fluorescent intensity with maxima at 519 nm in tris buffer with physiological pH 7.4. in this complexation followed the Dexter type energy or electron transfer mechanism.

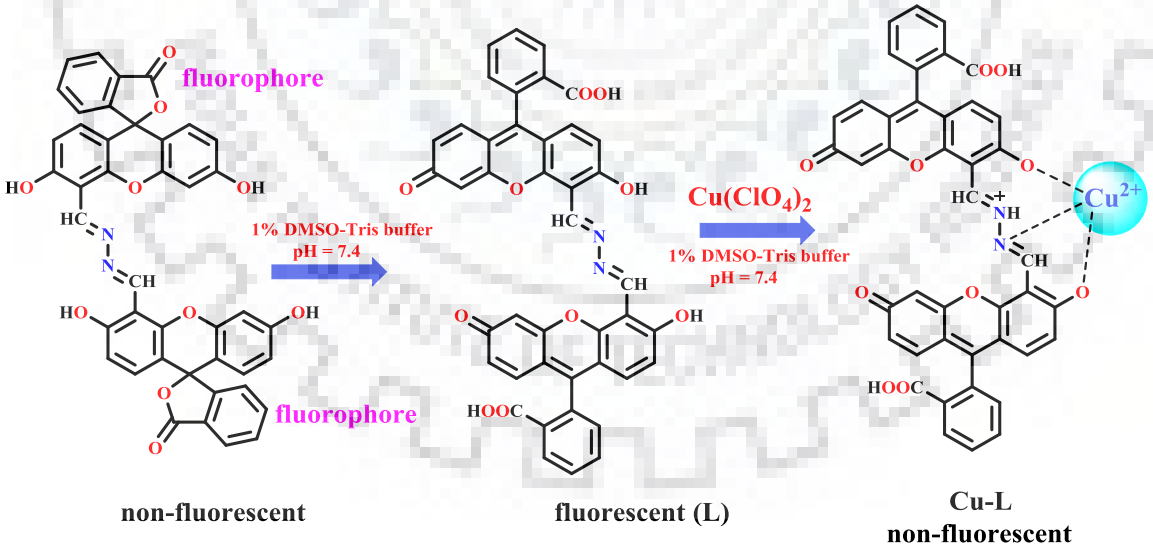


**Scheme 1.9.** $Cu^{2+}$ selective fluorescent probe based on Dexter type energy transfer.

### *1.7.2.2.4.5 Excimer/Exciplex formation*

An excited molecule that have two monomers unit forms by the absorption of electromagnetic radiation and combine or overlap with unexcited species and generate a dimer in the excited state. This dimer is called excimer or exciplex that represents different emission spectrum from initial monomers. The relative difference between the equilibrium shape of the excited to ground state generates a broad, red-shifted emission that indicates the formation of excimer/exciplex [135,136]. The contact between structurally distinct species (e.g. an electron donor and an acceptor), generates an excited state complex called as exciplex (from "excited complex"). The development of excimer/exciplex is a reversible process and both are luminescent chemical entities. When an analyte is present (metal ion or anion), the formation of excimer/exciplex is either strongly strengthen or disturb, that varied the emission spectra of excimer/exciplex. The ratio of fluorescence intensity of excimer and monomer provides a quantitative amount of metal ion present in solution mixture [137]. These types of sensors are called as "ratiometric sensors".

Cho *et al.* [138] have been reported 1,8-naphthalimides based some molecules and describe their aggregation behavior in both extremely polar and nonpolar solvents (Scheme 1.10). The emission of the molecules is induced by the aggregation in the solvent and shifted to longer wavelength. It ascribed the intermolecular excimer or intramolecular exciplex formation.

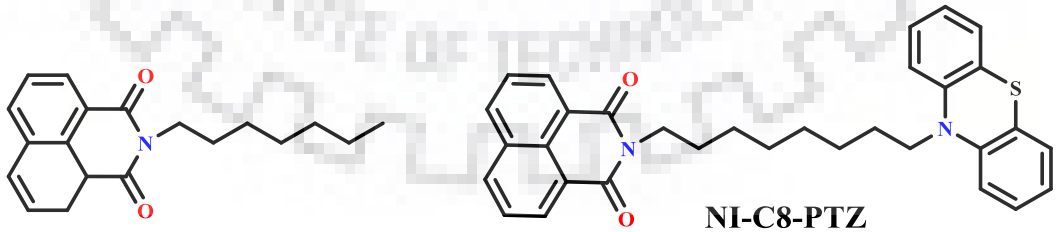


**NI-C7** **NI-C8-PTZ**

**Scheme 1.10.** 1,8-naphthalimide based molecules represented excimer and exciplex formation.

### *1.7.2.2.4.6 CHEF and CHQF mechanism*

Chelation enhancement fluorescence and chelation quenched fluorescence both are familiar mechanism in fluorescence sensors. The changes in fluorescence intensity (enhanced or quenched) may be occurred due to the recognition of metal ion or anions and when it is enhanced or quenched then called as CHEF or CHQF mechanism respectively [139]. In the presence of paramagnetic metal ions, the fluorescence intensity may be quenched in proximity of fluorophore and forbidden intersystem crossing process become faster, this effect is called as paramagnetic effect [140,141]. Chelation of probes affect the molecular system, it increases the rigidity of the molecular system *via* blocked rotation of the fluorophore.

Earlier in 2015, Goswami et al. [142] reported a quinoline based chemosensor (Scheme 1.11), it was directly used in the sensing of $Cd^{2+}$ ion among other biologically important metal ions. The fluorescence intensity was enhanced with $Cd^{2+}$ ion with large spectral shift (38 nm) may be occurred due to chelation enhanced fluorescence (CHEF) and intramolecular charge transfer (ICT) mechanism. In competitive experiment there, no interference occurred by the other metal ions specially $Zn^{2+}$ metal ion. further this probe was used in different applications such as non-cytotoxic effect with live raw cells and cadmium detection with paper strip. The LOD of the $Cd^{2+}$ ion with this probe is $9.9\times10^{-8}$ M level.

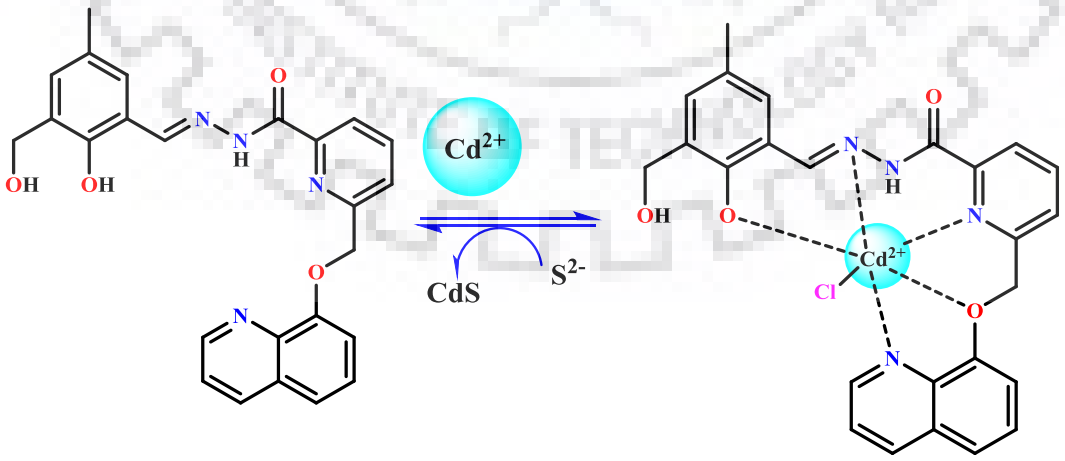


**Scheme 1.11.** $Cd^{2+}$ ion selective CHEF based fluorescent based chemosensor.

### *1.7.2.2.4.7 Excited State Intramolecular proton transfer (ESIPT)*

ESIPT processes have more importance among molecular probes [143], luminescent materials [144-146] and molecular logic gates [147]. Excited state intramolecular proton transfer (ESIPT) mechanism was discovered by Weller in 1956. The molecules which shows ESIPT mechanism possesses both a proton acceptor (carbonyl oxygen or azo nitrogen) and a proton donor (e.g. hydroxyl or amino group), that can form a five-, six- or seven-membered ring *via* intramolecular hydrogen bond [148]. ESIPT processes involves the transfer of hydroxyl proton to the adjacent carbonyl oxygen which have distance between them is less than 2 Å [149]. The photophysical mechanism of ESIPT chromophores using 2-(2-hydroxyphenyl)-benzothiazole (HBT) in the figure 1.12. ESIPT examined as a fast photoinduced proton tautomerization switching methods. At ground state the molecule present in cis enol form which undergo ESIPT *via* intramolecular hydrogen bond equivalent to enol tautomer (E), whereas the keto (K) form is thermodynamically unstable. When the molecule is excited, proton transfer begins in the molecule and forms keto (K*) isomer in the excited state with large stokes shift (up to 10,000 $cm^{-1}$) comparatively energy of absorption. Further, dual emission is obtained by fluorescence for both enol and keto excited states. For cis-keto form, the deactivation channel is intersystem crossing that influence to triplet excited state of the keto tautomer. On the other hand, for trans-keto form the deactivation channel is isomerization. An energy barrier will cross by the molecule for the transformation of the trans-keto to cis-keto form, therefore this process is a slow process. The relatively slow decay of triplet state and trans-keto to cis-keto processes are at similar time scale [150].

Ghosh et al. [151] has been reported a ESIPT based ratiometric fluorescent sensor 1H. This fluorescent sensor is highly selective for aluminum ion among other biologically active metal ions in 90% aqueous system (Scheme 1.12). The photophysical properties of probe as well as selectivity of aluminum ion are explored by using different spectroscopic techniques such as UV-visible, emission spectroscopy, steady state and time resolved study. The selectivity towards aluminum ion increased in water/acetonitrile (9:1) medium with a change in fluorescence color from pale green to dark blue color with six-fold enhancement in the fluorescence intensity. The aluminum complex

$[Al(1H)(OH)]_2^{2+}$ was also analyzed by different techniques which reveals that the ESIPT mechanism is inhibited by the fluorescent sensor 1H after the interaction with aluminum ion.

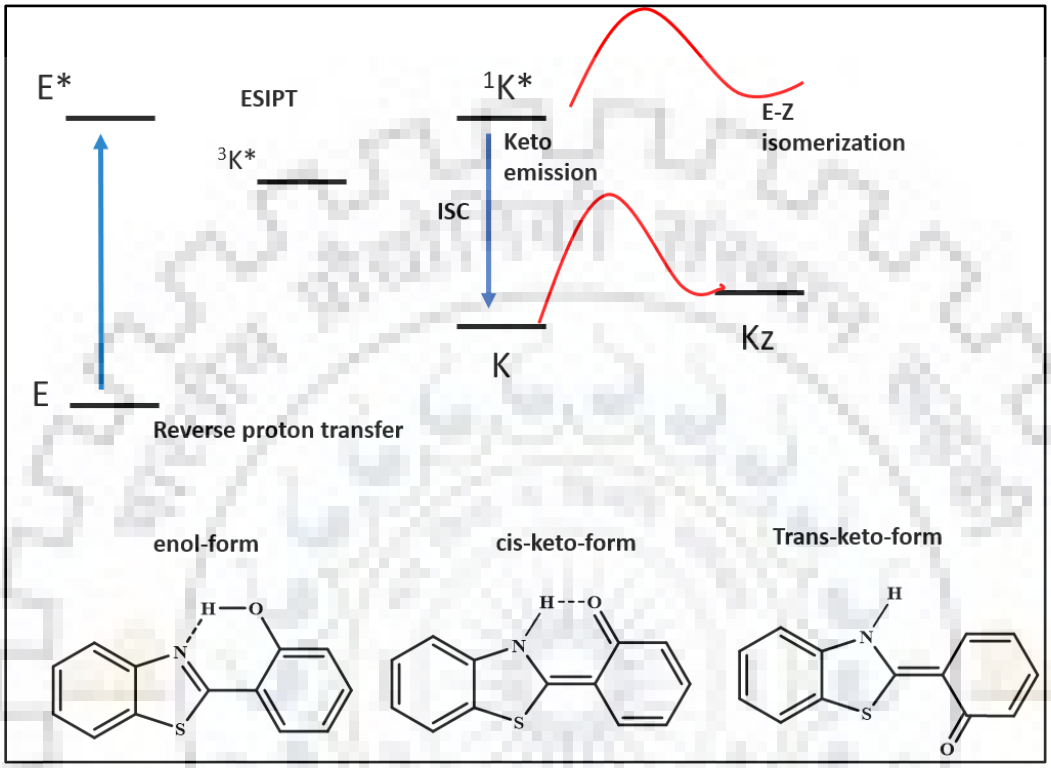


**Figure 1.12.** Mechanism of ESIPT, represented by 2-(2-hydroxyphenyl)-benzothiazole molecule.

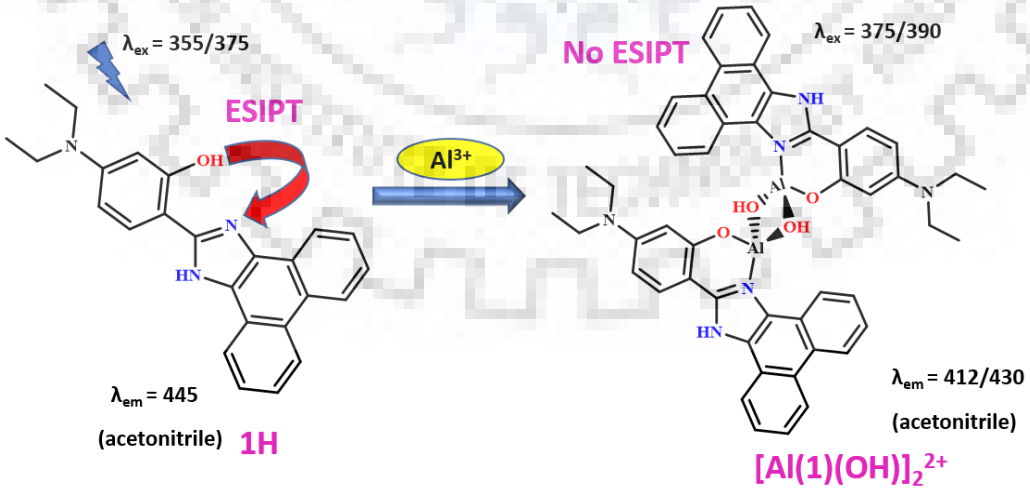


**Scheme 1.12.** The binding of aluminum ion with fluorescent probe 1H.

## References


1. M. Gokelma, A. Birich, S. Stopic, D. Friedrich, A review on alternative gold recovery reagents to cyanide, J. Mat. Sci. Chem. Engg. 4 (2016) 8-17.
2. P. A. Gale, R. Perez-Tomas and R. Quesada, Anion transporters and biological systems, Acc. Chem. Res. 46 (2013) 2801-2813.
3. P.A. Gale, Structural and molecular recognition studies with acyclic anion receptors, Acc. Chem. Res. 39 (2006) 465-475.
4. R. A. Manderville, Synthesis, proton-affinity and anti-cancer properties of the prodigiosin-group natural products, Curr. Med. Chem. 1 (2001) 195-218.
5. J. O. Egekeze and F. W. Oehme, Cyanides and their toxicity: A literature review, Veterinary Quarterly 2 (1980) 104-114.
6. J. Hamel, A review of acute cyanide poisoning with a treatment update, Crit. Care. Nurse 31 (2011) 72-81.
7. Z. Xu, X. Chen, H. N. Kim and J. Yoon, Sensor for the optical detection of cyanide ion, Chem. Soc. Rev. 39 (2010) 127-137.
8. J. Ma and P. K. Dasgupta, Recent development in cyanide detection: A review, Anal. Chim. Acta. 673 (2010) 117-125.
9. R. Kaushik, A. Ghosh, A. Singh, P. Gupta, A. Mittal and D. A. Jose, Selective detection of cyanide in water and biological samples by an off-the-shelf compound, ACS Sens. 1 (2016) 1265-1271.
10. M. Hosseini, M. R. Ganjali, B. Veismohammadi, F. Faridbod, S. D. Abkenar and M. Salavati-Niasari, Slective recognition of acetate ion based on fluorescence enhancement chemosensor, Luminescence 27 (2012) 341-345.
11. A. Singh, S. Tom and D. R. Trivedi, Aminophenol based colorimetric chemosensor for naked eye detection of biologically important fluoride and acetate ions in organo-aqueous medium: effective and simple anion sensor, J. Photochem. Photobiol. A 353 (2018) 407-420.
12. L. L. Zhou, X. H. Zhang and S. K. Wu, Colorimetric detection and differentiation of fluoride and dihydrogenphosphate anions, Sensor and Actuators B: Chemical 106 (2005) 343-346.

13. S.-I. Kondo and R. Takai, Selective detection of dihydrogen phosphate anion by fluorescence change with tetraamide-based receptors bearing isoquinolyl and quinolyl moieties, Org. Lett. 15 (2013) 538-541.
14. P. Norouzi, M. R. Ganjali, F. Faridbod, S. J. Shahtaheri and H. A. Zamani, Electrochemical anion sensor for monohydrogen phosphate based on nano-composite carbon paste, Int. J. Electrochem. Sci. 7 (2012) 2633-2642.
15. Archana, S. K. Sharma and R. C. Sobti, Nitrate removal from ground water: A review, E-J. Chem. 9 (2012) 1667-1675.
16. S. Dey and B. Giri, Fluoride fact on human health and health problems: A review, Medical and Clinical reviews 2 (2016) 1-6.
17. D. Kanduti, P. Sterbenk and B. Artnik, Floride: A review of use and effects on health, Mater. Sociomed. 28 (2016) 133-137.
18. N. Narsimha and V. Sudarshan, Contamination of fluoride in ground water and its effect on human health: A case study in hard rock aquifers of Siddipet, Telangana state, India, Appl. Water Sci. 7 (2017) 2501-2512.
19. M. G. M. G. Penido and U. S. Alon, Phosphate homeostasis and its role in bone health, Pediatr. Nephrol 27 (2012) 2012-2037.
20. K. K. Zadeh, L. Gutekunst, R. Mehrotra, C. P. Kovesdy, R. Bross, C. S. Shinaberger, N. Noori, R. Hirschberg, D. Benner, A. R. Nissenson and J. D. Kopple, Understanding sources of dietary phosphorous in the treatment of patients with chronic Kidney Disease, Clin. J. Am. Soc. Nephrol. 5 (2010) 519-530.
21. M. Laroche and J. F. Boyer, Phosphate diabetes, tubular phosphate reabsorption and phosphatonins, Joint Bone Spine 72 (2005) 376-381.
22. P. B. Tchounwou, C. G. Yedjou, A. K. Patlolla and D. J. Sutton, Heavy metal toxicity and the environment, In: Luch A. (eds) molecular, clinical and environmental toxicology. Experienentia Supplementum, vol 101. Springer, Basel, (2012) 133-164.
23. F. R. Peligro, I. Pavlovic, R. Rojas and C. Barriga, Removal of heavy metals from simulated wastewater by *in situ* formation of layered double hydroxides, Chem. Eng. J. 306 (2016) 1035-1040.

24. S. Gavryushov and P. Linse, Effective interaction potentials for alkali and alkaline earth metal ions in SPC/E water and prediction of mean ion activity coefficient, J. Phys. Chem. B 110 (2006) 10878-10887.
25. J. J. R. F. Da Silva and R. J. P. Williams. The biological chemistry of the elements: the inorganic chemistry of life. Oxford University Press (2001).
26. A. J. Wright, S. E. Mathews, W. B. Fischer and P. D. Beer, Novel resorcin[4] arenes as potassium-selective ion-channel and transporter mimics, Chem. Eur. J. 7 (2001) 3474-3481.
27. D. A. Doyle, J. M. Cabral, R. A. Pfuetzrer, A. Kuo, J. M. Golbis, S. L. Cohen, B. T. Chait and R. Mackinnon, The structure of the potassium channel: Molecular basis of $K^+$ conduction and selectivity, Science 280 (1998) 69-77.
28. P. R. A. Webber, A. Coeley, M. G. B. Drew and P. D. Beer, Potassium selective calix[4] semi tubes, Chem. Eur. J. 9 (2003) 2439-2446.
29. S. Bhattacharya and M. Dixit, Metallic radionuclides in the development of diagnostic and therapeutic radiopharmaceuticals, Dalton Trans. 40 (2011) 6112-6128.
30. H. Luo, S. Dai and P. V. Bonnensen, Solvent extraction of $Sr^{2+}$ and $Cs^+$ based on room-temperature ionic liquids containing monoaza-substituted crown ethers, Anal. Chem. 76 (20044) 2773-2779.
31. W. Jahnen-Dechent and M. Ketteler, Magnesium basics, Clin. Kidney J. 5 (2014) i3-i14.
32. S. Long and A. M. P. Romani, Role of cellular magnesium in human diseases, Astin J. Nutr. Food Sci. 2 (2014) 1051-1070.
33. C. B. Black, H.-W. Huang and J. A. Cowan, Biological co-ordination chemistry of magnesium, sodium and potassium ions protein and nucleotide binding sites, Coord. Chem. Rev. 135 (1994) 165-202.
34. R. J. P. Williams, Role of transition metal ions in biological processes, R. Int. Chem. Rev. 1 (1968) 13-38.
35. P. Faller, C. Hureau and O. Berthoumieu, Role of metal ions in the self-assembly of the Alzheimer's amyloid – β peptides, Inorg. Chem. 52 (2013) 12193-12206.

36. C. L. Dupont, G. Grass and C. Rensing, Copper toxicity and the origin of bacterial resistance-new insights and applications, Metallomics 3 (2011) 1109-1118.
37. N. C. Lloyd, H. W. Morgan, B. K. Nicholson and R. S. Ronimus, The composition of Ehrlich's Salvarsan: Resolution of a century -old debate, Angew. Chem. Int. Ed. 44 (2005) 941-944.
38. R. C. Gupta, Handbook of toxicology of chemical warfare agents, Elsevier. Inc. (2009) doi.org/10.1016/B978-0-12-374484-5.X0001-6.
39. World Health Organization's Arsenic Fact Sheet, (2016) available online: http://www.who.int/mediacentre/factsheet/fs372/en/
40. J.-Y. Chung, S.-D. Yu and Y.-S. Hong, Environmental source of arsenic exposure, J. Prev. Med. Public health 47 (2014) 253-251.
41. C.-H. Tseng, A review on environmental factors regulating arsenic methylation in humans, Toxicology and Applied Pharmacology 235 (2009) 338-350.
42. T. Chavez-Capilla, M. Beshai, W. Maher, T. Kelly and S. Poster, Bioaccessibility and degradation of naturally occurring arsenic species from food in the human gastrointestinal tract, Food Chemistry 212 (2016) 189-197.
43. M. N. Rana, J. Tangpong and M. M. Rehman, Toxicodynamics of lead, cadmium, mercury and arsenic-induced kidney toxicity and treatment strategy: A mini review, Toxicology Reports 5 (2018) 704-713.
44. M. E. Hillburn, Environmental lead perspective, Chem. Rev. 8 (1979) 63-84.
45. P. F. Schuster, D. P. Krabbenhaft, D. L. Naftz, L. D. Cecil, M. L. Olson, J. F. Dewild, D. D. Susong, J. R. Green and M. L. Abbott, Atmospheric mercury deposition during the last 270 years: A Glacial ice core record of natural and anthropogenic sources, Environ. Sci. Technol. 36 (2002) 2303-2310.
46. R. A. Bernhoft, Mercury toxicity and treatment: A review of the literature, J. Environ. Public Health (2012) 460508, 1-10.
47. K. B. Jacobson and J. E. Turner, The interaction of cadmium and certain other metal ions with proteins and nuelic acids, Toxicology 16 (1980) 1-37.
48. A. W. Czarnik, Fluorescent chemosensors for ion and molecule recognition, American Chemical Society, Washington DC, (1993).

49. N. H. Bings, A. Bogaerts and J. A. C. Broekaert, Atomic Spectroscopy: A review, Anal. Chem. 82 (2010) 4653-4681.
50. D. Beauchemin, Inductively coupled plasma spectrometry, Anal. Chem. 82 (2010) 4786-4810.
51. V. A. Fassel and R. N. Kniseley, Inductively coupled plasma-optical emission spectroscopy, Anal. Chem. 46 (1974) 1110 A-1120 A.
52. T. E. Edmonds, (eds.), Chemical sensors, Blackie and sons Ltd., London, (1988).
53. J. J. Rebek, Introduction to the molecular recognition and self-assembly special feature, Proc. Natl. Acad. Sci. U.S.A. 106 (2009) 10423-10424.
54. P. Yin, J. Zhang, T. Li, X. Zuo, J. Huo, A. M. warner, S. Chattopadhyay, T. shibata, Y. wei and T. Liu, Self-recognition of structurally identical, rod shaped macroions with different central metal atoms during their assembly process, J. Am. Chem. Soc. 135 (2013) 4529-4536.
55. S. K. Kim, G. I. Vargas-Zuniga, B. P. Hay, N. J. Young, L. H. Delmau, C. Masselin, B. A. Moyer and J. L. Sessier, Controlling cesium cation recognition *via* cation metathesis within an ion pair receptor, J. Am. Chem. Soc. 134 (2012) 1782-1792.
56. T. Terashima, M. Kawabe, Y. Miyabara, H. Yoda and M. Sawamoto, Polymeric pseudo-crown ether for cation recognition *via* cation template-assisted cyclopolymerization, Nat. Commun. 4 (2013) 2321.
57. A. S. Moomaw and M. E. Maguir, Cation selectivity by the CorA $Mg^{2+}$ channel requires a fully hydrated cation, Biochemistry 49 (2010) 5998-6008.
58. G. G.Talanova, H.-S. Hwang, V. S. Talanov and R. A. Bartsch, Chromogenic lariat ethers for selective alkali metal cation recognition, Anal. Chem. 73 (2001) 5260-5265.
59. N. Wanichacheva, E. R. Soto, C. R. Lambert and W. G. McGimpsey, Surface-based lithium ion sensor: An electrode derivatized with a self-assembled monolayer, Anal. Chem. 78 (2006) 7132-7137.
60. L. Lochman, J. Svec, J. Roh, K. Kirakci, K. Lang, P. Zimcik and V. Novakova, Metal-cation recognition in water by a tetrapyrazinoporphyrazine-based tweezer receptor, Chem. Eur. J. 22 (2016) 2417-2416.

61. S. K. Kim, S. H. Lee, J. Y. Lee. R. A. Bartsch and J. S. Kim, An excimer-based binuclear, on-off switchable calix[4] crown chemosensor, J. Am. Chem. Soc. 126 (2004) 16499-16506.
62. V. Mahendran and J. Philip, Sensing of biologically important cations such as $Na^{+}$, $K^{+}$, $Ca^{2+}$, $Cu^{2+}$ and $Fe^{3+}$ using magnetic nano-emulsions, Langmuir 29 (2013) 4252-4258.
63. J.-C. G. Bunzli, Lanthanide luminescence for biomedical analyses and imaging, Chem. Rev. 110 (2010) 2729-2755.
64. J.-C. G. Bunzli, Benefiting from the unique properties of lanthanide ions, Acc. Chem. Res. 39 (2006) 53-61.
65. I. Shtepliuk, N. M. Caffrey, T. Lakimov, V. Khranovskyy, I. A. Abrikosov and R. Yakimova, On the interaction of toxic heavy metals (Cd, Hg, Pb) with graphene quantum dots and infinite graphene, Sci. Rep. 7 (2017) 3934.
66. S. M. Pyle, J. M. Nocerino, S. N. Deming, J. A. Palasota, J. M. Palasota, E. L. Miller, D. C. Hillman, C. A. Kuharic, W. H. Cole, P. M. Fitzpatrick, M. A. Watson and K. D. Nichols, Comparison of AAS, ICP-AES, PSA, and XRF in determining lead and cadmium in soil, Environ. Sci. Technol. 30 (1995) 204-213.
67. S. Y. Lee, K. H. Bok and C. Kim, A fluorescence "turn-on" chemosensor for $Hg^{2+}$ and $Ag^{+}$ based on NBD (7-nitrobenzo-2-oxa-1,3-diazolyl), RSC Adv. 7 (2017) 290-299.
68. C. Erk, Cation recognition with fluorophore crown ethers, Ind. Eng. Chem. Res. 39 (2000) 3582-3588.
69. R. Shunungam, G. J. Gabriel, C. E. Smith, A. K. Aamer and G. N. Tew, A highly selective colorimetric aqueous sensor for mercury, Chem. Eur. J. 14 (2008) 3904-3907.
70. L. D. Chebrolu, S. Thurakkal, H. S. Balaraman and R. Danaboyina, Selective and dual naked eye detection of $Cu^{2+}$ and $Hg^{2+}$ ions using a simple quinoline-carbaldehyde chemosensor, Sens. Actuat. B: Chem. 204 (2014) 480-488.
71. S. A. Lee, G. R. You, Y. W. Choi, H. Y. Jo, A. R. Kim, I. S. J. Kim, Y. M. Kim and C. Kim, A new multifunctional Schiff base as a fluorescence sensor for $Al^{3+}$ and a

colorimetric sensor for $CN^-$ in aqueous media: an application to bioimaging, Dalton Trans. 43 (2014) 6650-6659.

72. E. Bianchi, K. Bowmann-James and E. Gracia-Espannia (Eds.), Supramolecular chemistry of anions, Wiley-VCH, New York (1997).
73. T. Gunnlaugsson, M. Glynn, G. M. Tocci, P.E. Kruger and F. M. Pfeffer, Anion recognition and sensing in organic and aqueous media using luminescent and colorimetric sensors, Coord. Chem. Rev. 250 (2006) 3094-3117.
74. K. Bowan-James, Alfred werner revisited: The co-ordination chemistry of anions, Acc. Chem. Res. 38 (2005) 671-678.
75. C. Suksai and T. Tuntulani, Chromogenic anion sensors, Chem. Soc. Rev. 32 (2003) 192-202.
76. S. Kubik, Anion recognition in water, Chem. Soc. Rev. 39 (2010) 3648-3663.
77. A. Okudan, S. Erdemir and O. Kocyigit, Naked eye detection of fluoride and acetate anions by using simple & efficient urea and thiourea based colorimetric sensor, J. Mol. Strut. 1048 (2013) 392-398.
78. M. Boiocchi, L. D. Boca, D. E. Gomez, L. Fabbrizzi, M. Licchelli and E. Monzani, Nature of urea-fluoride interaction: Incipient and definitive proton transfer, J. Am. Chem. Soc. 126 (2004) 16507-16514.
79. Y. Sun, Y. Liu, M. Chen and W. Guo, A novel fluorescent and chromogenic probe for cyanide detection in water based on the nucleophilic addition of cyanide to imine group, Talanta 80 (2009) 996-1000.
80. C.-L. Chen, Y.-H. Chen, C.-Y. Chen and S.-S. Sun, Dipyrrole carboxamide derived selective ratiometric probes for cyanide ion, Org. Lett. 8 (2006) 5053-5056.
81. R. M. Duke, J. K. O'Brien, T. McCabe and T. Gunnlaugsson, Colorimetric sensing of anions in aqueous solution using a charge neutral, cleft-like, amidothiourea receptor; tilting the balance between hydrogen bonding and deprotonation in anion recognition, Org. Biomol. Chem. 6 (2008) 4089-4092.
82. Y. Jia and J. Li, Molecular assembly of Schiff base interactions: Construction and application, Chem. Rev. 115 (2015) 1597-1621.

83. L. N. Neupane, J.-Y. Park, J. H. Park and K.-H. Lee, Turn-on fluorescent chemosensor based amino acid for Pb(II) and Hg(II) ions in aqueous solutions and role of tryptophan for sensing, Org. Lett. 15 (2013) 254-257.
84. Y. Zhou and J. Yoon, Recent progress in fluorescent and colorimetric chemosensors for detection of amino acids, Chem. Soc. Rev. 41 (2012) 52-67.
85. A. P. F. Turner, I. Karube and G. S. Wilson (eds.), Biosensors. Fundamentals and applications, Oxford University Press, New York (1987).
86. P. Xie, Q. H. Xiong, Y. Fang, Q. Qing and C. M. Lieber, Local electrical potential detection of DNA by nanowire-nanopore sensors, Nat. Nanotechnol. 7 (2012) 119-125.
87. A. Hulanicri, S. Glab and F. Ingman, Chemical sensors definition and classification, Pure Appl. Chem. 63 (1991) 1247-1250.
88. T. W. Bell and N. M. Hext, Supramolecular optical chemosensors for organic analytes, Chem. Soc. Rev. 33 (2004) 589-598.
89. S. Joo and R. B. Brown, Chemical sensors with integrated electronics, Chem. Rev. 108 (2008) 638-651.
90. V. K. Gupta, A. K. Singh and N. Mergu, A new beryllium ion-selective membrane electrode based on dibenzo(perhydrotriazino)aza-14-crown-4 ether, Anal. Chem. Acta 79 (2012) 44-50.
91. U. Yogeswaran and S.-M. Chen, A review on the electrochemical sensors and biosensors composed of nanowires as sensing material, Sensors 8 (2008) 290-313.
92. E. Bakker and E. Pretsch, Potentiometric sensors for trace-level analysis, Trends Analyst Chem. 4 (2004) 589-598.
93. J. B. Raoof, R. Ojani and M. Kolbadinezhad, Voltammetric sensor for gluthaione determination based on ferrocene- modified carbon paste electrode, J. Solid State Electrochem. 13 (2009) 1411-1416.
94. C. McDonagh, C. S. Burke and B. D. MacCraith, Optical chemical sensors, Chem. Rev. 108 (2008) 400-422.
95. S. M. Borisov and O. S. Wolfbeis, Optical Biosensors, Chem. Rev. 108 (2008) 423-461.

96. K. N. Shinde, S. J. Dhoble, H. C. Swart and K. Park, Basic mechanism of photoluminescence, phosphate phosphors for solid-state lighting, Springer Berlin Heidelberg (2012) 41-59.
97. M. Adachi and Y. Nagao, Design of near infrared dyes based on π-conjugation system extension 2, theoretical elucidation of framework extended derivatives of perylene chromophore, Chem. Mater. 13 (2001) 662-669.
98. D. F. Swinehart, The Beer Lambert Law, J. Chem. Educ. 39 (1962) 333-335.
99. B. Wardle, Principle and applications of photochemistry, Jhon Wiley & Sons, Chichester (2009).
100. M. Derksen and S. Grimme, An efficient approach for the calculation of Franck-Condon integrals of large molecules, J. Chem. Phys. 122 (2005) 244101-1-244101-9.
101. F. Santoro, R. Improta, A. Lami, J. Bloino and V. Barone, Effective method to compute Franck-Condon integrals for optical spectra of large molecules in solution, J. Chem. Phys. 126 (2007) 84509.
102. M. Kasha, Characterization of electronic transitions in complex molecules, Discuss. Faraday Soc. 9 (1950) 14-19.
103. M. Montalti, A. Credi, L. Prodi and M. T. Gandolfi, Handbook of photochemistry, 3rd Edition, Taylor & Francis (2006).
104. I. Berlman, Handbook of fluorescence spectra of aromatic molecules. Elsevier (2012).
105. K. P. Carter, A. M. Young and A. E. Palmer, Fluorescent sensors for measuring metal ions in living systems, Chem. Rev. 114 (2014) 4564-4601.
106. X. Zhang, J. Yin and J. Yoon, Recent advancement in development of chiral fluorescent and colorimetric sensors, Chem. Rev. 114 (2014) 4918- 4959.
107. A. P. de Silva, T. S. Moody and G. D. Wright, Fluorescent PET (Photoinduced electron transfer) sensors as potent analytical tools, Analyst 134 (2009) 2385-2393.
108. M. Natali, S. Campagna and F. Scandola, Photoinduced electron transfer across molecular bridges: electron- and hole-transfer super exchange pathways, Chem. Soc. Rev. 43 (2014) 4005-4018.

109. B. Daly, J. Ling and A. P. de Silva, Current developments in fluorescent PET (photoinduced electron transfer) sensors and switches, Chem. Soc. Rev. 44 (2015) 4203-4211.
110. S. Fukuzumi, T. Honda and T. Kojima, Structures and photoinduced electron transfer of protonated complexes of porphyrins and metallophthalocyanines, Coor. Chem. Rev. 256 (2012) 2488-2502.
111. X. Zhou, P. Li, Z. Shi, X. Tang, C. Chen and W. Liu, A highly selective fluorescent sensor for distinguishing cadmium from zinc ions based on a quinoline platform, Inorg. Chem. 51 (2012) 9226-9231.
112. L. N. Neupane, J. Y. Park, J. H. Park and K. H. Lee, Turn–on fluorescent chemosensor based on an amino acid for Pb(II) and Hg(II) Ions in aqueous Solutions and role of tryptophan for sensing, Org. Lett. 15 (2013) 254–257.
113. S. Banerjee, P. Brandao and A. Saha, A robust fluorescent chemosensor for aluminum ion detection based on a Schiff base ligand with an azo arm and application in a molecular logic gate, RSC Adv. 6 (2016) 101924-101936.
114. S. K. Kim, N. J. Singh, S. J. Kim, H. G. Kim, J. K. Kim, J. W. Lee, K. S. Kim and J. Yoon, New fluorescent photoinduced electron transfer chemosensor for the recognition of $H_2PO_4^-$, Org. Lett. 5 (2003) 2083-2086.
115. R. Misra and S. P. Bhattacharya, Intramolecular charge transfer: theory and applications, Published by Wiley-VCH Verlag GmbH & Co. KGaA (2018).
116. A. Prasanna de Silva, H. Q. N. Gunaratne, T. Gunnlaugsson, A. J. M. Huxley, C. P. McCoy, J. T. Rademacher and T. E. Rice, Signaling recognition events with fluorescent sensors and switches, Chem. Rev. 97 (1997) 1515-1566.
117. V. Tharmaraj, S. Devi and K. Pitchumani, An intramolecular charge transfer (ICT) based chemosensor for silver ion using 4-methoxy-N-((thiophen-2-yl)methyl)benzenamine, Analyst 137 (2012) 5320-5324.
118. R. Ali, S. S. Razi, M. Sahid, P. Srivastava and A. Misra, Off-On-Off fluorescence behavior of an intramolecular charge transfer probe towards anions and $CO_2$, Spectrochimica Acta. Part A, Molecular and Bimolecular Spectroscopy 168 (2016) 21-28.

119. J. Zhang, Y. Fu and J. R. Lakowicz, Enhanced Förster resonance energy transfer (FRET) on single metal particle, J. Phy. Chem. C Nanometer Interfaces, 111 (2007) 50-56.
120. A. Sharma and S. G. Schulman, Introduction of Fluorescence spectroscopy, John Wiley & Sons, Chichester (1999).
121. T. Förster, 10th spiers memorial lecture, Transfer mechanism of electronic excitation, Discuss. Faraday Soc. 27 (1959) 7-17.
122. H. J. Carlson and R. E. Campbell, Genetically encoded FRET-based biosensors for multiparameter fluorescence imaging, Curr. Opin. Biotechnol. 20 (2009) 19-27.
123. J. M. Serin, D. W. Brousmiche and J. M. J. Frechet, A FRET-Based ultraviolet to near-infrared frequency converter, J. Am. Chem. Soc. 124 (2002) 11848-11849.
124. L. Yuan, W. Lin, K. Zheng and S. Zhu, FRET based small molecule fluorescent probes: Rational design and bioimaging applications, Acc. Chem. Res. 46 (2013) 1462-1473.
125. K. E. Sapsford, L. Berti and I. L. Medintz, Materials for fluorescence resonance energy transfer analysis: Beyond traditional donor-acceptor combinations, Angew. Chem. Int. Ed. 45 (2006) 4562-4589.
126. C.-Y. Li, Y. Zhou, Y.-F. Li, C.-X. Zou and X.-F. Kong, Efficient FRET based colorimetric and ratiometric fluorescent chemosensor for $Al^{3+}$ in living cells, Sensor and Actuators B Chemical, 186 (2013) 360-366.
127. M. Xu, S. Wu, F. Zeng and C. Yu, Cyclodextrin supramolecular complex as a water soluble ratiometric sensor for ferric ion sensing, Langmuir 26 (2010) 4529-4534.
128. D. L. Dexter, A theory of sensitized luminescence in solids, J. Chem. Phys. 21 (1953) 836-850.
129. C. B. Murphy, Y. Zhang, T. Troxier, V. Ferry, J. J. Martin and W. E. Jones, Probing Förster and Dexter energy-transfer mechanism in fluorescent conjugated polymer chemosensors, J. phy. Chem. B 108 (2004) 1537-1543.
130. N. Kumar, V. Bhalla and M. Kumar, Resonance energy transfer–based fluorescent probes for $Hg^{2+}$, $Cu^{2+}$ and $Fe^{2+}$/$Fe^{3+}$ ions, Analyst 139 (2014) 543–558.
131. Y. J. Gong, X. B. Zhang, A. L. Luo, T. Fu, W. Tan, G. L. Shen and R. Q. Yu, Through bond energy transfer: A convenient and universal strategy toward efficient

ratiometric fluorescent probe for bioimaging applications, Anal. Chem. 84 (2012) 10777-10784.

132. X. Zhang, Y. Xiao, L. He and Y. Zhang, Through-bond energy transfer cassettes for multicolor encoding, J. Org. Chem. 79 (2014) 6315-6320.
133. S. Adhikari, A. Ghosh, S. Guria and A. Sahana, A through bond energy transfer based ratiometric probe for fluorescent imaging of $Sn^{2+}$ ions in living cells, RSC Adv. 6 (2016) 39657-39662.
134. R. V. Rathod, S. Bera, M. Singh and D. Mondal, A colorimetric and fluorometric investigation of Cu(II) ion in aqueous medium with a fluorescein-based chemosensor, RSC Adv. 6 (2016) 34608-34615.
135. W. T. Yip and D. H. Levy, Excimer/Exciplex formation in Vander Waals dimer of aromatic molecules, J. Phy. Chem. 100 (1996) 11539-11545.
136. J. Vollbrecht, Excimers in organic electronics, New J. Chem. 42 (2018) 11249-11254.
137. J. Hoche, H.-C. Schmitt, A. Humeniuk, Z. Fisher, R. Mitric and M. I. S. Röhr, The mechanism of excimer formation: An experimental and theoretical study on the pyrene dimer, Phys. Chem. Chem. Phys. 19 (2017) 25002-25015.
138. D. W. Chao and D. W. Cho, Excimer and exciplex emissions of 1,8-naphthalimides caused by aggregation in extremely polar or nonpolar solvents, New J. Chem. 38 (2014) 2233-2236.
139. A. T. Afaneh and G. Schreckenbach, Fluorescence enhancement/quenching based on metal orbital control: Computational studies of a 6-thienyllumazine-based mercury sensor, J. Phys. Chem. A 119 (2015) 8106-8116.
140. J. H. Chang, Y. M. Choi and Y. K. Shin, A significant fluorescence quenching of anthrylaminobenzocrown ethers by paramagnetic metal cations, Bull. Korean Chem. Soc. 22 (2001) 527-530.
141. Y. Dong, R. Fan, W. Chen, P. Wang and Y. Yang, A simple quinolone Schiff-base containing CHEF based fluorescence 'turn-on' chemosensor for distinguishing $Zn^{2+}$ and $Hg^{2+}$ with high sensitivity, selectivity and reversibility, Dalton Trans. 46 (2017) 6769-6775.

142. S. Goswami, K. Aich, S. Das, C. D. Mukhopadhyay, D. Sarkar and T. K. Mondal, A new visible-light-excitable ICT-CHEF-mediated fluorescence 'turn-on' probe for the selective detection of $Cd^{2+}$ in a mixed aqueous system with live-cell imaging, Dalton Trans. 44 (2015) 5763-5770.
143. J. Wu, W. Liu, J. Ge, H. Zhang and P. Wang, New sensing mechanisms for design of fluorescent chemosensors emerging in recent years, Chem. Soc. Rev. 40 (2011) 3483-3495.
144. S. Park, J. E. Kwon, S. H. Kim, J. Seo, K. Chung, S. Y. Park, D. J. Jang, B. M. Medina, J. Gierschner and S. Y. Park, A white-light-emitting molecule: Frustrated energy transfer between constituent emitting centers, J. Am. Chem. Soc. 131 (2009) 14043-14049.
145. K. C. Tang, M. J. Change, T. Y. Lin, H. A. Pan, T. C. Fang, K. Y. Chen, W.Y. Hung, Y. H. Hsu and P. T. Chou, Fine tuning the erengetics of excited-state intramolecular proton transfer (ESIPT): White light generation in A single ESIPT system, J. Am. Chem. Soc. 133 (2011) 17738-17745.
146. C. C. Hsieh, C. M. Jiang and P. T. Chou, Recent experimental advances on excited-state intramolecular proton coupled electron transfer reaction, Acc. Chem. Res. 43 (2010) 1364-1374.
147. V. Luxami and S. Kumar, Molecular half-subtractor based on 3,3'–bis(1H-benzimidazolyl-2-yl)[1,10]-binaphthalenyl-2,2'-diol, New J. Chem. 32 (2008) 2074-2079.
148. H. Yuan, S. Feng, K. Wen, X. Guo and J. Zhange, The excited-state intramolecular proton transfer in N-H-type dye molecules with a seven-membered-ring intramolecular hydrogen bond-A theoretical insight, Spectrochim. Acta A 191 (2018) 421-426.
149. M. M. Henary and C. J. Fahrni, Excited state intramolecular proton transfer and metal ion complexation of 2-(2-hydroxyphenyl)benzazoles in aqueous solution, J. Phy. Chem. A 106 (2002) 5210-5220.
150. J. Zhao, S. Ji, Y. Chen, H. Guo and P. Yang, Excited state intramolecular proton transfer (ESIPT): From principal photophysics to the development of new

chromophores and applications in fluorescent molecular probes and luminescent materials, Phys. Chem. Chem. Phys. 14 (2012) 8803-8817.

151. S. Sinha, B. Chowdhury and P. Ghosh, A highly sensitive ESIPT-based ratiometric fluorescence sensor for selective detection of $Al^{3+}$, Inorg. Chem. 55 (2016) 9212-9220.

# CHAPTER 2

## "THIOSEMICARBAZIDE BASED CHEMOSENSOR FOR CYANIDE AND ARSENITE IONS"

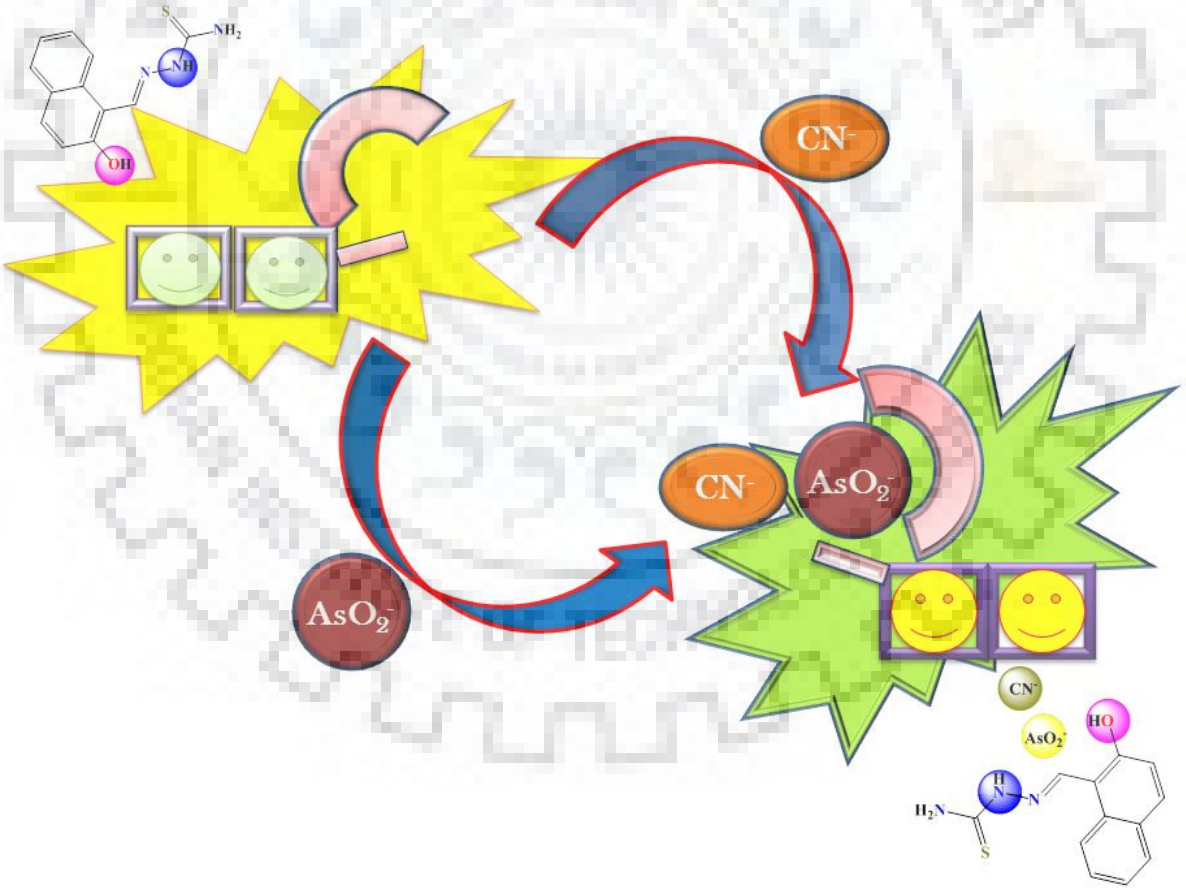

# CHAPTER 2

## 2.1 INTRODUCTION

Anions demonstrate their necessity in a broad range of chemical and biological processes. Various efforts have been devoted to generate numerous receptors for anionic species since two decades [1]. Among all the anions, it is well-known that arsenic (in the form of anions) and cyanide ion are extremely toxic and lethal for living organisms. Arsenic is the 20$^{th}$ most abundant element in the earth's crust. It mainly exists in the four oxidation states, As(V), As(III), As(0) and As(-3), in the environment [2]. Inorganic arsenic, *viz.* arsenite, As(III) and arsenate As(V) is more toxic than organic arsenic, *viz.* monomethylarsonic acid and dimethylarsonic acid [3]. Arsenite [As(III)] is more toxic than arsenate [As(V)] due to its binding with the sulfhydryl unit of proteins, which can intervene with the reactions of other enzymes and proteins [4]. The binding of trivalent arsenic with specific proteins can convert the conformation and functionality of the protein as well as hamper their reaction with other proteins. As(V) can also interrupt the conversion of ATP to ADP *via* the permanent replacement of phosphate groups due to its resemblance to phosphite ions [5]. The main source of arsenic exposure in the environment is from ground water or drinking water [6,7]. The chronic toxicity of arsenic has adverse effect on human health such as skin cancer, skin lesions, neurotoxicity, cardiovascular diseases and diabetes [8]. Similarly, cyanide anions are also detrimental to biological systems and environment. It's acute poisoning can damage the body's central respiratory system because it can easily bind with heme-proteins to block cytochrome c oxidase, which hindered the electron transfer chain in the mitochondria [9]. It is released in the environment by ammonia manufacturing, electroplating, steel production and extraction of gold [10]. Inhalation of toxic cyanide can occur from absorption by the lungs and exposure *via* the skin, polluted drinking water and contaminated food [11]. As per as the guidelines of the World Health Organization (WHO) and U.S. Environment Protection Agency (USEPA), the permissible limits of arsenic and cyanide in drinking water is 0.01 ppm or 10 ppb and 0.2 ppm, respectively [12]. There have been many methods developed for the detection of arsenite and cyanide ions. Electrochemical analysis and ion chromatography are the traditional methods, which require time consuming procedures and the use of sophisticated instrumental techniques [13], whereas chemical sensors are another approach, which are simple, affordable and expeditious in

real time monitoring. The sensing process frequently uses absorption and emission spectroscopy, which precisely monitor and sometimes detect using naked eye [14]. Chemical sensors for arsenite anion are rarely available with fluorescence intensity enhancement. The cyanide ion analyzed by their Lewis basicity, nucleophilicity [15] and quality of making hydrogen bonds in a solution [16]. There are so numerous mechanisms, including internal charge transfer [17], single electron transfer [18], fluorescence resonance energy transfer [19] and plated electrode [20-22], which support the fluorescence behavior for anions.

In this chapter, a single probe was developed that can sense both arsenite and cyanide ions. The sensing mechanism involves the probe having two acidic protons, which results in deprotonation *via* interaction of both anions as well as hydrogen bonding as revealed by NMR spectroscopy and detailed theoretical studies. To date, no reports are available based on the direct detection of both the toxic arsenite and cyanide anions together using a single chemical sensor with high limit of detection in the range of μM to nM. Most of the previous reports on chemical sensor that detect multiple anions using the same probe molecule only detect common anions. The present protocol detects those anions, which attract more interest from researchers due to their high toxicity and adverse effect *i.e.* $AsO_2^-$ and $CN^-$ with the same platform. The as-synthesized probe is a potential candidate to sense multiple anions whilst maintaining a high limit of detection using the same platform. Sensing using this probe is cost effective in terms of the reagents used for its synthesis as well as reduce number of steps used in sensing because it can sense both the anions simultaneously.

## 2.2 EXPERIMENTAL SECTION

### 2.2.1 Reagents and instruments

The sodium salts of the anions used were of analytical grade, purchased from Merck and used without further purification. 2-hydroxy-1-naphthaldehyde and thiosemicarbazide were purchased from Sigma Aldrich (99%). All absorption spectra were recorded in Shimadzu, UV-3600 double beam spectrophotometer using a square quartz cell with a path length of 10 mm. The NMR spectra were recorded on a JEOL 400

MHz spectrophotometer. All emission spectra were recorded on a Horiba RF-5301PC using a standard quartz cell (path length, 3 cm). Vibrational spectra were recorded on a Perkin-Elmer FT-IR 1000 Spectrophotometer. Elemental analysis (CHNS) was performed on Elementar Model Vario El-III instrument. Cyclic voltammetry was carried out on an CHI760E electroanalyser with glassy carbon electrode as a working electrode, Ag/AgCl as the reference electrode and platinum wire used as an auxiliary electrode with 0.1 M tetrabutylammonium perchlorate used as the supporting electrolyte at a scan rate of 0.1 V/s. The mass of the probe and the probe with the anions was analyzed using a WATERS Q-TOF premier-HAB213 mass spectrometer. Fluorescence lifetime was recorded using a Horiba Jobin Yvon fluorocube fluorescence life time system.

### 2.2.2 Synthesis of Probe (L1)

**2-((2-Hydroxynaphthalen-1-yl)methylene)hydrazinecarbothioamide (L1):**

Thiosemicarbazide (1 mmol, 0.091 g) was dissolved in ethanol (10 ml) in a round bottom flask and 2-hydroxy-1-naphthaldehyde (1 mmol, 0.158 g) in ethanol (10 ml) was added dropwise to the solution with stirring. After completion of the reaction, the reaction mixture was refluxed for 5 h according to a previously reported literature procedure [23]. A yellow colored precipitate was obtained, which was filtered and recrystallized from DMF : ethanol (1:4) (Scheme 2.1).

**Yield:** 80%. Calcd. for $C_{12}H_{11}N_3OS$: C, 58.76; H, 4.52; N, 17.13; S, 13.07; O, 6.52 and found: C, 59.02; H, 4.182; N, 17.16; S, 12.927, O, 6.711. FT-IR data (KBr $\upsilon_{max}$ $cm^{-1}$): $NH_2$: 3254, N-H: 3165, C=S: 1394, C=N: 1611, O-H: 3447, UV-Visible (DMF: $H_2O$ (9:1), $\lambda_{max}$ nm): 331, 368 nm. $^1H$ NMR (DMSO, 400 MHz, δ/ppm): N-H: 11.36 (s, 1H), O-H: 10.51 (s, 1H), CH=N: 9.00 (s, 1H), $NH_2$: 8.48 (s, 1H), 8.16(s, 1H), 7.83 (d, *J* = 9.0 Hz, 1H), 7.80 (d, *J* = 8.1 Hz, 2H), 7.53 (t, *J* = 7.5, 1H),7.33 (t, *J* = 7.5 Hz, 1H), 7.15 (d, *J* = 9.0 Hz, 1H). $^{13}C$ NMR (DMSO, 100 MHz, δ/ppm):177.81, 157.16, 143.60, 133.04, 132.05, 129.23, 128.60, 128.44, 124.01, 123.44, 118.89, 110.29. ESI-mass of probe **L1** m/z 246.0547, $(M+H)^+$.

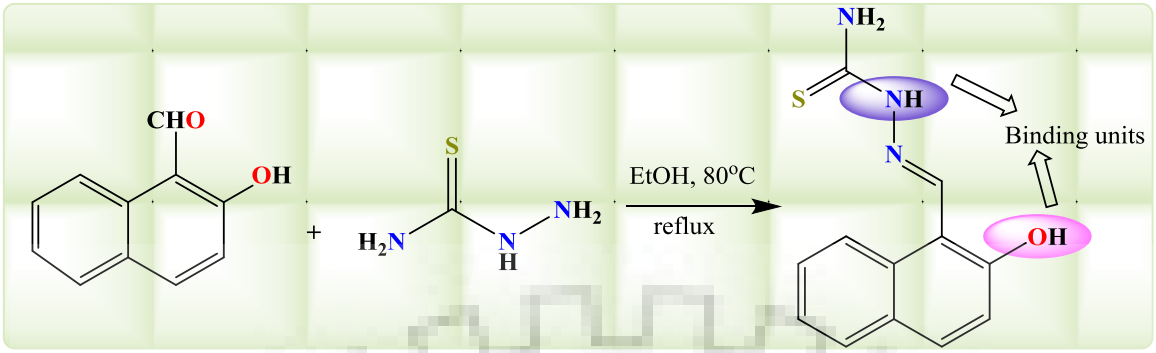


**Scheme 2.1.** Synthesis of probe (**L1**).

## 2.3 RESULTS AND DISCUSSION

### 2.3.1 Visualization test

The preliminary test for the detection of both anions was performed *via* a colorimetric test. Figure 2.1 shows the performance an equimolar concentration ($5.0\times10^{-5}$ M) of probe in DMF: $H_2O$ (HEPES buffer, pH= 7.2) (9:1, v/v solution) with 5 equivalents of the anion solutions (1 mM). A sudden color change was observed, which turned light yellow to dark yellow with arsenite and cyanide ions among other anions. The color change was observed due to deprotonation or strong hydrogen bonding between the probe and the anions ($AsO_2^-$ and $CN^-$). Moreover, the selectivity of arsenite and cyanide ions with probe was analyzed using absorption and emission spectra.

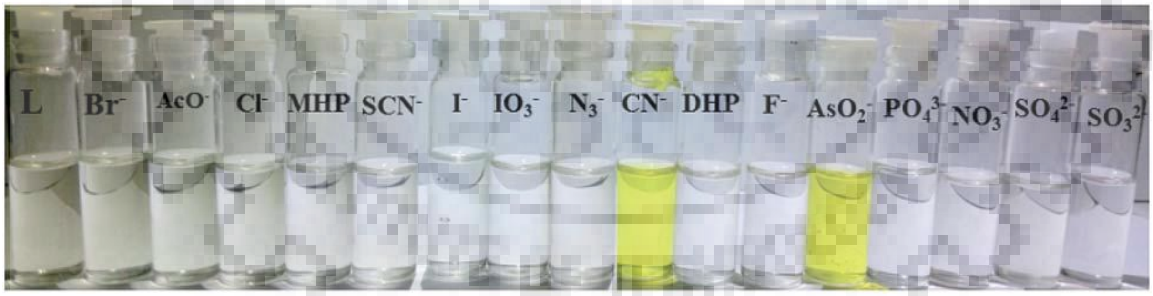


**Figure 2.1.** The visualization test of **L1** with different anions in DMF:$H_2O$ (9:1, v/v solution, HEPES buffer 7.2) medium.

### 2.3.2 UV-Vis studies of probe with different anions

The selectivity of anions ($AsO_2^-$ and $CN^-$) with probe **L1** was investigated using UV-Vis studies among different anions including $Cl^-$, $Br^-$, $F^-$, $I^-$, $SCN^-$, $H_2PO_4^-$, $HPO_4^{2-}$,

$CH_3COO^-$, $NO_3^-$, $SO_4^{2-}$, $SO_3^{2-}$, $PO_4^{3-}$, $IO_3^-$, $N_3^-$ in the DMF : $H_2O$ (9:1, v/v solution) medium. The probe showed two absorption peaks at 332 (due to π-π* transitions) and 369 nm (due to n-π* transitions). Arsenite and cyanide ions have the ability to abstract hydrogen or make hydrogen bonds with the probe. Upon the addition of all anions investigated, a new absorption band appeared at 452 nm in the UV-Vis spectra in the case of arsenite and cyanide ions, while this band was absent for the other anions. The selectivity of probe for only these two anions over the others may be attributed to its dissociation energy *i.e.* p*K*a value with these anions, which provide more stability to the probe. Figure 2.2 represents the selectivity with $AsO_2^-$ and $CN^-$ ions among other anions. The experiment was performed using fluorescence spectroscopy and the intensity enhancement was observed with $AsO_2^-$ and $CN^-$ among all the other anions studied. This study revealed that the probe was selective for arsenite and cyanide anions.

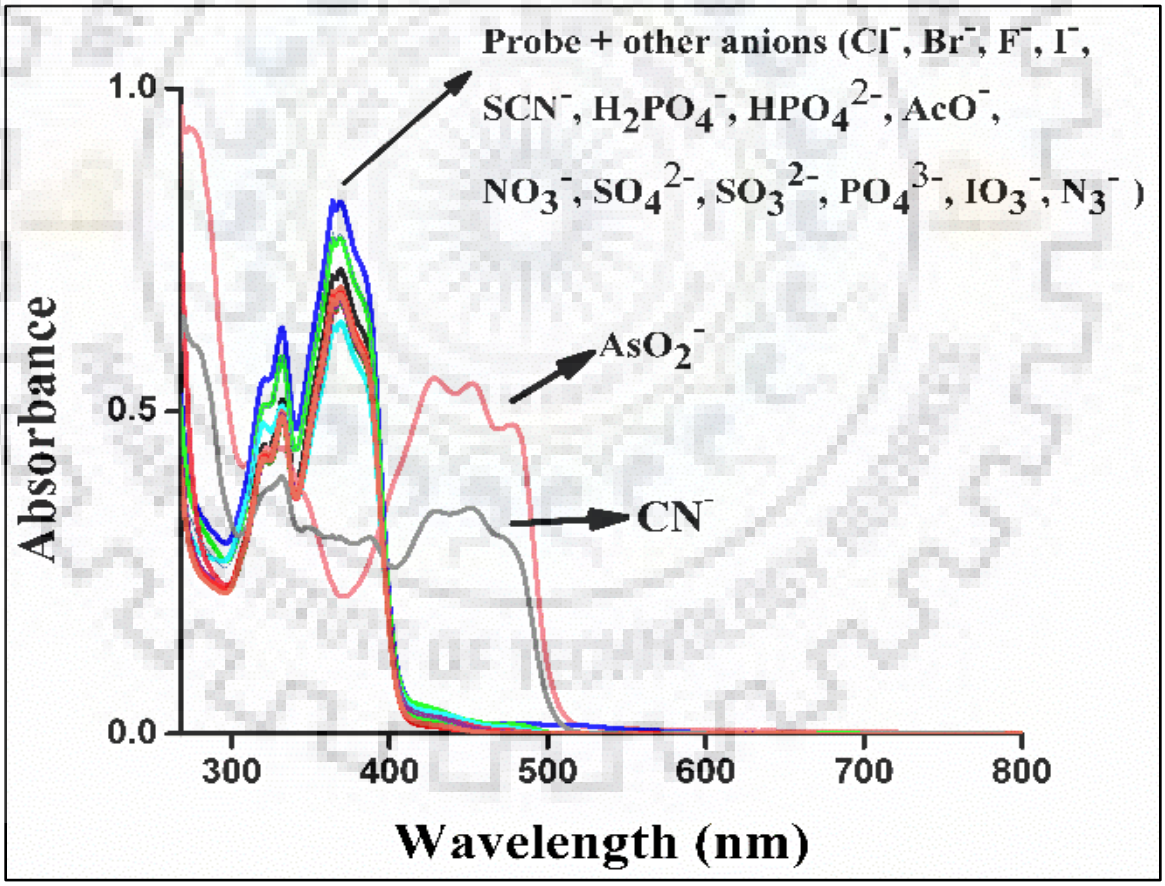


**Figure 2.2.** The selectivity of $AsO_2^-$ and $CN^-$ ion among different anions with **L1** in DMF:$H_2O$ (9:1, v/v solution, HEPES buffer 7.2) medium *via* absorption spectroscopy**.**

### 2.3.3 Binding sites and stoichiometry

The binding stoichiometry of the probe **L1** with arsenite and cyanide ions was observed in the absorption spectra of equimolar solutions (50 μM) of probe **L1** upon gradual variation in the mole fraction with anions ($AsO_2^-$ and $CN^-$). Figure 2.3(a) and 2.3(b) show the change in the absorption spectra with different mole fraction of anions in the Job's plot [24, 25], which support the 1:1 and 1:2 stoichiometry with arsenite and cyanide ions (50 μM) respectively. Using the Job's plot, the mole fraction value for arsenite ion was 0.55 and for cyanide ion it was 0.66, which endorse the 1:1 and 1:2 stoichiometry. The absorption spectra show the changes upon the addition of the anions to the probe (**L1**); the bands at 332 nm and 369 nm were quenched with an increase in the absorption band at 452 nm due to interaction of the anions with probe (**L1**). The isosbestic point was revealed from the non-interacted to interacted probe with anions by absorption titration of probe **L1** with both anions (Figure 2.4(a) & 2.4(b)). The formation constants were calculated and found to be $3.6\times10^5$ $M^{-1}$ and $5.8\times10^6$ $M^{-1}$ for the arsenite and cyanide ions, respectively, by Job's continuous variation method.

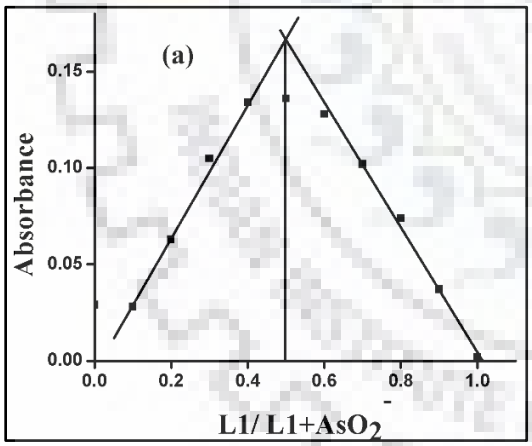


**Figure 2.3(a).** The Job's plot obtained with an equivalent mole concentration of probe **L1** (50 μM) and arsenite ion (50 μM).

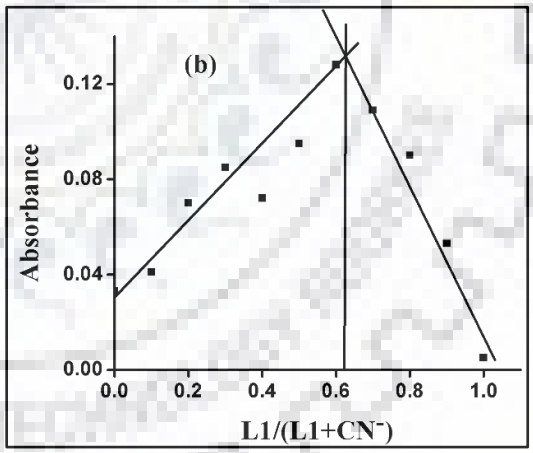


**Figure 2.3(b).** The Job's plot obtained with an equivalent mole concentration of probe **L1** (50 μM) and cyanide ion (50 μM).

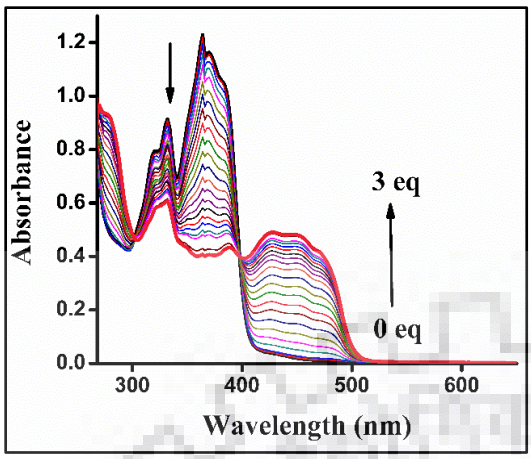


**Figure 2.4(a).** UV-Vis titration of **L1** with $AsO_2^-$ ion.

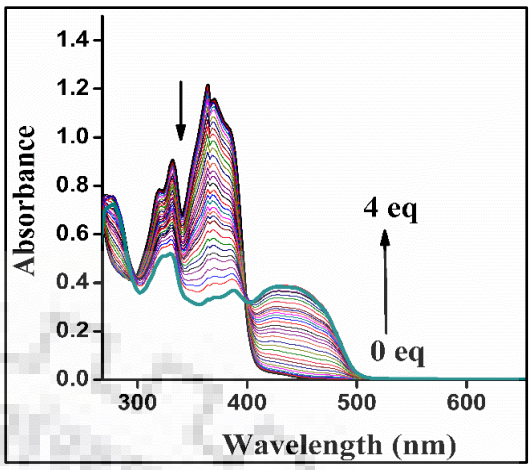


**Figure 2.4(b).** UV-Vis titration of **L1** with $CN^-$ ion.

### 2.3.4 Fluorescence emission spectra

Fluorescence studies were carried out in the same medium with a 10 µM concentration of the probe (**L1**); Figure 2.5 shows the selectivity test using the emission spectra. First, the selectivity test was performed with probe **L1** (10 µM) and 2 equivalent of all anions (40 µM). At an excitation wavelength of 363 nm, a "turn-on" emission occurred in the case of arsenite and cyanide ions over all other anions studied ($Cl^-$, $Br^-$, $F^-$, $I^-$, $SCN^-$, $H_2PO_4^-$, $HPO_4^{2-}$, $CH_3COO^-$, $NO_3^-$, $SO_4^{2-}$, $SO_3^{2-}$, $PO4^{3-}$, $IO_3^-$, $N_3^-$). The deprotonation and strong hydrogen bonding between the probe and both the anions (arsenite and cyanide) caused an enhancement in the emission. Hydrogen was deprotonated from the –OH group and hydrogen bonding with the –NH group occurred. Absorption and emission studies are strong evidence, which indicates that the probe is more selective for arsenite and cyanide ions among all the other anions studied. To confirm the sensitivity of **L1** towards $CN^-$ and $AsO_2^-$, dual anion treatment was also performed with probe **L1**. In favour of dual anion studies, equal concentrations (10 µM + 10 µM) of the anions were used with probe **L1**. Figure [2.6(a) & 2.6(b)] reveals the interference effect of the secondary anion in both case *viz.* $AsO_2^-$ and $CN^-$. Single anions ($Cl^-$, $Br^-$, $F^-$, $I^-$, $SCN^-$, $H_2PO_4^-$, $HPO_4^{2-}$, $CH_3COO^-$, $NO_3^-$, $SO_4^{2-}$, $SO_3^{2-}$, $PO_4^{3-}$, $IO_3^-$, $N_3^-$) treatment of the probe is indicated by the green bars, blue bar represents for **L1** and the red bars for **L1**+$CN^-$ with other anions in Figure 2.6(a). In the case of **L1**+$AsO_2^-$ Figure 2.6(b), blue bar showed **L1** where as red bars represented with interfering anions and

green bar for single anions with probe **L1**. The interference studies revealed that there is no interference by the other anion in case of both anions whereas $AsO_2^-$ and $CN^-$ act as interfering ions with each other. Therefore, with the help of interference studies it can be concluded that probe was highly selective for $AsO_2^-$ and $CN^-$ anions. These findings were strongly supported by UV-vis analysis of the probe with the various ions mentioned.

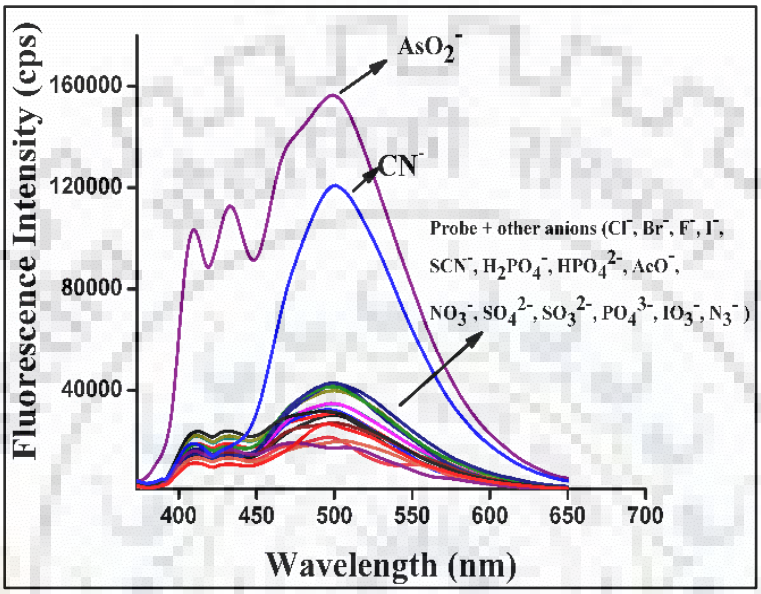


**Figure 2.5.** The fluorescence emission spectra of probe **L1** (10 μM) with different anions in DMF:$H_2O$ (9:1, v/v solution, HEPES buffer).

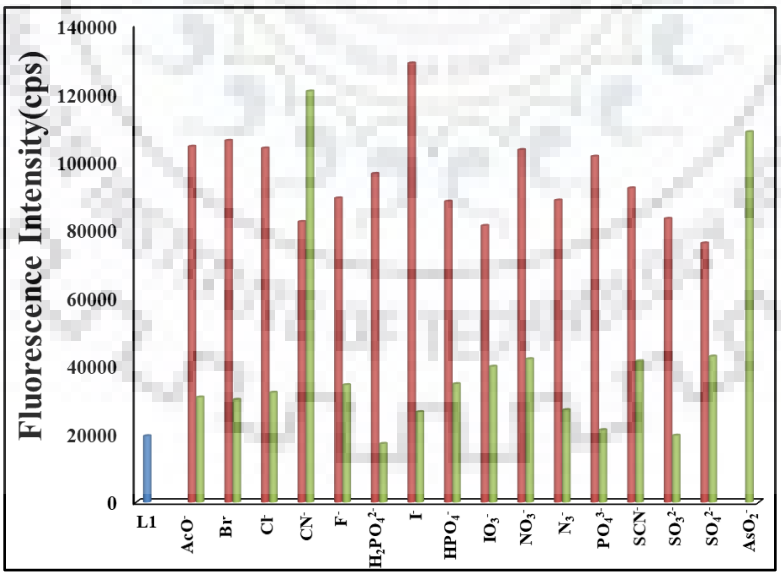


**Figure 2.6(a).** The interference study of **L1** in the presence of other anions, in figure the blue bar for **L1**, green bar represents **L1**+ other anions and red bar shows **L1**+$AsO_2^-$+ different anions.

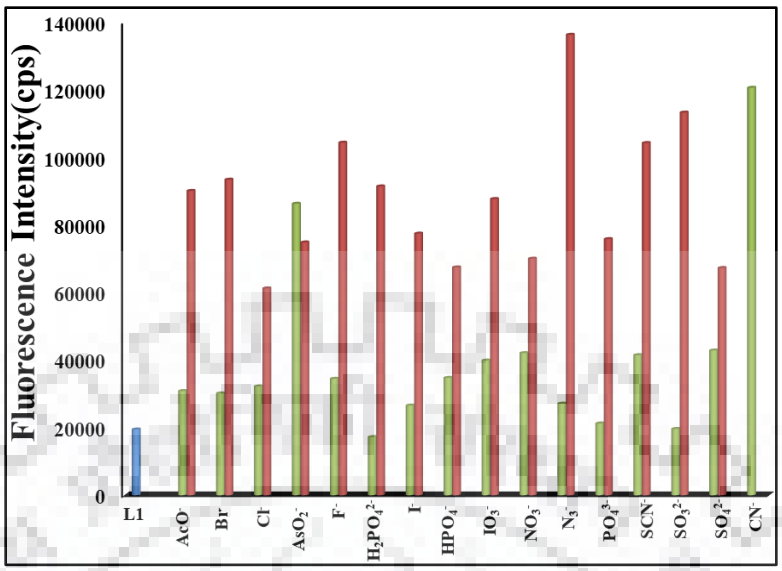


**Figure 2.6(b).** The interference study of **L1** in the presence of other anions, in figure the blue bar for **L1**, green bar represents **L1**+ other anions and red bar shows **L1**+$CN^-$+ different anions.

### 2.3.5 Emission Titration of probe L1 with $AsO_2^-$ and $CN^-$

An emission titration was performed with 2.5 ml of probe **L1** (10μM) and each anions ($AsO_2^-$ and $CN^-$) were added gradually to the same amount of probe in DMF : H2O (HEPES buffre, pH = 7.2, 9 :1, v/v solution). The association constant of both anions with probe were calculated from fluorescence titration *i.e.* $3.1\times10^5$ $M^{-1}$ and $1.9\times10^6$, respectively for the anions ($AsO_2^-$ and $CN^-$) using Benesi-Hildebrand plot [26]**.** The B-H plot was constructed between $1/(I-I_o)$ and $1/[A^-]$, where I is the emission intensity [27] of probe **L1**, $I_o$ for **L1** + anion ($AsO_2^-$ and $CN^-$) and $I_{max}$ is the emission intensity of complete binding of anions with **L1** and $A^-$ is the concentration of anions. Figure 2.7(a) and 2.7(b) represents the B-H plots of **L1**+$CN^-$ and **L1**+$AsO_2^-$, respectively. Similarly, the limit of detection (LOD) was calculated using the plot between $(I - I_o)/(I_{max} - I_o)$ and log (anions). Figure 2.8(a), 2.8(b) are the plots for the LOD for $AsO_2^-$ and $CN^-$ with probe **L1** *i.e.* 66 nM ($6.6\times10^{-8}$ M) and 77 nM ($7.7\times10^{-8}$ M), respectively in DMF: $H_2O$ (9:1, HEPES buffer, pH = 7.2), which are significantly less than the permissible limit cited by the WHO.

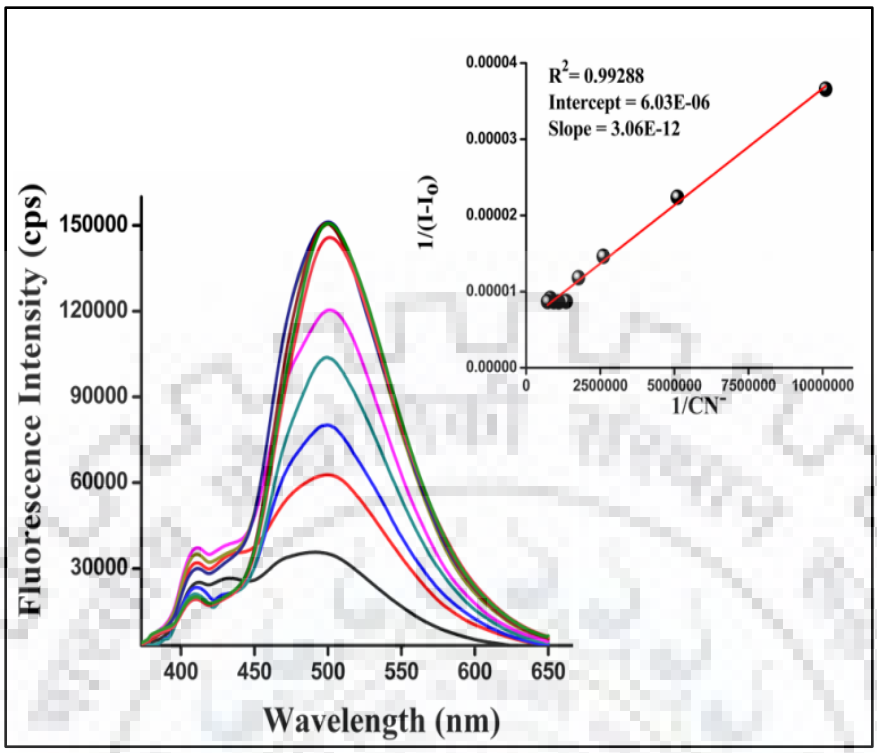


**Figure 2.7(a).** The emission titration of **L1** with $CN^-$ and inset shows the B-H plot of **L1** with CN- ion in medium (DMF:$H_2O$, v/v solution HEPES buffer 9:1).

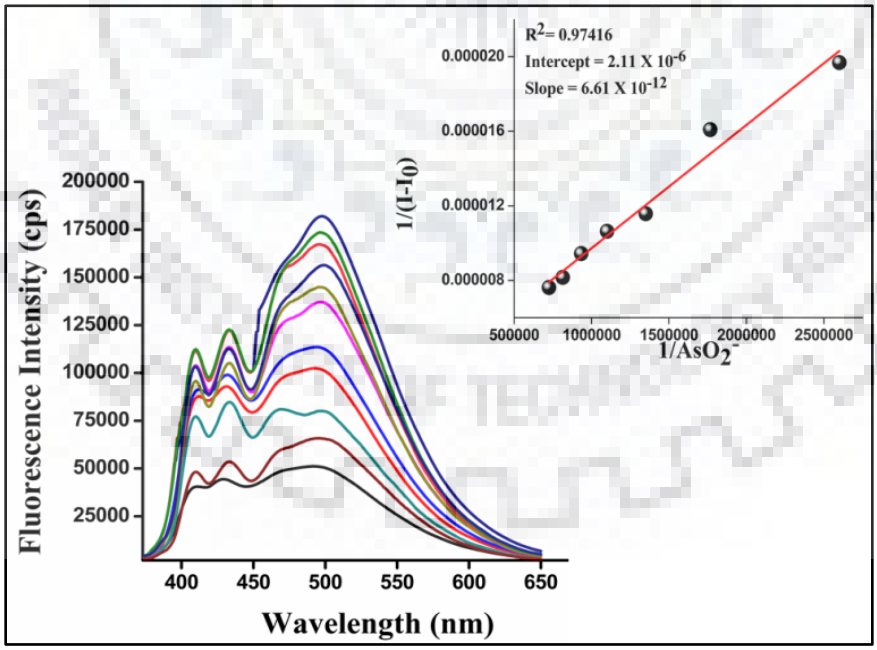


**Figure 2.7(b).** The emission titration of **L1** with $AsO_2^-$ and inset shows the B-H plot of **L1** with $AsO_2^-$ ion in medium (DMF:$H_2O$, v/v solution HEPES buffer 9:1).

In a previous report a minimum detection limit of 0.18 µM to 2.1 µM for $CN^-$ and 10.0 µM to 1.32 µM for $AsO_2^-$ were observed [28-31] whereas, in this work the LOD for $AsO_2^-$ and $CN^-$ is 0.066 µM and 0.077 µM, respectively.

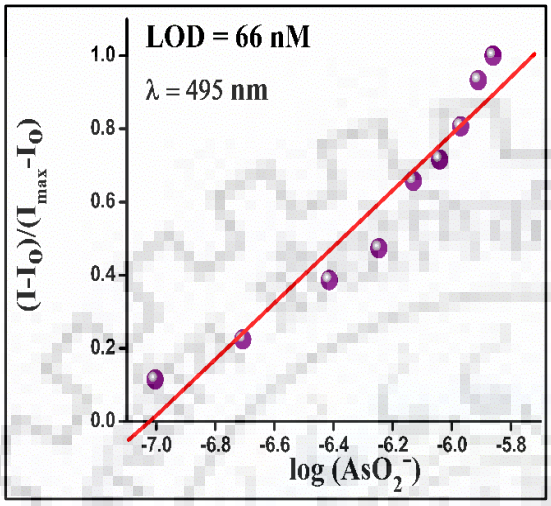


**Figure 2.8(a).** Limit of detection graph of **L1** with $AsO_2^-$.

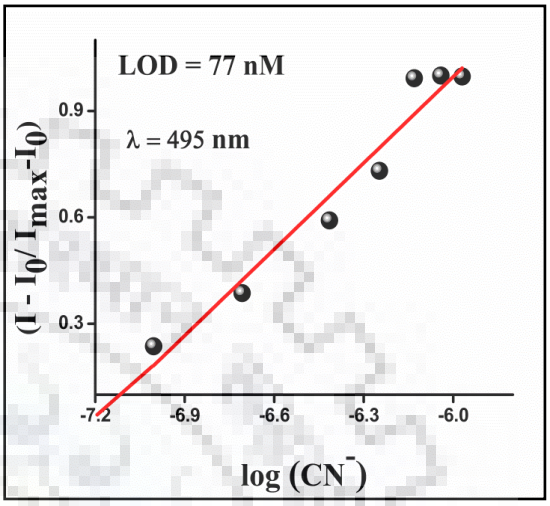


**Figure 2.8(b).** Limit of detection graph of **L1** with $CN^-$.

### 2.3.6 pH studies

The performance of the probe **L1** and the probe when treated with both anions was found to be strongly dependent on the pH of the medium because the probe was enriched with proton sensitive donar sites. It was essential to investigate the pH dependence of the probe and the probe with both anions. The pH study of probe **L1** showed that at acidic pH the intensity did not change as much as at basic pH and pH maintained by NaOH and HCl in basic and acidic range. On further enhancement in pH, deprotonation occurred as well as increase in the fluorescence intensity. The same experiment was performed with **L1**+$AsO_2^-$ and **L1**+$CN^-$, which exhibited that in case of **L1**+$AsO_2^-$ the compound was stable between pH 8-11 and after that the intensity decreased and the compound became turbid. However, probe **L1** with $CN^-$ demonstrated that the compound was stable from pH 7-11 and beyond this pH range, the compound was found to degrade [Figure 2.9(a) & 2.9(b)]. The pH studies of the probe with anions revealed that the pH range between 7 and 11 was suitable for sensing of anions.

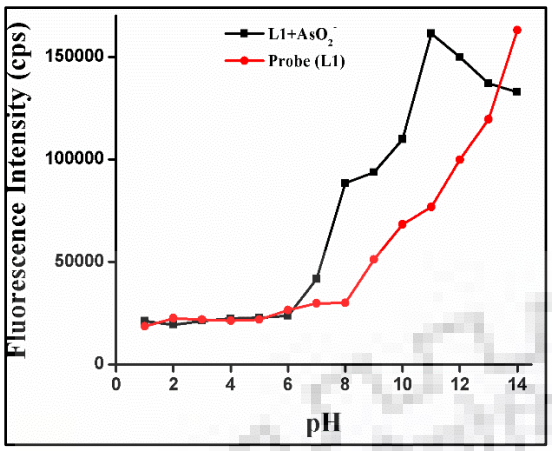


**Figure 2.9(a).** The activity of **L1** and **L1** in presence of $AsO_2^-$ ion at various pH.

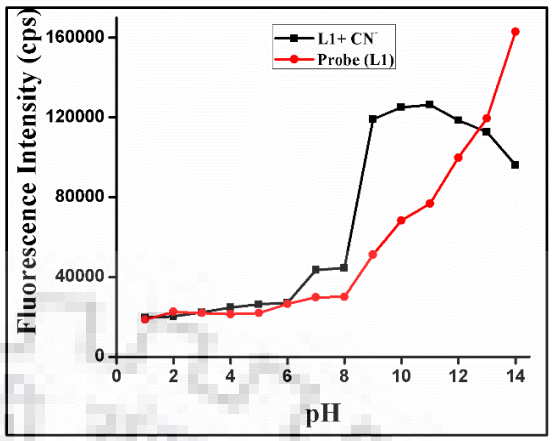


**Figure 2.9(b).** The activity of **L1** and **L1** in presence of $CN^-$ ion at various pH.

### 2.3.7 Binding Interaction

Further, the interaction of the probe with $AsO_2^-$ and $CN^-$ ions were demonstrated using an $^1H$ NMR titration study. Experiments of the probe **L1** and both anions was performed in DMSO. In the NMR spectrum of the probe **L1** the peaks at δ 9.04 ppm, δ 11.38 ppm, δ 10.49 ppm was designated as the –CH proton, -NH proton and –OH proton, respectively and other doublet and triplet corresponded to the aromatic protons. Upon addition of the $CN^-$ and $AsO_2^-$ ions, the proton signals were shifted towards upfield in both cases. In case of $AsO_2^-$, a substantial upfield shift ($\Delta\delta$ = 0.01 ppm) was observed due to the resonance of the –OH proton with π-$e^-$ cloud of aromatic region whereby, the electronegativity on the molecule increased. The peak for the –OH proton (10.49 ppm) was found to be completely disappear and similarly, the peak of –NH proton (11.38 ppm) decreased. On the other hand, the addition of $CN^-$ ion to the probe lead to a significant upfield shift ($\Delta\delta$= 0.02 ppm) and the peaks corresponding to –NH and –OH completely disappeared. Meanwhile, the aromatic signals were also shifted upfield. The $^1H$ NMR studies clearly illustrate that both anions interacted with the probe **L1** *via.* deprotonation of the –NH and –OH groups in the case of $CN^-$ whereas, in the case of $AsO_2^-$ deprotonation and hydrogen bonding occurred with –OH and –NH protons, respectively. Figure 2.10(a) & 2.10(b) show the binding interactions with and without the anions.

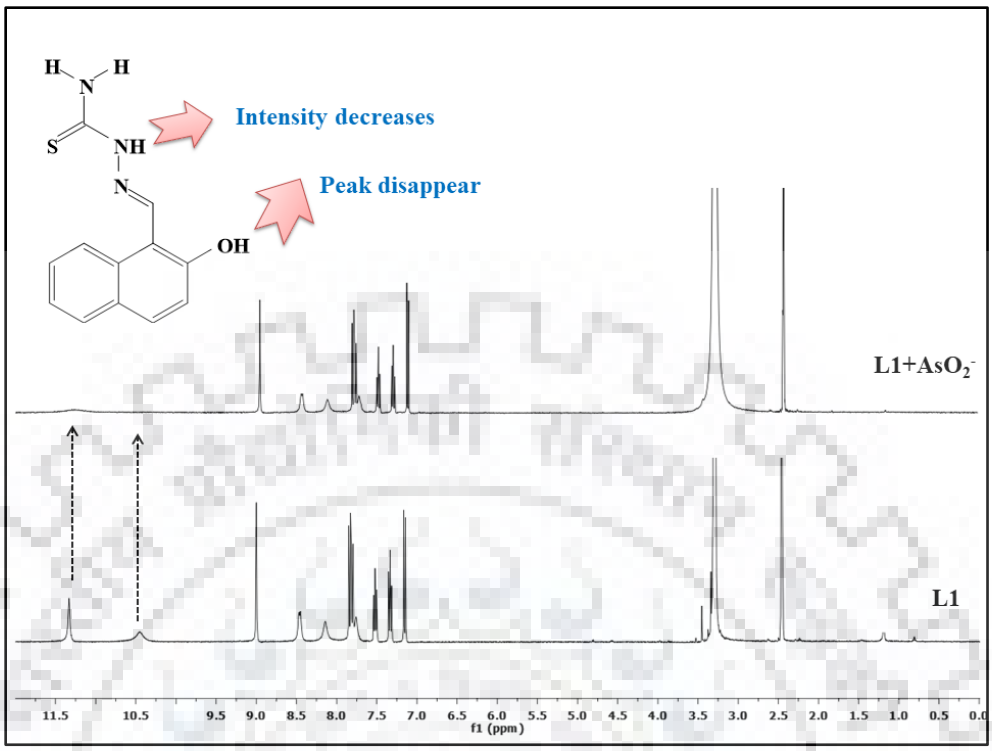


**Figure 2.10(a).** Repesents the varied NMR spectra without and with addition of $AsO_2^-$ ion with **L1** in DMSO-$d^6$.

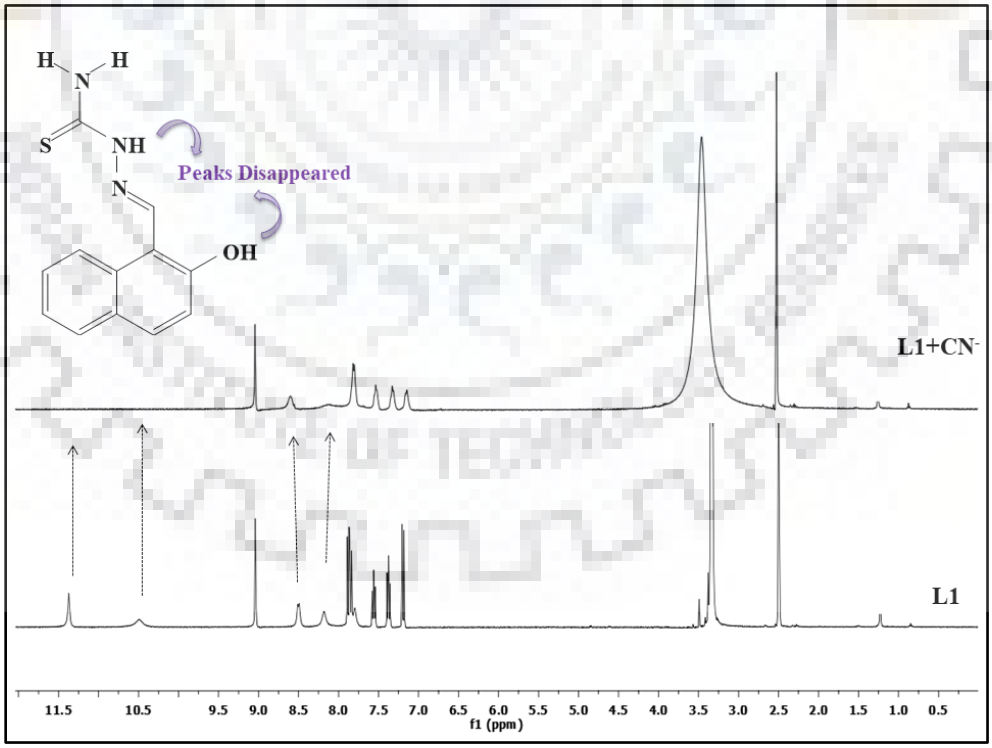


**Figure 2.10(b).** Repesents the varied NMR spectra without and with addition of $CN^-$ ion with **L1** in DMSO-$d^6$.

Further, the deprotonation behavior of probe **L1** in the case of both anions ($AsO_2^-$ &$CN^-$) was confirmed using ESI-mass spectrometry. Figure 2.11(a) & (c) represented the ESI-mass of **L1** with both anions. The mass (*m/z*) of the probe **L1** was 246.0547 $(M+H)^+$, which changed upon the addition of the anions to *m/z* = 244.0547 $(M-2H+H)^+$ in case of cyanide and with arsenite the *m/z* value was 245.0587 $(M-H+H)^+$, which supported the 1:2 and 1:1 stoichiometry between anions and the probe **L1**. Figure 2.11(b) & (d) shown the binding mode of **L1** with $CN^-$ and $AsO_2^-$ ion respectively.

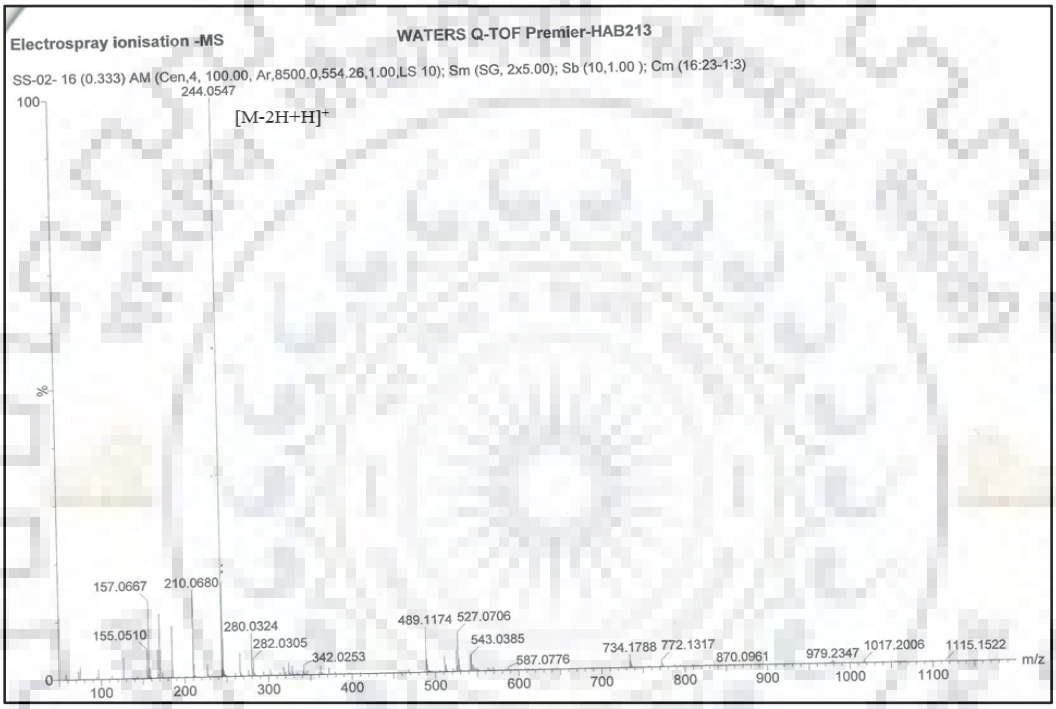


**Figure 2.11(a).** ESI-MS of **L1** with $CN^-$.

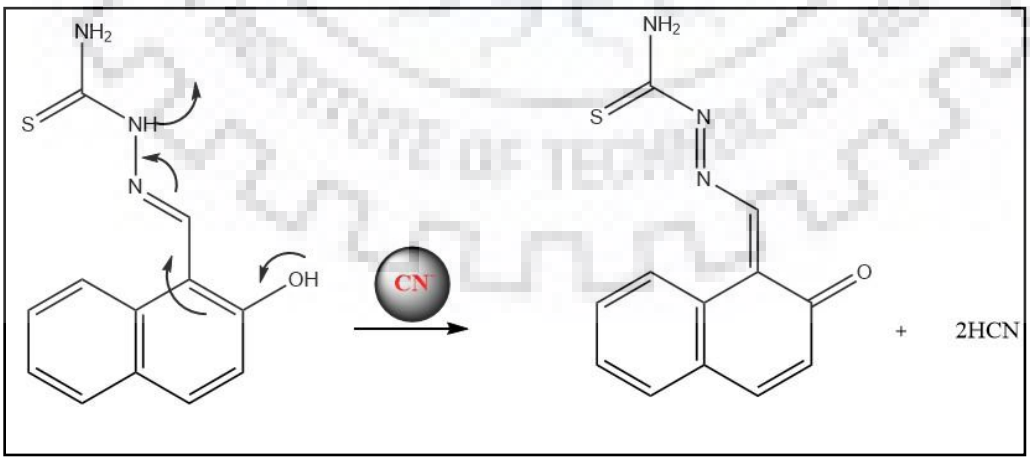


**Figure 2.11(b).** The binding mode of **L1** with $CN^-$ ion.

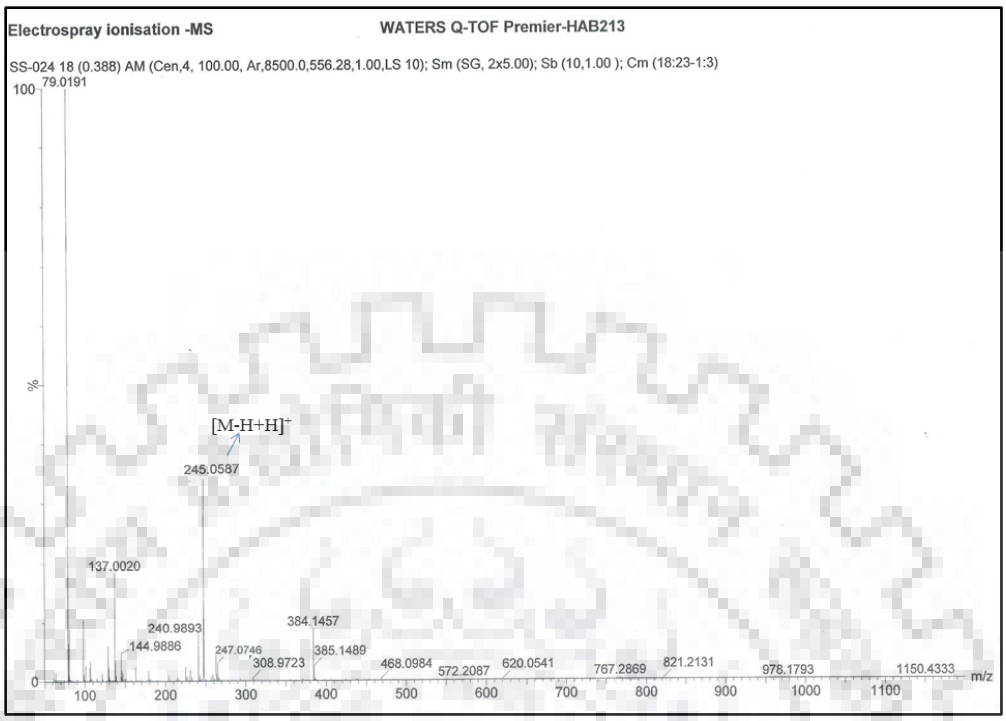


**Figure 2.11(c).** ESI-MS of **L1** with $AsO_2^-$.

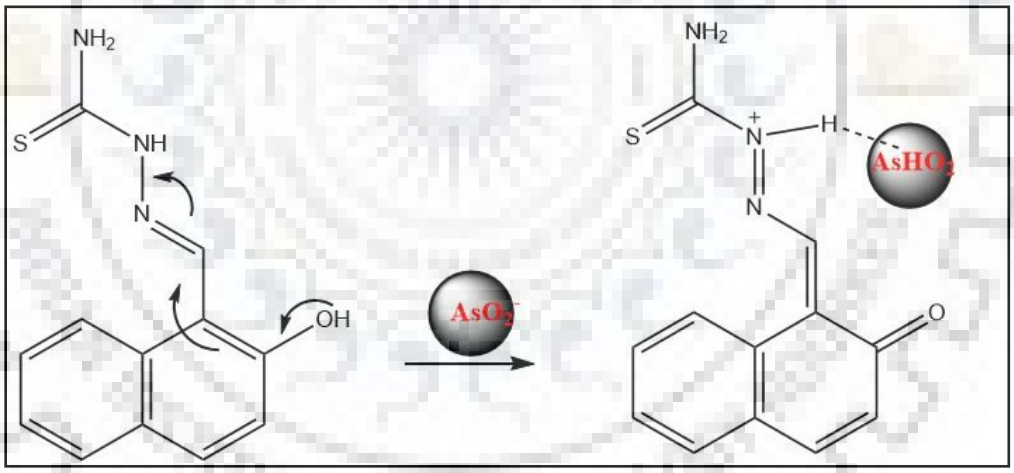


**Figure 2.11(d).** The binding mode of **L1** with $AsO_2^-$ ion.

### 2.3.8 Theoretical studies

The host and guest interaction was varified using density functional theory (DFT) calculations. The optimizied geometry of probe **L1** and **L1**+ anions ($AsO_2^-$ and $CN^-$) was obtained in gas phase using the Gaussian 09 W computational program [32]. This was performed with B3LYP functions and basis sets 6-31G(d, p) for probe **L1** and **L1**+ anions. In the HOMO, the electron density of probe **L1** was spread over the

thiosemicarbazone unit while in the LUMO, the electron density was localized on the naphthalene unit. However, The energy band gap calculated between HOMO-LUMO of probe **L1** was 3.732 eV.

The electron density of probe **L1** in HOMO – LUMO was effected by the deprotonating agent like $CN^-$ and $AsO_2^-$. As these anions deprotonate the proton from the probe the electron density increased in the HOMO in the case of $CN^-$. Similarly, in the case of $AsO_2^-$ electron density was more effected than $CN^-$ due to influence of hydrogen bonding. As a result, the decrease in the energy band gap and optimized structures in both cases are shown in the Figure 2.12. In the case of **L1**+$CN^-$ and **L1**+$AsO_2^-$, the energy band gap was diminished up to 1.822 eV and 0.961 eV respectively. The electron distribution in the case of **L1**+2$CN^-$ in the HOMO was around the thiosemicarbazone unit while in the LUMO it was mostly distributed around the naphthalene unit. Similarly, for **L1**+$AsO_2^-$, the electron cloud was localized around the naphthalene unit in the HOMO and in the LUMO, the electron density was localised on the $AsO_2^-$ unit, which supports the deprotonation and hydrogen bonding mechanism [33].

### 2.3.9 Cyclic Voltametric studies

Furthermore, the electrochemical demeanour of probe **L1** and **L1**+ anions ($AsO_2^-$ & $CN^-$) were analysed in DMF solution containing 0.1M TBAP as the supporting electrolyte. The voltammogram of probe **L1** represented one irreversible reduction peak at -1.65 V and one oxidation peak at 1.01 V. After the addition of $AsO_2^-$ solution to the probe there was not any change in the irreversible reduction peak at -1.65 V but the current was droped-off in comparison to the previous case and a new peak appeared at 0.36 V that support As(0) was oxidised to As(III) [34]; simultaneously the peak at 1.01 V was diminished with an electrochemical difference of 0.07 V. On the other hand, the oxidation and reduction peaks at -1.65 V, 1.01 V was shifted upto -0.85 V and 1.06 V respectively, which supports the formation of anoinic species and an increased in π-conjugation in case of cyanide [35,36], concurrently, a new oxidation peak appeared at 0.21 V that supports the interaction between probe **L1** and cyanide ion. Figure 2.13 (a), (b) and (c) shows all voltammogram.

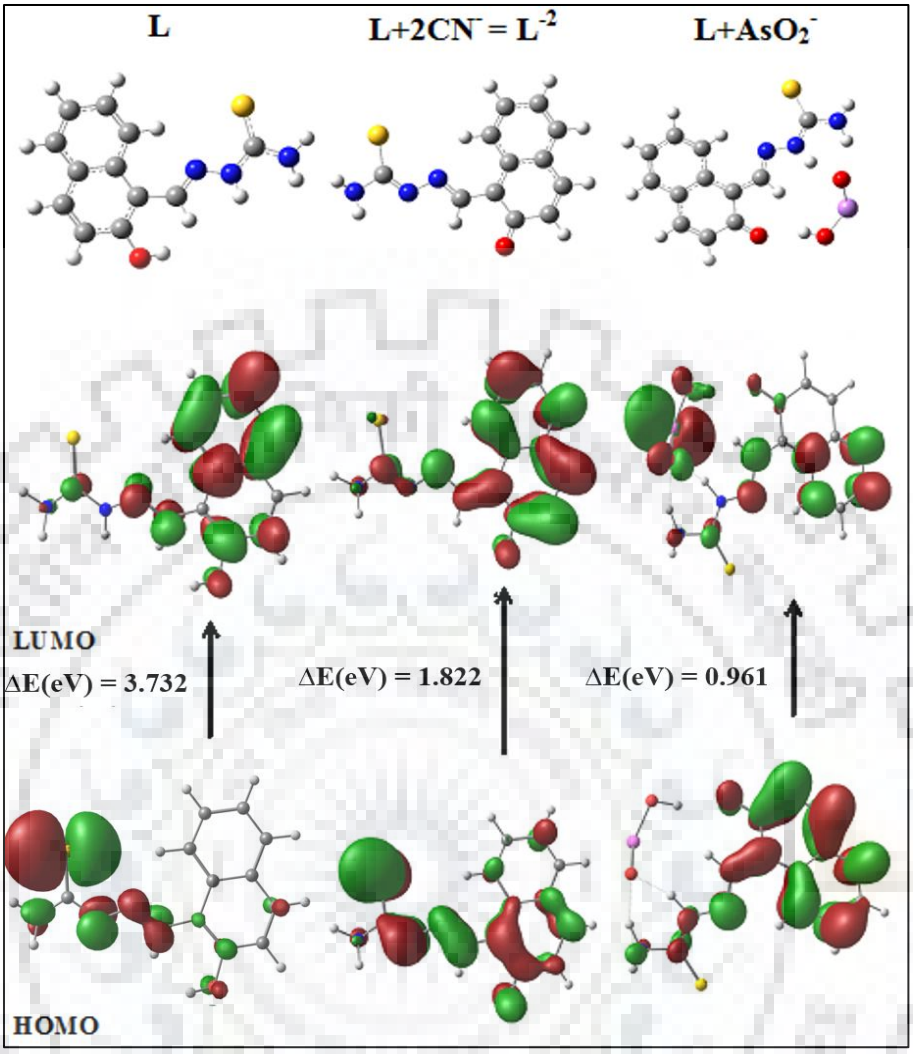


**Figure 2.12.** The optimized structure of **L1** and after interacction with both anions ($AsO_2^-$ & $CN^-$) by using 6-31G(d, p) basis set.

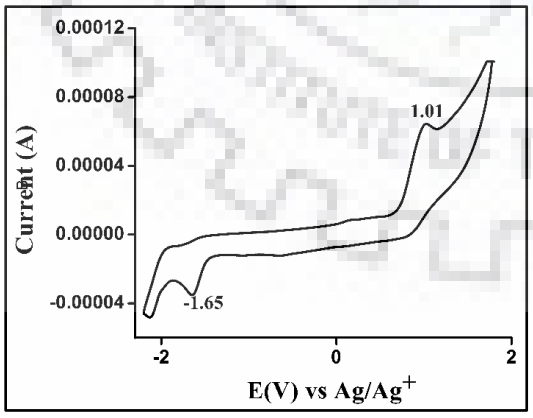


**Figure 2.13(a).** The cyclic voltammogram of **L1**.

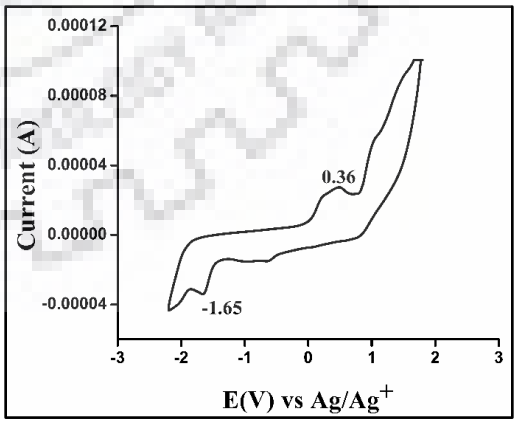


**Figure 2.13(b).** The cyclic voltammogram of **L1** with $AsO_2^-$ ion.

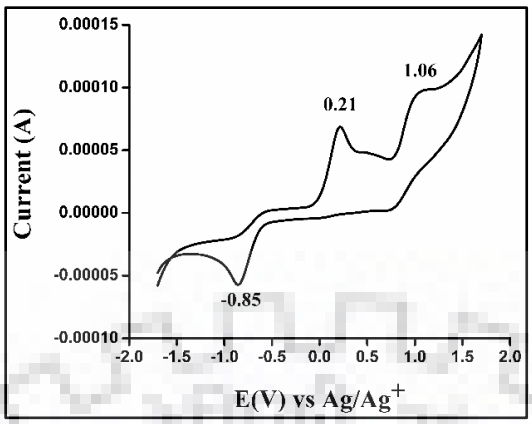


**Figure 2.13(c).** The cyclic voltammogram of **L1** with $CN^-$ ion.

### 2.3.10 Life Time Decay Measurement

In order to confirm the turn-on emission behavior of probe **L1** with arsenite and cyanide, the life time was meseaured of probe **L1** with both the anions ($AsO_2^-$ & $CN^-$). The lifetime follows the mono-exponencial decay of probe **L1** with arsenite ion and the life time was 0.98 ns. Similarly, the probe **L1** with cyanide ion also follow the mono-exponential decay which depicts that the lifetime of the probe **L1** with cyanide was 0.90 ns as the probe **L1** with cyanide and arsenite ion shows trun-on emission at an excitation wavelength of 363 nm [37]. Figure 2.14(a) and 2.14(b) represents the plot of the life time decay curves.

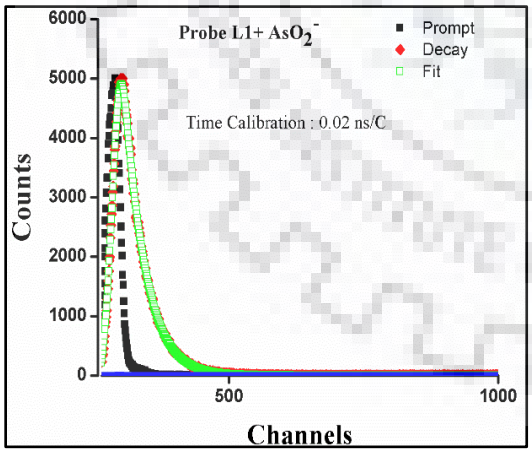


**Figure 2.14(a).** Lifetime profile of probe **L1** with arsenite ion.

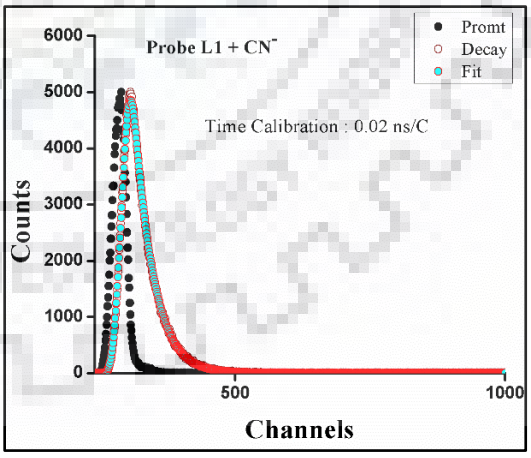


**Figure 2.14(b).** Lifetime profile of probe **L1** with $CN^-$ ion.

## 2.4 APPLICATIONS

### 2.4.1 Sensitivity test

The concentration of probe **L1** was maintained at 10 μM, while the concentration of arsenite ion was varied from 0-20 μM. The fluorescence intesity was measured at 363 nm of all the solution. Then, a calibration plot was plotted between the concentration and the change in the intensity resulting in a linear relationship. A similar experiment was performed with cyanide ions, which results in a similar linear plot (figure 2.15(a) & 2.15(b)). Using this plot, an unknown concentration of arsenite and cyanide ion can be determined by measuring the fluorescence intensity in water and also in the presence of all other anions studied.

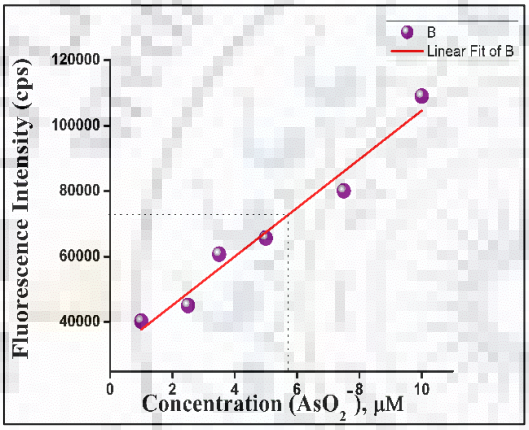


**Figure 2.15(a)**. Calibration plot between change in fluorescence intensity of the probe **L1** at 363 nm *vs* arsenite ion for the quantitative analysis of arsenite ion in water.

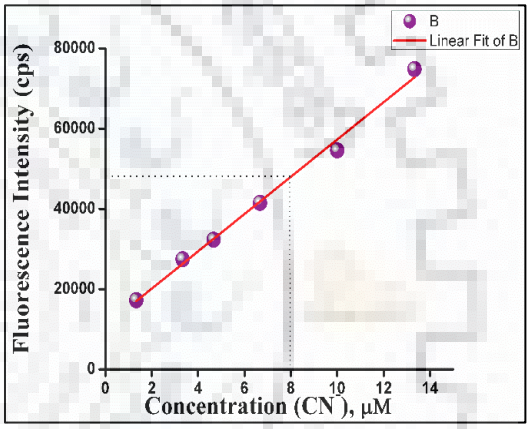


**Figure 2.15(b)**. Calibration plot between change in fluorescence intensity of the probe **L1** at 363 nm *vs* cyanide ion for the quantitative analysis of cyanide ion in water.

### 2.4.2 Real water analysis

For the assessment of the pratical application of probe **L1**, the probe was applied to analyse real water samples. The water sample used was tap water from Roorkee and known amounts of cyanide and Arsenite were added into the water samples. The assay was calculated by spiking a known amount of standard cyanide and arsenite solutions followed by evaluating its recovery. The water samples was compared with a controlled sample of same concentration and find the value of the concentration of the spiked

anions. The recovery of the different known amounts of cyanide added was acquired from 95% to 104%, whereas for arsenite ion, it was from 93% to 99%, which showed that the application of probe **L1** in real water samples was quite feasible. Table 2.1 & 2.2 represent the study with real water sample analysis.

**Table 2.1:** The determination of cyanide ions in tap water sample using probe **L1**.

| Sample | Added $CN^-$ (M) | Found[a] $CN^-$ (M) ± SD | Recovery (%) |
|---|---|---|---|
| **Tap water** | $5.0 \times 10^{-5}$ | $5.2 \pm 0.4 \times 10^{-5}$ | 104 % |
| | $10.0 \times 10^{-5}$ | $9.5 \pm 0.2 \times 10^{-5}$ | 95 % |
| | $15.0 \times 10^{-5}$ | $14.8 \pm 0.2 \times 10^{-5}$ | 98.6 % |

[a] Standard deviation calculation for three measurements.

**Table 2.2:** The determination of arsenite ions in tap water samples using probe **L1**.

| Sample | Added $AsO_2^-$ (M) | Found[a] $AsO_2^-$ (M) ± SD | Recovery (%) |
|---|---|---|---|
| **Tap water** | $5.0 \times 10^{-5}$ | $4.9 \pm 0.1 \times 10^{-5}$ | 99 % |
| | $10.0 \times 10^{-5}$ | $9.3 \pm 0.3 \times 10^{-5}$ | 93 % |
| | $15.0 \times 10^{-5}$ | $14.7 \pm 0.3 \times 10^{-5}$ | 98 % |

[a] Standard deviation calculation for three measurements.

## 2.5 CONCLUSIONS

The probe **L1** was synthesized and characterised using different techniques like UV-Vis, FT-IR, ESI-mass and NMR spectroscopy. The probe displayed high selectivity as well as sensitivity towards both the toxic arsenite and cyanide anions, when comparing to other biologically admissible anions. The probe acts as a chemodosimeter for both ions ($AsO_2^-$ & $CN^-$) with LOD as low as *ca.* 66 nM for arsenite ions and 77 nM for cyanide ions. The binding affinitty of probe **L1** to arsenite and cyanide ion was confirmed by NMR, DFT optimization, ESI-MS, electrochemical behaviour and optical studies. The probe can also used for the determination of unknown concentration of arsenite and cyanide ion in water using the calibration plot of known concentration *vs* fluorescence intensity as well as in real water sample analysis.

**References**


1. R. Martinez-Manez and F. Sancenon, Fluorogenic and chromogenic chemosensors and reagents for anions, Chem. Rev. 103 (2003) 4419−4476.
2. H. Hasegawa, M. Matsui, S. Okamura, M. Hojo, N. Iwasaki and Y. Sohrin, Arsenic speciation including 'Hidden' arsenic in natural waters, Appl. Organometal. Chem. 13 (1999) 113–119.
3. W. R. Cullen and K. J. Reimer, Arsenic speciation in the environment, Chem. Rev. 89 (1989) 713-764.
4. H. Kaur, R. Kumar, J. N. Babu and S. Mittal, Advances in arsenic biosensor development – A comprehensive review, Biosens. Bioelectron. 63 (2015) 533–545.
5. S. Shen, X. - F. Li, W. R. Cullen, M. L. Weinfeld and X. C. Le, Arsenic binding with proteins, Chem. Rev. 113 (2013) 7769−7792.
6. S. D. Richardson**,** Water analysis, Anal. Chem. 71 (1999) 181R-215R.
7. A. R. Keimowitz, B. J. Mailloux, P. Cole, M. Stute, H. J. Simpson and S. N. Chillrud, Laboratory investigation of enhanced sulphatereduction as a groundwater arsenic remediation strategy, Environ. Sci. Technol. 41 (2007) 6718-6724.
8. N. Yogarajaha and S. S. H. Tsai, Detection of trace arsenic in drinking water: Challanges and opportunities for microfluidics, Environ. Sci.: Water Res.Technol. 1 (2015) 426-447.
9. M. Jamkratoke, V. Ruangpornvisuti, G. Tumcharern, T. Tuntulani and B. Tomapatanaget, A-D-A sensors based on naphthoimidazoledione and boronic acid as trun-on cyanide probes in water, J. Org. Chem. 74 (2009) 3919–3922.
10. S.-J. Hong, J. Yoo, S.-H. Kim, J. S. Kim, J. Yoon and C.-H. Lee, β-Vinyl subsituted calix[4]pyrrole as a selective ratiometric sencor for cyanide anion, Chem. Commun. (2009) 189-191.
11. Z. Xu, X. Chen, H. N. Kim and J. Yoon, Sensors for the optical detection of cyanide ion, Chem. Soc. Rev. 39 (2010) 127–137.
12. WHO. Guidelines for drinking-water quality, World Health Organization, Geneva, Switzerland. 4th. (2011).

13. M. Baglan and S. Atilgan, Selective and sensitive trun-on fluroscent sensing of arsenite based on cysteine fused tetraphenylethene with AIE characteristics in aqueous media, Chem. Commun. 49 (2013) 5325-5327.
14. R. Manivannan, A. Satheshkumar and K. P. Elango, Highly selective colorimetric/fluorometric chemodosimeters for cyanide ions in aqueous solution based on michael addition to C-atom possessing different polar substituents, Tetrahedron Lett. 55 (2014) 6281–6285.
15. M. Tomasulo, S. Sortino, A. J. P. White and F. M. Raymo, Chromogenic oxazine for cyanide detection, J. Org. Chem. 71 (2006) 744-753.
16. S.-S. Sun and A. J. Lees, Anion recognition through hydrogen bonding: A simple, yet highly sensitive, luminescent metal-complex receptor, Chem. Commun. (2000) 1687–1688.
17. N. Kumari, S. Jha and S. Bhattacharya, Colorimetric probes based on anthraimidazolediones for selective sensing of fluoride and cyanide ion *via* intramolecular charge transfer, J. Org. Chem. 76 (2011) 8215-8222.
18. M. R. Ajayakumar and P. Mukhopadhyay, Single-electron transfer driven cyanide sensing: A new multimodal approach, Org. Lett. 12 (2010) 2646-2649.
19. S. Goswami, S. Paul and A. Manna, FRET based selective and ratiometric 'Naked Eye' detection of $CN^-$ in aqueous solution on fluorescein-Zn-naphthalene ensemble plateform, Tetrahedron Lett. 55 (2014) 3946–3949.
20. U. P. Azad and V. Ganesan, Tris(4,4′-dimethyl-2,2′-bipyridine)iron(II)-exchanged nafion for arsenite determination in water samples, Chem. Electro. Chem. 1 (2014) 379–383.
21. R. Touilloux, M.-L. Tercier-Waeber and E. Bakker, Direct arsenic(III) sensing by a renewable gold plated Ir-based microelectrode, Analyst 140 (2015) 3526-3534.
22. N. Gupta, A. K. Singh, S. Bhardwaj and D. Singhal, Electroanalytical studies of chromone based ionophores for the selective determination of arsenite ion, Electroanalysis 27 (2015) 1166–1175.
23. I. Dilovic, M. Rubc, V. Vrdoljak, S. K. Pavelie, M. Karlj, I. Piantanida and M. Cindric, Novel thiosemicarbazone derivatives as potential antitumor agents:

Synthesis, physicochemical and structural properties, DNA interactions and antiproliferative activity, Bioorg. Med. Chem. Lett. 16 (2008) 5189–5198.

24. A. Kumar and H.-S. Kim, A pyrenesulfonyl-imidazolium derivative as a selective cyanide ion sensor in aqueous media, New J. Chem. 39 (2015) 2935-2942.
25. J. H. Lee, A. R. Jeong, I.-S. Shin, H.-J. Kim and J.-I. Hong, Fluorescence trun-on sensor for cyanide based on a cobalt(II)-coumarinylsalen complex, Org. Lett. 12 (2010) 764-767.
26. S. Goswami, K. Aich, S. Das and A. K. Das, A highly selective and sensitive probe for colorimetric and fluorogenic detection of $Cd^{2+}$ in aqueous media, Analyst 138 (2013) 1903-1907.
27. S. Lohar, A. Sahana, A. Banerjee, A. Banik, S. K. Mukhopadhyay, J. S. Matalobos and D. Das, antipyrine based arsenate selective fluorescent probe for living cell imaging, Anal. Chem. 85 (2013) 1778−1783.
28. W.-C. Lin, S.-K. Fang, J.-W. Hu, H.-Y. Tsai, and K.-Y. Chen, Ratiometric fluorescent/colorimetric cyanide-selective sensor based on excited-state intramolecular charge transfer-excited-state intramolecular proton transfer switching, Anal. Chem. 86 (2014) 4648−4652.
29. J. Liu, Y. Liu, Q. Liu, C. Li, L. Sun and F. Li, Iridium(III) complex-coated nanosystem for ratiometric upconversion luminescence bioimaging of cyanide anions, J. Am. Chem. Soc.133 (2011) 15276-15279.
30. M. A. Kaloo and J. Sankar, Reusable and specific proton transfer signalling by inorganic cyanide in solution and solid phase, Chem. Comm. 51 (2015) 14528-14531.
31. S. Mardanya, S. Karmakar, D. Mondal and S. Baitalik, An imidazolyl-pyreno-imidazole conjugate as a cyanide sensor and a set-reset memorized sequential logic device, Dalton Trans. 44 (2015) 15994-16012.
32. H. B. Schlegel, G. E. Scuseria, M. A. Robb, J. R. Cheeseman, G. Scalmani, V. Barone, B. Mennucci, G. A. Petersson, H. Nakatsuji, M. Caricato, X. Li, H. P. Hratchian, A. F. Izmaylov, J. Bloino, G. Zheng, J. L. Sonnenberg, M. Hada, M. Ehara, K. Toyota, R. Fukuda, J. Hasegawa, M. Ishida, T. Nakajima, Y. Honda, O. Kitao, H. Nakai, T. Vreven, J. A. Montgomery Jr, J. E. Peralta, F. Ogliaro, M.

Bearpark, J. J. Heyd, E. Brothers, K. N. Kudin, V. N. Staroverov, R. Kobayashi, J. Normand, K. Raghavachari, A. Rendell, J. C. Burant, S. S. Iyengar, J. Tomasi, M. Cossi, N. Rega, J. M. Millam, M. Klene, J. E. Knox, J. B. Cross, V. Bakken, C. Adamo, J. Jaramillo, R. Gomperts, R. E. Stratmann, O. Yazyev, A. J. Austin, R. Cammi, C. Pomelli, J. W. Ochterski, R. L. Martin, K. Morokuma, V. G. Zakrzewski, G. A. Voth, P. Salvador, J. J. Dannenberg, S. Dapprich, A. D. Daniels, O. Farkas, J. B. Foresman, J. V. Ortiz, J. Cioslowski and D. J. Fox, Gaussian 09, Revision A.02, Gaussian, Inc., Wallingford CT (2009).

33. A. S. M. Islam, R. Alam, A. Katarkar, B. K. Chaudhuri and M. Ali, Di-Oxime based selective selective fluorescent probe for arsenate and arsenite ions in a purely aqueous medium with living cell imaging applications and H-bonding induced microstructure formation, Analyst 140 (2015) 2979–2983.
34. J. P. Mafa, N. Mabuba and O. A. Arotiba, An exfoliated graphite based electrochemical sensor for as(iii) in water, Electroanalysis 28 (2016) 1462–1469.
35. K. Kaur, S. K. Mittal, A. Kumar S. K., A. Kumar and S. Kumar, Viologen substituted anthrone derivatives for selective detection of cyanide ions using voltammetry, Anal. Methods 5 (2013) 5565-5571.
36. D. Nematollahi, M. Alimoradi and S. W. Husain, Cyclic voltammetric study of the oxidation of catechols in the presence of cyanide ion, Electroanalysis 16 (2004) 1359-1365.
37. G. Balamurugan, P. Venkatesan, S. P. Wub and S. Velmathi, Novel ratiometric turn-on fluorescent probe for selective sensing of cyanide ions, effect of substitution and bio-imaging studies, RSC Adv. 6 (2016) 24229-24235.

# CHAPTER 3

## "DICARBOHYDRAZIDE BASED CHEMOSENSOR FOR COPPER AND CYANIDE IONS"

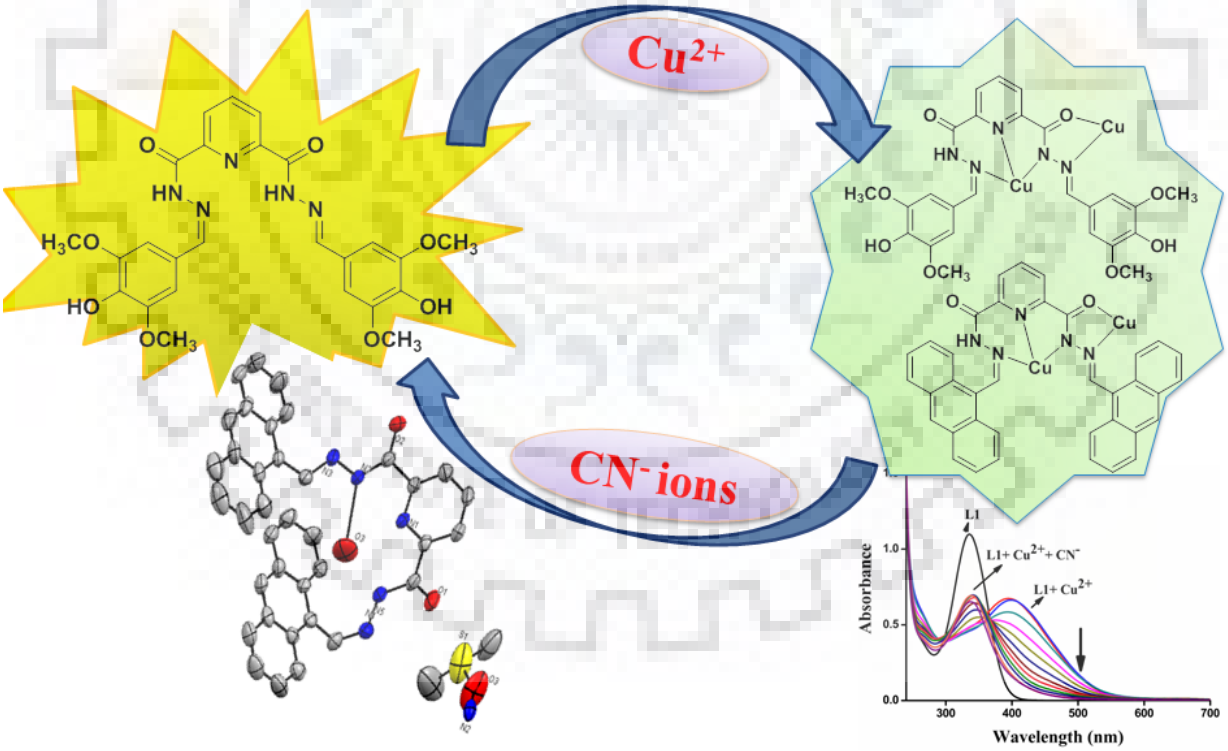

# CHAPTER 3

## 3.1 INTRODUCTION

Transition metals such as iron, zinc, magnesium and copper, play an important role in living systems. Among transition metals, copper is the third most essential trace metal and performs a foremost role in human nervous system as the cofactor of many metalloenzymes [1,2]. It is essential for a wide range of physiological processes, such as in bone growth, hemoglobin biosynthesis, dopamine production, nerve function regulation, the functional and structural augmentation of protein and enzymatic functions. Copper also generates cellular energy, induced signal transduction and diminishes molecular oxygen [3]. However, the presence of unregulated copper and disrupted copper ion homeostasis [4] can lead to numerous neurogenerative diseases such as Menkes syndrome, Alzheimer's disease, Wilson's syndrome [5], Amyotrophic lateral sclerosis, Parkinson's disease and Prion diseases [6,7]. Menkes syndrome [8] is due to copper deficiency, while Wilson syndrome is due to copper toxicosis, and both are human genetic disorders [9-12]. Cyanide ions are more toxic ion compared to other anions, although cyanide is very vital reagent for many industrial processes in different areas such as mining, synthetic fiber production and electroplating [13-16]. The "excessive" utilization of cyanide [17] in these factories and its fundamental transportation, expands the likelihood of human exposure. Its acute toxicity destroys the central respiratory system of the body and block the electron transfer chain in mitochondria [18,19].

The extensive use of copper within daily life is the prime reason of copper pollution in the environment, and although copper is essential metal ion, it is harmful for living systems when found in concentration higher than required. This is similar with cyanide ions, as its frequent use in industries to make environment polluted. According to World Health Organization (WHO), the permissible limit of copper ions and cyanide ions in drinking water is 2 ppm (30 μM) and 0.2 ppm [20,21] respectively. In blood, the maximum concentration of copper ions should not be greater than 100-150 μg-dL$^{-1}$[22,23]. The Environmental protection Agency has advised that the safe maximum limit of copper in drinking water 1.3 ppm (*ca.* 20 μM) [24].

There are many sensors, which can sense copper ions, using different mechanism. Aside from this, the multidentate chemosensors also have the ability to sense other

specific metal ions. In this chapter, multidentate ligands have been synthesized and applied as chemosensors. This chapter shows that the ligands, which have large number of donor atom and hydroxyl group, are highly sensitive and selective for copper ions. The chapter presents four ligands, each with different molecule added and with a common backbone of pyridine dicarbohydrazide. All four of these ligands were highly selective and sensitive towards copper ions among the metal ions. The complexation occurred *via*. PET (photoinduced electron transfer) mechanism. Furthermore, anion sensing was performed with **L**+ $Cu^{2+}$ and result shown that the ligands with copper ion can sense cyanide ion with good limit of detection *via.* metal displacement path.

## 3.2 EXPERIMENTAL SECTION

### 3.2.1 Materials and Measurements

The acetate and chloride salts used were of analytical grade purchased from Merck and used without further purification. All other chemicals were purchased from Sigma-Aldrich and distilled solvents were used throughout the experiments. The elemental analysis (CHNS) was performed using a Verio MICROV3.1.1 instrument. The vibrational spectrum was acquired using a Perkin Elmer FT-IR 1000 spectrophotometer. A Specord 600 thermo scientific PC double beam spectrophotometer (with a path length 3cm) was used to obtain absorption spectra and the emission spectra obtained using a Horiba RF-5301PC with standard quartz cell (path length 3cm). A JEOL 400 MHz spectrometer was used to obtain the NMR spectra. A CHI760E Electro-analyser was used to obtain electrochemical studies, with three electrodes configuration of pyrolytic graphite as a working electrode, $Ag/AgCl_2$ as a reference electrode, Pt wire used as a counter electrode and 0.1 M tetrabutylammonium hexafluorophosphate ($nBu_4NPF_6$) as a supporting electrolyte. The mass spectrum gleaned *via* Bruker micrOTOF$^{TM}$-Q II mass spectrometry.

### 3.2.2 Synthesis of the ligands:

**Synthesis of precursor (1)**

The pyridine-2,6-diester obtained by the refluxing pyridine-2,6-dicarboxyclic acid with thionyl chloride in methanol solvent 6hr. Pyridine-2,6-dicarbohydrazide (**1**) was synthesized by stirring hydrazine (4.4 mmol, 0.223 g) with pyridine ester (2 mmol, 0.390 g) in the presence of ethanol.

**Yield: (95%).** FT-IR data (KBr, $\nu_{max}/cm^{-1}$): -$NH_2$: 3440 and 3277, C=O: 1681, N-H: 1516 and 1640, and C-N: 1442. $^{1}H$ NMR Spectra: NMR (DMSO, 400 MHz) δ(ppm) 10.64 (s, 2H), 8.105 (d, 2H), 8.152 (t, 1H), and 4.621 (s, 4H). $^{13}C$-NMR (DMSO,100 MHz): δ(ppm) 124, 139, 148, and 162.

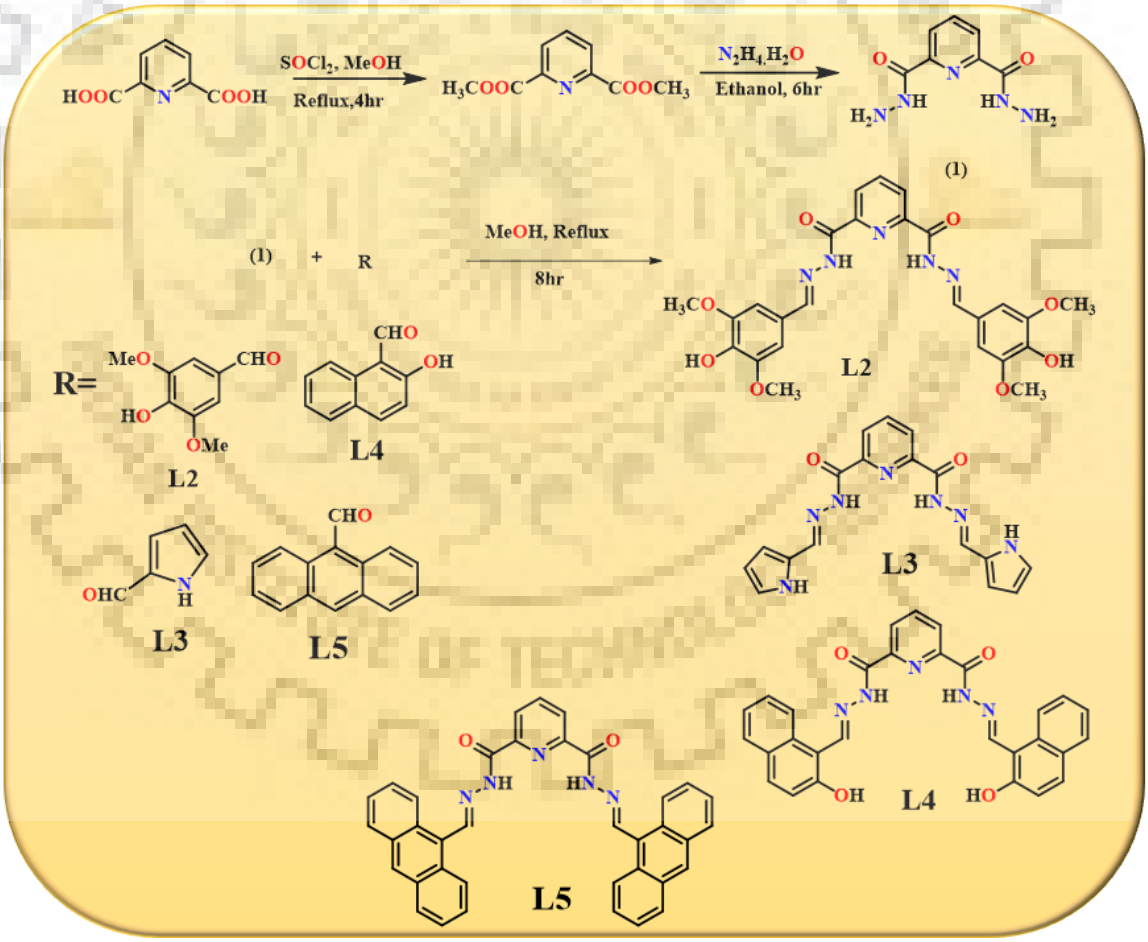


**Scheme 3.1.** Synthesis of **L2** to **L5**.

**Synthesis of Ligand L2 [Bis(4-hydroxy-3,5-dimethoxybenzylidene)pyridine-2,6-dicarbohydrazide]:**

Pyridine-2,6-dicarbohydrazide **(1)** (1mmol, 0.196 g) was refluxed with syringaldehyde (2 mmol, 0.364 g) for 6hr in methanol lead to the formation of ligand **L2**. Light-yellow colored precipitate was occurred (Scheme 3.1). Same procedure was followed for the synthesis of other ligands.

**Yield:** (**74**%). Calc. for $C_{25}H_{25}N_5O_8$: C, 57.36; H, 4.81; N, 13.38 and O, 24.45 and found: C, 55.73; H, 4.784; N, 13.29 and O, 26.196. FT-IR data (KBr, $\nu_{max}/cm^{-1}$): -N-H: 3506, 3279, O-H: 3495, C-H: 2938, C=O: 1678, C-N: 1456, C-O: 1113, and N-H: 1588. UV-Visible (MeOH:$H_2O$, $\lambda_{max}$/nm): 337 nm (n-π*). $^1$H-NMR (DMSO, 400 MHz, δ/ppm) 12.24 (s, 2H), 9.05 (s, 2H), 8.66 (s, 2H), 8.33 (d, 2H), 8.28 (t, 1H), 7.10 (s, 4H), and 3.85 (s, 12H). $^{13}$C-NMR (DMSO, 100 MHz, δ/ppm) 159, 151.37, 151.29, 148.93, 148.73, 138.81, 124, 105.49, 105.34, and 56.10. ESI-mass of **L2** m/z: 546.1865, $(M+Na)^+$.

**Synthesis of Ligand L3: Bis((1H-pyrrol-2-yl)methylene)pyridine-2,6-dicarbohydrazide**

**Yield (50%)**, Calc. for $C_{17}H_{15}N_7O_2$: C, 58.45; H, 4.33; N, 28.07 and O, 9.15 and found: C, 58.59; H, 4.441; N, 28.45 and O, 8.519. FT-IR data (KBr, $\nu_{max}/cm^{-1}$): -N-H: 3389, C-H: 3208, C=O: 1652, C-N: 1416, C-O: 1118, and N-H: 1527. UV-Visible (MeOH, $\lambda_{max}$/nm): 339 nm (n-π*). $^1$H-NMR (DMSO, 400 MHz, δ/ppm) 12.04 (s, 2H), 11.66 (s, 2H), 8.54 (s, 2H), 8.32 (d, 2H), 8.25 (t, 1H), 6.98 (s, 1H), 6.61 (s, 1H), and 6.19 (s, 1H). $^{13}$C-NMR (DMSO, 100MHz, δ/ppm) 159.36, 148.91, 143.36, 140.31, 127.30, 125.53, 123.49, 114.57, and 109.98. ESI-mass of **L3** m/z: 372.4048, $(M+Na)^+$.

**Synthesis of ligand L4 bis((2-hydroxynaphthalen-1-yl)methylene)pyridine-2,6-dicarbohydrazide**

**Yield (60%)**, Calc. for $C_{29}H_{21}N_5O_4$: C, 69.18; H, 4.20; N, 13.91 and O, 12.71 and found: C, 69.39; H, 3.860; N, 14.34 and O, 12.41. FT-IR data (KBr, $\nu_{max}/cm^{-1}$): -O-H: 3435, -N-H: 3236, C-H: 3054, C=O: 1680, C-N: 1465, C-O: 1190, and N-H: 1575. UV-Visible (MeOH, $\lambda_{max}$/nm): 317, 330 (n-π*), 372 nm (n-π*). $^1$H-NMR (DMSO, 400 MHz, δ/ppm)

12.59 (s, 2H), 12.51 (s, 2H), 9.81 (s, 2H), 8.53 (d, *J* = 8.6 Hz, 2H), 8.40 (d, *J* = 6.9 Hz, 2H), 8.36 – 8.31 (m, 1H), 7.99 (d, *J* = 9.0 Hz, 2H), 7.94 (d, *J* = 7.9 Hz, 2H), 7.68 (t, *J* = 7.6 Hz, 2H), 7.47 (t, *J* = 7.4 Hz, 2H), and 7.29 (d, *J* = 8.9 Hz, 2H). $^{13}$C-NMR (DMSO, 100MHz, δ/ppm) 159.39, 158.81, 149.72, 148.36, 133.78, 132.27, 129.62, 128.50, 128.39, 126.10, 124.29, 121.66, 119.41, and 109.17. ESI-mass of **L4** m/z: 526.1512, $(M+Na)^+$.

**Synthesis of ligand L5: Bis(anthracen-9-ylmethylene)pyridine-2,6-dicarbohydrazide Yield (50%)**, Calc. for $C_{35}H_{25}N_5O_2$: C, 77.74; H, 4.41; N, 12.25 and O, 5.60 and found: C, 77.59; H, 4.31; N, 12.05 and O, 6.05. FT-IR data (KBr, $\nu_{max}/cm^{-1}$): -N-H: 3449, C-H: 3047, C=O: 1679, C-N: 1533, and C-O: 1165. UV-Visible (MeOH, $\lambda_{max}$/nm): 386 nm (n-π*), $^1$H-NMR Spectra: NMR (DMSO, 400 MHz) δ(ppm) 12.64 (s, 2H), 9.97 (s, 2H), 8.91 (d, *J* = 8.8 Hz, 4H), 8.74 (s, 2H), 8.44 (d, *J* = 7.3 Hz, 2H), 8.39 – 8.33 (m, 1H), 8.15 (d, *J* = 8.3 Hz, 4H), 7.66 – 7.60 (m, 4H), and 7.60–7.54 (m, 4H). $^{13}$C-NMR (DMSO, 100MHz) δ(ppm) 159.91, 149.96, 148.86, 131.51, 130.64, 130.37, 129.64, 127.90, 126.20, 125.55, and 125.40. ESI-mass of **L5** m/z: 594.1910, $(M+Na)^+$.

### 3.2.3 X-ray Crystallography

Structural measurement of single crystal of **L4** and **L5** were performed on a Bruker Kappa Apex four circle- 5 CCD diffractometer. Single crystal of **L4** and **L5** compounds, which were suitable for X-ray diffraction, were developed in DMSO that mounted on nylon 7 Cryoloop. SMART/SAINT software was used for data reduction. Graphite monochromatic Mo*Kα* radiation (0.7107 A$^o$) at 298 K was used in intensity data collection. Structural solutions, refinement and data collection were collected using the SHELXTL program as a direct method. Images and hydrogen bonding interaction were constructed of the crystal lattice with mercury software. The refinement parameters of **L4** and **L5** are shown in Table 3.1. The 3*3 packing interaction representations of **L4** and **L5** ligands is shown in figure 3.2 (a) and (b). The Crystallographic data for both compounds has been deposited with Cambridge Crystallographic Data Centre (the deposition numbers of **L4** and **L5** are **CCDC 1577825** and **CCDC 1552443**) (Figure 3.1).

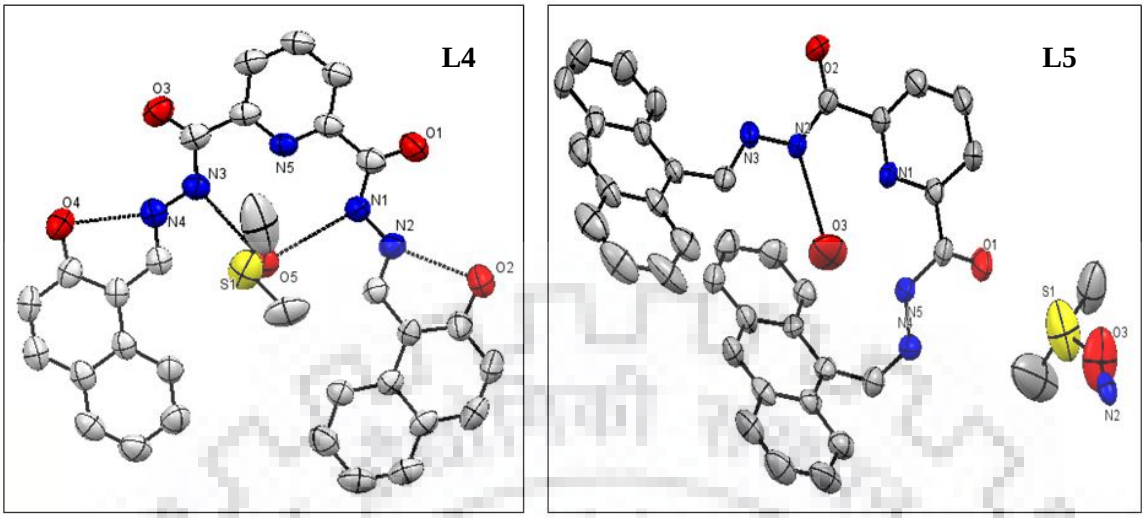


**Figure 3.1.** ORTEP diagram of **L4** and **L5** molecule with hydrogen bonding interaction.

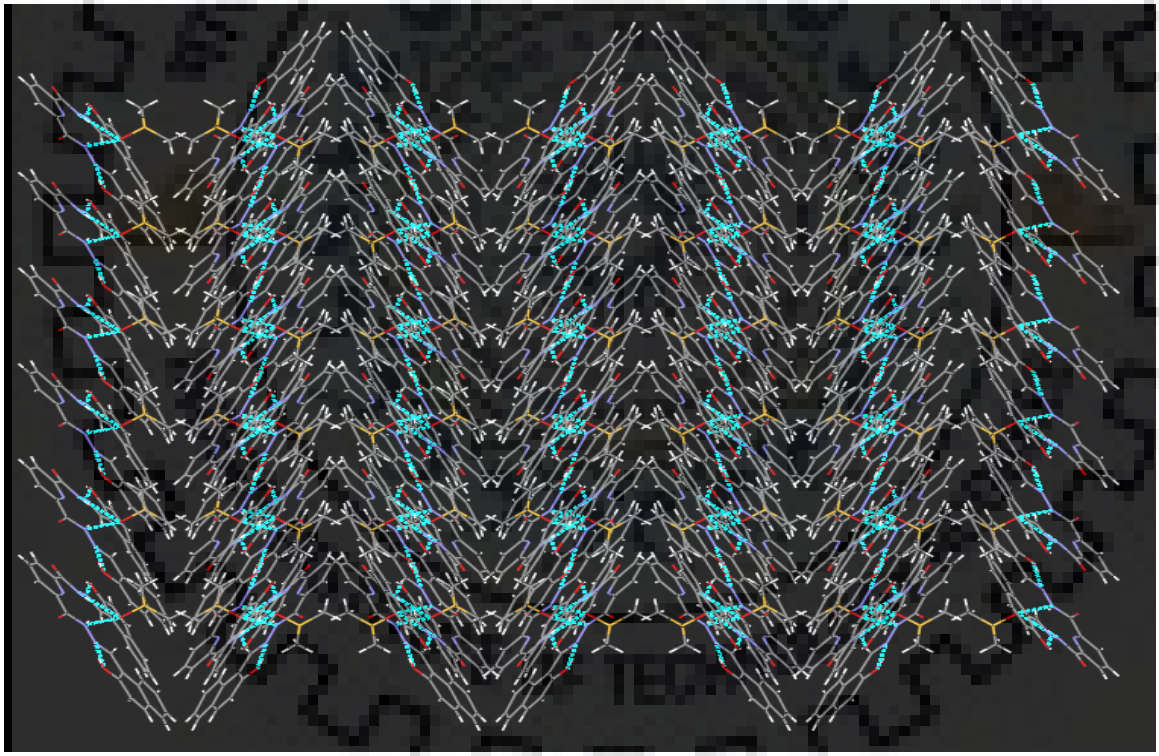

**Figure 3.2(a).** The 3*3 packing diagram of **L4** along ‘a’ axis with hydrogen bonding interaction.

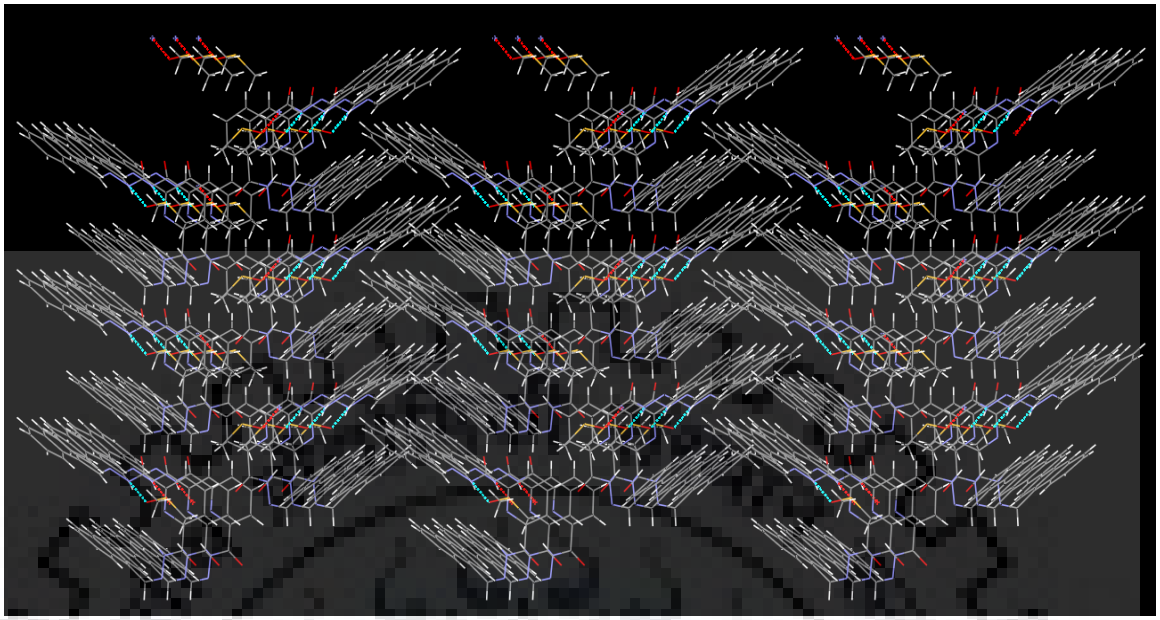

**Figure 3.2(b).** The 3*3 packing diagram of **L5** along 'a' axis with hydrogen bonding interaction.

**Table 3.1:** Crystal data and structure refinement parameters of **L4** and **L5**.

| | **L4** | **L5** |
|---|---|---|
| Empirical formula | C31 H27 N5 O5 S | C39 H31 N5 O3 S |
| Formula weight | 581.64 | 649.75 |
| Crystal system | Monoclinic | Monoclinic |
| Space group | C 2/c | P 21 |
| a/Å | 30.297 | 10.0344 |
| b/Å | 12.301 | 8.1177 |
| c/Å | 16.640 | 20.1951 |
| β/Å | 112 | 97.782 |
| $V$/Å$^3$ | 5750 | 1629.87 |
| $Z$ | 8 | 2 |

| | | |
|---|---|---|
| $D_{calc}$(g cm$^{-3}$) | 1.344 | 1.324 |
| $\mu/mm^{-3}$ | 0.162 | 0.147 |
| $\Theta$ range/$^{o}$ | 0.926 - 29.158 | 2.408 – 28.314 |
| Reflections collected | 7191 | 8135 |
| Independent reflections | 3666 | 2584 |
| Parameters | 403 | 449 |
| GOF ($F^2$) | 1.040 | 0.794 |
| $R_1$; $wR_2$[I>2 sigma(I)] | 0.0863 – 0.2384 | 0.0603 – 0.1320 |
| $R_1$; $wR_2$ (all data) | 0.1561 – 0.2939 | 0.1767– 0.1593 |

## 3.3 RESULTS AND DISCUSSION

### 3.3.1 The binding mode of Ligands with Copper Ion

The binding of copper with these four ligands is evidenced by the FT-IR spectra and mass spectra. The FT-IR spectra of **L2** and **L2** with $Cu^{2+}$ ions showed that the fingerprint reason with $Cu^{2+}$ ions was different to the **L2** vibrational spectra. There are some bands present at 3279 (–NH), 1678 (-C=O), and other bands, which disappeared upon complexation with the $Cu^{2+}$ ions. New bands generated at 1627, 1434, 1328 cm$^{-1}$ supports that the complexation occurred with C=O, -NH. Similarly, the vibrational spectrum of **L3** with $Cu^{2+}$ ions was different to that of **L3**. In the vibrational spectra of complexed and decomplexed **L3**, bands disappeared at 3208 (pyrole -NH), 3383 (-NH), 1652 (-C=O), 1641, 1527 and band at 1416 was shifted to 1441 cm$^{-1}$ and new bands are generated at 1609, 1035 cm$^{-1}$ that confirmed the complexation with $Cu^{2+}$ ion.

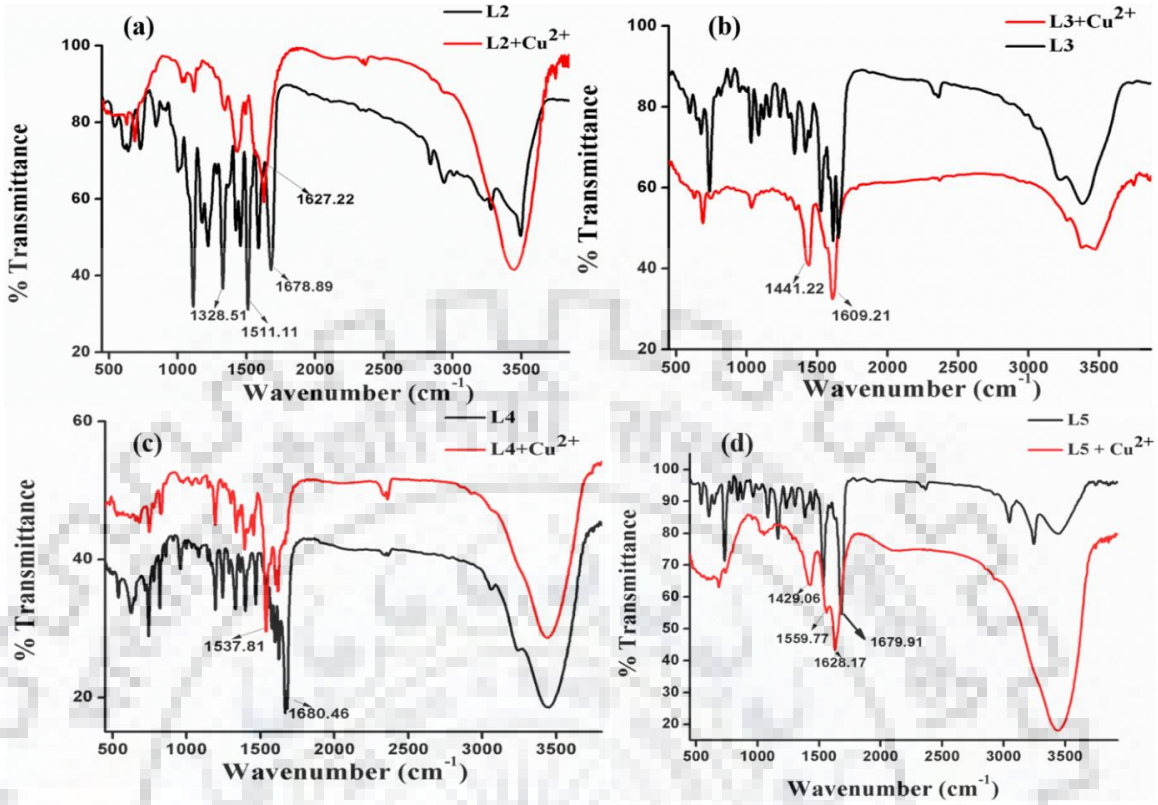


**Figure 3.3.** (a) FT-IR Spectrum of ligand **L2** and **L2+ $Cu^{2+}$**, (b) FT-IR Spectrum of ligand **L3** and **L3+ $Cu^{2+}$**, (c) FT-IR Spectrum of ligand **L4** and **L4+ $Cu^{2+}$**, (d) FT-IR Spectrum of ligand **L5** and **L5+ $Cu^{2+}$.**

The vibrational spectra of **L4** also showed that the bands disappeared on metalation with $Cu^{2+}$ ions *i.e.* 3232, 3062, 1680, 1666, 1578 $cm^{-1}$, and some are shifted from 1624 to 1618 $cm^{-1}$, 1598 to 1602 $cm^{-1}$, 1548 to 1537 $cm^{-1}$. This was due to the $Cu^{2+}$ ions combining with –NH, -C=O and hydroxyl group of the ligands. There were new bands at 3451, 1454 $cm^{-1}$ which appeared after the binding with $Cu^{2+}$ ions. Like the **L4** ligand, the FT-IR spectra of **L5** with $Cu^{2+}$ ion the obscured bands were at 3445 (-NH), 3247, 1682 (-C=O), 1538,1450 $cm^{-1}$, and new bands were visible at 3448, 1632, 1561, 1425 $cm^{-1}$ This affirmed metalation of all four ligands with $Cu^{2+}$ ions. Figure 3.3 represents the binding mode of ligand with copper ions and ligand in FT-IR spectrum. The binding of $Cu^{2+}$ ion with ligands was also confirmed by mass spectrometry [25]. The mass of **L2** with $Cu^{2+}$ ion is 926.68 which represented 1:2 stoichiometry, *i.e.* 2 $Cu^{2+}$ with one **L2**. The mass of **L3** with copper ion showed the 1:3 stoichiometry, *i.e.* 570.86. Similarly, **L4** also displayed 1:2 stoichiometry in its mass spectrum, which was 701.41.

**L5** also exposed 1:2 stoichiometry with $Cu^{2+}$ ion, the mass was 815.51. It was demonstrated in the Figure 3.4, 3.5, 3.6, and 3.7 for **L2**, **L3**, **L4**, and **L5** respectively. Binding mode with copper ion represents by the figure 3.8.

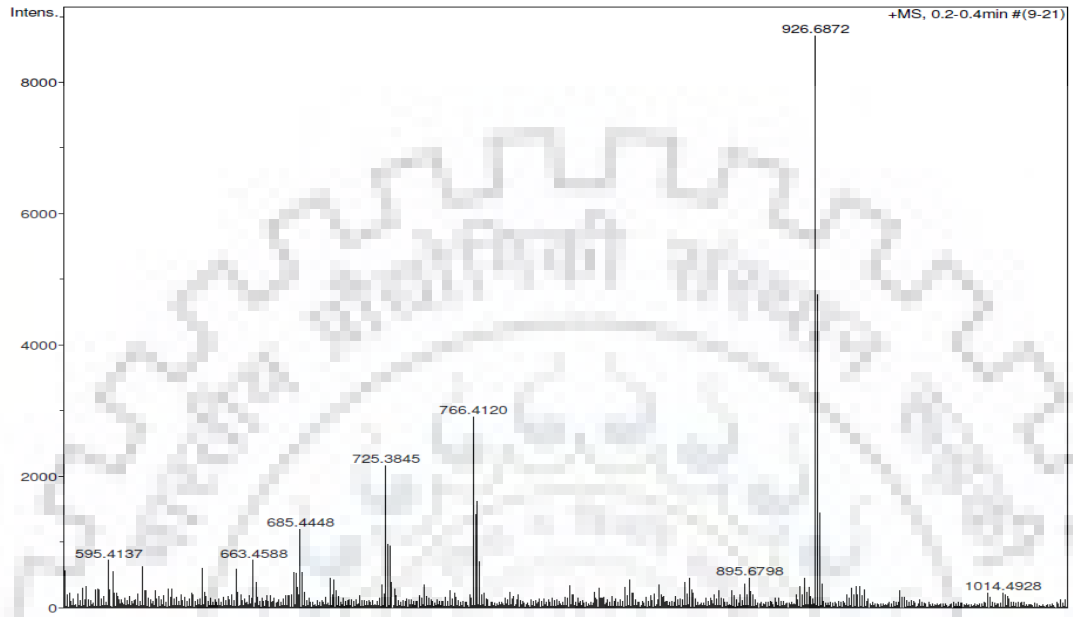


**Figure 3.4.** Mass Spectrum of ligand **L2** with copper ion **($L2+2Cu^{2+}+4ACO^{-}+H_2O+Na^{+}$).**

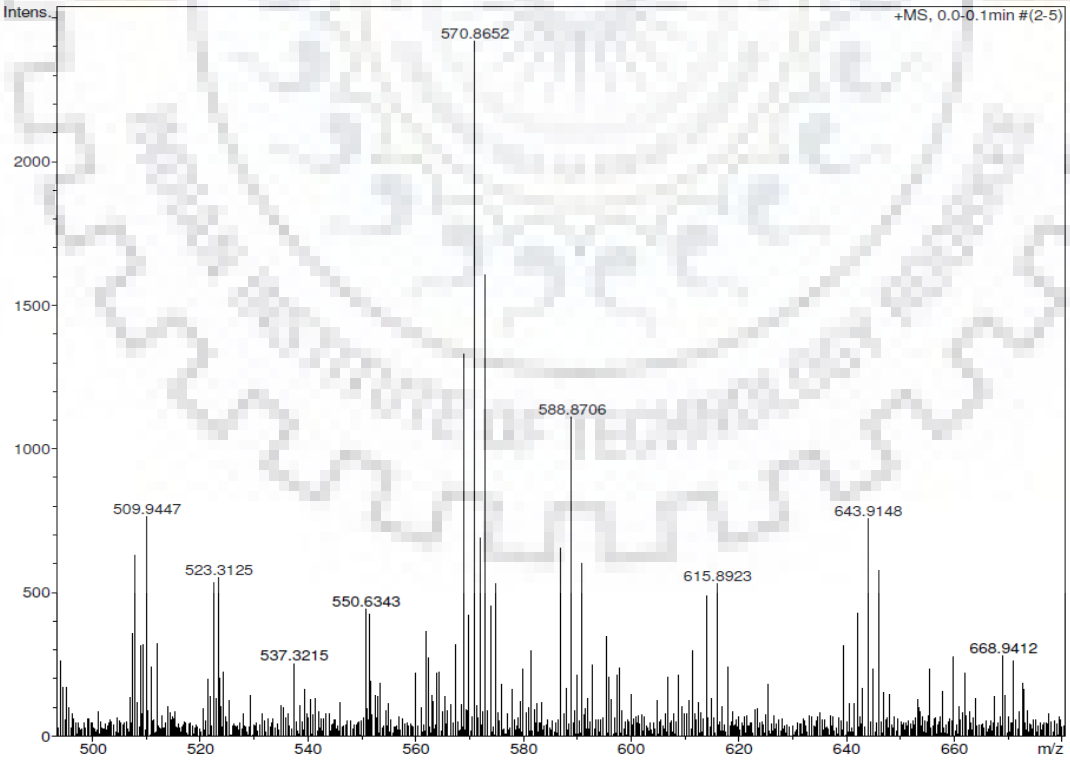


**Figure 3.5.** Mass Spectrum of ligand **L3** with copper ion **($L3+3Cu^{2+}+2H_2O+H^{+}$).**

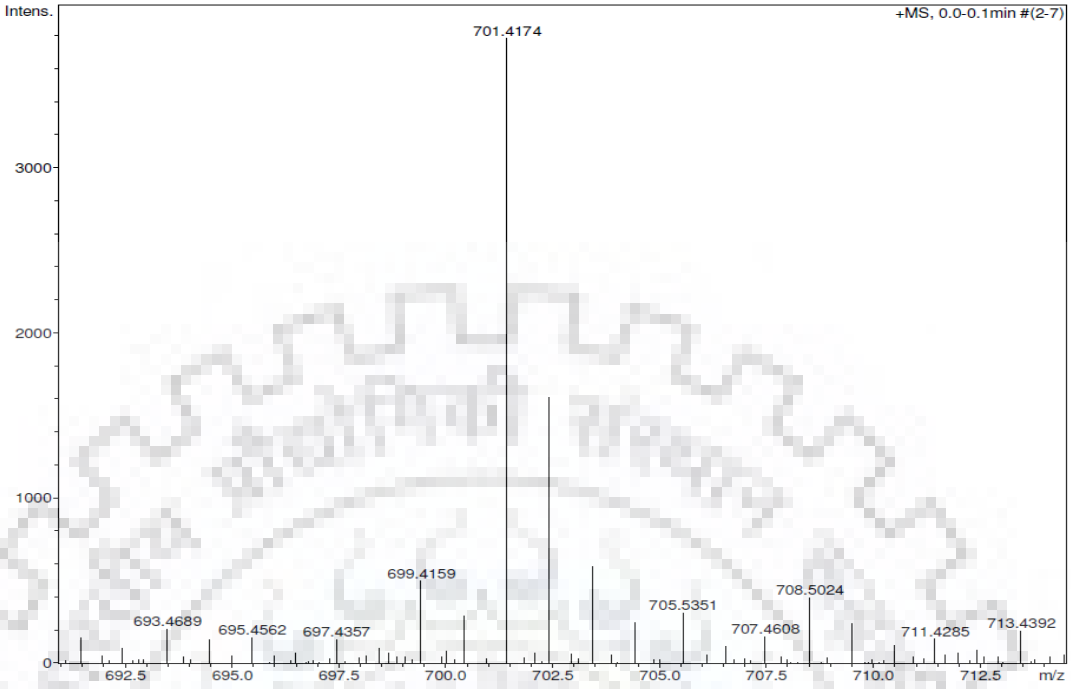


**Figure 3.6.** Mass Spectrum of ligand **L4** with copper ion **($L4+2Cu^{2+}+ CH_3COO^-$).**

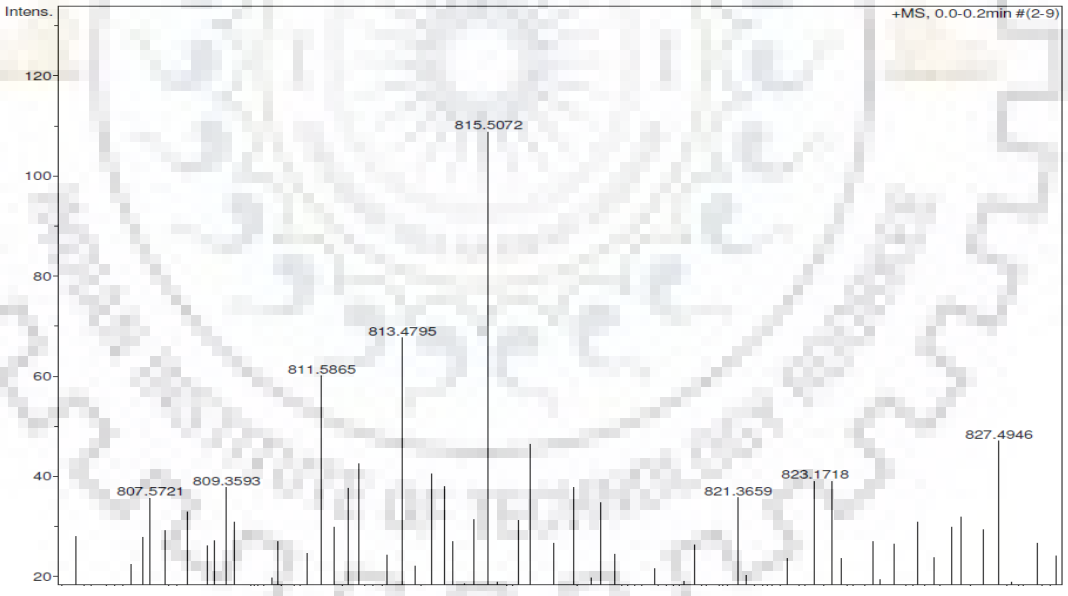


**Figure 3.7.** Mass Spectrum of ligand **L5** with copper ion **($L5+ 2Cu^{2+}+ 2ACO^-+ 1H^+$).**

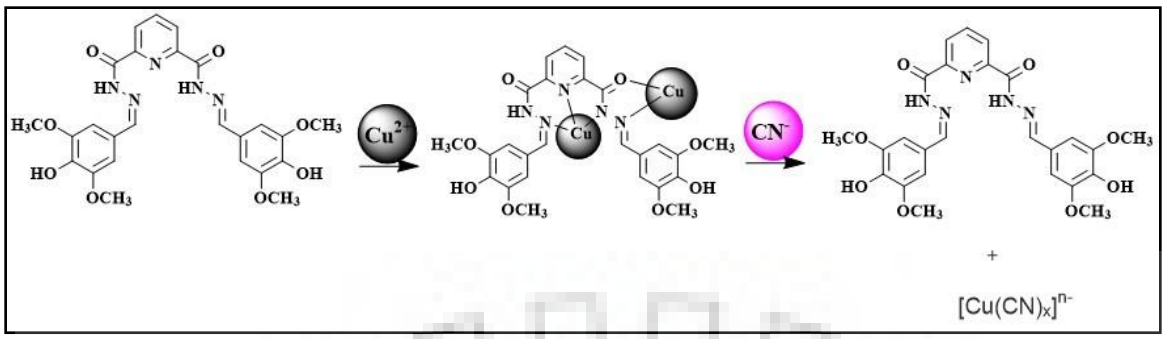


**Figure 3.8.** Binding mode of **L2** with copper ion with metal displacement *via* cyanide ion.

### 3.3.2 Photo-physical properties

The photophysical properties of all four ligands **L2**, **L3**, **L4** and **L5** were recorded *via.* UV-vis absorption and emission spectroscopy in MeOH: $H_2O$ (9:1) as a solvent. Ligand **L2** displayed one broad absorption band at 337 nm due to π - π* transition from the conjugated system of the ligand. Similarly, **L3** showed a broad absorption peak at 339 nm that was most likely again due to π-π* transition. **L4** showed three absorption band at 316, 330, and 372 nm which were ascribed to n - π* and π - π* transitions. Similarly, **L5** displayed two bands at 379 and 386 nm, corresponding to n - π* and π - π* transition. **L2**, **L3**, **L4** and **L5,** when investigated with a pool of different metal ions such as $Mg^{2+}$, $Fe^{3+}$, $Na^{+}$, $Li^{+}$, $Ca^{2+}$, $Ba^{2+}$, $Cr^{3+}$, $Mn^{2+}$, $Co^{2+}$, $Ni^{2+}$, $Cu^{2+}$, $Zn^{2+}$, $Al^{3+}$, $Hg^{+}$, $Hg^{2+}$ and $V^{5+}$, displayed the most expressive binding with $Cu^{2+}$ ions, as recognized from the modulation of absorption spectra. On addition of $Cu^{2+}$ (5 mM) salt in **L2** (20 μM) the absorption profile was shifted from 337 to 399 nm towards red shifting due to the d-d transition between $Cu^{2+}$ and Ligand. Similarly, the absorption spectrum of **L3** also shifted to red shift from 339 to 450 nm on addition of copper salt, among other metal salts. Likewise, the absorption profile of **L4** and **L5** were shifted from 372 to 447 nm and 386 to 395 nm respectively, after interaction with $Cu^{2+}$ ions, but with **L5** there was a new band which appeared at 322 nm. This demonstrated the interaction with $Cu^{2+}$ ions because of d-d transition of $Cu^{2+}$ ions with ligands and π-π interaction between the aromatic rings (Figure 3.10). The stoichiometry of $Cu^{2+}$ ions with **L2** was determined by the addition of mole fraction of $Cu^{2+}$ ion in the ligand **L** (**L2**, **L3**, **L4**, **L5**) by plotting Job's plot. The 1:2,

1:3, 1:2, 1:2 stoichiometry was presented for **L2**, **L3**, **L4**, **L5** respectively (Figure 3.9 (a), (b), (c), (d)).

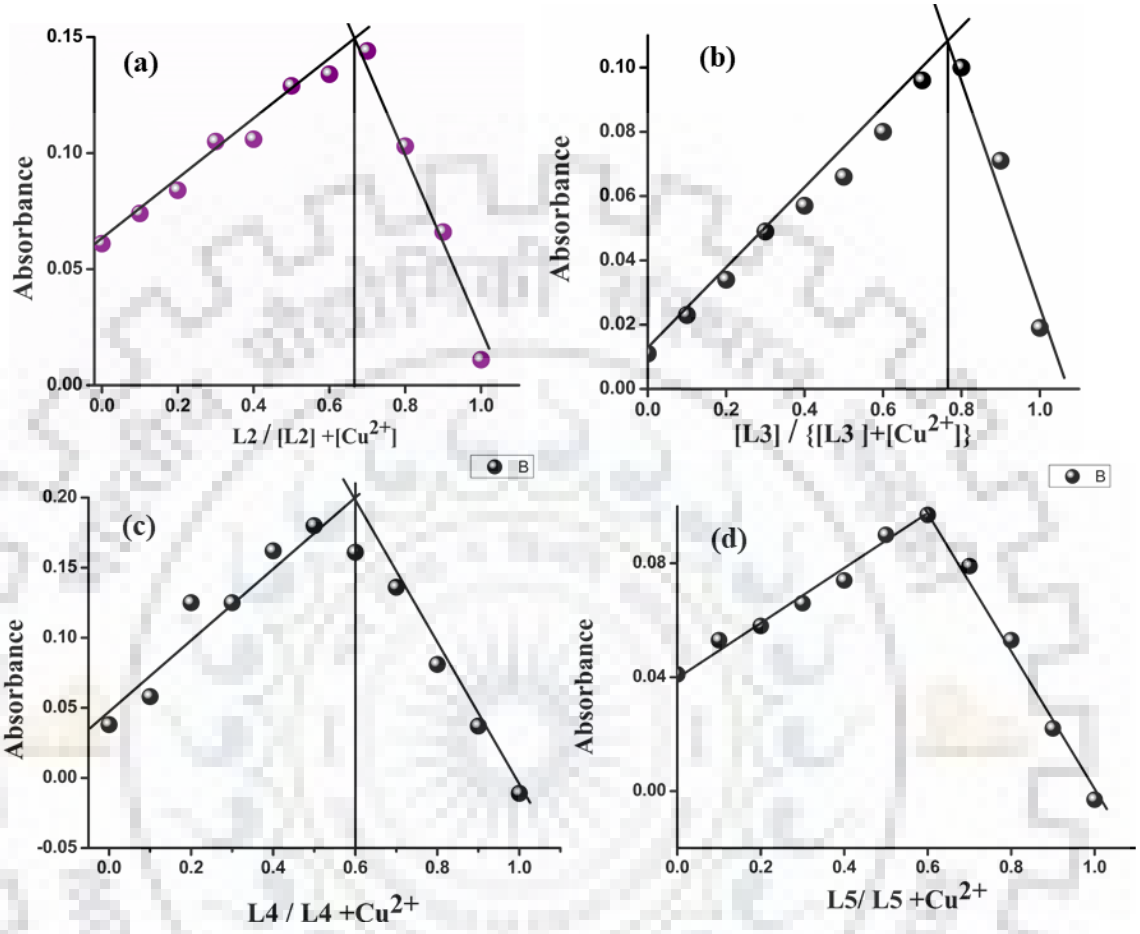


**Figure 3.9.** Demonstrated the Job's plot with the mole fraction of ligands (**L2**, **L3**, **L4** and **L5**) and copper ion.

Further, the titration experiments for the four ligands with 20 μM concentration were performed with gradual addition of $Cu^{2+}$ ions and absorption spectra were recorded after each addition. The consecutive addition of $Cu^{2+}$ ions to **L2** resulted in an increase in the absorbance at 399 nm with two isosbestic points at 295 and 370 nm. The new absorption band originating at 399 nm was due to d-d transition of copper complex, as shown in Figure 3.11.

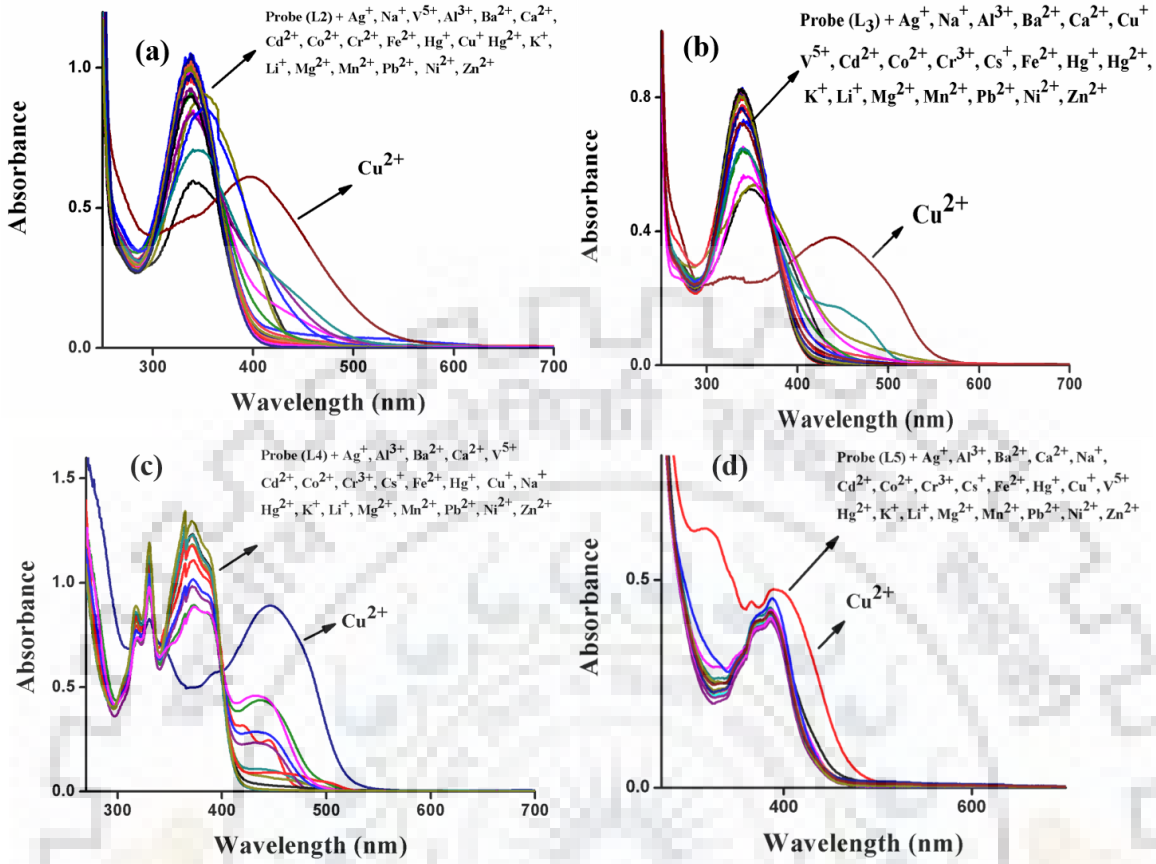


**Figure 3.10.** Selectivity spectra of **L2** to **L5** with 20 μM solution of ligand with 5mM of metal ion solutions by absorption spectra in that was selective for copper ion among other metal ion.

The **L3** was investigated with the same metal ions which were used for **L2**, and a significant change in absorbance was observed. The titration experiment with **L3** was implemented to validate the reproducibility of the binding of $Cu^{2+}$ ions with **L3**. The addition of consecutive amounts of $Cu^{2+}$ to **L3** lead to an increase in the absorbance band at 450 nm. The absorbance band at 450 nm correlates to d-d transition of the copper complex and is shown in Figure 3.11. Similarly, titration experiments were also implemented to confirm the binding of $Cu^{2+}$ with **L4** and **L5**. It was confirmed by the graphs that the intensity of absorbance band at 447 nm with **L4** was increased by subsequent addition of $Cu^{2+}$ to ligand solution and with **L5** the absorbance band was also increased at 395 nm and 322 nm with consecutive addition of $Cu^{2+}$ ion (Figure 3.11).

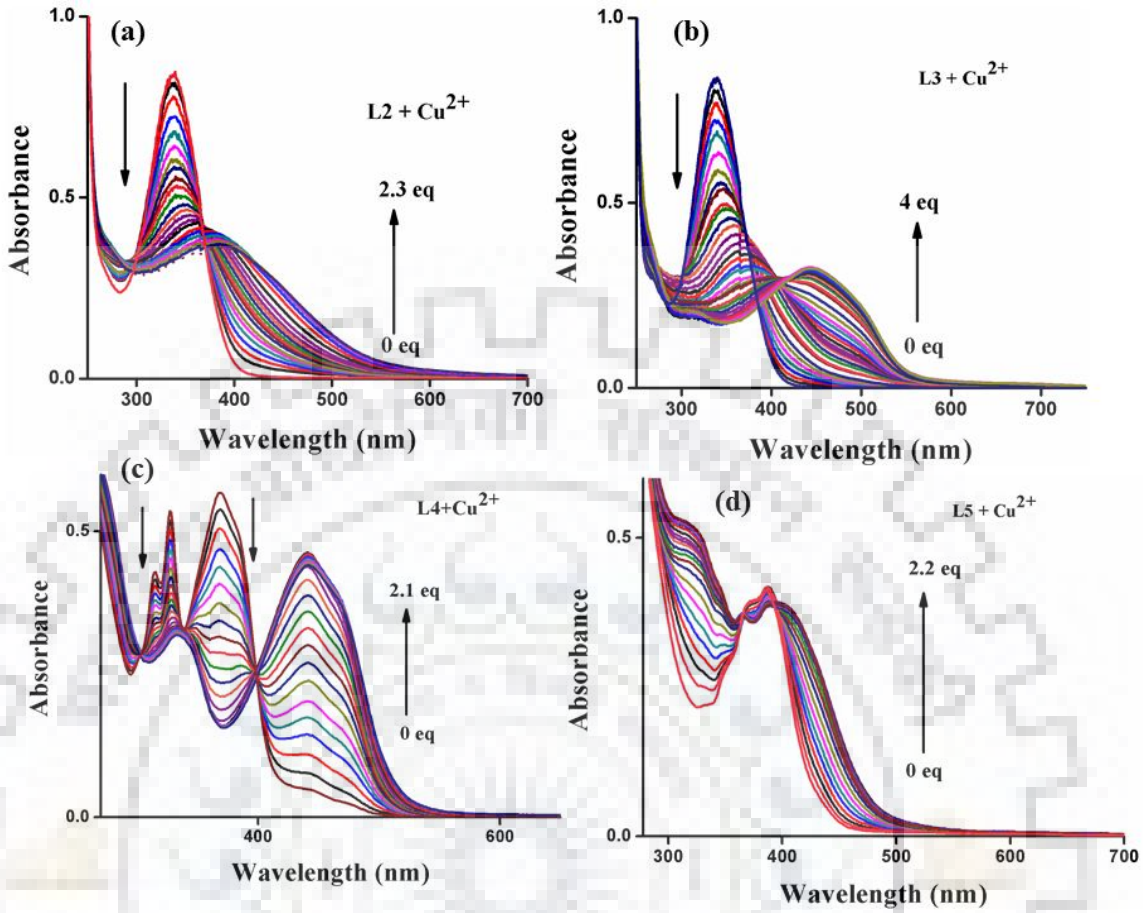


**Figure 3.11.** Titration experiment of **L2**, **L3**, **L4** and **L5** (20 μM) with gradual addition of $Cu^{2+}$ ion.

The selectivity and sensitivity of $Cu^{2+}$ ion among various metal ions were also confirmed using emission studies of all four ligands. The $Cu^{2+}$ ions were selective for all four ligands and there was quenching in the fluorescence intensity due to photoinduced electron transfer mechanism which is presented in the Figure 3.12.

Furthermore, the titration experiment performed with a gradual addition of $Cu^{2+}$ to a 10 μM solution of all four ligands showed the interaction of copper ions (10μM) with all ligands and the quenching in fluorescence intensity was prominent in titration experiments due to the photoinduced electron transfer from nitrogen atom as shown in Figure 3.14. Moreover, competitive experiments were also performed with $Cu^{2+}$ ion in the presence of other metals ions with all four ligands, and the results of these showed that there was no interference from the other metal ions in the selectivity of $Cu^{2+}$ ion. The

results of these competitive studies with $Cu^{2+}$ ions, in which blue bar represents the ligand + metal ions and red bar show ligand+ $Cu^{2+}$+ other metal ions are shown in the Figure 3.13 (a), (b), (c), (d). Using the emission spectra, the S-V plot shows the static nature of quenching by addition of $Cu^{2+}$ (Figure 3.14).

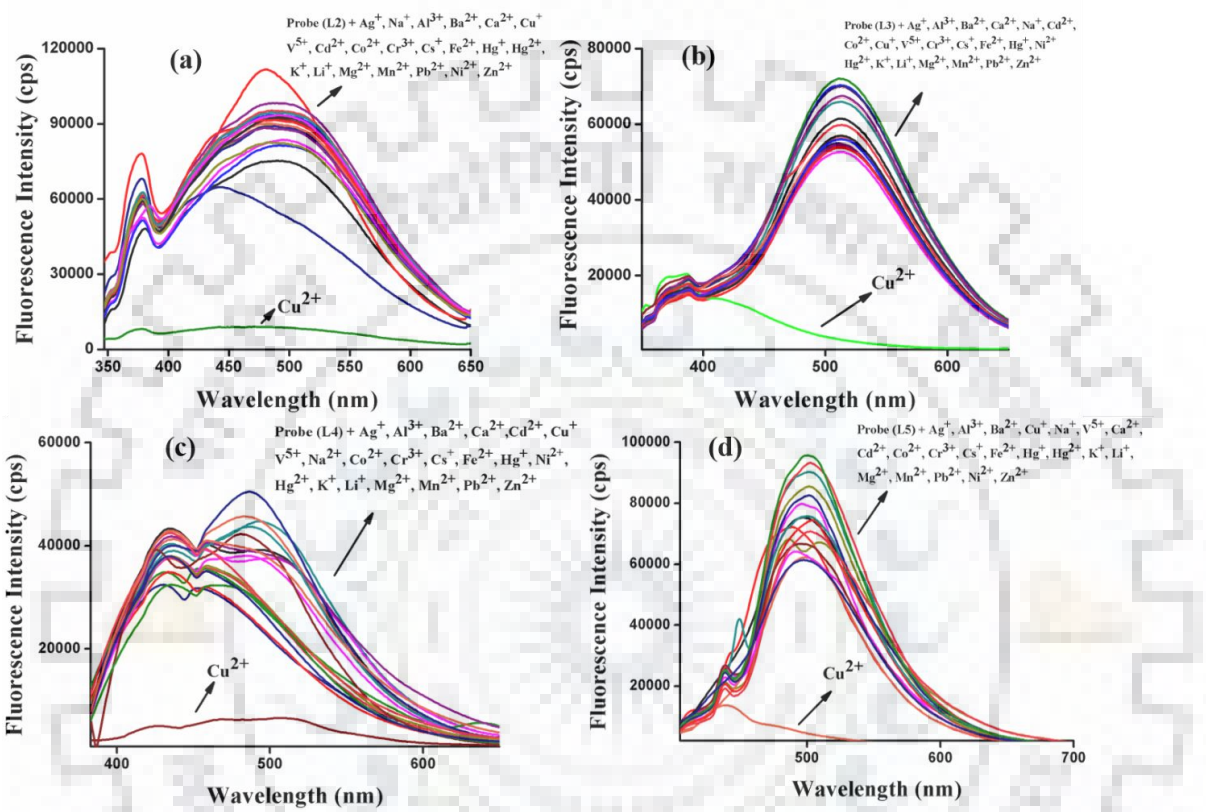


**Figure 3.12.** The selectivity of $Cu^{2+}$ ion with all four ligands where (a) shows the selectivity with **L2** ligand, (b) shows selectivity with **L3** ligand, (c) represents the selectivity of **L4** ligand and (d) shows the selectivity with **L5** ligand.

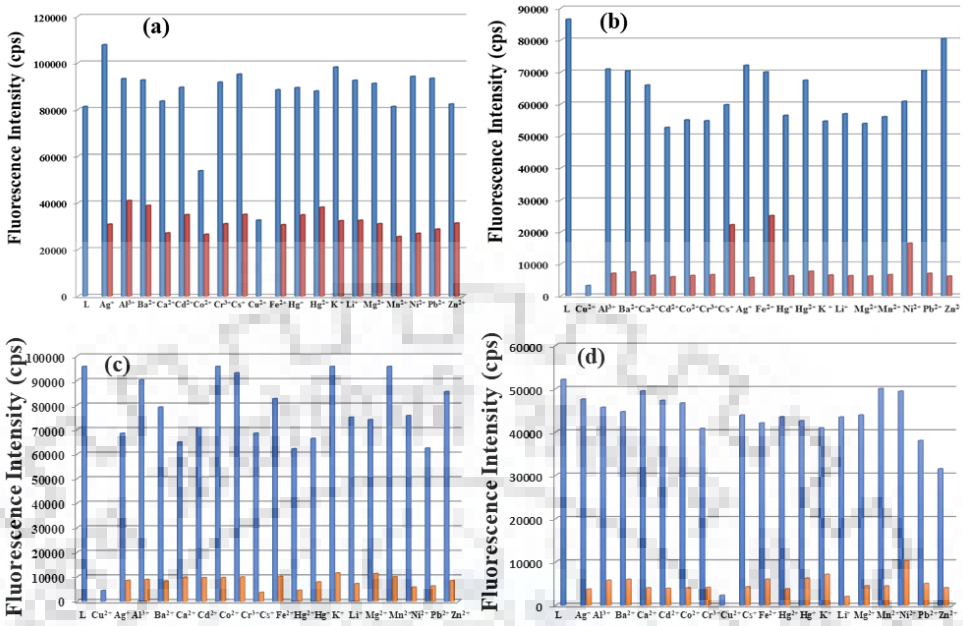


**Figure 3.13.** The (a), (b), (c) and (d) represents the competitive experiment of all four ligands **L2, L3, L4** and **L5** respectively with various metal ions in the presence of copper ion.

**Table 3.2:** Photophysical properties, binding constant and limit of detection.

| | **Absorbance maxima** | **Emission maxima** | **Stoichiometry** | **Stock shift** | **Binding constant (log *β*)** | **LOD** |
|---|---|---|---|---|---|---|
| **L2** | 337(π-π*) | 494 nm | - | - | - | - |
| **L3** | 339 (π-π*) | 514 nm | - | - | - | - |
| **L4** | 316, 330, 372 (π-π*) & (n-π*) | 485 nm | - | - | - | - |
| **L5** | 379, 386 (π-π*) & (n-π*) | 499 nm | - | - | - | - |
| $Cu_2$(**L2**) | 399 | Fluorescence quenching at 494 nm | 1:2 | 62 nm | 8.866 | 0.12 µM |
| $Cu_3$(**L3**) | 450 | Fluorescence quenching at 514 nm | 1:3 | 111 nm | 17.645 | 0.10 µM |
| $Cu_2$(**L4**) | 447 | Fluorescence quenching at 485 nm | 1:2 | 72 nm | 11.145 | 0.097 µM |
| $Cu_2$(**L5**) | 395 | Fluorescence quenching at 499 nm | 1:2 | 16 nm | 6.45 | 0.098 µM |

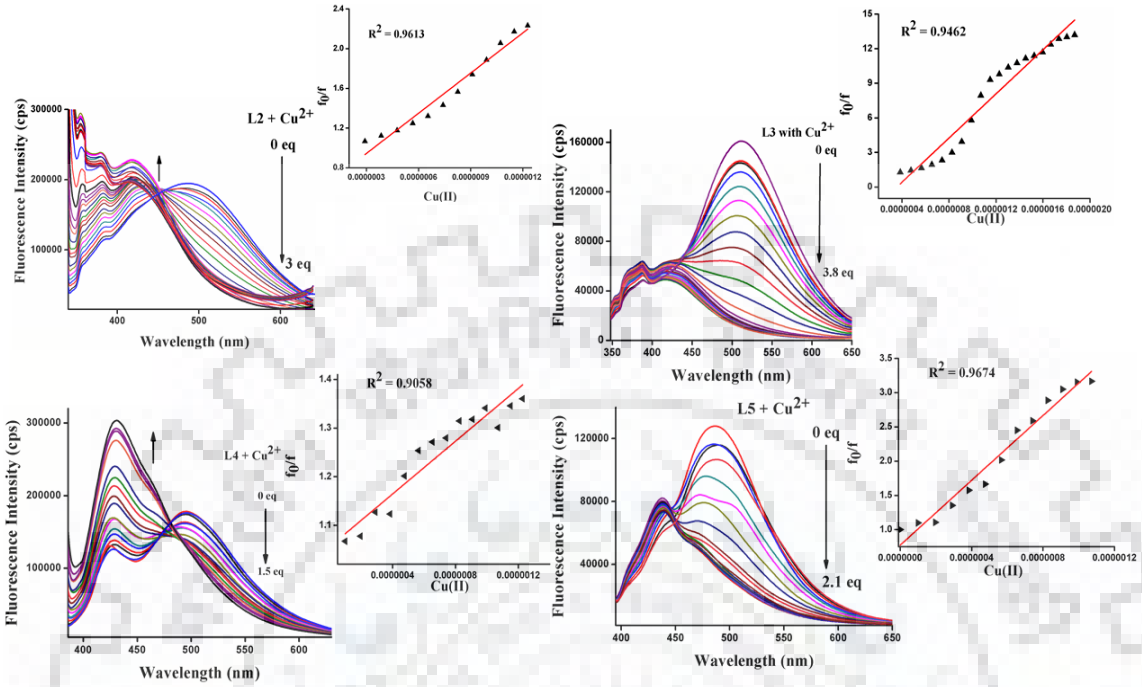


**Figure 3.14.** These all figures represent the titration experiment by emission spectra of **L2** to **L5** with copper ion at excitation wavelength 340 nm, 348 nm, 383nm and 394 nm respectively and inset shows the S-V curve of **L2** to **L5**.

The Hill plot [26] has been plotted between $\log(Cu^{2+})$ and $\log(I - I_{min})/(I_{max} - I)$ for binding constant where I represents the intensity by the gradual addition of $Cu^{2+}$ ion, $I_{min}$ represents intensity without the addition of $Cu^{2+}$ ions, $I_{max}$ shows the intensity on complete addition of copper ions in the solution of ligands and the value of association constant ($K_a$) for **L2**, **L3**, **L4**, **L5** (log $\beta$) was 8.866, 17.645, 11.145, and 6.45 respectively. Figure 3.15 shows the Hill Plot of all four ligands with Copper ions. The limit of detection (LOD) of **L2** to **L5** were 0.12, 0.10, 0.097 and 0.098 μM respectively, which are all less than the permissible limit of copper ions given by the WHO, all data was summarized in Table 3.2. The Figure 3.16 (a), (b) (c) (d) shows the plots of limit of detection. Comparison with previous reported data is summarized in Table 3.3.

**Table 3.3:** Comparison table with previously reported data.

| **Previous literature** | **Chemosensor** | **Detection limit of copper ion** | **Applications** | **Binding constant** | **L+$Cu^{2+}$ As Anion sensor** |
|---|---|---|---|---|---|
| Sensors and Actuators B 211 (2015) 498–506. [27] | Maleonitrile based | 7.3 μM | - | $2.8\times10^{4}\ M^{-1}$ | - |
| Tetrahedron letters 48 (2007) 5525-5529. [28] | Dioxotetraamine and 1,8-naphthalimide based | 0.3 μM | - | - | - |
| Tetrahedron 70 (2014) 2822-2828. [29] | Quinolin based | $1.4 \times 10^{-5}$ M | - | $3.3\times10^{3}\ M^{-1}$ | Selective for $CN^-$ ion with 0.57 μM detection limit |
| Sensors and Actuators B 211 (2015) 325–331. [30] | Rhodamine B-based | $1.8 \times 10^{-7}$ M | Real water analysis, Paper strips test | $2.28 \times 10^{5}\ M^{-1}$ | - |
| Tetrahedron 68 (2012) 9076-9084. [31] | Acenaphthene based | 2 μM | | $1.18\times10^{5}\ M^{-1}$ | Selective for $CN^-$ ion with 1 μM detection limit |
| Anal. Methods, 9 (2017) 618-624. [32] | Picolinamide based | 0.67 μM | Real Water analysis | - | - |
| present work | Pyridine dicarbohydrazided based | 0.09 to 0.12 μM | Logic gate behavior, real water analysis | 6.45 to 17.645 | Selective for $CN^-$ ion with 0.31 and 0.53 μM detection limit |

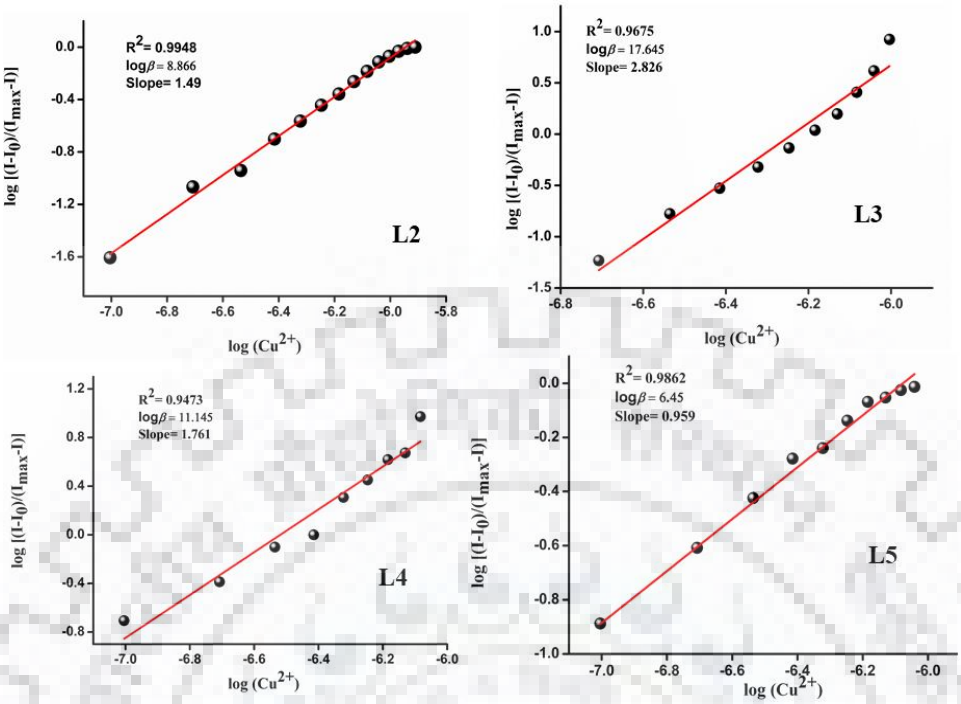


**Figure 3.15.** The Hill plot of all four ligands **L2**, **L3**, **L4** and **L5**.

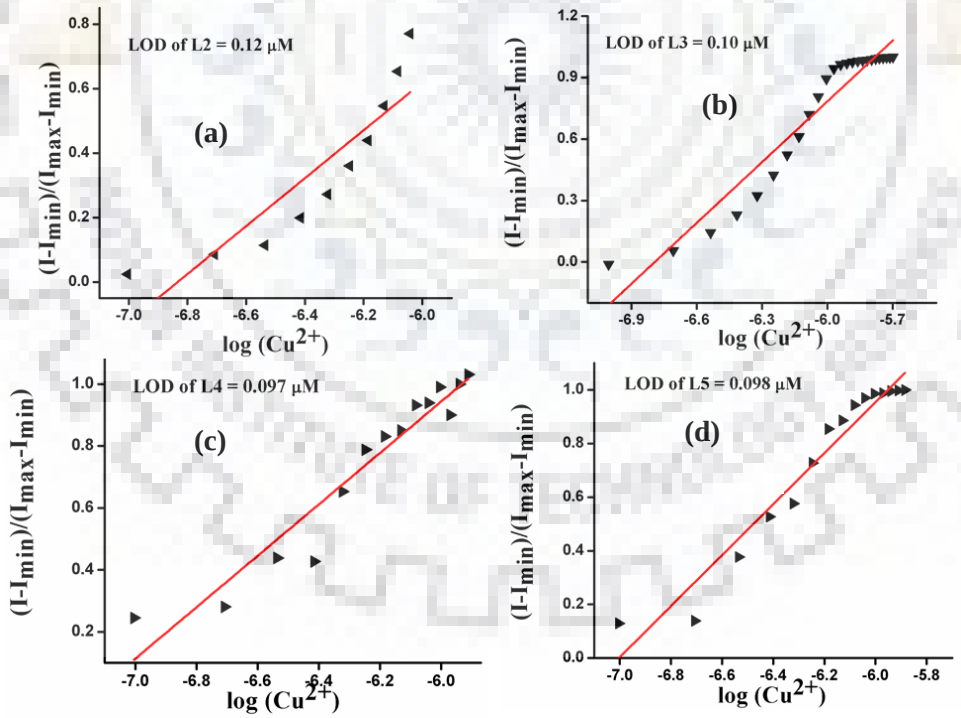


**Figure 3.16.** (a) Limit of detection plot for copper ion with **L2**, (b) Limit of detection plot for copper ion with **L3**, (c) Limit of detection plot for copper ion with **L4**, (d) Limit of detection plot for copper ion with **L5**.

### 3.3.3 Electrochemistry

The redox behavior of all four ligands and their metal complex with copper ions was measured in distilled methanol in the potential range of +2.0 to -2.0 V and electrochemical data is abridged in the Table 3.4. All the copper complexes have shown one quasi-reversible peak in the range -0.9 to -1.2 V. The $Cu^{2+}$ complex with **L2** a cathodic peak ($E_{pc}$) at -1.194 and an anodic peak ($E_{pa}$) at 0.57 V, as represented in the figures, that was attributed to $Cu^{2+}$/Cu The other copper complexes with other ligands **L3**, **L4** and **L5** also displayed cathodic peaks at -1.190, -1.080 and -1.003 and anodic peaks at 0.57, 0.67, 0.935 V, respectively. Aside from these potentials, the current was also simultaneously increased in the anodic region. The redox potential of all copper complexes was negative, due to the presence of a conjugated aromatic ring [33]. In the positive potential of all of the copper complexes, oxidation peaks in the range of 0.57 to 1.49 V, represented Cu/$Cu^{2+}$. However, all four ligands showed a positive potential in the range of 0.0922 to 1.54 V and negative potential in the range of -0.58 to 1.50 V which was diminished after complexation with copper ions. The new potential peaks were different to the other potentials due to complexation of copper ions with the ligands. The Figures 3.17 shows all of the changes resulting from the presence of the $Cu^{2+}$ ion from decomplexation to complexation.

**Table 3.4:** Electrochemical behavior of all ligands and their copper complexes.

| | **I Oxidation peak** | **II Oxidation peak** | **I Reduction Peak** | **II Reduction peak** |
|---|---|---|---|---|
| **L2** | 1.056 | 1.54 | -0.985 | - |
| **L3** | 1.06 | - | -0822 | - |
| **L4** | 0.122 | 0.182 | -0.58 | -0.79 |
| **L5** | 0.092 | 1.13 | -0.935 | -1.500 |
| $Cu_2$(**L2**) | 0.57 | - | -0.82 | -1.194 |
| $Cu_3$(**L3**) | 0.57 | 1.06 | - | -1.190 |
| $Cu_2$(**L4**) | - | 0.325 | -0.67 | -1.08 |

| | | | | |
|---|---|---|---|---|
| $Cu_2$(**L5**) | 0.63 | 1.49 | - | -1.003 |

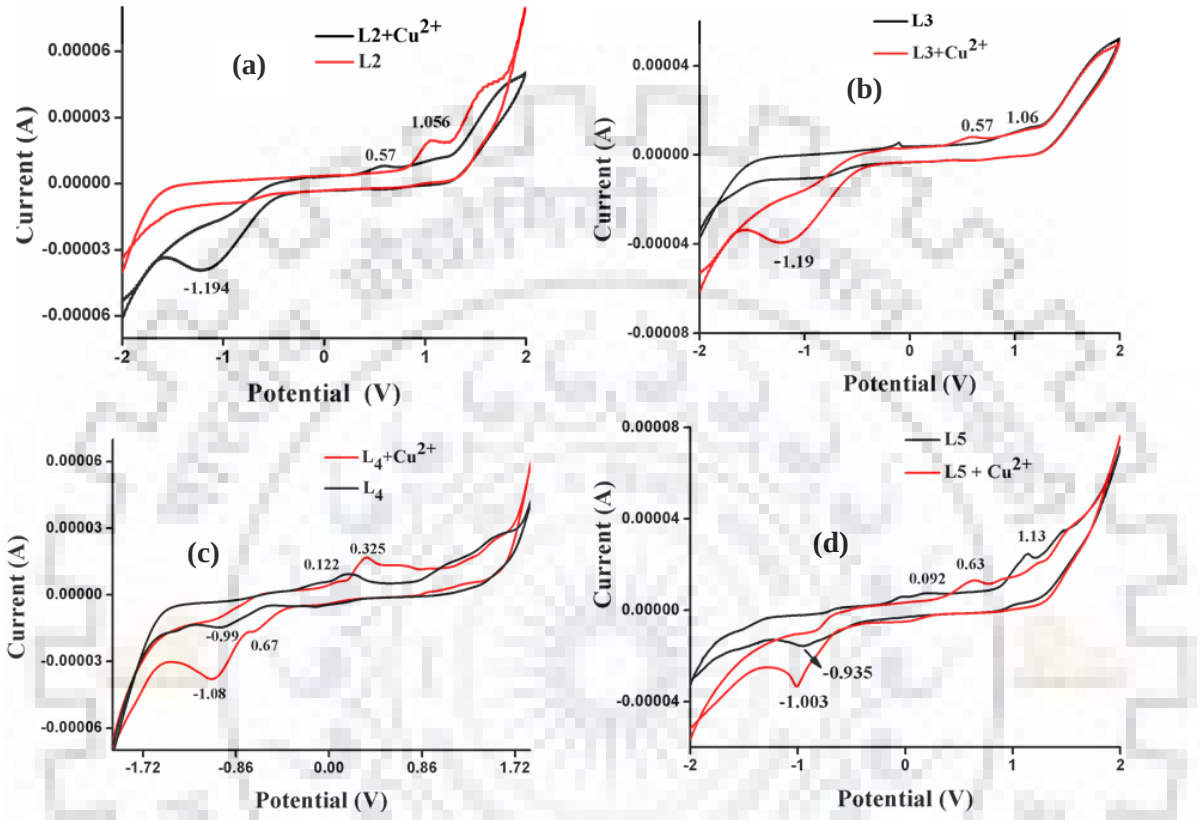


**Figure 3.17**. (a) Electrochemical behavior of **L2** and **L2** +$Cu^{2+}$, (b) Electrochemical behavior of **L3** and **L3** +$Cu^{2+}$, (c) Electrochemical behavior of **L4** and **L4**+ $Cu^{2+}$, (d) Electrochemical behavior of **L5** and **L5**+ $Cu^{2+}$.

### 3.3.4 pH study of ligands

The efficiency of all four ligands with or without copper ion at different pH levels was studied. The results showed that at acidic pH, the intensity of the ligand not change as much as when it was at basic pH. The pH study showed that the intensity was increased at basic pH because of ligands are enriched with sensitive proton donor sites. At high pH, deprotonation occurred simultaneously as fluorescence intensity increased. This study revealed that ligands were stable between 4-10 pH, outside of this range the ligand properties changed. The same experiment was performed with **L** (**L2**-**L5**) + $Cu^{2+}$

and it was found that in case of **L2**+$Cu^{2+}$, the compound was stable between 4-11 pH and outside of this range the compound became turbid and intensity changed. In the case **L3**+$Cu^{2+}$, a range of 4-11 pH was suitable and apart from this range the compound deteriorated. From the pH study, the suitable pH range for **L4** and **L5** with $Cu^{2+}$ was found to be 3-10 pH and aside of this the properties of compounds changed. So, the results showed that the 4-11 pH range was the most convenient for all four ligands. Figure 3.18 demonstrate the pH study of all four ligands in the absence or presence of copper ions.

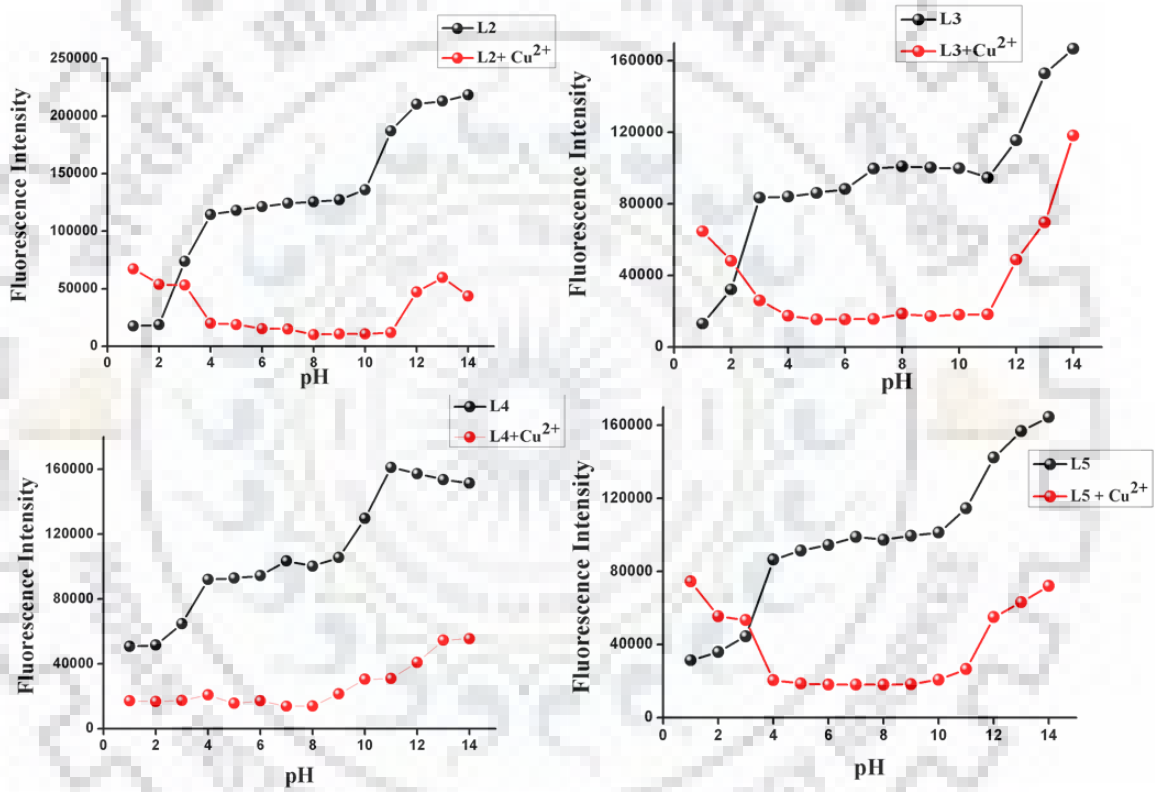


**Figure 3.18.** Represents the spam of pH for all four ligands in the absence and presence of $Cu^{2+}$ ions.

### 3.3.5 *In-situ* photophysical study with different anions

As indicated by the displacement approach of all four ligands, their fluorogenic activity was completely quenched by the complexation with copper ions [34-36]. On exposure with $CN^-$ [$Cu^{2+}$ with chelating ligands], $CN^-$ can combine with $Cu^{2+}$ to produce the extremely stable species $[Cu(CN)_x]^{n-}$, resulting in the arrival of a free ligand among

other anions ($Cl^-$, $Br^-$, $F^-$, $CN^-$, $NO_3^-$, $SO_3^{2-}$, $SO_2^-$, $SO_4^{2-}$, $S^{2-}$, $H_2PO_4^-$, $HPO_4^{2-}$, $SCN^-$, $CO_3^{2-}$ and Cys). Figure 3.19(a) and (b) shows the selectivity of cyanide ion among other anions. This led us to estimate that the **L** (**L2**-**L5**)-$Cu^{2+}$ gathering is a potential sensor for cyanide ions among other anions. The *in-situ* $CN^-$ induced decomplexation was investigated using UV-vis studies. The results show that, *in-situ*, **L2** and **L5** with copper ions have an affinity towards cyanide ions among other anions due to the decomplexation of **L2** and **L5** from copper ions, but **L3** and **L4** are not subject to any interference by different anions because of their high affinity towards $Cu^{2+}$ ions. As a result, the study shown that in the cases of **L2** and **L5**, $CN^-$ ions encountered decomplexation with $Cu^{2+}$ ions, whereas **L3** and **L4** did not previously develop the ligand after the *in-situ* reaction with $CN^-$ ions. The Figures 3.19(c) and (d) show the changes in absorption spectra on gradual addition of cyanide ions with **L2**+$Cu^{2+}$ and **L5**+$Cu^{2+}$, respectively. Using plot of log($CN^-$) *vs* A-$A_0$/$A_{max}$-$A_0$. The limit of detection of cyanide with **L2** and **L5** are 0.31 μM and 0.53 μM respectively, which are much less than the permissible limit of cyanide ions prescribed by the World Health Organization (WHO). Figure 3.20 (a) and (b) expressed the detection limit graphs for cyanide ions.

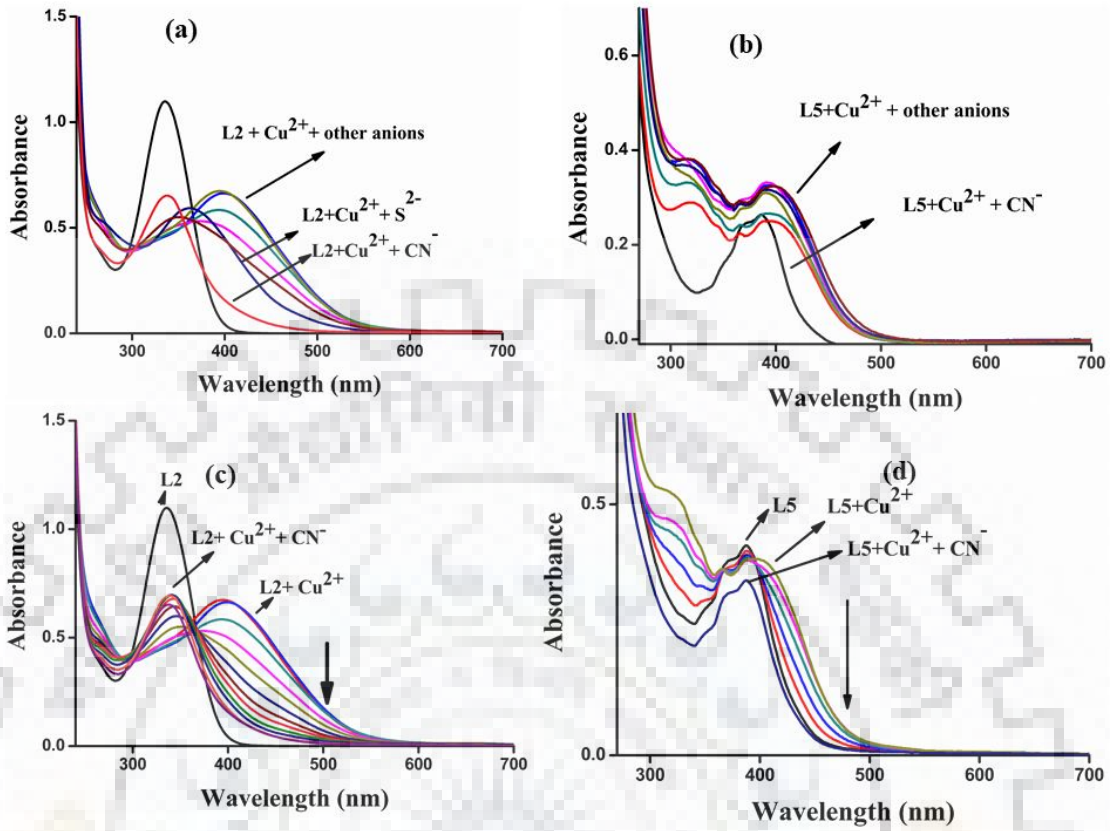


**Figure 3.19.** (a) & (b) Show the selectivity of $CN^-$ ion *via* absorption studies of in-situ **L2** and **L5** with different anions in the presence of copper ion and (c) & (d) shows the titration graph of **L** (**L2** and **L5**) + $Cu^{2+}$ (20 µM) ion *in-situ* by gradual addition of $CN^-$ (20 to 200 µM).

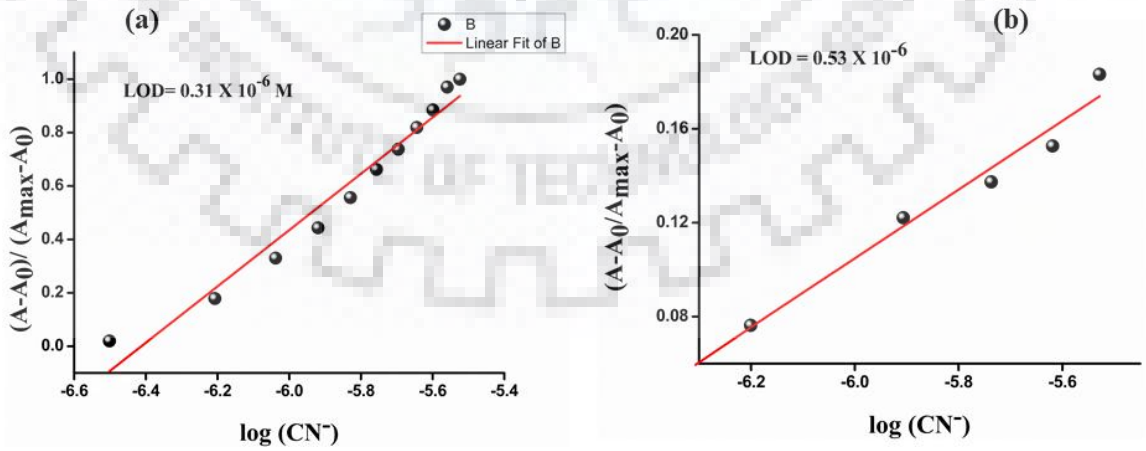


**Figure 3.20.** (a) & (b) represents the limit of detection graph of **L2**+$Cu^{2+}$ and **L5**+$Cu^{2+}$ with $CN^-$ (20 to 200 µM).

## 3.4. APPLICATIONS

### 3.4.1 Real sample analysis

To evaluate the potential uses of synthesized ligands (**L2**-**L5**), the ligands are applied in the analysis of different water samples. The water samples used were tap water and the Ganga river water from Roorkee, and known amounts of copper were added to the water samples. The assessment was determined by spiking with a known amount of standard copper ion solution followed by calculating its recovery. The resulting recovery of different known amounts of copper ions added was noted to be 94% to 99% from tap water and 99.4% to 103% from Ganga river water. This result shows that the application of ligands for real water analysis was quite achievable. Table 3.5 represents the real water analysis. The same experiment was performed for $CN^-$ ions in water samples, which is represented in Table 3.6. The in-situ experiment was carried out using $CN^-$ ions. This experiment was analyzed only for **L2** and **L5** because only these two ligands showed the metal displacement approach. The results revealed that the recovery of $CN^-$ ions from tap water was between 99% to 99.7% and from 93% to 96% for Ganga river water.

**Table 3.5:** Determination of copper ion in different water samples by using **L2**, **L3**, **L4** and **L5** ligand.

| | Samples | Spiked $Cu^{2+}$ (M) | Found $^{a}Cu^{2+}$ ± SD (M) | Recovery (%) |
|---|---|---|---|---|
| **L2** | Tap water | $5 \times 10^{-5}$ | $4.95 \pm 0.1 \times 10^{-5}$ | 99 % |
| | Ganga River water | $5 \times 10^{-5}$ | $5.00 \pm 0.2 \times 10^{-5}$ | 100 % |
| **L3** | Tap water | $5 \times 10^{-5}$ | $4.73 \pm 0.3 \times 10^{-5}$ | 94.6 % |
| | Ganga River water | $5 \times 10^{-5}$ | $5.1 \pm 0.1 \times 10^{-5}$ | 102 % |
| **L4** | Tap water | $5 \times 10^{-5}$ | $4.94 \pm 0.1 \times 10^{-5}$ | 98.8 % |
| | Ganga River water | $5 \times 10^{-5}$ | $5.15 \pm 0.5 \times 10^{-5}$ | 103 % |
| **L5** | Tap water | $5 \times 10^{-5}$ | $4.89 \pm 0.2 \times 10^{-5}$ | 97.8 % |

| | | | |
|---|---|---|---|
| Ganga River water | $5 \times 10^{-5}$ | $4.97 \pm 0.1 \times 10^{-5}$ | 99.4 % |

[a] Standard deviation was calculated for three measurements.

**Table 3.6:** Determination of cyanide ion in different water samples by using **L2** and **L5** ligand.

| Samples | | Spiked $CN^-$ | [a]Found $CN^-$ ± SD | Recovery |
|---|---|---|---|---|
| **L2**+$Cu^{2+}$ | Tap water | $4 \times 10^{-5}$ | $3.96 \pm 0.1 \times 10^{-5}$ | 99% |
| | River water | $4 \times 10^{-5}$ | $3.87 \pm 0.2 \times 10^{-5}$ | 96.7% |
| **L5**+ $Cu^{2+}$ | Tap water | $4 \times 10^{-5}$ | $3.99 \pm 0.1 \times 10^{-5}$ | 99.7% |
| | River water | $4 \times 10^{-5}$ | $3.75 \pm 0.3 \times 10^{-5}$ | 93% |

[a] Standard deviation was calculated for three measurements.

### 3.4.2 Logic gate operation for L2 and L5

Studies were carried out based on metal displacement approach of **L2**-$Cu^{2+}$ and $CN^-$, with consistent changes in its absorption intensity at 397 nm. Furthermore, these changes were applied as a molecular switch which uses on Boolean logic operations [37]. For the explanation of the design of the logic gate, 1 logic assigned for input and 0 for output. The four plausible input combinations are (0,0), (1,0), (0,1), (1,1) [38] which are shown in the Figure 3.20, and it was observed that in the absence or presence of $Cu^{2+}$ and $CN^-$ ($Cu^{2+}$, $CN^-$ = 1 or $Cu^{2+}$, $CN^-$ = 0) there was no output signal. However, in the presence of a $Cu^{2+}$ only input signal ($Cu^{2+}$ = 1, $CN^-$ = 0) at maximum absorption, 397 nm was accomplished as the output signal, but inverse of that ($Cu^{2+}$ = 0, $CN^-$ = 1) did not show any output signal. The truth table was integrated for logic circuit with two inputs as $Cu^{2+}$ ($In_1$), and $CN^-$ ($In_2$). **L2** and **L5** have the ability to expose INHIBIT job through absorption output with the AND logic gate as an inverter to invert the input signal. A similar experiment was performed with the **L5** molecule and the absorption changed at 398 nm, which showed the same logic gate after applying same inputs. Figure 3.21 showed the molecular switch for **L2**.

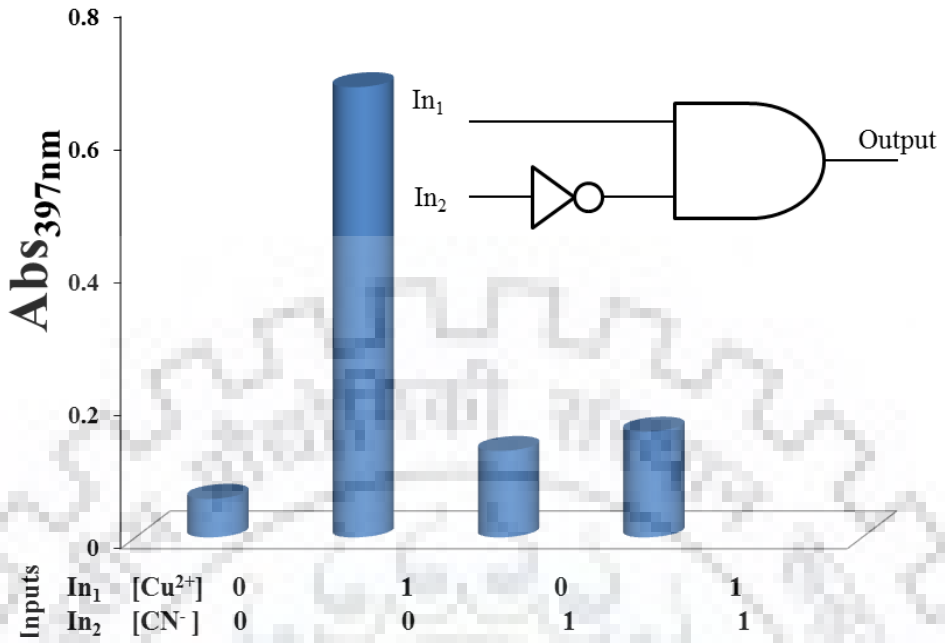


**Figure 3.21.** Change in absorbance of **L2** at four different input conditions: inset shows implicated logic diagram.

## 3.5 CONCLUSIONS

Multidentate dicarbohydrazide based ligands were successfully synthesized and well characterized through NMR, FTIR, elemental analysis, crystal structure analysis, mass spectrometry and investigation into their photophysical properties. These ligands show high selectivity and sensitivity towards copper ions amongst other metal ions. The Job's plot analysis showed that $Cu^{2+}$ forms 1:2, 1:3, 1:2, and1:2 complexes with **L2**, **L3**, **L4**, **L5** respectively. The good binding constants were demonstrated by **L2**, **L3**, **L4**, and **L5** with copper ions to be 8.86, 17.645, 11.145 and 6.45 respectively, and good detection limits were established by the ligands between 0.097 to 0.12 μM. The studies using FT-IR and ESI Mass spectroscopy proved the coordination site of the $Cu^{2+}$ ion with all four ligands. Furthermore, these *in situ* experiments were explored for anion detection, where the results showed that only **L2**+$Cu^{2+}$ and **L5**+$Cu^{2+}$ could detect cyanide ions with good sensitivity at *ca.* 0.31 and 0.53 μM *i.e.* less than the permissible limit given by WHO. The *in-situ* experiments showed that **L2** and **L5** could sense cyanide ions in presence of copper ions. The data was also applied in molecular switch and represents an INHIBIT logic gate.

## References


1. D. E. Kang, C. S. Lim, J. Y. Kim, E. S. Kim, H. J. Chun and B. R. Cho, Two-Photon probe for $Cu^{2+}$ with an internal reference: Quantitative estimation of $Cu^{2+}$ in human tissues by two-photon microscopy, Anal. Chem. 86 (2014) 5353−5359.
2. D. J. Waggoner, T. B. Bartnikas and J. T. Gitlin, The role of copper in neurodegenerative disease, Neurobiology of Disease 6 (1999) 221-230.
3. K. Mariappan, M. Alaparthi, G. Caple, V. Balasubramanian, M. M. Hoffman, M. Hudspeth ans A. G. Sykes, Selective fluorescence sensing of copper(II) and water *via* competing imine hydrolysis and alcohol oxidation pathways sensitive to water content in aqueous acetonitrile mixtures, Inorg. Chem. 53 (2014) 2953–2962.
4. S. L. Fontaine and J. F. B. Mercer, Trafficking of the copper-ATPases, ATP7A and ATP7B: Role in copper homeostasis, Archives of Biochemistry and Biophysics 463 (2007) 149–167.
5. D. Strausak, J. F. B. Mercer, H. H. Dieter, W. Stremmel and G. Multhaup, Copper in disorders with neurological symptoms: Alzheimer's, Menkes, and Wilson diseases, Brain Research Bulletin 55 (2001) 175-185.
6. C. Vulpe, B. Levinson, S. Whitney, S. Packman and J. Gitschier, Isolation of a candidate gene for Menkes disease and evidence that it encodes a copper–transporting ATPase, Nature Genetics 3 (1993) 7 – 13.
7. E. Gaggelli, H. Kozlowski, D. Valensin and G. Valensin, Copper homeostasis and neurodegenerative disorders (Alzheimer's, Prion, and Parkinson's Diseases and Amyotrophic Lateral Sclerosis), Chem. Rev. 106 (2006) 1995−2044.
8. C. Ge, Q. Luo, D. Wang, S. Zhao, X. Liang, L. Yu, X. Xing and L. Zeng, Colorimetric detection of copper(II) ion using click chemistry and Hemin/G-Quadruplex Horseradish Peroxidase-Mimicking DNA enzyme, Anal. Chem. 86 (2014) 6387−6392.
9. F. J. Huo, C. X. Yin, Y. T. Yang, J. Su, J. B. Chao and D. S. Liu, Ultraviolet-Visible light (UV-Vis)-reversible but fluorescence-irreversible chemosensor for copper in water and Its application in living cells, Anal. Chem. 84 (2012), 2219-2223.

10. J. F. B. Mercer, The molecular basis of copper-transport diseases, TRENDS in Molecular Medicine 7 (2001) 64-69.
11. L. C. Jackson, Possible adaptation to serum thiocyanate overload associated with chronic sublethal dietary cyanide ingestion, Human biology 60 (1988) 615-622.
12. Y. Wang, H.-Q. Chang, W.–N. Wu, X.-J. Mao, X.-L. Zhao, Y. Yang, Z.-Q. Xu, Z.-H. Xu and L. Jia, A highly sensitive and selective colorimetric and Off-On fluorescent chemosensor for $Cu^{2+}$ based on rhodamine 6G hydrazide bearing thiosemicarbazide moiety, J. Photochem. Photobiol. A 335 (2017) 10-16.
13. M. Jamkratoke, V. Ruangpornvisuti, G. Tumcharern, T. Tuntulani and B. Tomapatanaget, A-D-A sensors based on naphthoimidazoledione and boronic acid as turn-On cyanide probes in water, J. Org. Chem. 74 (2009) 3919-3922.
14. R. Jackson, R. P. Oda, R. K. Bhandari, S. B. Mohan, M. Brenner, G. A. Rockwood and B. A. Logue, Development of a fluorescence-based sensor for rapid diagnosis of cyanide exposure, Anal. Chem. 86 (2014) 1845–1852.
15. T. Liu, F. Huo, J. Li, F. Cheng and C. Yin, Two novel $CN^-$ turn on fluorescent imaging with twin binding groups, Sens. Actuators B 239 (2017) 526-535.
16. F. Huo, Y. Zhang, Y. Yue, J. Chao, Y. Zhang and C. Yin, Isophorone-based aldehyde for "Ratiometric" detection of cyanide by hampering ESIPT, Dyes Pigm. 143 (2017) 270-275.
17. N. Yadav and A. K. Singh, Dual anion colorimetric and fluorometric sensing of arsenite and cyanide ions, RSC Adv. 6 (2016) 100136–100144.
18. A. Ishii, H. Seno, K. Watanabe-Suzuki and O. Suzuki, Determination of cyanide in whole blood by capillary gas chromatography with cryogenic oven trapping, Anal. Chem. 70 (1998) 4873–4876.
19. J. Li, W. Wei, X. Qi, G. Zuo, J. Fang and W. Dong, Highly selective colorimetric/fluorometric dual-channel sensor for cyanide based on ICT off in aqueous solution, Sens. Actuators B, 228 (2016) 330-334.
20. Guidelines for Drinking-Water Quality, World Health Organization, Geneva, (1996).
21. WHO, Guidelines for Drinking-Water Quality, World Health Organization, Geneva, Switzerland, 4th edn, (2011).

22. S. R. Patil, J. P. Nandre, P. A. Patil, S. K. Sahoo, M. Devi, C. P. Pradeep, Y. Fabiao, L. Chen, C. Redshaw and U. D. Patil, A uracil nitroso amine based colorimetric sensor for the detection of $Cu^{2+}$ ions from aqueous environment and its practical applications, RSC Adv. 5 (2015) 21464–21470.
23. H. S. Jung, P. S. Kwon, J. S. Kim, C. S. Hong, J. W. Kim, S. Yan, J. Y. Lee, J. H. Lee, T. Joo, and J. S. Kim, Coumarin-derived Cu(2+)-selective fluorescence sensor: Synthesis, mechanisms, and applications in living cells, J. Am. Chem. Soc. 131 (2009) 2008–2012.
24. G. Y. Lan, C. C. Huang and H. T. Chang, Silver nanoclusters as fluorescent probes for selective and sensitive detection of copper ions, Chem. Commun. 46 (2010) 1257–1259.
25. P. Raj, A. Singh, A. Singh and N. Singh, Synthesis and photophysical properties of schiff base Ni(ii) complexes: Application for sustainable antibacterial activity and cytotoxicity, ACS Sustainable Chem. Eng. 5 (2017) 6070–6080.
26. D. Singhal, N. Gupta and A. K. Singh, Chromogenic 'Naked Eye' and fluorogenic 'turn-on' sensor for mercury metal ion using thiophene based schiff base, RSC Adv. 5 (2015) 65731- 65738.
27. T. G. Jo, Y. J. Na, J. J. Lee, M. M. Lee, S. Y. Lee and C. Kim, A multifunctional colorimetric chemosensor for cyanide and copper(II) ions, Sens. Actuators B, 211 (2015) 498–506.
28. H. Mu, R. Gong, Q. Ma, Y. Sun and E. Fu, A novel colorimetric and fluorescent chemosensor: Synthesis and selective detection for $Cu^{2+}$ and $Hg^{2+}$, Tetrahedron Letters 48 (2007) 5525–5529.
29. G. J. Park, I. H. Hwang, E. J. Song, H. Kim and C. Kim, A colorimetric and fluorescent sensor for sequential detection of copper ion and cyanide, Tetrahedron 70 (2014) 2822-2828.
30. G. Li, F. Tao, H. Wang, Y. C. Li and L. Wang, A novel reversible colorimetric chemosensor for rapid naked-eye detection of $Cu^{2+}$ in pure aqueous solution, Sens. Actuators B 211 (2015) 325–331.
31. M. Shahid, S. S. Razi, P. Srivastava, R. Ali, B. Maiti and A. Misra, A useful scaffold based on acenaphthene exhibiting $Cu^{2+}$ induced excimer fluorescence and

sensing cyanide *via* $Cu^{2+}$ displacement approach, Tetrahedron 68 (2012) 9076 - 9084.

32. L. Yang, N. Huang, L. Huang, M. Liu, H. Li, Y. Zhang and S. Yao, An electrochemical sensor for highly sensitive detection of copper ions based on a new molecular probe Pi-A decorated on graphene, Anal. Methods 9 (2017) 618-624.
33. P. Gayathri and A. S. Kumar, Electrochemical behavior of the 1, 10-Phenanthroline ligand on a multiwalled carbon nanotube surface and its relevant electrochemistry for selective recognition of copper ion and hydrogen peroxide sensing, Langmuir, 30 (2014) 10513-10521.
34. Z. Xu, X. Chen, H. N. Kim and J. Yoon, Sensors for the optical detection of cyanide ion, Chem. Soc. Rev. 39 (2010) 127–137.
35. X. Chen, S.-W. Nam, G.-H. Kim, N. Song, Y. Jeong, J. Shin, S. K. Kim, J. Kim, S. Park and J. Yoon, A near-infrared fluorescent sensor for detection of cyanide in aqueous solution and its application for bioimaging, Chem. Commun. 46 (2010) 8953-8955.
36. F. Wang, L. Wang, X. Chen and J. Yoon, Recent progress in the development of fluorometric and colorimetric chemosensors for detection of cyanide ions, Chem. Soc. Rev. 43 (2014) 4312-4324.
37. L. Lu, C. Chen, D. Zhao, J. Sun and X. Yang, Europium luminescence used for logic gate and ions sensing with enoxacin as the antenna, Anal. Chem. 88 (2016) 1238–1245.
38. J. Liu, X. He, J. Zhang, T. He, L. Huang, J. Shen, D. Li, H. Qiu and S. Yin, A BODIPY derivative for colorimetric and fluorometric sensing of fluoride ion and its logic gates behavior, Sens. Actuators B 208 (2015) 538–545.

# CHAPTER 4

## "PYRIMIDINE BASED CHEMOSENSOR FOR ALUMINUM IONS"

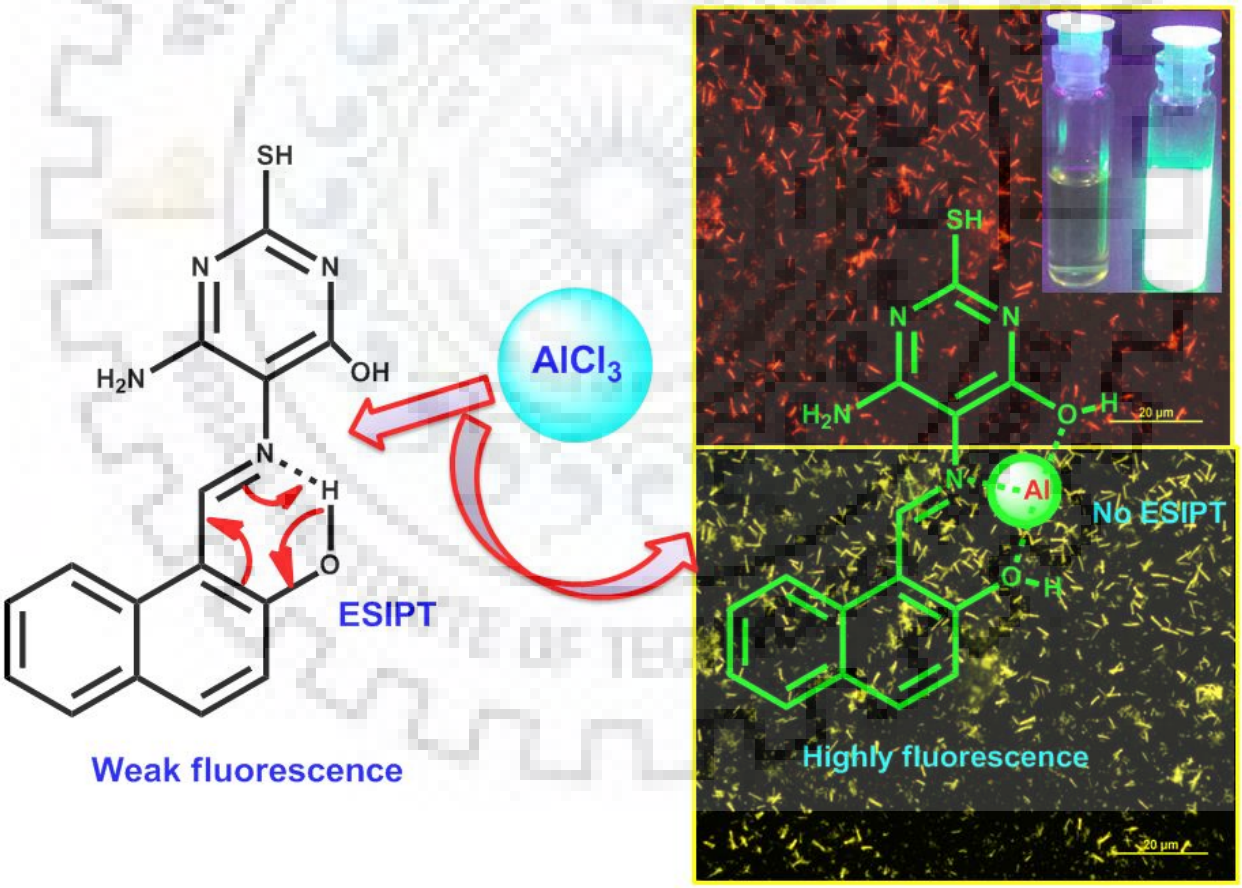

# CHAPTER 4

## 4.1 INTRODUCTION

Aluminum is the 3rd generous element in the earth's crust. Acid rain is one of the main sources of leaching of free aluminum ion in the environment and surface water. Its uses have been increased drastically in day-to-day activities from last few years *i.e.* cooking utensils, aluminum foil which raises the amount of aluminum metal ion in daily food and drinking water [1,2], as well as pervasive use in diverse field like automotive and aeronautic transport, food additive, space industries, construction, packaging and aluminum-based pharmaceuticals, which creates adverse effect on the environment. Its toxicity causes many deceases such as Alzheimer's disease [3,4], Amyotrophic lateral sclerosis, Parkinson's disease *i.e.* damages the human nervous system as well as it also deadly hindered the plants growth [5,6] *etc.* According to FAO/WHO the tolerable limit of aluminum ion is 7.0 mg/Kg body weight in a week which was suggested based on short term toxicity [7,8]. Therefore, to prevent the direct impact on the human being and biosphere by $Al^{3+}$, it is needed to control the concentration levels of $Al^{3+}$ in the environment. Due to poor coordination ability and insufficient spectroscopic characteristics, it is difficult to detect the aluminum ion concentration in the environment and surface water. Therefore, it is required to promote $Al^{3+}$ sensors, which possess easy synthetic route, and sensitive, selective mechanisms.

Some tedious, time consuming and sophisticated techniques such as graphite furnace atomic absorption spectroscopy and inductively coupled plasma atomic emission spectroscopy are used in the detection of aluminum ion. Due to the drawbacks of these techniques, in recent years, fluorescent sensing has great attraction by virtue of its high efficiency to sense numerous biological and chemical species. Therefore, many fluorescent sensors have been synthesized and used them in the detection of different metal ions with different mechanism [9-17]. ESIPT mechanism (Excited state intramolecular proton transfer) has unique properties in practical application because of its attractive photophysical property such as large Stokes shift that avoided the self-absorption of molecule or inner filter effect, which improve the fluorescence analysis with this type of molecule. Another property is keto tautomer or transient character of molecule in the ground state. Those molecules which has H-bond donor group such as

phenolic or amino group established photo-tautomer by transferring the proton to an adjoining atom in electronically excited state. Similarly, here C=N isomerization is also occurred.

On the basis of these properties the chapter demonstrated the sensor that has –OH group adjacent to the imine nitrogen which exemplifies intramolecular proton transfer from –OH to imine nitrogen *i.e* represents ESIPT mechanism. Here the C=N isomerization is also inhibited after addition of aluminum ion and showed high fluorescent properties. This sensor depicts specific affinity towards $Al^{3+}$ ion unlike other metal ions with large spectral shift (58 nm) due to the presence of polar groups such as hydroxyl groups, amine group which shows high affinity with $Al^{3+}$ ion. As result of interaction between host with $Al^{3+}$ ion leads to hinder ESIPT mechanism and C=N isomerization of host. The sensor reveals low detection limit in nano molar range (99 nM) for $Al^{3+}$ ion in ACN. Photoluminescence of host with $Al^{3+}$ ion emits green and red fluorescent light for imaging of bacterial cell (E. coli DHα). It also acts as a reversible chemosensor and represents INHIBIT logic gate. The host **L6** represents ESIPT mechanism that was hampered with $Al^{3+}$ ion after that it was used in various practical applications. The synthesis process of the sensor is a simple and easy one-step method. The synthesis did not involve costly chemicals or sophisticated techniques.

## 4.2 EXPERIMENTAL SEGMENT

### 4.2.1 Reagents and instruments

Chloride and nitrate salts of metals were purchased from SDFine and Merck of analytical reagent grade and used them for analytical studies without any purification. Reagent 2-hydroxy-1-naphthaldehyde and 5,6-diamino-2-mercaptopyrimidin-4-ol was purchased from Sigma Aldrich (>90%). Absorption spectra was measured by Shimadzu, UV-3600 double beam spectrophotometer with quartz cell. Vibrational spectra recorded in Perkin-Elmer FT-IR 1000 spectrophotometer. The Elementar Model Vario EI-III instrument was used for the elemental analysis. JEOL 400 MHz spectrophotometer was used to record all NMR spectra. Emission spectra was recorded on Horiba RF-5301PC by standard quartz cell (3 cm path length). The electrochemical was documented on

CHI760E electro analyzer Ag/AgCl as reference electrode, glassy carbon electrode as working electrode and platinum wire as auxiliary electrode with 0.1 M $nBu_4NPF_6$ (as supporting electrolyte), 0.1 $Vs^{-1}$ scan rate and -2.0 to 2.0 potential range. Mass spectrum was analyzed on WATERS Q-TOF premier-HAB213 mass spectrometer and Bruker micrOTOF$^{TM}$ -Q II mass spectrometer.

**4.2.2 Synthesis of ligand L6, L7:**

**A) Synthesis of ligand L6 (6-amino-5-(((2-hydroxynaphthalen-1-yl)methylene)amino)-2-mercaptopyrimidin-4-ol):**

Ligand **L6** was synthesized by adding methanolic solution of 2-hydroxy-1-naphthaldehyde (1.5 mmol, 0.2582 g) in methanolic solution of 5,6-diamino-2-mercaptopyrimidin-4-ol (1 mmol, 0.1581 g) with continuous stirring. After completion the adding of reagent, reflux the reaction mixture for 12 hr. A dark yellow colored precipitate was obtained, which was recrystallized with ethanol (Scheme 4.1) [18].

**Yield.** 80%. Calc. for $C_{15}H_{12}N_4O_2S$: C, 57.68; H, 3.87; N, 17.94; O, 10.24; S, 10.27 and found: C, 57.79; H, 3.623; N, 17.84: O, 10.724; S, 10.023. FT-IR data (KBr $\upsilon_{max}$ $cm^{-1}$): O-H: 3490, $NH_2$: 3387, C-H str.: 3169, S-H: 2895, C=N: 1568, C=C: 1626, C-S: 1477. UV-Visible ($CH_3CN$, $\lambda_{max}$ nm): 400 nm. $^1$H NMR (DMSO, 400 MHz, δ/ppm) 14.12 (s, 1H), 12.17 (s, 1H), 11.90 (s, 1H), 10.50 (s, 1H), 8.10 (d, *J* = 8.5 Hz, 1H), 7.87 (d, *J* = 9.0 Hz, 1H), 7.83 (d, *J* = 8.9 Hz, 1H), 7.53 (t, *J* = 7.1 Hz, 1H), 7.34 (t, *J* = 7.2 Hz, 1H), 7.12 (d, *J* = 9.0 Hz, 1H), 6.57(s, 2H). $^{13}$C NMR (DMSO, 100 MHz, δ/ppm) 172.20, 160.94, 157.97, 155.72, 150.59, 133.89, 132.61, 129.57, 128.33, 128.04, 123.95, 120.56, 119.75, 110.80, 102.42. ESI-mass of **L6** *m/z* 313.0750, $(M+H)^+$.

**B) Synthesis of ligand L7 (6-amino-5-((4-bromobenzylidene)amino)-2-mercaptopyrimidin-4-ol):**

Ligand **L7** was synthesized by adding methanolic solution of 4-bromobenzaldehyde (1 mmol, 0.1850 g) in methanolic solution of 5,6-diamino-2-mercaptopyrimidin-4-ol (1 mmol, 0.1581 g) with continuous stirring. After complete

addition of reagent, reflux the reaction mixture for 5-6 hr. A light-yellow colored precipitate was obtained, which was recrystallized with ethanol (Scheme 4.1).

**Yield.** 70%. Calc. for $C_{11}H_9BrN_4OS$: C, 40.62; H, 2.79; N, 17.23; S, 11.72 and found: C, 39.95; H, 2.540; N, 17.72; S, 11.525. FT-IR data, (KBr $\upsilon_{max}$ $cm^{-1}$): O-H: 3433, $NH_2$: 3323, C-H str.: 3202, S-H: 2909, C=C: 1634, C=N: 1599, C-S: 1477. UV-Visible ($CH_3CN$, $\lambda_{max}$ nm): 367 nm. $^1H$ NMR (DMSO, 400 MHz, δ/ppm) 11.96 (s, 1H), 11.81(s, 1H), 9.58 (s, 1H), 7.81 (d, *J* = 8.1 Hz, 2H), 7.54 (d, *J* = 8.1 Hz, 2H), 6.75 (s, 2H). $^{13}C$ NMR (DMSO, 100 MHz, δ/ppm) 172.51, 157.60, 152.91, 150.51, 138.02, 131.98, 129.88, 123.29, 102.40. ESI-mass of **L7** *m/z* 346.96 $(M+Na)^+$.

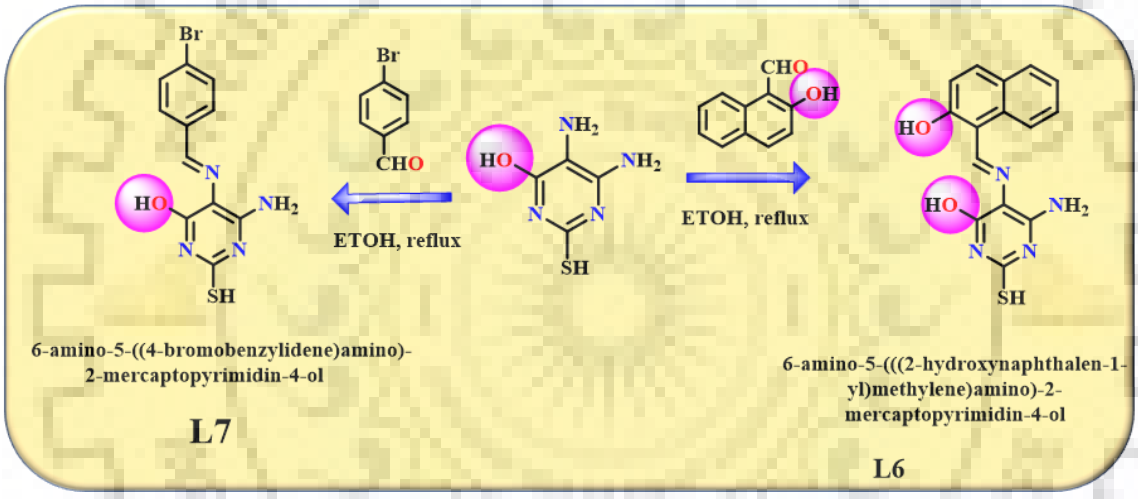


**Scheme 4.1.** Synthesis of **L6** and **L7** ligand.

## 4.3 RESULT AND DISCUSSION

### 4.3.1 Solvochromic test

The solvochromic trends was checked with different solvent such as MeOH, ACN, DMF, DMSO, THF, Hexane and Water. A new peak was appeared at 482 nm with MeOH, DMF, DMSO and THF solvent due to the hydrogen bonding takes place between ligands (**L6**, **L7**) and with these solvents. In case of Hexane then precipitate occurred and with water the ligands generated strong hydrogen with decreases the intensity of absorbance. DCM is also not chosen due to the less miscibility of this solvent. Therefore, ACN was selected as a solvent for all further studies because of less tendency of

hydrogen bonding with the ligands (**L6**, **L7**). Figure 4.1 shows the solvent study with the both ligands.

Further the binary mixture study of ACN was also performed with different volume of water. This study revealed that the peak corresponds to 400 nm was found to decrease, simultaneously, with increasing the water concentration. However, a new peak at 482 nm was observed due to hydrogen bonding of water content with ligands; which was increased with water concentration. Hence, ACN solvent without water was used to avoid the peak of hydrogen bonding at 482 nm. Figure 4.2 demonstrate the binary mixture study of both the ligands.

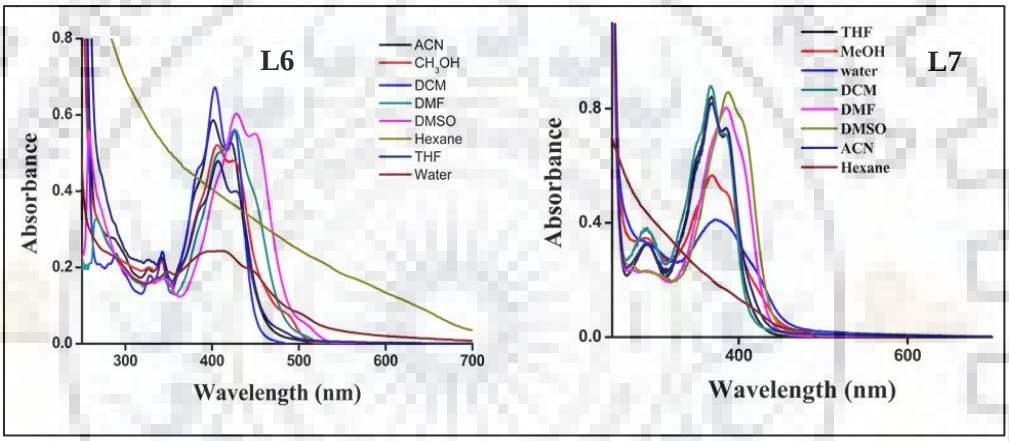


**Figure 4.1.** The solvent study of **L6** and **L7** respectively with different solvent.

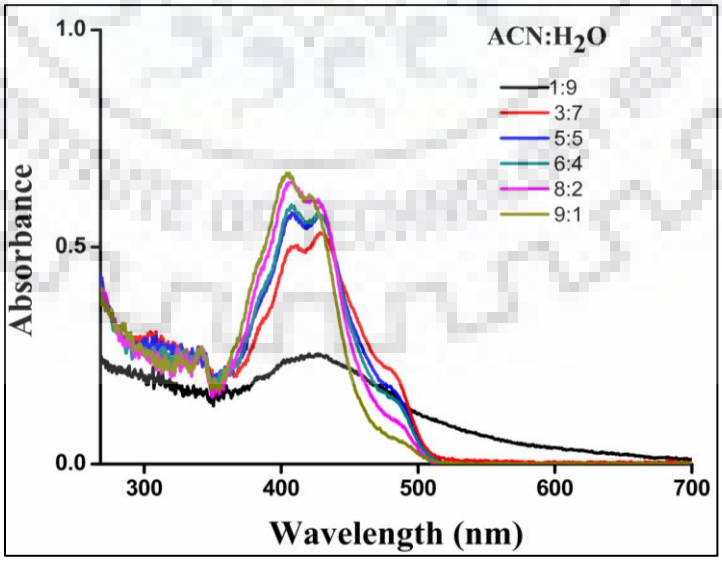


**Figure 4.2.** The binary mixture study of **L6** in ACN with water.

### 4.3.2 Visualization test

Initiatory test for the detection of aluminum ion was performed as fluorometric test in UV light. Figure 4.3 represents the performance of equi-molar concentration ($4.0\times10^{-4}$ M) of **L6** in $CH_3CN$ with 5 equivalents of all metal ion solution (1mM). A sudden highly green fluorescent has emitted with aluminum metal ion among other metal ions in UV light. Whereas, in case of **L7** there was no change with $Al^{3+}$ ion in daylight as well as in UV light.


**Figure 4.3. L6** + different metal ion in UV light.

### 4.3.3 Photo-physical Studies of both ligands L6, L7 with different metal ions

The selectivity of $Al^{3+}$ ion with both the ligand **L6**, **L7** was investigated by UV-vis and emission studies among different metal ions such as $Ag^{+}$, $Al^{3+}$, $Ca^{2+}$, $Ba^{2+}$, $Co^{2+}$, $Cd^{2+}$, $Cr^{3+}$, $Cs^{+}$, $Cu^{2+}$, $Fe^{3+}$, $Hg^{+}$, $Hg^{2+}$, $K^{+}$, $Li^{+}$, $Ni^{2+}$, $Mn^{2+}$, $Pb^{2+}$, $Zn^{2+}$. In UV-vis studies, the ligand **L6** showed the $\lambda_{max}$ at 400 nm due to n - $\pi^*$ transition and **L7** represented at 367 nm due to n - $\pi^*$ transition. The $\lambda_{max}$ difference in both ligand **L6** and **L7** has due to the more conjugation shown by naphthalene ring in **L6** as compared to **L7**. In case of **L6**, the 400 nm peak was shifted by 58 nm bathochromic shift at 458 nm with the addition of aluminum salt whereas, the absorption spectra of **L7** did not show any change with aluminum salt or other metal ion due to the deficiency of aldimine nitrogen with adjacent two hydroxyl group moiety. In case of **L6**, this red shift is due to the addition of aluminum ion by figure 4.4. On the other hand, in order of selectivity the emission spectra at excitation wavelength 405 nm was represented an immediate enhancement in the fluorescence intensity of **L6** with $Al^{3+}$ metal salt rather than other different metal ions which shown in figure 4.4. This enhancement supports the behavior of complexation of **L6** with aluminum ion. A turn-on fluorescent emission with $Al^{3+}$ ion indicates inhibition

of keto-enol form and C=N isomerization of **L6**. In ESIPT mechanism, the compound was presented in the keto-enol form but after addition of $Al^{3+}$ metal ion with **L6**, the formation of keto-enol form in **L6** was hampered and showed high fluorescence intensity. Further, the emission study was performed with **L7** ligand but there was not much more change in **L7** emission spectra that didn't show any change with aluminum ion (Figure 4.5). therefore, further studies were performed only with **L6** ligand not with **L7**.

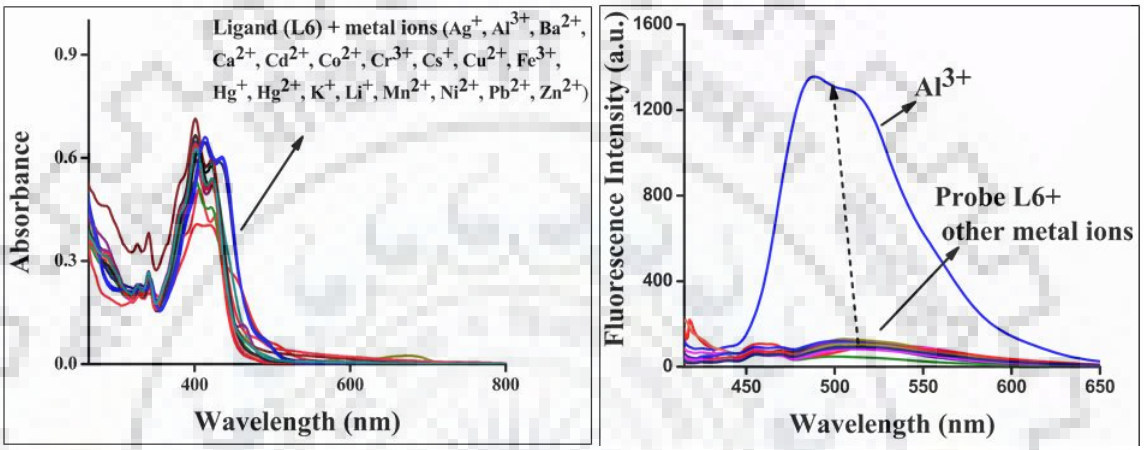


**Figure 4.4.** UV-vis study and Emission spectra for selectivity test of **L6** with various metal ions.

Furthermore, for the justification of high selectivity of **L6** towards $Al^{3+}$ metal ion the competitive experiment was performed with other metal ions. **L6** (5 μM) was served with 1.0 equivalent of $Al^{3+}$ ion and 1.0 equivalent of different metal ions. Figure 4.6 demonstrated the interfering study with different metal ions, which represented that there is slight decrease in the fluorescent intensity with copper ion while no interference was observed with other metal ions in the detection of $Al^{3+}$ metal ion. In this figure 4.6 the orange and blue bar represents **L6**, **L6** + metal ions ($Ag^{+}$, $Al^{3+}$, $Ca^{2+}$, $Ba^{2+}$, $Co^{2+}$, $Cd^{2+}$, $Cr^{3+}$, $Cs^{+}$, $Cu^{2+}$, $Fe^{3+}$, $Hg^{+}$, $Hg^{2+}$, $K^{+}$, $Li^{+}$, $Ni^{2+}$, $Mn^{2+}$, $Pb^{2+}$, $Zn^{2+}$) respectively and red bar indicates the **L6** + $Al^{3+}$+ different metal ions. This study was supported that **L6** is highly selective for $Al^{3+}$ ion in ACN.

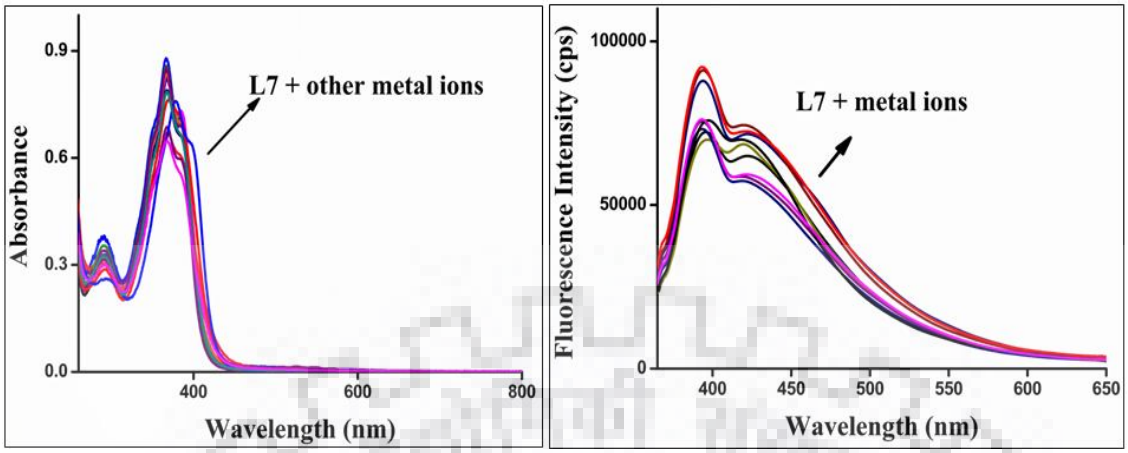


**Figure 4.5.** UV-vis study and fluorescence spectra for selectivity experiment of **L7** ligand with different metal ions.

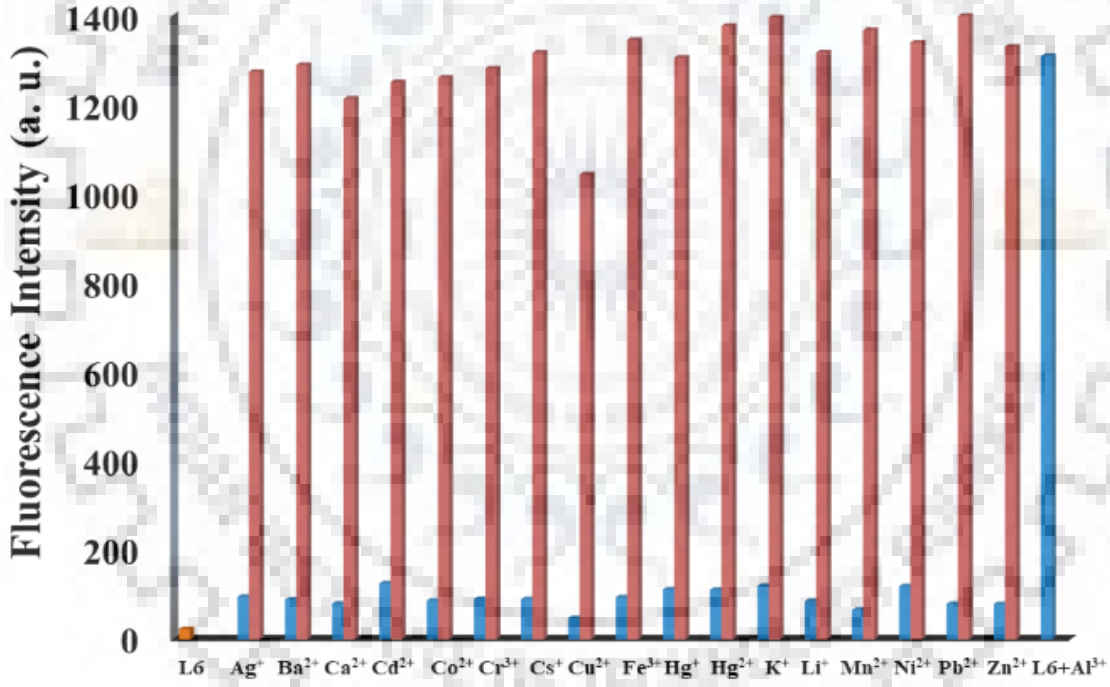


**Figure 4.6.** Interference study with different metal ion in the presence of $Al^{3+}$ here blue bar represents **L6**+metal ion and red bar shown **L6**+$Al^{3+}$+ different metal ions.

Further, the fluorescence changes were also studied at different pH of **L6** in the presence and absence of $Al^{3+}$ metal ion. The weak fluorescence intensity was manifested by **L6** from 5 to 10 pH after that in basic pH the intensity was increased due to proton ejection from the **L6** molecule. However, the same experiment was performed with

aluminum ion, which exhibited from pH 4-10, the fluorescence intensity was increased, apart from this pH the fluorescence intensity was not that much change only some decrement was observed in intensity which was depicted in figure 4.7. This increment was because of the complexation with aluminum ion. This broad span of pH makes **L6** useful in various applications [19].

The binding stoichiometry of **L6** with $Al^{3+}$ metal ion was examined by the emission spectra of equimolar solution (10 μM) of **L6** with concomitant variation in mole fraction of $Al^{3+}$ ion. Figure 4.8 represents the change in fluorescence spectra with different mole fraction of $Al^{3+}$ ion in Job's plot which results the 1:1 stoichiometry was confirmed through the Job's plot. Moreover, the binding constant and limit of detection were calculated through B-H plot by fluorescence titration of **L6** with $Al^{3+}$ ion.

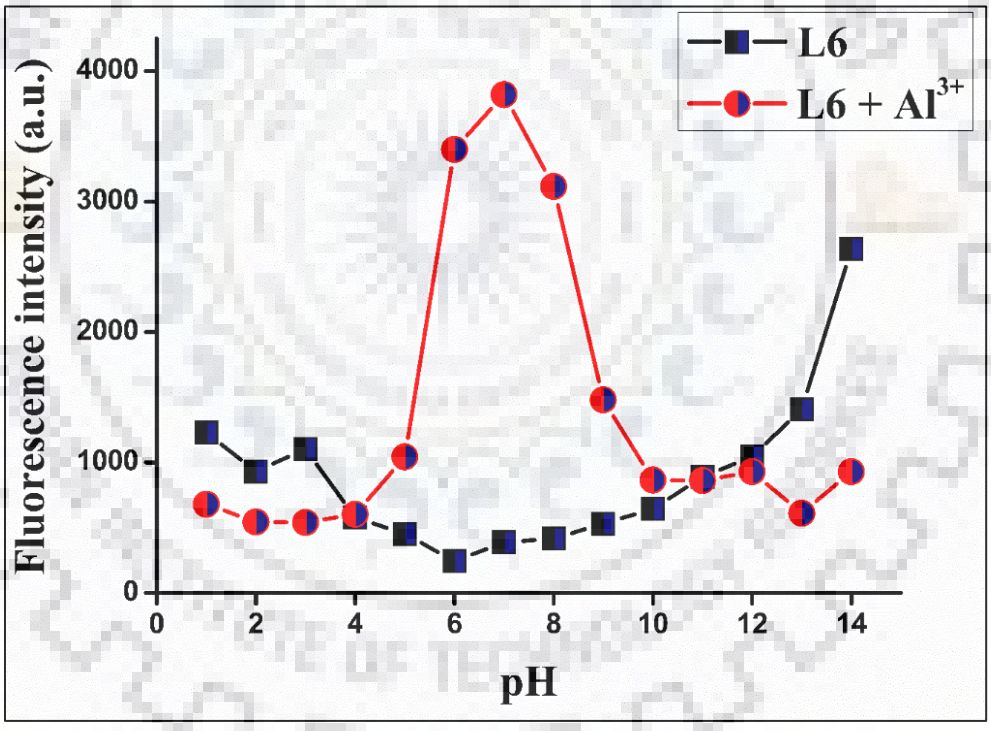


**Figure 4.7.** Change in fluorescence intensity of **L6** and **L6**+$Al^{3+}$ at different pH.

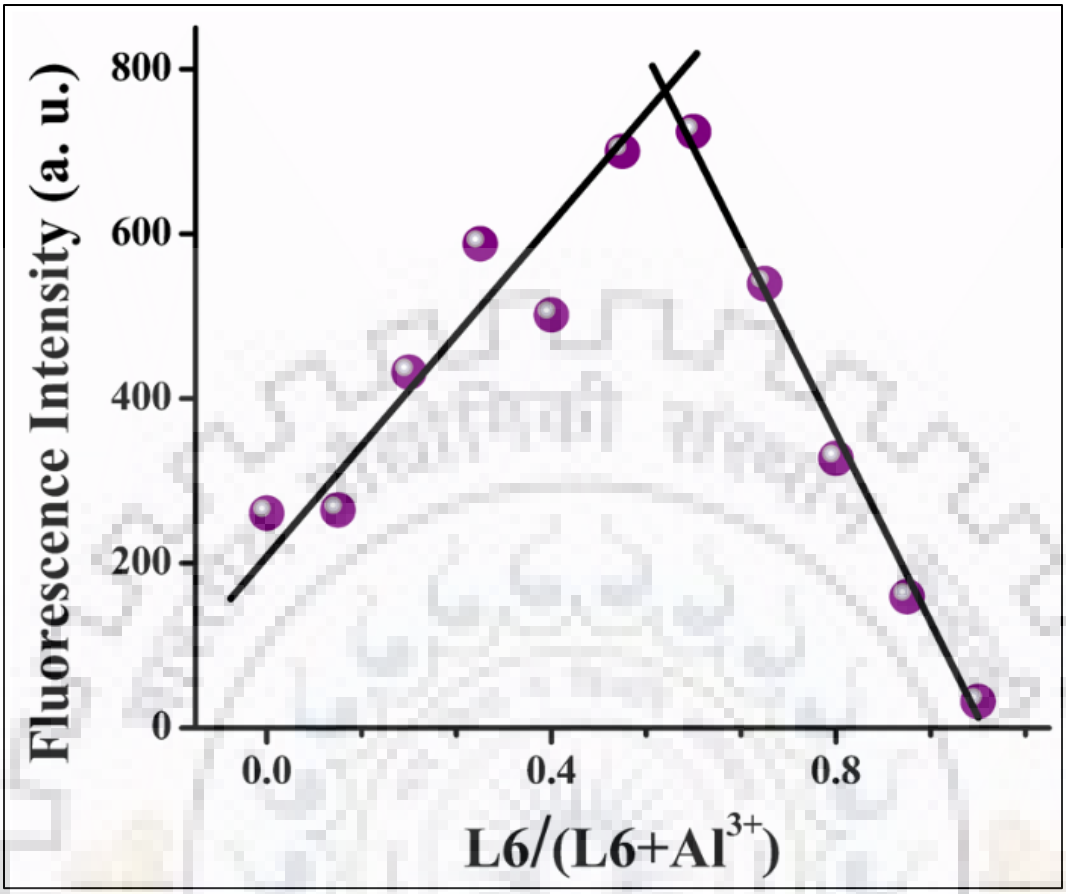


**Figure 4.8.** Maxima at 1:1 by Job's plot.

The Benesi-Hildebrand plot [20] (B-H plot) was plotted between $1/Al^{3+}$ and $1/(I-I_0)$ which was shown in figure 4.9 and the association constant $K_a$ was found to be $3.5 \times 10^4$ which was within the range ($10^3$-$10^9$) and has high limit of detection (LOD) as $9.9 \times 10^{-8}$ (99 nM), which is remarkably less than the admissible limit specified by the WHO. Figure 4.10 represents the LOD graph. It is also less than the previously reported limit of detection [21-27] which was represented in table 4.1.

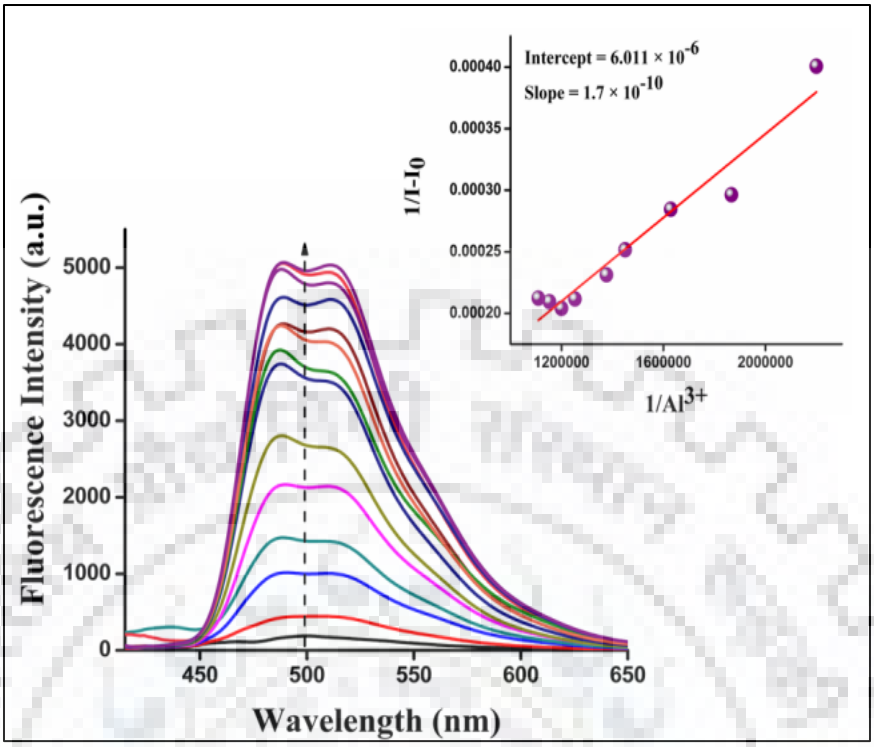


**Figure 4.9.** Emission titration of **L6** with $Al^{3+}$ ion in ACN medium.

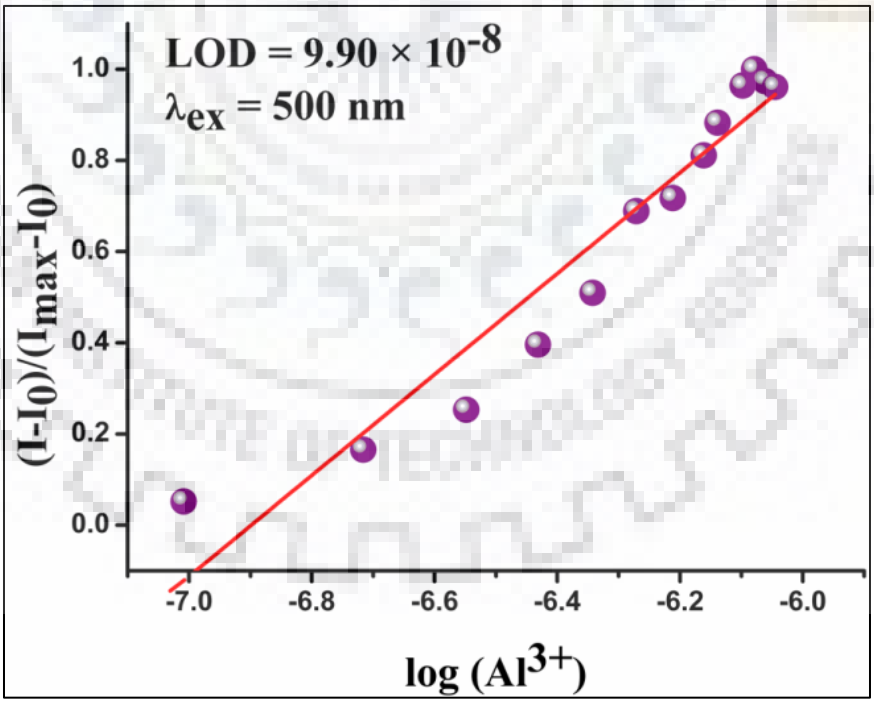


**Figure 4.10.** Determination of limit of Detection limit (LOD) for aluminum ion by using emission spectra.

**Table 4.1:** Comparison with some previously reported work.

| Previous literature | Chemosensor | Detection limit | Applications |
|---|---|---|---|
| Chem. Commun. 48 (2012) 1039-1041.(ref. 21) | quinoline-triazolyl-pyrrolidinyl-coumarin | < 10 μM | - |
| Chem. Commun., 47 (2011) 8778–8780. (ref. 22) | Calix[4]arene based | 1.2 - $10^{-7}$ μM | - |
| RSC Adv. 5 (2015) 63338–63344. (ref. 23) | 1,1-bis-[2-hydroxy-3-acetyl-5-methylphenyl]methane | 0.7 μM | - |
| Inorg. Chem. 49 (2010) 7229–7231. (ref. 24) | Coumarin-Triazolyl-Bipyridyl based | 25 μM | - |
| Chem. Commun. 50 (2014) 11833-11836. (ref. 25) | Naphthalene based | 2.8 - 50 μM | Cell Imaging |
| Tetrahedron Lett. 55 (2014) 1347–1352. (ref. 26) | Quinoline based | 1 μM | - |
| Analytica Chimica Acta 853 (2015), 596-601. (ref. 27) | Aminoquinoline based | 1.08 μM | Cell imaging |
| Present work | Pyrimidine based | 99 nM | Cell imaging, Dipstrip test |

The reversibility factor is very important for practical application. For reversibility, the EDTA was used with **L6**+$Al^{3+}$ mixture as chelating ligand, which was quenched the fluorescence intensity due to the formation of well-known complex between EDTA and $Al^{3+}$ ion. Figure 4.11 described the reversibility of **L6** with $Al^{3+}$ and EDTA. After that, again the addition of $Al^{3+}$ ion in the mixture of **L6** + $Al^{3+}$ +EDTA the fluorescence intensity was turned-on. These results offering that **L6** is the reversible chemosensor and it can be used as recyclable sensor over analyzed with $Al^{3+}$ with binding agent *i.e.* EDTA [28].

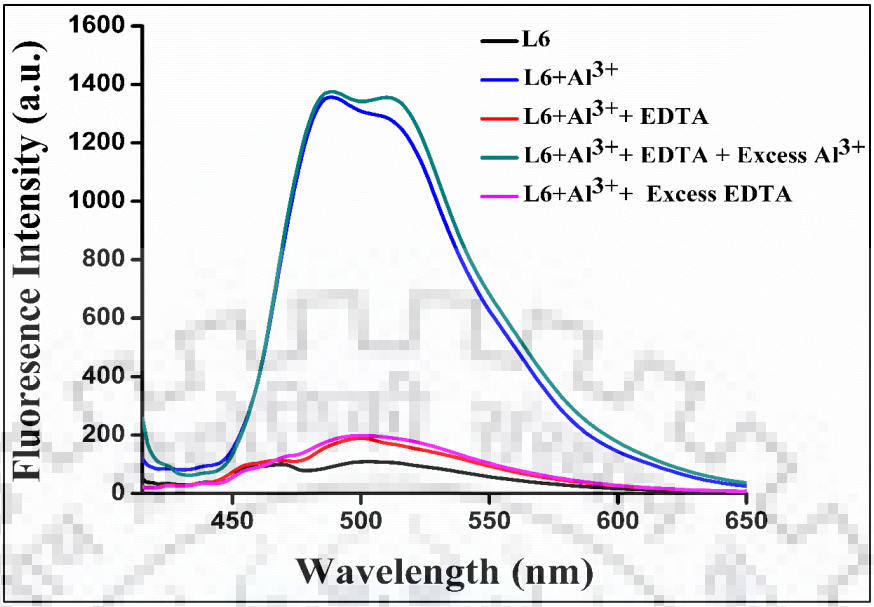


**Figure 4.11.** The reversibility behavior of **L6** by using EDTA as binding agent.

### 4.3.4 $^{1}$H-NMR titration

The binding mode of **L6** with $Al^{3+}$ ion, $^{1}$H-NMR titration was performed in DMSO-$d_6$. The complexation of **L6** with aluminum ion was also influence the NMR spectra, that changes was represented in the figure 4.12. It was clearly shown by the NMR spectrum the peaks at δ 14.20, 12.17, 11.90, 10.50, 6.57 ppm designated $–OH^{1}$, -SH, $-OH^{2}$, -CH=N, $-NH_2$ respectively, in which some was shifted to downfield region and some was shifted to upfield due to the co-ordination of $Al^{3+}$ with **L6**. An attractive observation was that $–OH^{1}$ proton was experienced exceptionally upfield shifting with $Al^{3+}$ ion from 14.20 δ ppm to 14.13 δ ppm, which was assigned as the proton for keto-amine tautomerization of **L6**. The aldimine proton along with $–OH^{2}$ was showed downfield shifting from δ 10.49 to δ 10.500 ppm and δ 11.90 to δ 11.93 ppm respectively. This all assignment was demonstrated in figure 4.12. Other proton signals were also shifted downfield region due to the decrement of electron density on **L6** chemosensor. During the NMR titration of **L6** with $Al^{3+}$, the all changes in the chemical shift clearly demonstrated that the N-atom of aldimine along with $O^{1}$ and $O^{2}$ (keto) as the donor atom in a tridentate form which represents the hard acid – hard base interaction [29].

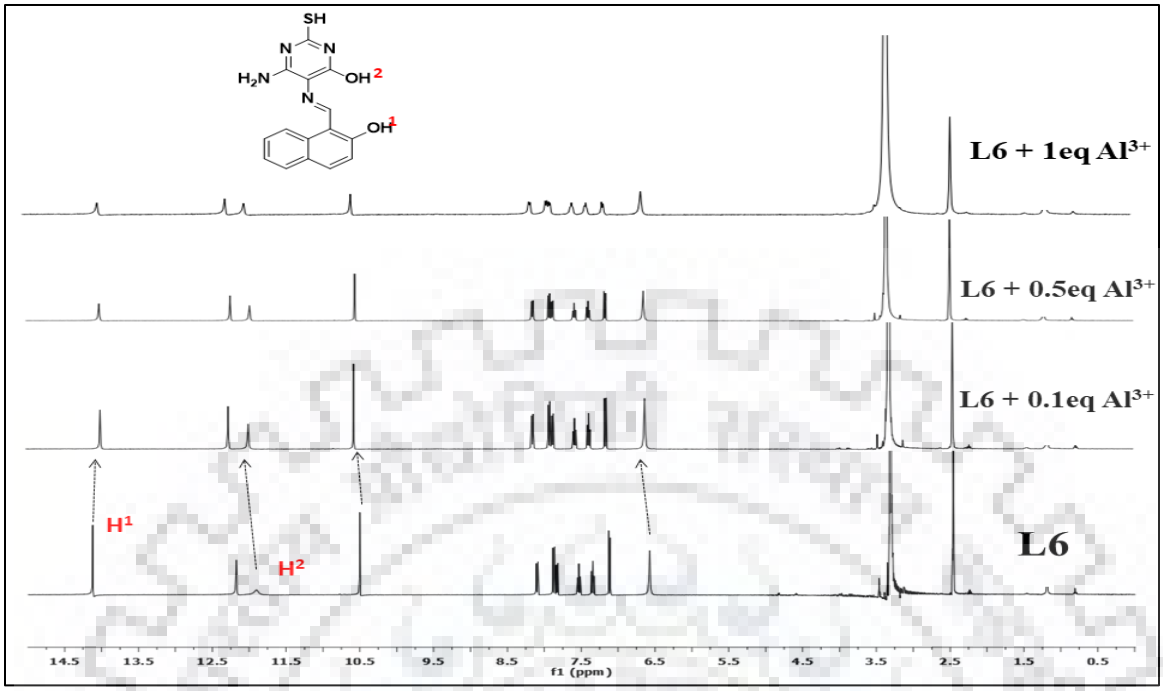


**Figure 4.12.** Binding affinity by $^{1}$H NMR titration of **L6** with $Al^{3+}$ in DMSO-$d_6$.

### 4.3.5 Computational studies

In theoretical context, the host-guest interaction was documented by Density Functional theory (DFT) method. The optimized geometry of **L6**, **L7** and **L6**+$Al^{3+}$ were gleaned in solution phase by Gaussian 09 W computational program with B3LYP functions and 6-31G(d, p) basis set for metal free chemosensor apart from this LaNL2DZ basis sets for **L6**+$Al^{3+}$ was used [30]. Figure 4.13 and figure 4.14 advertised the all optimized structure of **L6** and **L6** + $Al^{3+}$. The inter conversion of proton in keto - enol form of **L6** was also optimized by Gaussian 09 W program. The bond length of hydrogen bond of **L6** in keto – enol form was different the O-NH (the bond length is 1.553 Å) and OH-N (1.633 Å) which was clearly indicated the tautomerization of **L6** which support the ESIPT mechanism. In HOMO of **L6** the electron density was spread over the pyrimidine unit but in LUMO the electron cloud was localized over the naphthalene unit. The energy band gap of **L6**, **L7** was 3.43 eV (Figure 4.13, 4.14 and figure 4.15) and 2.71 eV respectively. After the addition of aluminum ion with **L6** the energy band gap was diminished up to 2.04 eV. HOMO of **L6**+$Al^{3+}$ represented that the electron distribution was focalized on whole molecule but in LUMO the electron density was spread over the

naphthalene unit. The decrement in energy band gap with aluminum ion supports that after complexation with metal ion ESIPT mechanism was hindered [31].

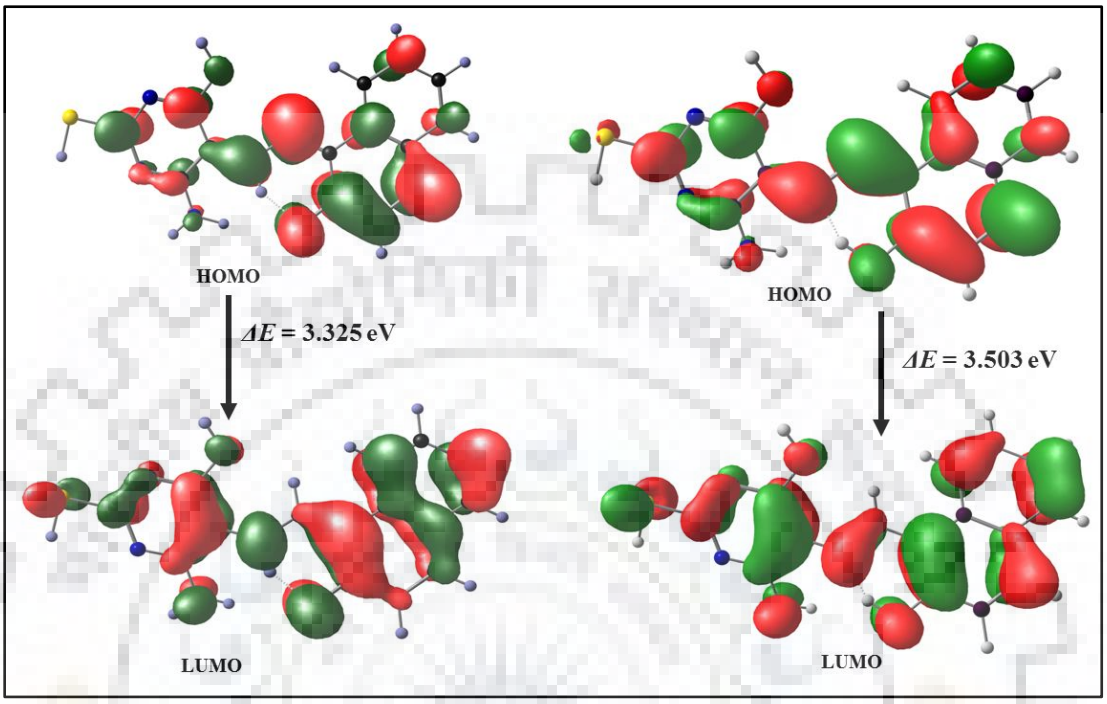


**Figure 4.13.** Computational study of **L6** the Keto-enol form in solution phase (solvent =ACN).

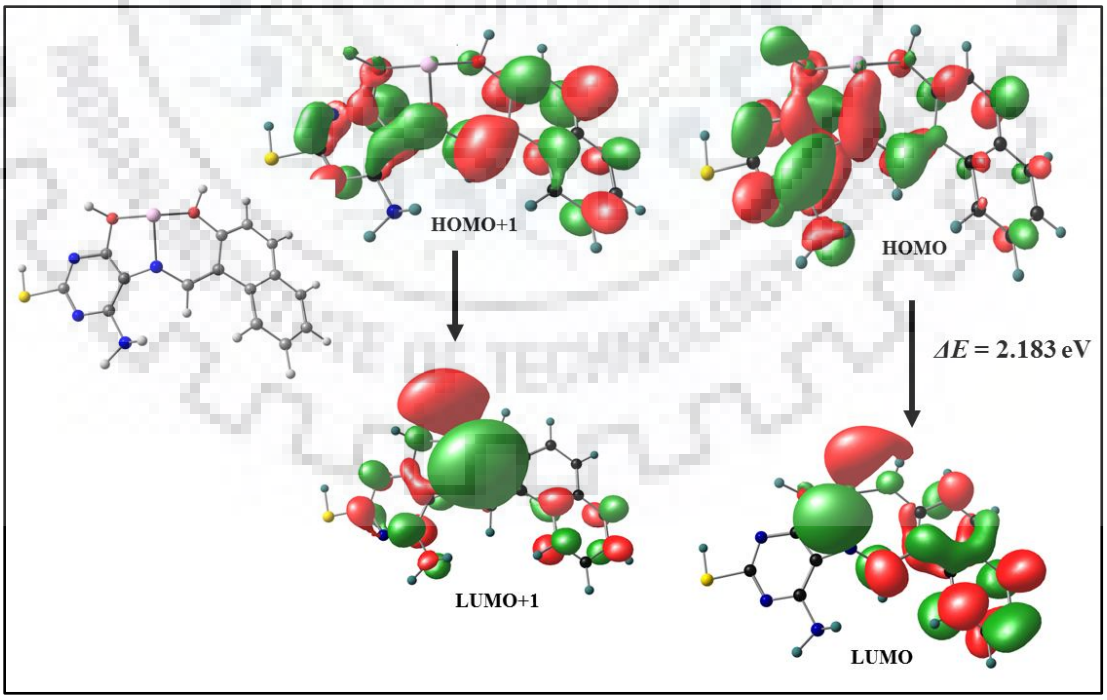


**Figure 4.14.** Computation study of **L6** with $Al^{3+}$ ion in solution phase (Solvent = ACN).

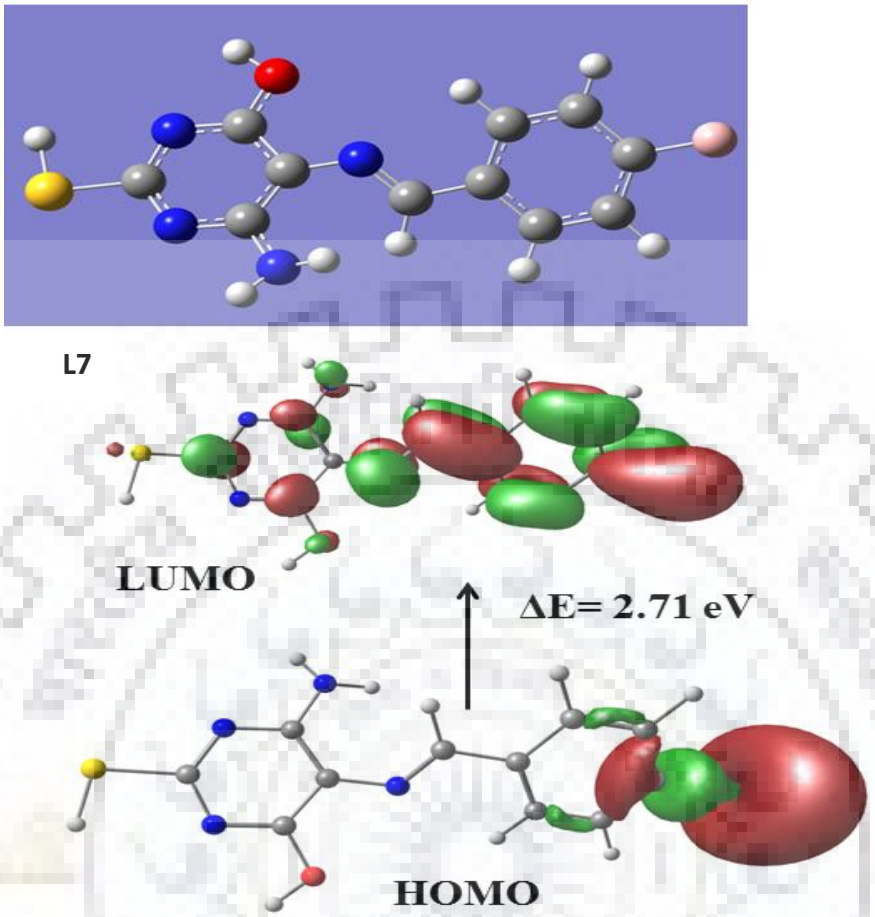


**Figure 4.15.** Optimized structure of **L7**.

### 4.3.6 Electrochemical demeanor

Further the electrochemical behavior of **L6** and **L6**+$Al^{3+}$ were evaluated in ACN solution with 0.1 M TBAP as supporting electrolyte. The voltammogram of probe **L6** described one oxidation peak at 1.465 V and one reduction peak at -0.690 V. Upon the addition of $Al^{3+}$ solution in the **L6** solution there was one new oxidation peak appeared at 0.92 V and one reduction peak at -0.94 V, simultaneously the current was increased due to the complexation with metal ion [32]. This anodic shift in the peaks specified the electrostatic interaction between **L6** and $Al^{3+}$. Figure 4.16 presented the cyclic voltammogram of **L6** and **L6**+$Al^{3+}$.

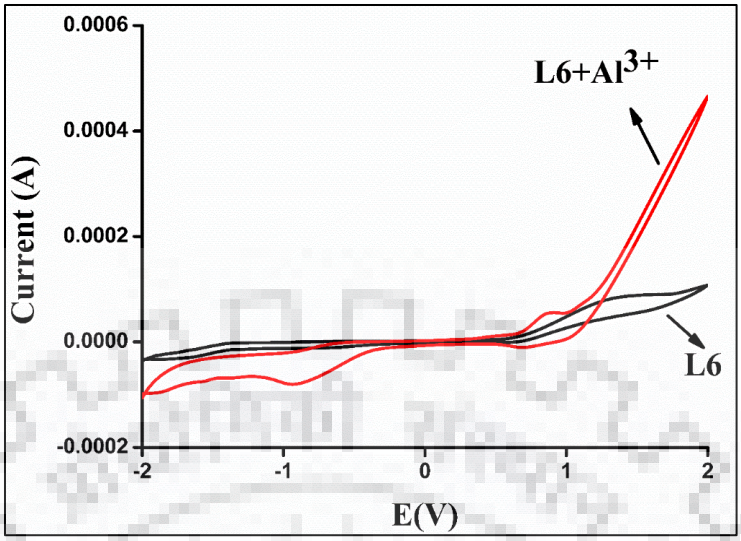


**Figure 4.16.** Cyclic Voltammogram of **L6** and **L6**+$Al^{3+}$.

### 4.3.7 Receptivity of sensor

The fluorescence life-time decay was measured of **L6** with $Al^{3+}$ by Horiba Jobin Yvon fluorocube instrument using time resolved fluorescence plot. The life time decay measurement was shown in figure 4.17, this life time decay plot of **L6** + $Al^{3+}$ followed the mono-exponential decay which revealed that decay time of **L6** with aluminum ion was 2.31 ns [33].

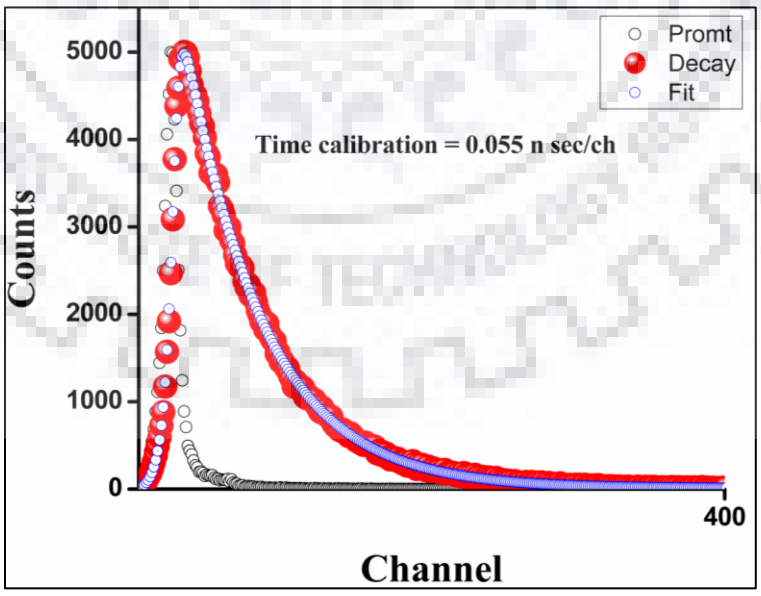


**Figure 4.17.** Time decay profile of **L6**+$Al^{3+}$.

### 4.3.8 OFF-ON switching behavior of L6

Based on reversibility behavior of **L6** receptor and consequent changes in fluorescent intensity at 500 nm, it can be implemented on Boolean logic operations [34, 35]. This was used as combinational logic circuit. In this context the strong fluorescence at 500 nm was prescribed by ON state (output= 1) whereas, the weak fluorescence corresponds to OFF state (output=0). There are two inputs IN1 $Al^{3+}$ and IN2 EDTA, whose presence and absence were itemized as 1 and 0. Figure 4.18 validated the logic gate behavior. The threshold value of intensity was determined as 400. The weak fluorescence intensity was observed below threshold value in the absence (0, 0), in presence of both inputs (1, 1) and also alone EDTA (0, 1). So, by analyzing the fluorescence intensity behavior with two inputs IN1 and IN2 an INHIBIT logic gate was entrenched at molecular level.

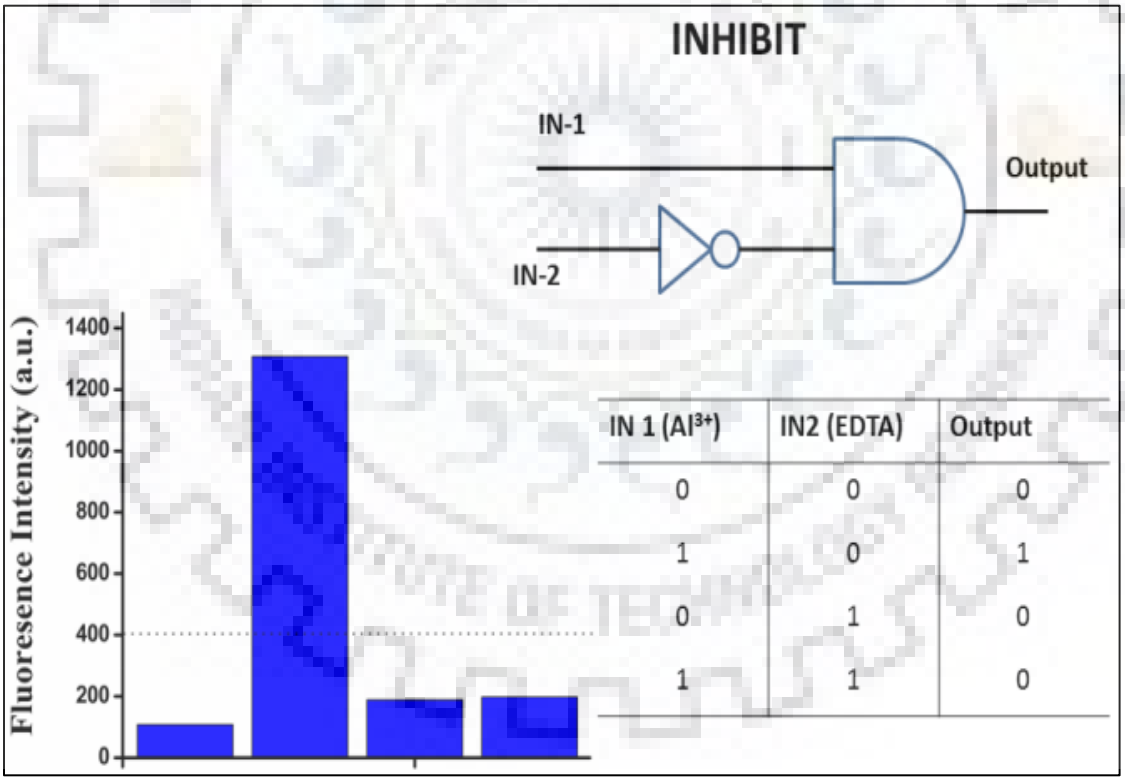


**Figure 4.18.** Represents the logic gate behavior which follow the **INHIBIT** gate.

## 4.4 APPLICATIONS

### 4.4.1 Bacterial cell imaging

For bacterial cell imaging, the E.coli DH5-α bacterial cell were grown overnight in LB (Luria Bertani) medium at 37 $^{O}$C in a shaker incubator. Overnight grown bacterial cells was incubated with 10 μM of $Al(Cl)_3$ in PBS at 37 $^{O}$C for 4 h. PBS solution was used for washing and remove the remaining $Al(Cl)_3$, the bacterial cells were then incubated with 10 μM of **L6** in ACN:PBS for half an hour at room temperature. Again, the incubated bacterial cells were washed with PBS solution and recorded onto a glass slide. Fluorescence images of fixed bacterial cells were gleaned using a Nikon Eclipse LV 100 fluorescence microscope at 20X magnification. This test reveals that the bacterial cell emits red and green fluorescence with $Al^{3+}$ in the presence of **L6** under fluorescence microscope. Figure 4.19 displayed the fluorescence images of bacterial cell in the presence of $Al^{3+}$ with **L6**.

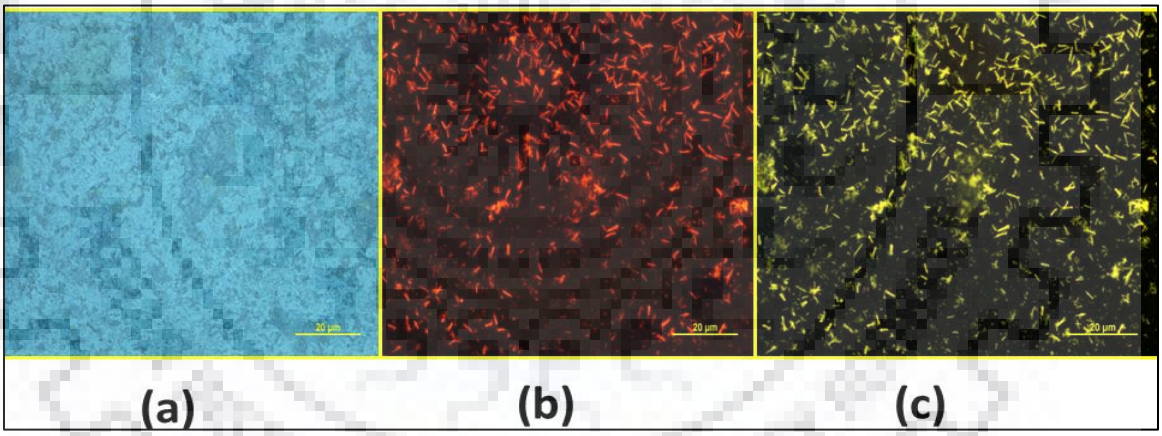


**Figure 4.19.** Fluorescent imaging of bacterial cell (E.coli DH5-α) a gram negative bacterial cell (a) represents the bacterial cell on glass slide with 20X magnification, in (b), (c) shows that it emits red and green fluorescent of bacteria with $Al^{3+}$ ion and **L6**.

### 4.4.2 Dip-strip test

Further for the practical application, **L6** used as chemosensor for aluminum metal ion, test paper strips easily prepared by normal filter paper and baptizing in the solution of **L6** (10μM) and dried these paper strips in open air for 3-4 hours.

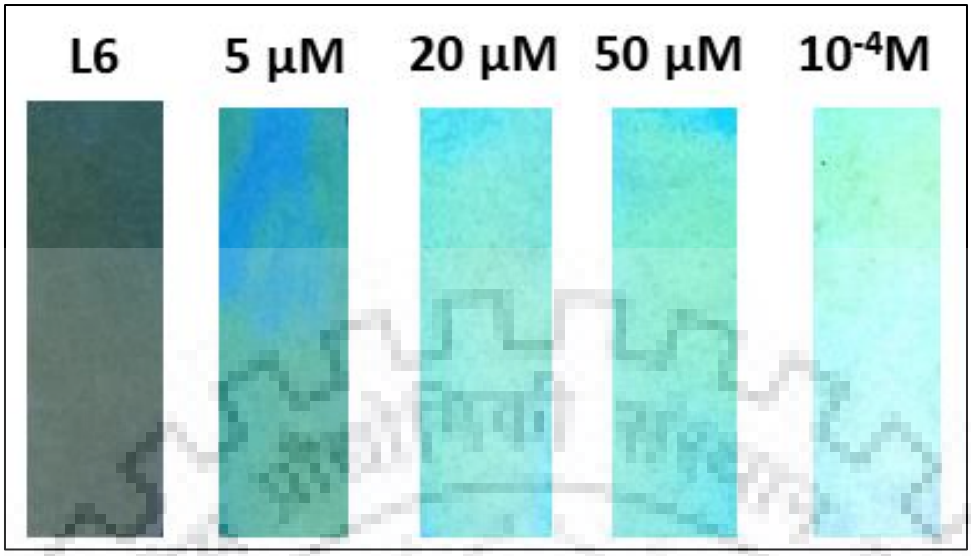


**Figure 4.20.** Represents the Paper strips of **L6** with different concentration of $Al^{3+}$.

Furthermore, the dried strips were drenched into diversified concentration of $Al^{3+}$; these strips advertised a significant change in UV light [36]. The result change in fluorescent behavior of these strips shown in figure 4.20, it is a small kit for the detection of $Al^{3+}$ in UV light.

## 4.5 CONCLUSIONS

The pyrimidine-based ligands **L6** and **L7**, was successfully synthesized and characterized *via* different tools such as NMR, UV-vis, Mass spectrometry, fluorescence spectroscopy, FTIR and elemental analysis. Apart from this, in both ligands only **L6** was highly selective for aluminum ion among other admissible metal ions as colorimetric and fluorescent chemosensors. The reversible chemosensor **L6** demonstrated low detection limit with aluminum ion *ca.* 99 nM. The binding interaction of **L6** with $Al^{3+}$ was successfully demonstrated by NMR, DFT optimization, cyclic voltammetry and optical studies. **L6** with aluminum ion was also represented the molecular switching behavior. Further, **L6** was successfully applied in different practical application *viz.* cell imaging and dip-strip test.

## References


1. M. I. S. Verıssimo, J. A. B. P. Oliveira and M. T. S. R. Gomes, Leaching of aluminium from cooking pans and food containers, Sens. Actuators B 118 (2006) 192– 197.

2. C.-H. Chen, D.-J. Liao, C.-F. Wan and A.-T. Wu, A turn-on and reversible Schiff base fluorescence sensor for $Al^{3+}$ ion, Analyst 138 (2013) 2527–2530.

3. G. D. Fasman, Aluminum and Alzheimer's disease: Model studies, Coor. Chem. Rev. 149 (1996) 125-165.

4. D. P. Perl, Relationship of aluminum to Alzheimer's disease, Environ. Health Persp. 63 (1985) 149-153.

5. T. L. Macdonald and R. B. Martin, Aluminum ion in biological system, Trends in Biochem. Sci. 13 (1988) 15-19.

6. N. E. Alstad, W. B. M. Kjelsberg, L. A. Vollestad, E. Lydersen and A. B. S. Poleo, The significance of water ionic strength on aluminium toxicity in brown trout (Salmo trutta L.), Environmental Pollution 133 (2005), 333–342.

7. World Health Organization, *In FAO/WHO Expert Committee report on food additives*, Report Series, (1989) WHO Tech, 33rd Report.

8. World Health Organization, Background document for development of WHO guidelines for drinking water quality. Geneva : Health Criteria and Other Supporting Information (1998) 2nd Addendum to, volume 2.

9. M. Shyamal, P. Mazumdar, S. Maity, G. P. Sahoo, G. Salgado-Morán and A. Misra, Pyrene scaffold as real-time fluorescent turn-on chemosensor for selective detection of trace-level Al(III) and its aggregation-induced emission enhancement, J. Phys. Chem. A 120 (2016) 210−220.

10. S. Sen, T. Mukherjee, B. Chattopadhyay, A. Moirangthem, A. Basu, J. Marek and P. Chattopadhyay, A water soluble $Al^{3+}$ selective colorimetric and fluorescent turn-

on chemosensor and its application in living cell imaging, Analyst 137 (2012) 3975-3981.

11. S. K. Kim and J. Yoon, A new fluorescent PET chemosensor for fluoride ions, Chem. Commun. (2002) 770-771.

12. D. Maity and T. Govindaraju, Pyrrolidine constrained bipyridyl-dansyl click fluoroionophore as selective $Al^{3+}$ sensor, Chem. Commun. 46 **(**2010) 4499–4501.

13. J. Wanga, Y. Pang, A simple sensitive ESIPT On-Off fluorescent sensor for selective detection of $Al^{3+}$ in water, RSC Adv. 4 (2014) 5845–5848.

14. M. J. Kim, R. Konduri, H. Ye, F. M. MacDonnell, F. Puntoriero, S. Serroni, S. Compagna, T. Holder, G. Kinsel and K. Rajeshwar, Dinuclear ruthenium(II) polypyridyl complexes containing large, redox-active, aromatic bridging ligands: synthesis, characterization, and intramolecular quenching of MLCT excited states, Inorg. Chem. 41 (2002) 2471–2476.

15. A. Sahana, A. Banerjee, S. Lohar, A. Banik, S. K. Mukhopadhyay, D. A. Safin, M. G. Babashkina, M. Bolte, Y. Garcia and D. Das, FRET based tri-color emissive rhodamine–pyrene conjugate as an $Al^{3+}$ selective colorimetric and fluorescence sensor for living cell imaging, Dalton Trans. 42 (2013) 13311–13314.

16. M. Arduini, F. Felluga, F. Mancin, P. Rossi, P. Tecilla, U. Tonellato and N. Valentinuzzi, Aluminium fluorescence detection with a FRET amplified chemosensor, Chem. Commun. (2003) 1606–1607.

17. S.-Z. Zhan, M. Li, X.-P. Zhou, D. Li and S. W. Ng, Excimer and exciplex formation in a pair of bright phosphorescent isomers constructed from $Cu_3$(pyrazolate)$_3$ and $Cu_3I_3$ coordination luminophores, RSC Adv. 1 (2011) 1457–1459.

18. S. J. Kirubavathy, J. Saranya, N. Sathya, I. V. M. V. Enoch, P. M. Selvakumar and S. Chitra, Synthesis, characterization and biological evaluation of Ru(III) mercaptopyrimidine Schiff base complexes, Appl. Organomet. Chem. (2017) 1–11.

19. J.-L. Tang, C.-Y. Li, Y.-F. Li, X. Lu and H.-R. Qi, A highly sensitive and selective fluorescent probe for trivalent aluminum ion based on rhodamine derivative in living cells, Analytica Chimica Acta 888 (2015), 155-161.

20. H. A. Benesi and J. H. Hildebrand, A spectrophotometric investigation of the interaction of iodine with aromatic hydrocarbons, J. Am. Chem. Soc. 71 *(*1949**)** 2703–2707.

21. D. Maity and T. Govindaraju, A differentially selective sensor with fluorescence turn-on response to $Zn^{2+}$ and dual-mode ratiometric response to $Al^{3+}$ in aqueous media, Chem. Commun. 48 (2012) 1039-1041.

22. F. K.-W. Hau, X. He, W. H. Lam, V. W.-W. Yam, Highly selective ion probe for $Al^{3+}$ based on Au(I)----Au(I) interactions in a bis-alkynyl calix[4]arene Au(I) isocyanide scaffold, Chem. Commun. 47 **(**2011) 8778–8780.

23. S. M. Hossain, A. Lakma, R. N. Pradhan, A. Chakraborty, A. Biswas and A. K. Singh, Synthesis and characterization of a novel, ditopic, reversible and highly selective, "Turn-On" fluorescent chemosensor for $Al^{3+}$ ion, RSC Adv. 5 **(**2015**)** 63338–63344.

24. D. Maity and T. Govindaraju, Conformationally constrained (coumarin-triazolyl-bipyridyl) click fluoroionophore as a selective $Al^{3}$þ, Inorg. Chem. 49 (2010) 7229–7231.

25. S. Samanta, S. Goswami, Md. N. Hoque, A. Ramesh and G. Das, An aggregation-induced emission (AIE) active probe renders Al(III) sensing and tracking of subsequent interaction with DNA, Chem. Commun. 50 **(**2014) 11833-11836.

26. K. B. Kim, D. M. You, J. H. Jeon, Y. H. Yeon, J. H. Kim and C. Kim, A fluorescent and colorimetric chemosensor for selective detection of aluminum in aqueous solution, Tetrahedron Letters 55 (2014) 1347–1352.

27. T. anand, G. Sivaraman, A. Mahesh and D. Chellappa, Aminoquinoline based highly sensitive fluorescent sensor for lead(II) and aluminum(III) and its application in live cell imaging, Anal. Chim. Acta 853 (2015) 596–601.

28. J. C. Qin, Z.-Y. Yang and P. Yang, Recognition of $Al^{3+}$ based on a naphthalene-based "Off–On" chemosensor in near 100% aquous media, Inorg. Chim. Acta 432 (2015) 136–141.

29. N. A. Kumar, V. Kumar, R. Prajapati, S. K. Asthana, K. K. Upadhyay and J. Zhao, A remarkable effect of N,N-diethylamino functionality on the optoelectronic properties of a salicylimine-based probe for $Al^{3+}$, Dalton Trans. 43 (2014) 5831–5839.

30. H. B. Schlegel, G. E. Scuseria, M. A. Robb, J. R. Cheeseman, G. Scalmani, V. Barone, B. Mennucci, G. A. Petersson, H. Nakatsuji, M. Caricato, X. Li, H. P. Hratchian, A. F. Izmaylov, J. Bloino, G. Zheng, J. L. Sonnenberg, M. Hada, M. Ehara, K. Toyota, R. Fukuda, J. Hasegawa, M. Ishida, T. Nakajima, Y. Honda, O. Kitao, H. Nakai, T. Vreven, Jr J. A. Montgomery, J. E. Peralta, F. Ogliaro, M. Bearpark, J. J. Heyd, E. Brothers, K. N. Kudin, V. N. Staroverov, R. Kobayashi, J. Normand, K. Raghavachari, A. Rendell, J. C. Burant, S. S. Iyengar, J. Tomasi, M. Cossi, N. Rega, J. M. Millam, M. Klene, J. E. Knox, J. B. Cross, V. Bakken, C. Adamo, J. Jaramillo, R. Gomperts, R. E. Stratmann, O. Yazyev, A. J. Austin, R. Cammi, C. Pomelli, J. W. Ochterski, R. L. Martin, K. Morokuma, V. G. Zakrzewski, G. A. Voth, P. Salvador, J. J. Dannenberg, S. Dapprich, A. D. Daniels, O. Farkas, J. B. Foresman, J. V. Ortiz, J. Cioslowski and D. J. Fox, Gaussian 09, Revision A.02, Gaussian, Inc., Wallingford CT, (2009).

31. W.-H. Ding, Wei, Cao, X.-J. Zheng, D.-C. Fang, W.-T. Wong and L.-P. Jin, A highly selective fluorescent chemosensor for Al(III) ion and fluorescent species formed in the solution, Inorg. Chem. 52 (2013) 7320−7322.

32. S. Goswami, S. Paul and A. Manna, Selective ''Naked Eye'' detection of Al(III) and PPi in aqueous media on a rhodamine–isatin hybrid moiety, RSC Adv. 3 (2013) 10639–10643.

33. A. Sahana, A. Banerjee, S. Lohar, B. Sarkar, S. K. Mukhopadhyay and D. Das, Rhodamine-based fluorescent probe for $Al^{3+}$ through time-dependent PET−CHEF−FRET processes and its cell staining, Inorg. Chem. 52 (2013) 3627−3633.

34. H.-S. Kim, S. K. Angupillai and Y.-A. Son, A dual chemosensor for both $Cu^{2+}$ and $Al^{3+}$: A potential $Cu^{2+}$ and $Al^{3+}$ switched YES logic function with an INHIBIT logic gate and a novel solid sensor for detection and extraction of $Al^{3+}$ ions from aqueous solution, Sens. Actuators B 222 (2016) 447–458.

35. S. S. Razi, R. Ali, R. C. Gupta, S. K. Dwivedi, G. Sharma, B. Koch and A. Misra, Phenylend- capped-thiophene (P-T type) based ICT fluorescent probe (D–π–A) for detection of $Hg^{2+}$ and $Cu^{2+}$ ions: Live cell imaging and logic operation at molecular level, J. Photochem. Photobiol. A 324 (2016) 106–116.

36. R. Ali, S. S. Razi, P. Srivastava, M. Shahid and A. Misra, A polynuclear hetero atom containing molecular organic scaffold to detect $Al^{3+}$ ion through a fluorescence turn-on response, RSC Adv. 5 (2015) 61513–61520.

# CHAPTER 5

## "OXALOHYDRAZONAMIDE BASED CHEMOSENSOR FOR MERCURY, CADMIUM AND COPPER IONS"

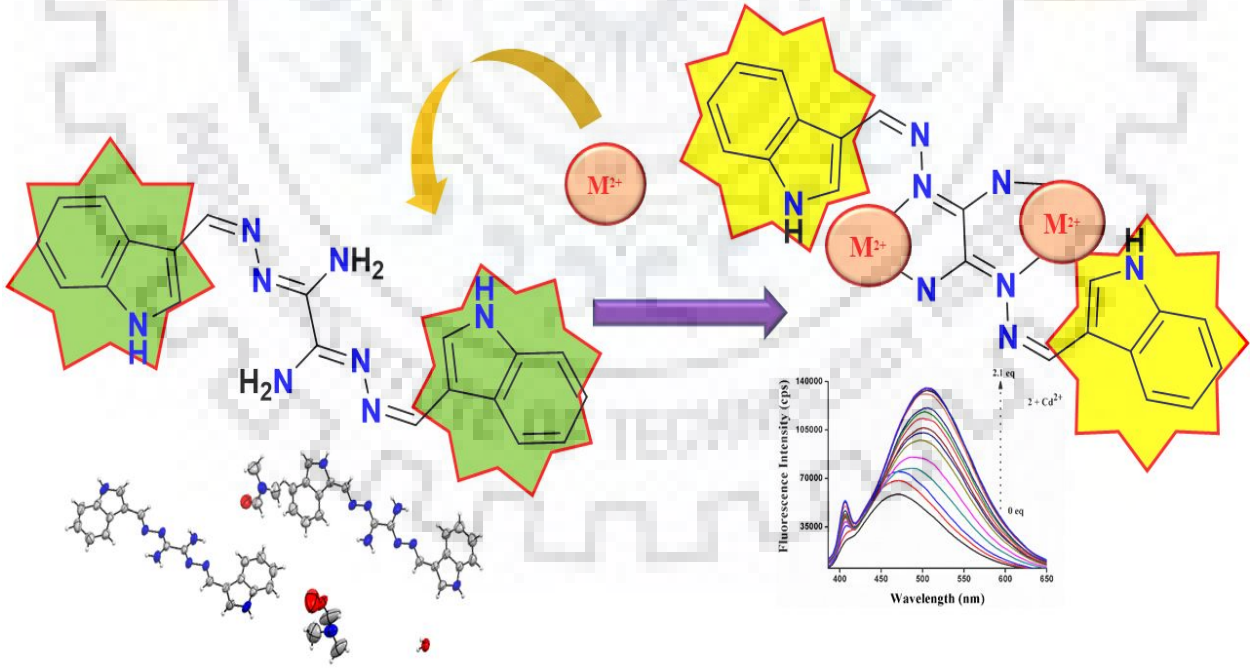

# CHAPTER 5

## 5.1 INTRODUCTION

The exposure and assessment of low contamination of transition and heavy metal ions are exclusively essential because these metal ions played a vital role in living systems and their high concentration showed extremely toxic impact on the environment [1,2]. This toxic effect of these metal ions attracts not only the scientific community, especially chemist, biologist, but progressively in general population who have knowledge of some disadvantages of these metal ions [3].

Among various metal ions mercury and cadmium are very toxic in nature due to their less solubility, not biodegradable, and thence can accumulate in the environment, that developed the contamination in food and water [4]. Apart from this, the slightly large concentration of copper ion also has the property to be an ecological pollutant and probably toxic to living cells [5]. Thus, these three metal ions have been involved in many diseases such as neurodegenerative diseases (Menkes, Alzheimer's and Wilson diseases) that related to copper ion high concentration [6-8]. Same as Hg(II) ion is highly toxic ion that can coordinate to biological ligands like DNA, enzyme and proteins which increases the toxic level of mercury ion that causes significant damage of kidney [9], brain [10] and central nervous system [11], accretion of Hg(II) in human body can supremacy of cognitive disorders and Minamata disease [12,13]. Cadmium is also an immensely toxic and carcinogenic metal ion whose higher level can associated with cardiovascular diseases, cancer morality and damage to kidneys and liver [14]. Therefore, it is necessary to develop the easy way to detect these ions in the environment. In this context, there are lots of instruments are available such as AAS, IES, ICP but these are very sophisticated and time consuming. Due to less biodegradability of these three metal ions it can accumulate in the environment, that contaminated the food and water. So, WHO (world health organization) and EPA (environmental protection agency) had rigidly determined the permissible limit of concentration of these metal ions that allowed in the drinking water.

Despite of, there are many sensors was designed for Copper, Mercury or Cadmium [15] *via* numerous mechanism such as ESIPT (excited state intramolecular proton transfer) [16], PET (photoinduced electron transfer) [17,18] and ICT (intramolecular charge transfer) [19,20]. On the next hand, still there are some flaws

among the noted chemosensors. Whereas, a smaller number of chemosensors that could analyze three cations simultaneously [21]. The detection of cations by the various fluorophores used are limited and usually organic solvent is the media for the detection of cations that limited many sensors for practical applications. The CHEF mechanism has some different quality rather than other mechanism such as large stock shift. Therefore, designed new chemosensor is highly sensitive towards the detection of $Cu^{2+}$, $Hg^{2+}$ and $Cd^{2+}$ simultaneously *via* CHEF mechanism in pure aqueous media. Moreover, the detection of these toxic metal ions in pure aqueous condition is still practical and challenging. In this context, this chemosensor detected copper, mercury and cadmium metal ion in aqueous media with good sensitivity. The present chemosensor has the multi donor atom *i.e.* the main reason to detect these ions.

## 5.2 MATERIALS AND METHODS

### 5.2.1 Materials and instruments

The distilled solvents were used throughout the whole experiments. The metal salts were used of analytical grade without further purification purchased from Merck. The FT-IR spectra was produced from Perkin Elmer FT-IR 1000 spectrophotometer. The NMR ($^{1}H$ and $^{13}C$) was received by JEOL 400 MHz spectrometer. All absorption spectra were gleaned by using Specord 600 Thermo Scientific PC double beam spectrophotometer with 3 cm path length quartz cell. Horiba RF-5301PC instrument was used for all emission spectra with standard quartz cell. The Verio MICROV3.1.1 instrument was used to perform elemental analysis (CHNS). The electrochemical studies executed on CHI760E Electro-Analyser instrument with three electrodes as, graphite electrode as working electrode, Pt wire had used as counter electrode and $Ag/AgCl_2$ electrode as reference electrode with 0.1 M tetrabutylammonium hexafluorophosphate ($nBu_4NPF_6$) supporting electrolyte. The mass spectra were received by using Brukar micrOTOF$^{TM}$-QII mass spectrometry.

### 5.2.2 Synthesis of ligand (L8)

**Synthesis of oxalohdrazonamide (1):** The ethanolic solution of dithiooxamide (1 mmol) and dropwise addition of 3 mmol hydrazine in the solution. After that this reaction

mixture was reflux for overnight. The dark brown precipitate was obtained after completion of the reaction by reported method [22].

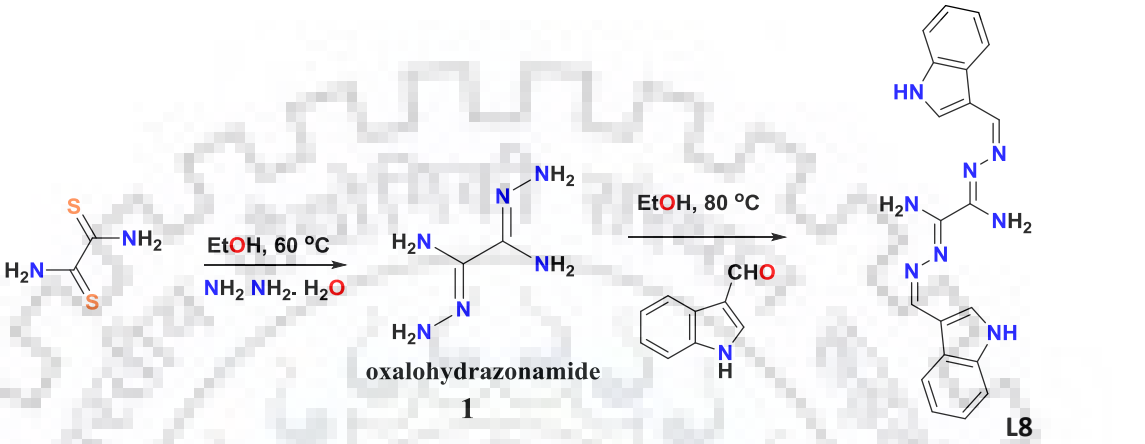


**Scheme 5.1.** Synthesis of compound **L8**.

**Synthesis of Bis((indol-3-yl)methylene)oxalohydrazonamide** (**L8**):

The ethanolic solution of **1** (1 mmol, 0.116g) was added dropwise to the ethanolic solution of indole 3-carboxaldehyde (2 mmol, 0.290g) with continuous stirring. The reaction mixture was refluxed for 6 hr. TLC was continuously checked up to completion of the reaction. A yellow coloured solution was acquired which was placed for crystallization for 7-8 days, after 7-8 days there was yellow coloured crystals appeared in block shaped. That crystals were separated from the solution and washed with ethanol and used for further studies. (Scheme 5.1)

**Yield:** 70%, Calculated for $C_{20}H_{18}N_8$; C: 68.28, H: 5.18, N: 26.54, and Found; C: 68.48, H: 5.099, N: 26.421, FTIR data (KBr, $\upsilon_{max}$ $Cm^{-1}$): $NH_2$: 3377, imidazole N-H: 3443, aromatic C-H: 3108, C=N: 1603, C-N: 1524, N=N: 1426. UV-Visible (water, $\lambda_{max}$ nm): 358 nm. $^1$H NMR (400 MHz) δ 11.62 (s, 2H), 8.64 (s, 2H), 8.31 (d, *J* = 7.5 Hz, 2H), 7.84 (d, *J* = 2.8 Hz, 2H), 7.43 (d, *J* = 7.6 Hz, 2H), 7.21–7.16 (m, 2H), 7.16–7.12 (m, 2H), 6.29 (s, 4H). $^{13}$C NMR (100 MHz) δ 153.01, 151.37, 137.64, 132.12, 125.03, 123.32, 122.85, 121.39, 113.09, 112.41. ESI mass: 393.2078 $(M + Na)^+$.

### 5.2.3 X-ray Crystallography

Bruker Kappa Apex four circle -5 CCD diffractometer was used for structural measurement of single crystal of **L8**. The suitable single crystal of **L8** was grown in the mixture of DMF: $H_2O$ (1:2) solution that escalated on nylon 7 Cryoloop. The data reduction was performed on SMART/SAINT software and the intensity data collection was mounted on Graphite monochromatic Mo$K\alpha$ radiation (0.7107 Å) at 298 K. All the data collection, structural solution and refinement were gained by SHELXTL program with direct method. Hydrogen bonding interaction with packing of 3*3 [figure 5.1(a)] and [figure 5.1(b)] images were designed in the crystal lattice by Mercury 3.9 software. Refinement parameter of **L8** is shown in table 5.1. Crystallographic data of **L8** has been deposited in Cambridge Crystallographic Data Centre with **CCDC 1835002**.

**Table 5.1:** Crystal data and structure refinement parameters of **L8**.

| | **L8** |
|---|---|
| Empirical formula | C28 H32 N10 O4 |
| Formula weight | 550.63 |
| Crystal system | Triclinic |
| Space group | P-1 |
| a/Å | 7.1650 |
| b/Å | 11.7125 |
| c/Å | 18.4026 |
| α/Å | 84.993 |
| β/Å | 81.868 |
| γ/Å | 74.095 |
| $V$/Å$^3$ | 1468.38 |
| $Z$ | 2 |
| $D_{calc}$ (g cm$^{-3}$) | 1.245 |
| $\mu/mm^{-3}$ | 0.088 |
| $\Theta$ *range*/$^{\circ}$ | 1.119-28.376 |
| Reflection collected | 7373 |
| Independent Reflection | 4575 |
| Parameters | 374 |

| | |
|---|---|
| GOF ($F^2$) | 1.116 |
| $R_1$; $wR_2$ [I>2 sigma(I)] | 0.0776-0.1145 |
| $R_1$; $wR_2$ (all data) | 0.2097-0.2468 |

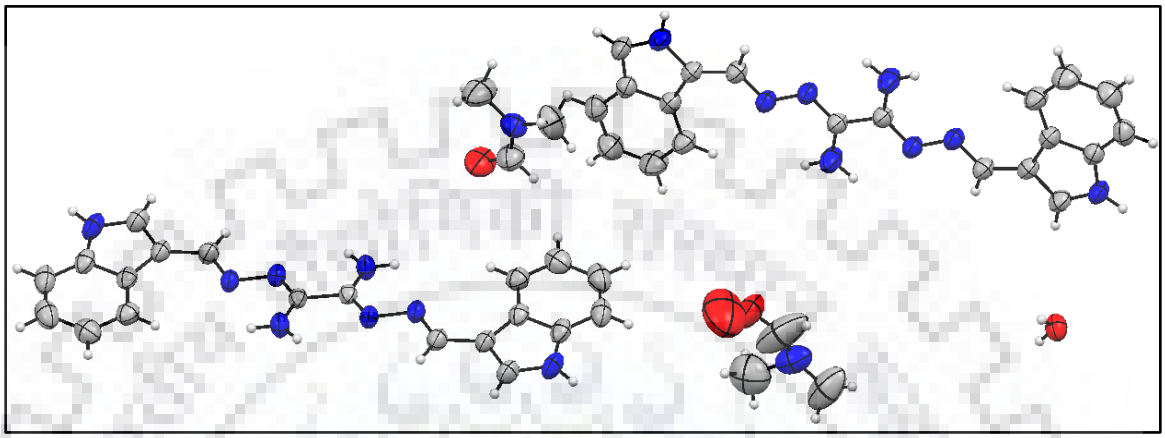

**Figure 5.1(a).** ORTEP diagram of compound **L8**.

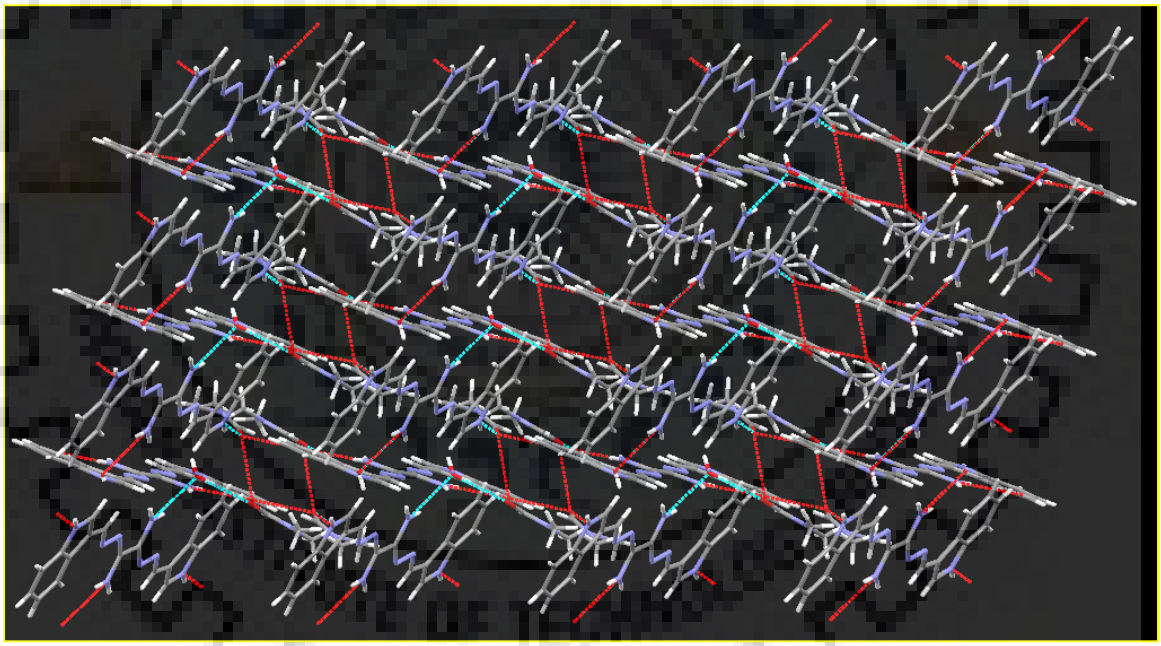

**Figure 5.1(b).** Packing of 3*3 diagram with hydrogen bonding interaction of compound **L8**.

## 5.3. RESULTS AND DISCUSSION

### 5.3.1 Visual test

The preliminary test for naked eye detection of metal ion is visualization test. This test was performed with $10 \times 10^{-4}$ M concentration of **L8** in water with various metal ions

(1mM). Figure 5.2 represented the colorimetric experiment that revealed the sudden color change was occurred with $Cu^{2+}$, $Hg^{2+}$ and with $Cd^{2+}$ ions among other metal ions [23]. This color change was from colorless to dark yellow in case of mercury and light yellow with cadmium ions whereas, dark green color was observed with copper ion. The color change refers to complexation of probe **L8** with metal ions.


**Figure 5.2.** The colorimetric test of **L8** with different metal ions in aqueous medium.

### 5.3.2 Photophysical properties of L8

Further, the absorption study was conducted of **L8** with all three ions by UV-Vis spectroscopy. Figure 5.3 represented the selectivity experiment of all three metal ions among other metal ions *via* absorption and emission studies. The absorption studies of **L8** were investigated by observing the absorption spectral demeanor upon the addition of various metal ions such as $Al^{3+}$, $Ag^{+}$, $Fe^{3+}$, $Ba^{2+}$, $Ca^{2+}$, $Cd^{2+}$, $Co^{2+}$, $Cu^{2+}$, $Cr^{3+}$, $Cs^{+}$, $Hg^{2+}$, $Hg^{+}$, $K^{+}$, $Pb^{2+}$, $Li^{+}$, $Mn^{2+}$, $Ni^{2+}$, and $Zn^{2+}$ in an 100% aqueous medium. **L8** showed an absorption band centered around 356 nm due to n-π* transition and this band remain unaffected by the addition of 10 equivalent of all metal ions except $Cd^{2+}$, $Cu^{2+}$ and $Hg^{2+}$. The absorption band at 356 nm was slightly shifted to red shift (3 nm) with the interaction with $Cd^{2+}$ ion, whereas in case of $Hg^{2+}$ ion it was shifted to red shift ($\Delta\lambda$ = 49 nm) at 405 nm due to ligand to metal charge transfer (LMCT). Similarly, in case of copper ion there was slight shifting ($\Delta\lambda$ = 18 nm) towards red shift from 356 nm to 374 nm that also support the LMCT behavior of complexation, which was shown in the figure 5.3.

Further, the selectivity and sensitivity of $Cu^{2+}$, $Hg^{2+}$ and $Cd^{2+}$ ions among different metal ions were proved by emission studies of **L8** with pool of various metal ions. The fluorescence studies were performed in aqueous medium with 10 µM

concentration of **L8** with 3 equiv. of all metal ions (50 μM). The emission spectra manifested that there was quenching occurred in the fluorescence intensity with $Cu^{2+}$ due to photoinduced electron transfer whereas in case of $Hg^{2+}$ ion quenching appeared with excellent red shift ($\Delta\lambda_{ex}$ = 81 nm) because of chelation fluorescence quenching behavior. Whereas, in case of $Cd^{2+}$ ion an immediate enhancement in the fluorescence intensity was occurred with some red sift ($\Delta\lambda_{ex}$= 53 nm) due to chelation enhanced fluorescence (CHEF) mechanism (Figure 5.3).

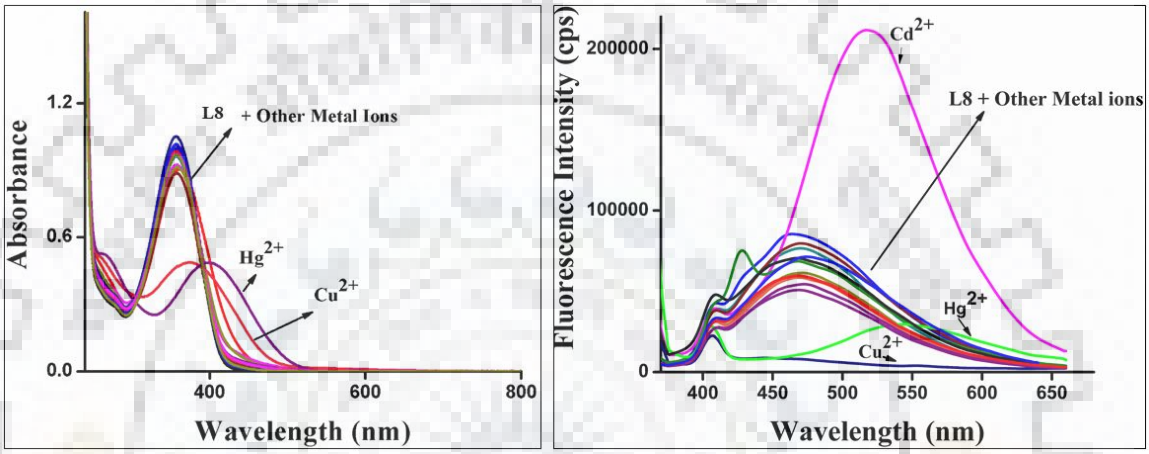


**Figure 5.3.** UV-vis and emission spectra of **L8** with the various metal ions.

After selectivity checking, the titration experiment was executed with a consecutive addition of metal ions to a 10 μM solution of **L8** one by one. Firstly, upon gradual addition of $Cu^{2+}$ to **L8** one strong high energy absorption band at $\lambda_{max}$ = 356 nm decreased with a simultaneous increment in intensity of the band at 374 nm. Similarly, with $Hg^{2+}$ the absorption band at 356 nm was gradually decreased with increasing in the band at 405 nm that was shown in figure 5.4. This shifting in the absorption bands revealed that the complexation occurred from the decomplexed probe **L8**. The titration experiment was also performed by emission spectroscopy that represented in the figure 5.5 (a), (b) & (c). The consecutive addition of $Cd^{2+}$ ion in the solution of **L8** supported the red shift by 53 nm due to the chelation enhanced fluorescence mechanism with the excitation wavelength of 373 nm. In case of $Cu^{2+}$ the fluorescence intensity was quenched due to photoinduced electron transfer from imine nitrogen atom. However, the continuous addition of mercury ion in probe **L8** solution demonstrated that the intensity

was also quenched due to the CHQF mechanism with shifting 81 nm bathochromic shift by figure 5.5 (c).

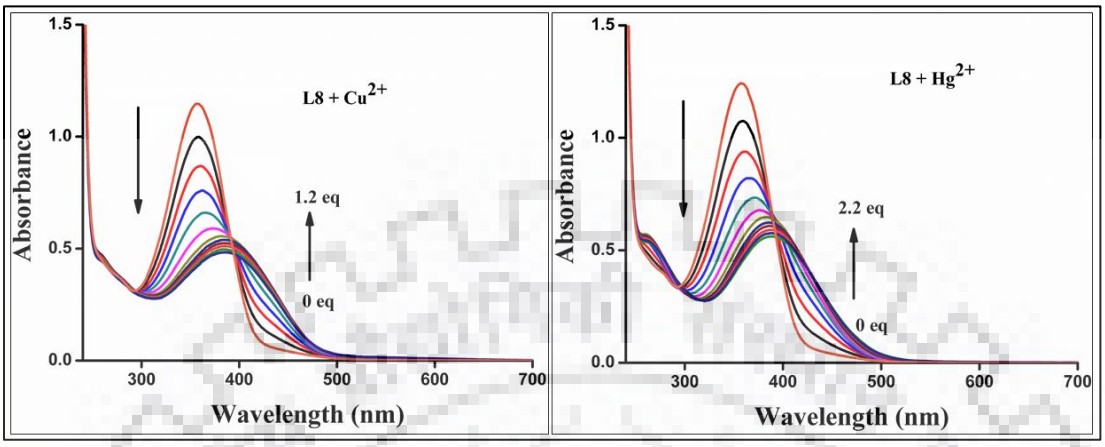


**Figure 5.4.** The titration experiment of **L8** with $Cu^{2+}$ and $Hg^{2+}$ ion on consecutive addition.

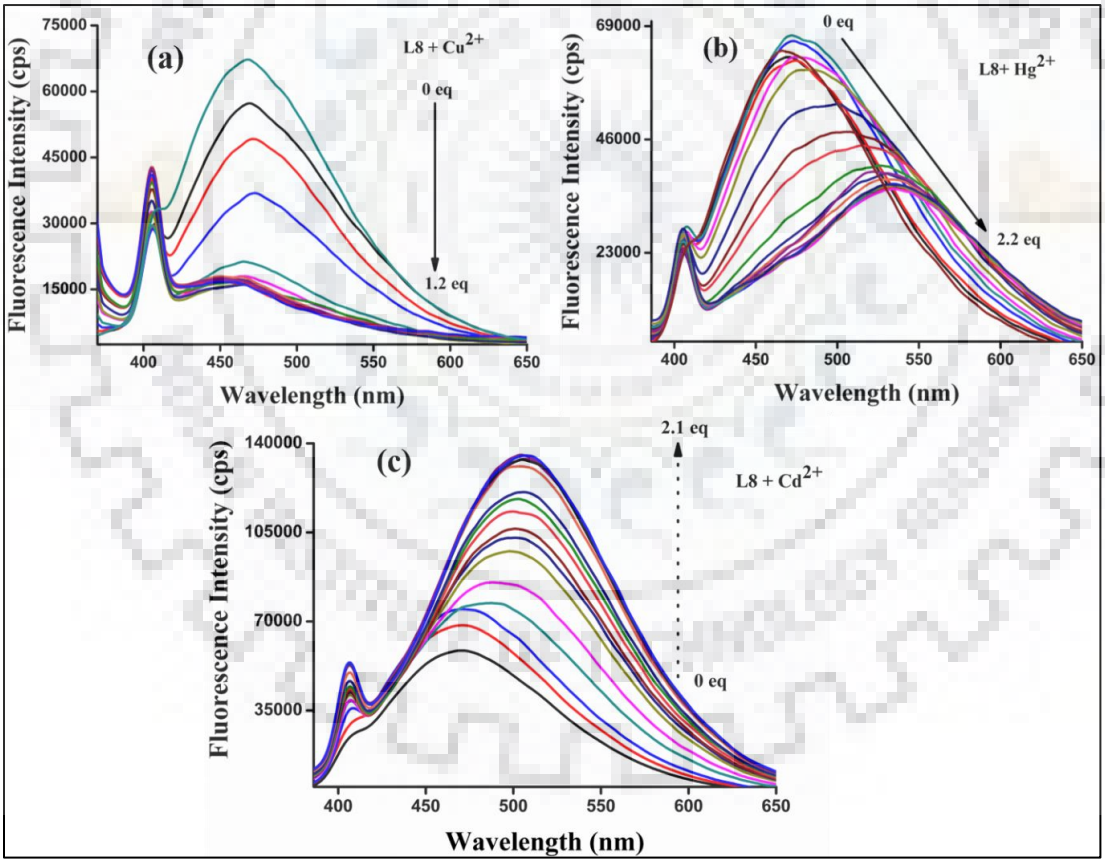


**Figure 5.5.** The emission titration of **L8** with three metal ions, (a) figure represent the $Cd^{2+}$ titration with probe L**8**, (b) titration with $Cu^{2+}$ ion, (c) shows titration of $Hg^{2+}$ with probe **L8**.

The binding assays was represented by utilizing the method of continuous variation in mole fraction (Job's Plot) that was plotted between continuously varied mole fraction and intensity/absorption of probe **L8** with metal ions. The Job's plot recommended 1:2 (Receptor: Cation) stoichiometry for $Cu^{2+}$, $Hg^{2+}$ and $Cd^{2+}$ metal ions respectively which is represented in Figure 5.6 (a), (b) and (c).

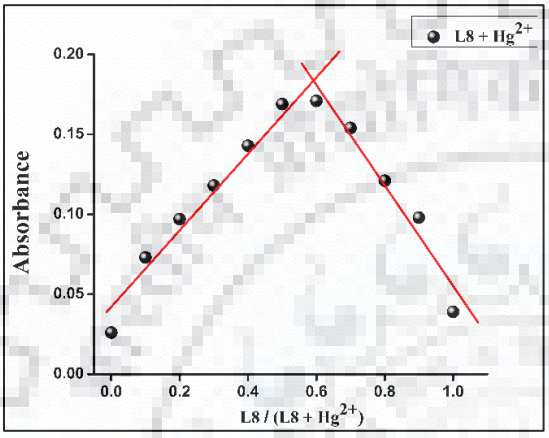


**Figure 5.6(a).** The Job's plot of $Hg^{2+}$ with **L8**.

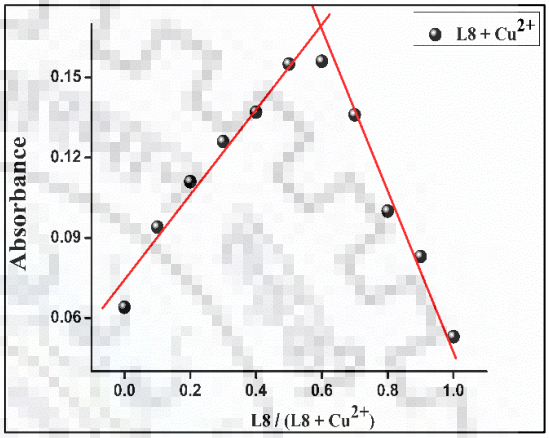


**Figure 5.6(b).** The Job's plot of $Cu^{2+}$ with **L8**.

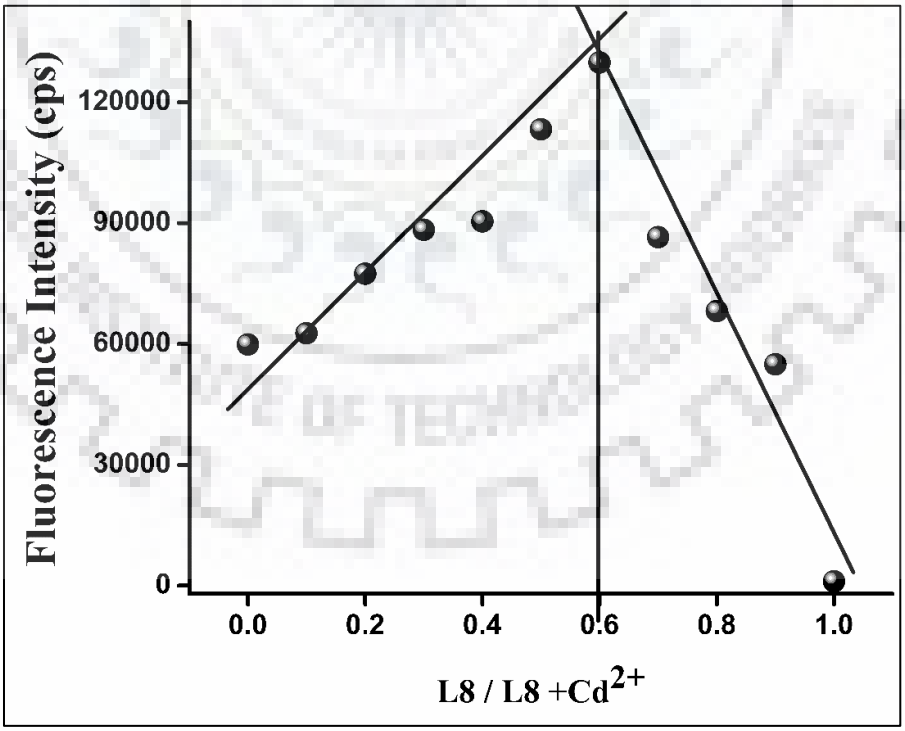


**Figure 5.6(c).** The Job's plot of $Cd^{2+}$ with **L8**.

Moreover, the stoichiometry of the complex has been endorsed by ESI-mass where peaks at m/z 791 for (**L8** + 2Cd + $2ClO_4^-$), m/z 610 for (**L8**+ 2Cu + $2AcO^-$) and m/z 839 for (**L8**+2Hg+$2Cl^-$) was examined which supported 1:2 stoichiometry between probe **L8** and all three metal ions that is shown in figure 5.7 (a), (b) and (c).

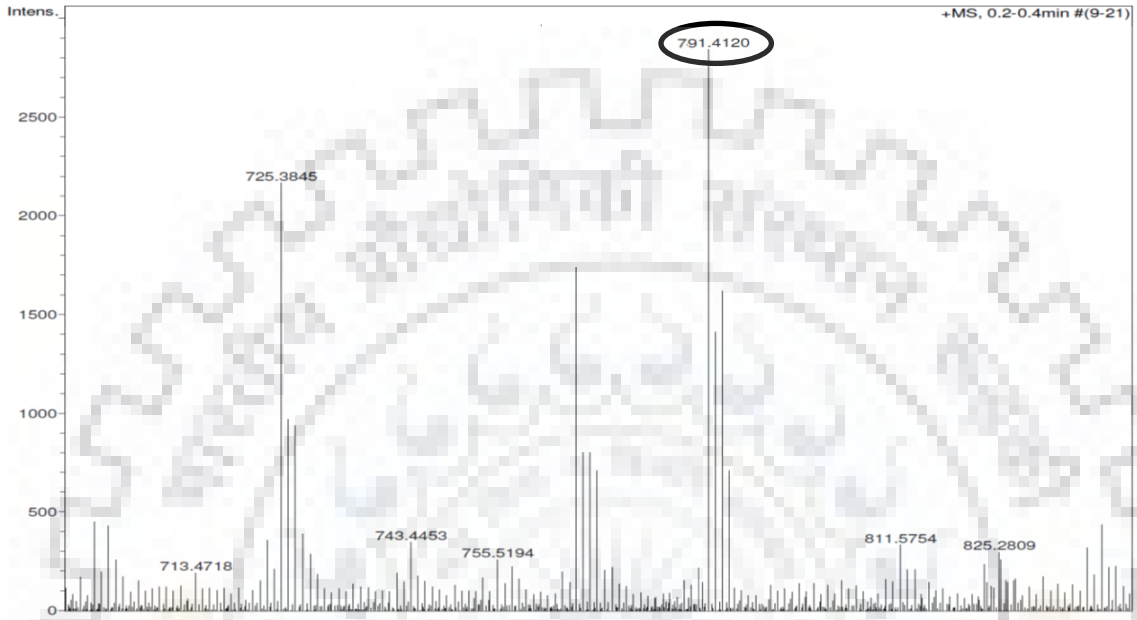


**Figure 5.7(a).** The mass spectra of [**L8 + 2Cd$^{2+}$ + 2ClO$_4^-$**].

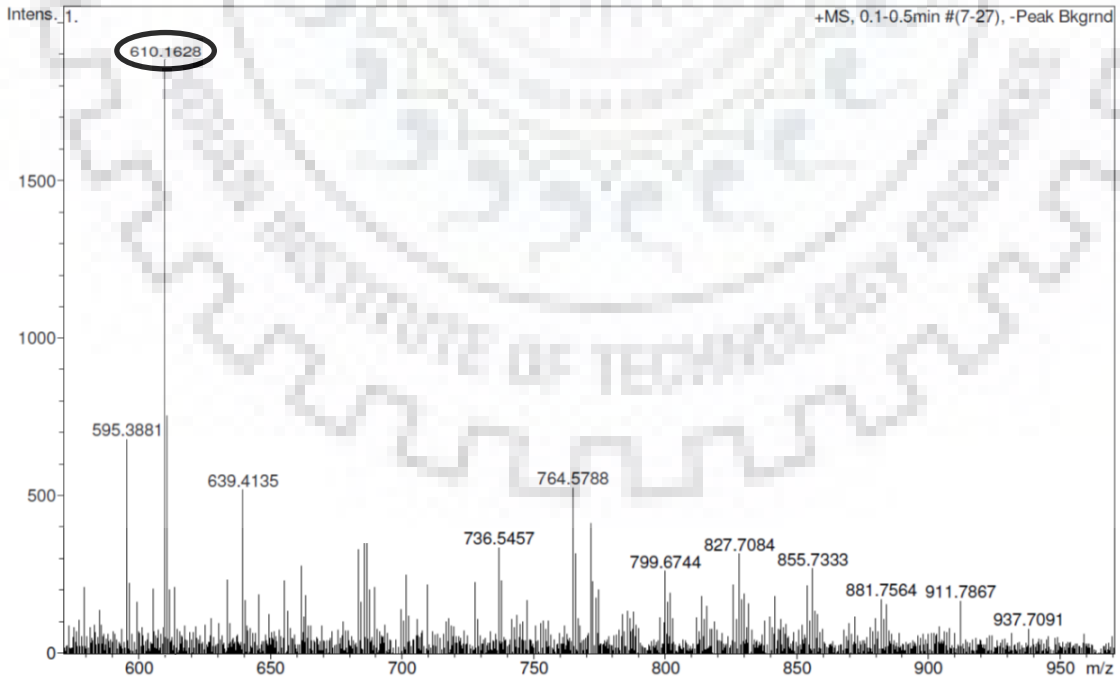


**Figure 5.7(b).** The mass spectra of [**L8 + 2Cu$^{2+}$ + 2AcO$^-$**].

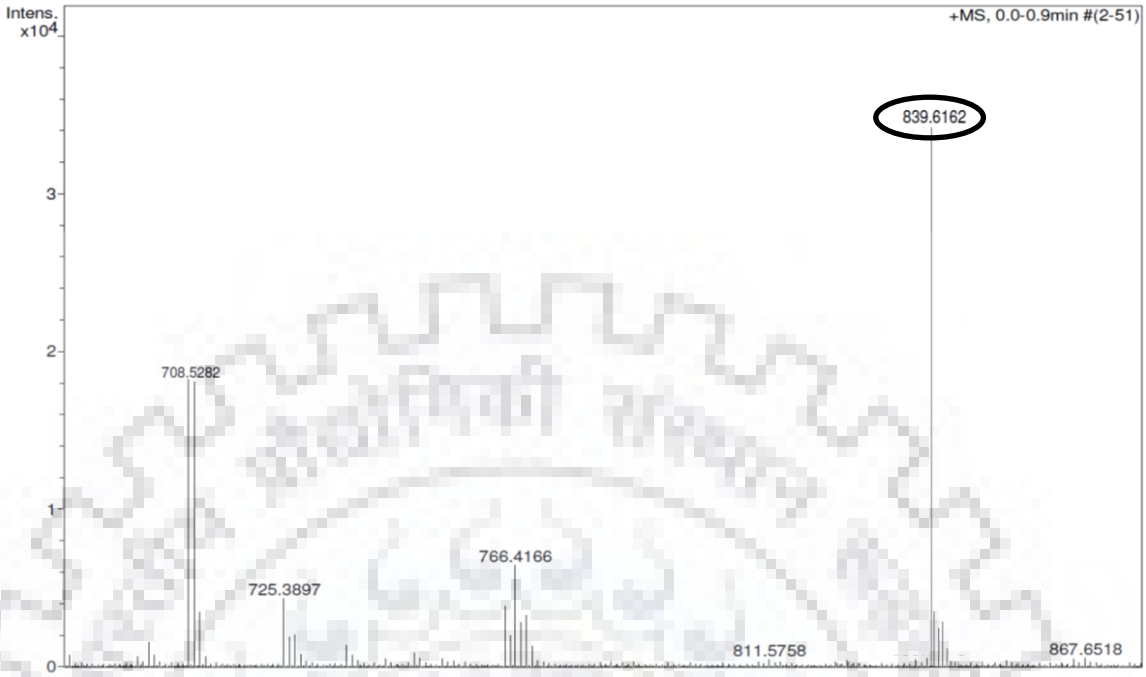


**Figure 5.7(c).** The mass spectra of [**L8** + $2Hg^{2+}$+$2Cl^{-}$].

Further, the sensitivity of **L8** was also affirmed by the performance of competitive experiments with all three-metal ion in the presence of other metal ions and the results revealed that there was no interference found besides $Cu^{2+}$ and $Hg^{2+}$ in case of $Cd^{2+}$ ion, the intensity was slightly decreased with copper and mercury ion. Similarly, the same experiment was performed with $Cu^{2+}$ and $Hg^{2+}$ ion in presence of other metal ions and monitored that there was no interference of other metal ions apart from $Cd^{2+}$ ion in which some increment in the intensity was found. Figure 5.8 (a), (b) and (c) shown the competitive experiment with other metal ions in presence of $Cu^{2+}$, $Hg^{2+}$and $Cd^{2+}$ ion.

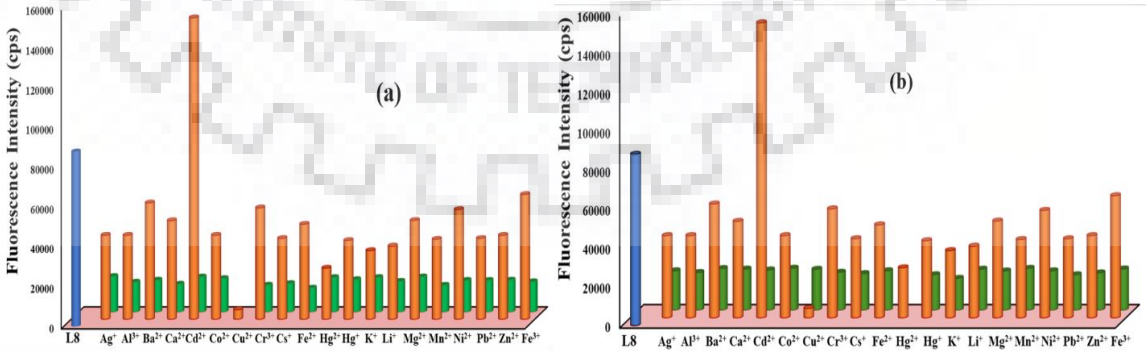


**Figure 5.8.** Competitive experiment of **L8** with $Cu^{2+}$ and $Hg^{2+}$ ion in the presence of different metal ions that is presented in (a) and (b) respectively.

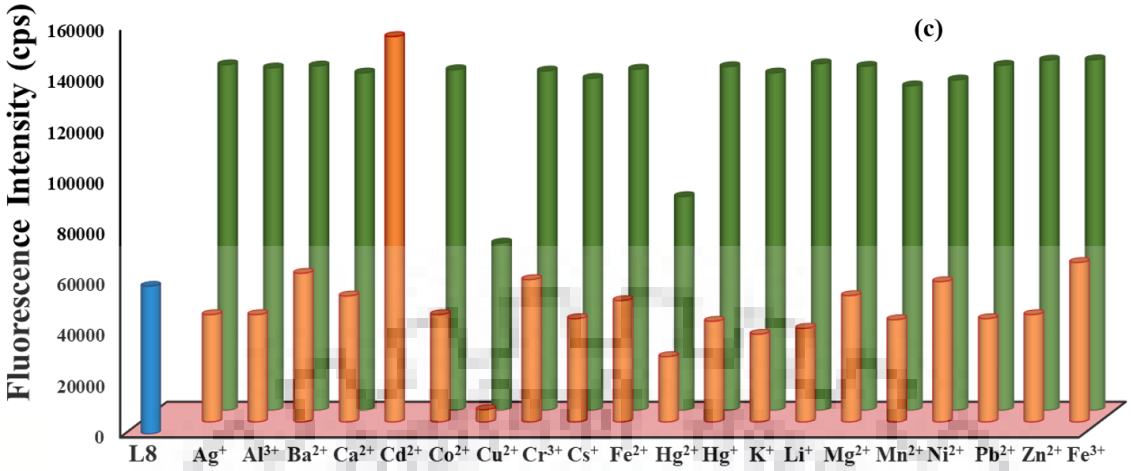


**Figure 5.8(c).** Represented the interference study of **L8** with $Cd^{2+}$ ion in the presence of other metal ions.

Moreover, determined the association constant ($K_a$) for $Cu^{2+}$, $Hg^{2+}$ ion with **L8** represented by Stern-Volmer plot [24-26] between concentration of metal ion ($Cu^{2+}$ & $Hg^{2+}$) and $F_0/F$ where $F_0$ represents the initial intensity of **L8** without addition of metal ion and F showed the intensity of the solution on gradual addition of metal ions. The S-V plot explained the static nature of quenching by the addition of metal ions. Figure 5.9 (a) & (b) and Figure 5.10 (a) & (b) represented the S-V plot of **L8** with $Cu^{2+}$ and $Hg^{2+}$ ions respectively. Similarly, the formation constant of $Cd^{2+}$ ion was established by Hill plot [27] that was constructed between log (1/metal ion concentration) and log $[(I-I_0)/(I_{max}-I)]$ that was demonstrate in figure 5.12 (a) & (b).

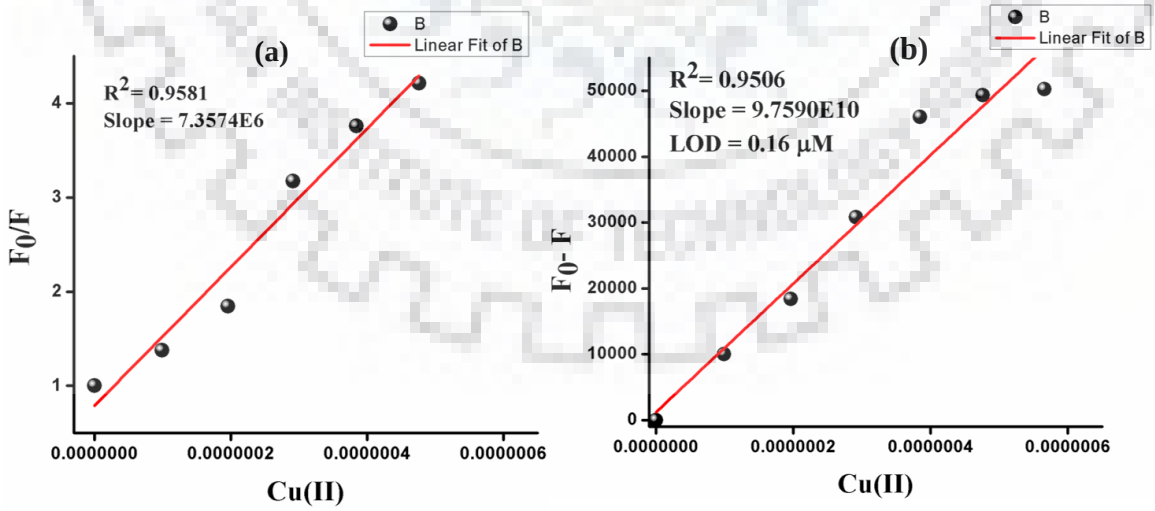


**Figure 5.9.** (a) Demonstrate the S-V plot of **L8** with $Cu^{2+}$ ion for binding constant and (b) shows limit of detection graph of **L8** with $Cu^{2+}$ ion.

The formation constant for $Cu^{2+}$, $Hg^{2+}$ ions were calculated $7.35 \times 10^6$, $2.33 \times 10^6$ by S-V plot and for $Cd^{2+}$ ion the $K_a$ value was 11.1621 (log $\beta$) by Hill Plot. Similarly, the limit of detection was calculated through 3σ/slope where σ represents the standard deviation calculated for different solution of same concentration of ligand **L8** (Figure 5.11). The limit of detection was 0.16 μM for $Cu^{2+}$, 0.33 μM for $Hg^{2+}$ ion and 0.11 μM for $Cd^{2+}$ ion. All data was summarized in table 5.2.

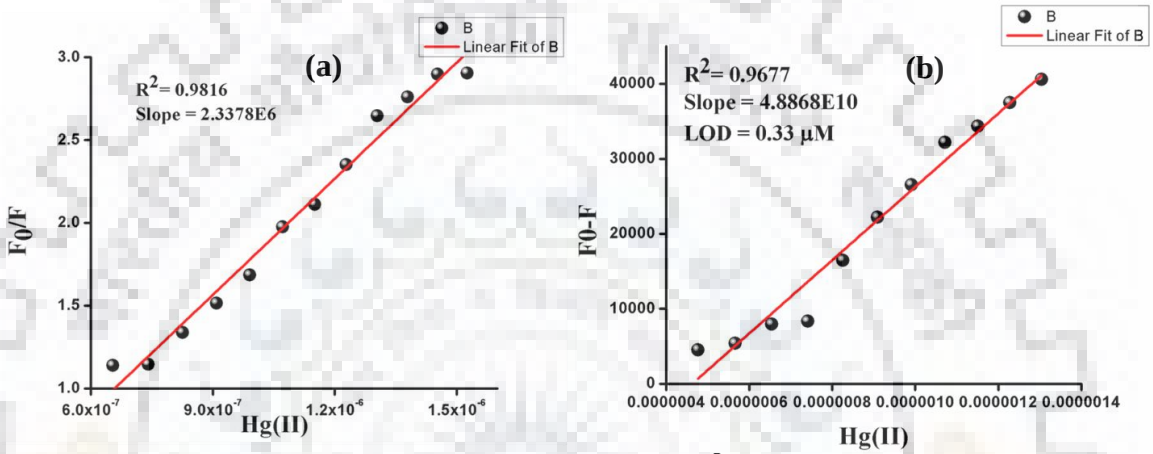


**Figure 5.10.** (a) Manifested the S-V plot of **L8** with $Hg^{2+}$ ion for binding constant and (b) shows limit of detection graph of **L8** with $Hg^{2+}$ ion.

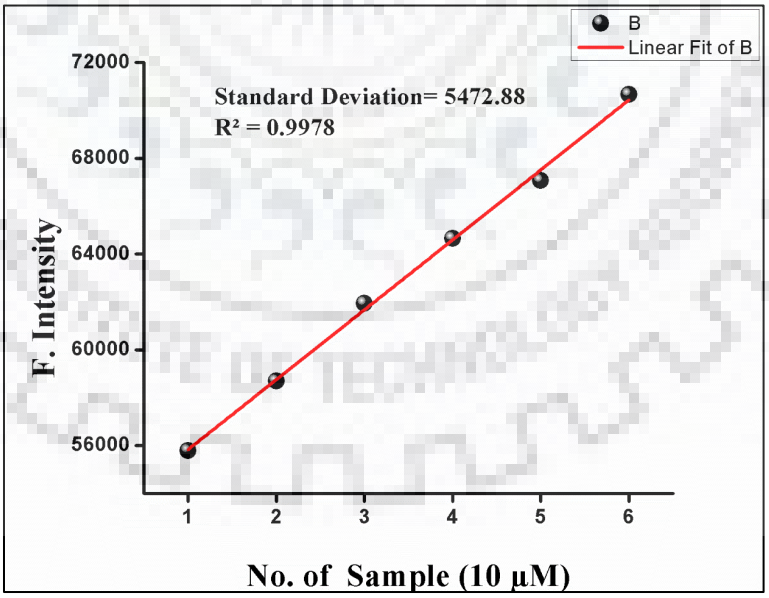


**Figure 5.11.** The standard deviation of six samples of **L8** (10 μM).

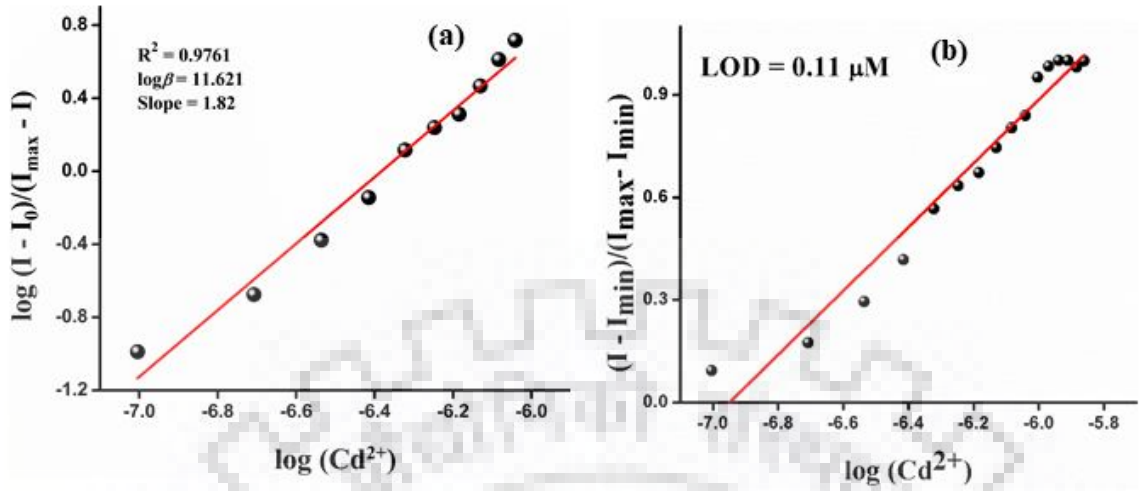


**Figure 5.12. (a)** Determined the B-H plot for $Cd^{2+}$ ion and **(b)** manifested the limit of detection of $Cd^{2+}$ ion.

**Table 5.2:** Summarized all data of photophysical properties of **L8**.

| | **Absorption Maxima ($\lambda_{max}$), nm** | **Emission Maxima ($\lambda_{em}$), nm** | **Stoichiometry** | **Stock shift (nm)** | **Binding Constant ($K_a$)** | **LOD (µM)** |
|---|---|---|---|---|---|---|
| **L8** | 356 | 468 | - | - | - | - |
| $Cu_2$(**L8**) | 374 | Fluorescence quenching at 468 nm | 1:2 | 18 nm | $7.35 \times 10^6$ | 0.16 |
| $Hg_2$(**L8**) | 405 | Fluorescence quenching at 468 nm with shifting by 68 nm | 1:2 | 49 nm | $2.33 \times 10^6$ | 0.33 |
| $Cd_2$(**L8**) | 360 | Fluorescence enhancement at 468 nm with shifting by 81 nm | 1:2 | 81 nm | 11.1621 (log $\beta$) | 0.11 |

### 5.3.3 $^1$H NMR studies, FT-IR spectra for binding mode

The binding mode of all three metal ions with probe **L8** was identified by FT-IR, NMR titration and mass analysis of **L8** with all three metals respectively. The FT-IR spectra of **L8** and **L8** with copper ion shown that the finger print region is not same of both spectra. There were few bands at 3482, 3443 for -$NH_2$, 3377 for pyrrole -NH and 3108 for aromatic -C-H, 1524 $cm^{-1}$ for -C=N were completely disappeared after complexation with copper ion. There were some new bands occurred at 1399 and 1118 and some was shifted from 1603 to 1601 $cm^{-1}$ that supported to -C=N, 749 to 747, 620 to 605 $Cm^{-1}$ that supported the complexation with copper ion from -C=N, pyrrole -NH and -$NH_2$ (figure 5.13 (a)). Likewise, the vibrational spectrum of **L8** with $Hg^{2+}$ ion was dissimilar to the vibrational spectra of **L8**. Some bands that represent the -$NH_2$ functional group disappeared and some was shifted 1426 to 1399 $cm^{-1}$, 1106 to 1102 $cm^{-1}$ and 620 to 597 $cm^{-1}$ that also support the complexation with mercury ion (figure 5.13 (c)). Similarly, the vibrational spectra of decomplexed and complexed **L8** with $Cd^{2+}$ ion was different to each other. In presented spectra with $Cd^{2+}$ showed that some bands at 3482, 3443 for -$NH_2$, 3377 for pyrrole was completely diminished whereas some was shifted from 1426 to 1399 $cm^{-1}$, 1106 to 1118 $cm^{-1}$ and 620 to 630 $cm^{-1}$ that affirmed the metalation of **L8** with $Cd^{2+}$ ion [28] (figure 5.13 (d)). Figure 5.13 (b) represents binding mode with metal ions.

Further, the binding mode of these metal ions with **L8** also entrenched by $^1$H NMR titration. The experiment was accomplished in DMSO-$d^6$ solvent and $^1$H NMR of **L8** the peaks at δ11.62, 8.64, 8.32 and 6.28 ppm were designated as the -NH(pyrrole) proton, -CH=N proton, aromatic ring protons and -$NH_2$ protons respectively. Other doublet and triplets was corresponded to aromatic proton. Figure 5.14 and figure 5.15 represents the $^1$H NMR spectra of after and before the addition of both ions ($Hg^{2+}$ and $Cd^{2+}$). The all proton signals were shifted towards downfield in both cases ($Hg^{2+}$ and $Cd^{2+}$). In case of $Hg^{2+}$ a significant downfield shift (Δδ = 0.34) of pyrrole -NH due to the complexation with $Hg^{2+}$ ion, the $NH_2$ protons was completely disappeared which supported to the complexation occurred from -$NH_2$, the downfield shift in aromatic protons (Δδ = 0.08, 0.24, 0.09, 0.05 ppm) sustained that the electronegativity on the molecule was decreased binding with $Hg^{2+}$ ions and aldimine proton was also shifted (Δδ

= 0.16) that supported in binding with $Hg^{2+}$ ion aldimine proton are also involved [29]. Figure 5.14 represented the NMR titration with $Hg^{2+}$ ion. On the other hand, the binding with $Cd^{2+}$ ion also presented by NMR titration that indicated there was downfield shift was observed in proton signals (Figure 5.15) $NH_2$ protons was completely diminished with the gradual addition of $Cd^{2+}$ ion and pyrrole proton have significant shift ($\Delta\delta$ = 0.09), aldimine proton was shifted (($\Delta\delta$ = 0.12 ppm) downfield, aromatic protons were also shifted downfield which supported decrement of electronegativity of molecule **L8** after complexation with $Cd^{2+}$ ion [30]. The complexation was also affirmed by the mass spectra with all three metal ions that manifested the interaction between **L8** and metal ions that was already discussed above.

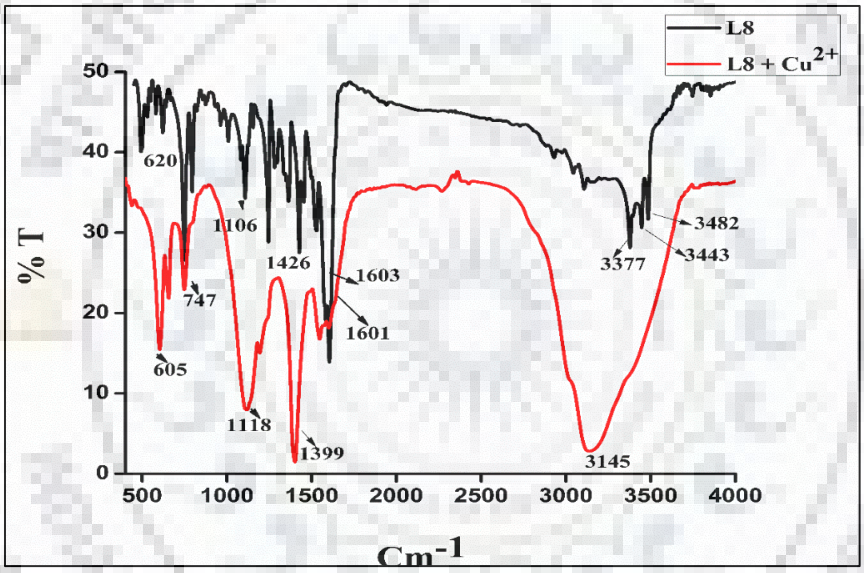


**Figure 5.13(a).** The combine FT-IR spectra of **L8** and **L8+Cu$^{2+}$** ion.

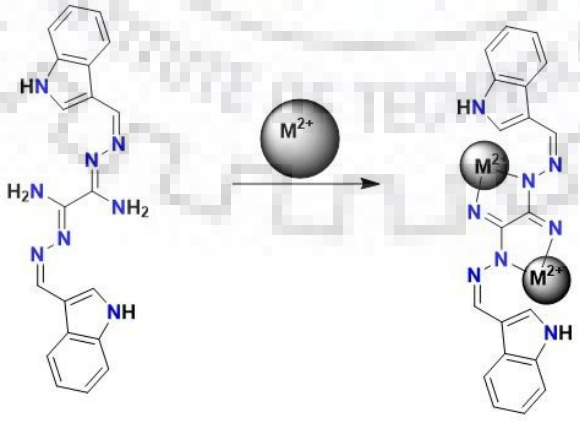


**Figure 5.13(b).** The binding mode of **L8** with metal ions.

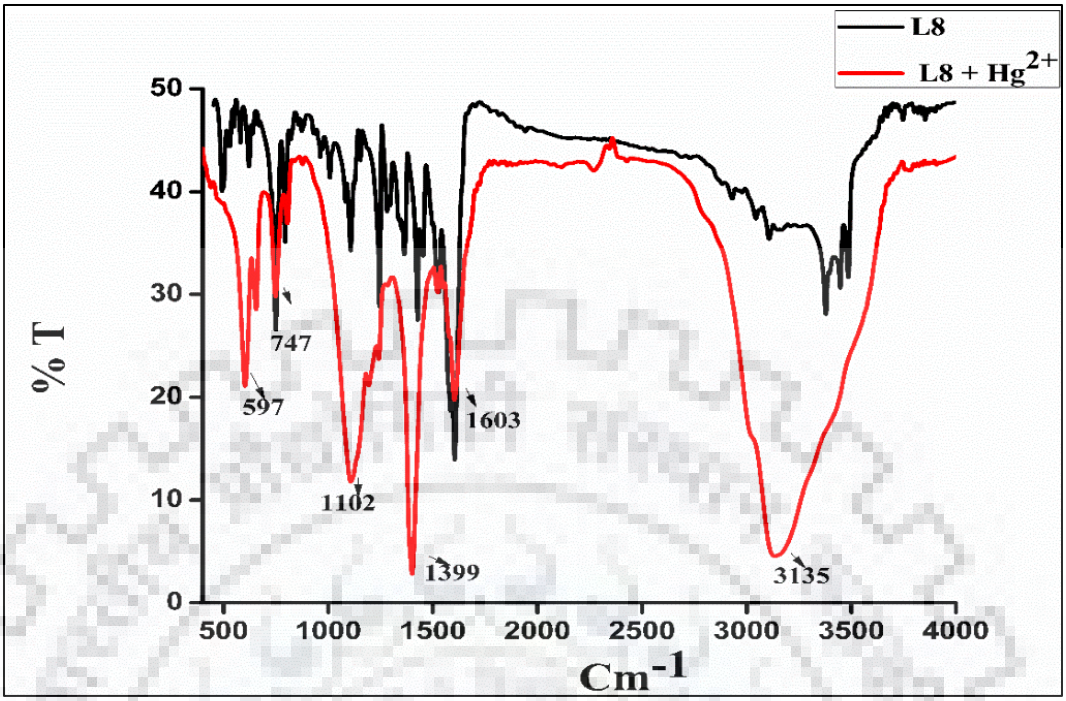


**Figure 5.13(c).** The combine FT-IR Spectra of **L8** and **L8+$Hg^{2+}$** ion.

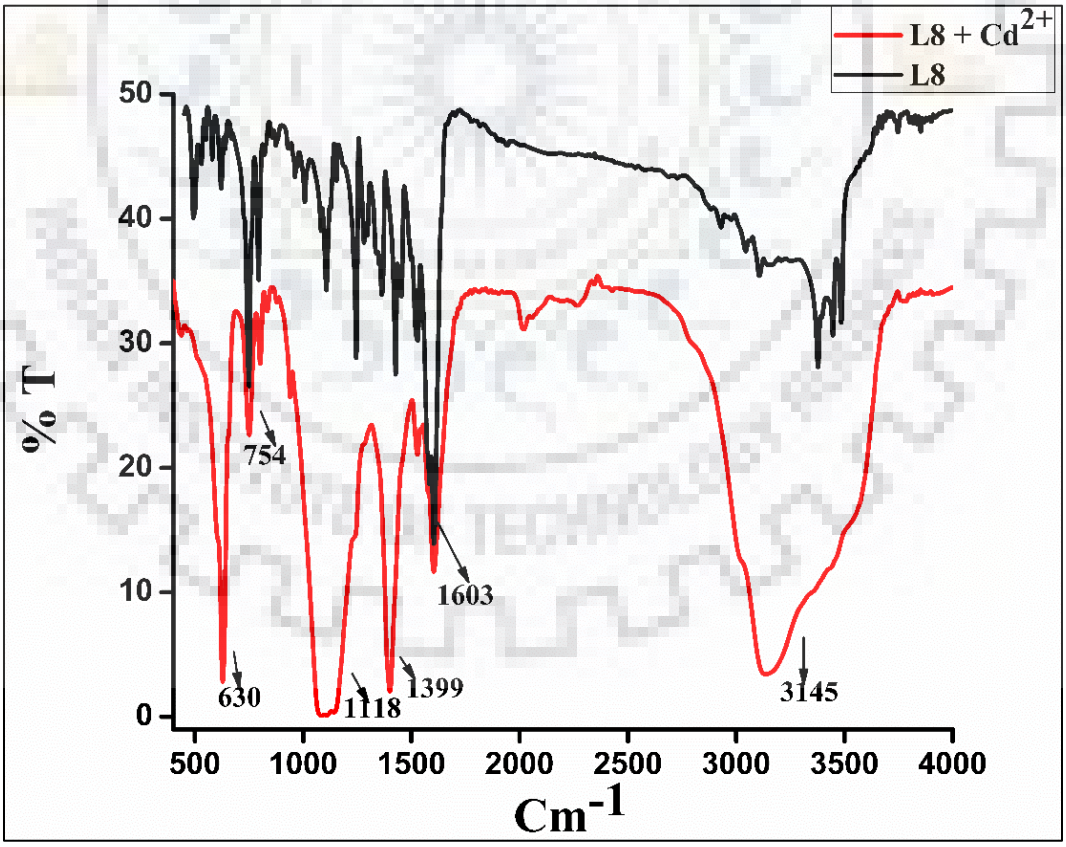


**Figure 5.13(d).** The combine FT-IR spectra of **L8** and **L8+$Cd^{2+}$** ion.

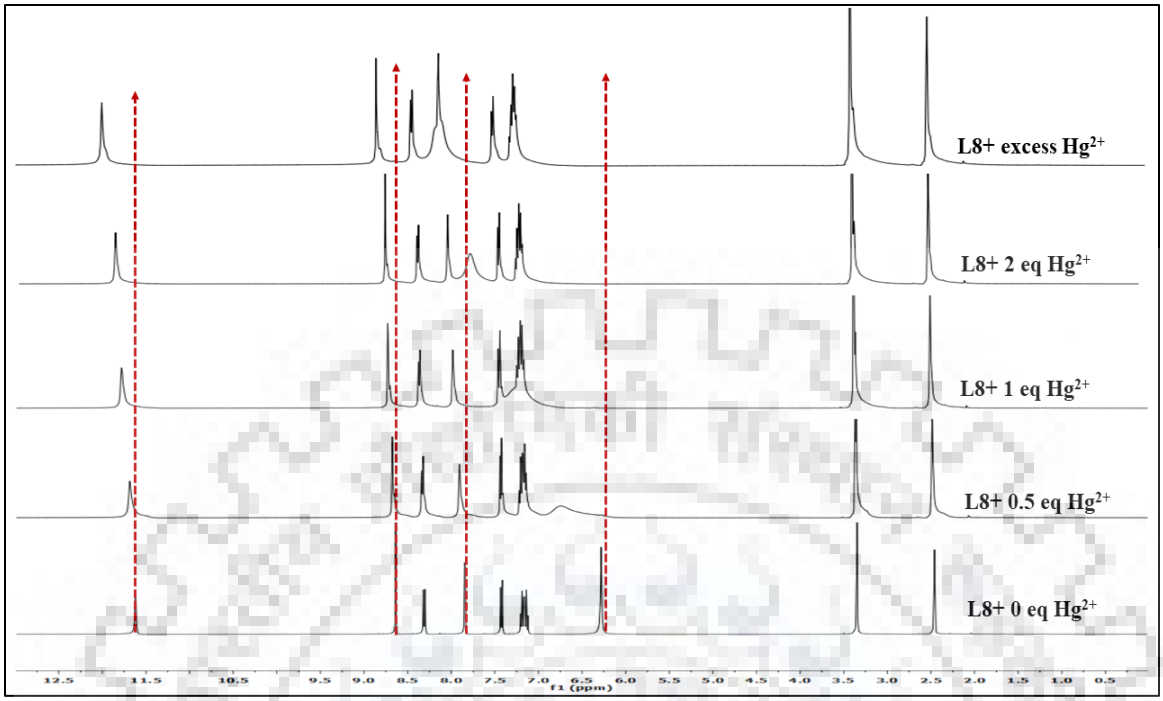


**Figure 5.14.** The NMR titration of **L8** with $Hg^{2+}$ in DMSO-$d_6$.

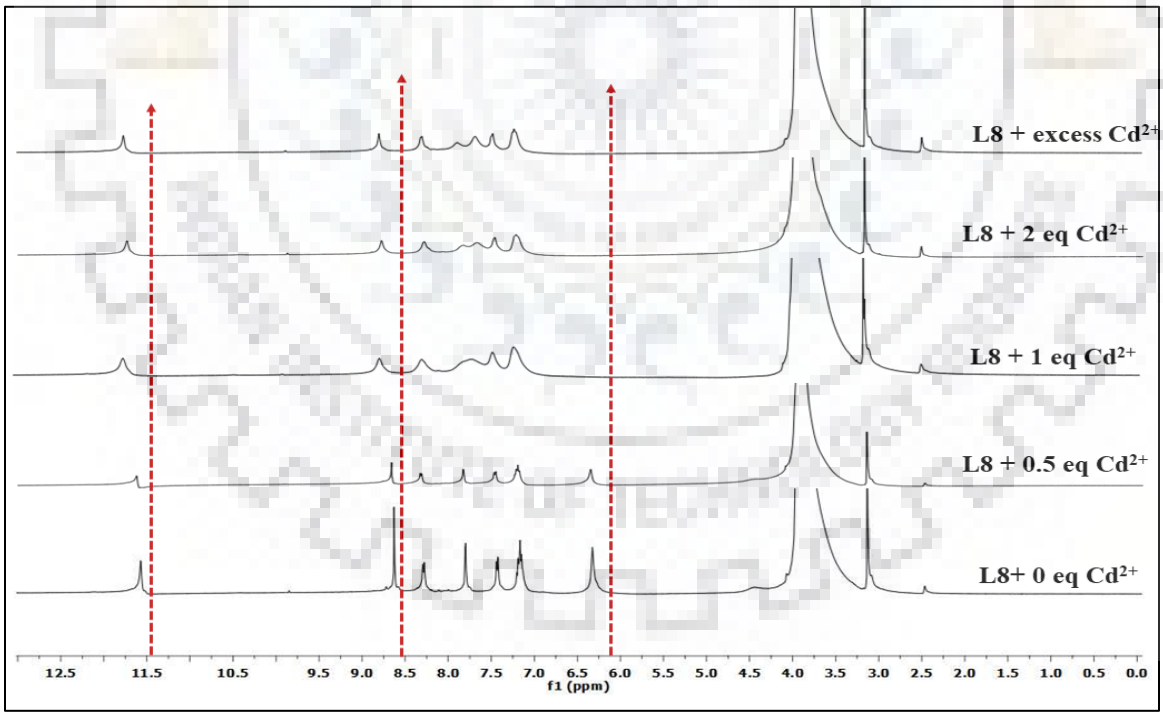


**Figure 5.15.** The NMR titration of **L8** with $Cd^{2+}$ in DMSO-$d_6$.

### 5.3.4 Electrochemical behavior of L8

The redox demeanor of L and all metal complexes was examined in $H_2O$ in the potential range -2 to +2 V and all electrochemical data encapsulated in the table 5.3 all three metal complexes have represented one irreversible reduction peak. The **L8**+$Cu_2$ complex manifested an anodic peak ($E_{pc}$) at 0.45 V and a cathodic peak ($E_{pa}$) at -0.63 that associated to Cu(II)/Cu(I) which was supported by Laviron equation for electron count in the redox process (Figure 5.17 (a)), on the other hand the probe displayed two irreversible anodic and two cathodic peaks at -1.82, -0.91, 1.21, 0.42 V respectively with simultaneous slight variation in current. The negative potential range for copper complex was -1.81 to -0.60 V represents one quasi-reversible peak. The voltammogram showed that the peak at -0.91 V was shifted to -0.63 on the complexation with copper ion [31] (Figure 5.16 (a)). Same as with $Hg^{2+}$ ion, the voltammogram of **L8**+$Hg^{2+}$ demonstrated one cathodic and one anodic peak at 0.35 V and -0.59 V respectively, which was occurred because of increment in conjugation of aromatic ring present in the molecule after interaction with $Hg^{2+}$ ion [32] with one electron transfer by the Laviron equation (Figure 5.17 (b)). Figure 5.16 (b) demonstrated the redox properties of **L8** with $Hg^{2+}$ ion. By the cyclic voltammogram of **L8** and all metal complexes the negative potential range was -1.82 to -0.59V. The voltammogram of **L8** with Cd(II) ion acquired one reversible peak at negative potential -0.59 and positive potential at 0.60 V that supported that the $Cd^{2+}$ ion bind with **L8** in reversible behavior [33] and there was some peaks occurred at -1.53 and 0.60 V, some peaks was shifted from -0.91 to -0.59V, 1.21 to 1.24 V and few new peaks was displayed after interaction with $Cd^{2+}$ ion at -1.53 and 0.75 (Figure 5.16 (c)) that represented the redox behavior in the solution with one electron transfer as $Cd^{2+}$/ $Cd^{+}$ by Laviron equation [34] which was plotted between log(scan rate) and different potential on different scan rate (Figure 5.17 (c)). All data was categorized in table 5.3.

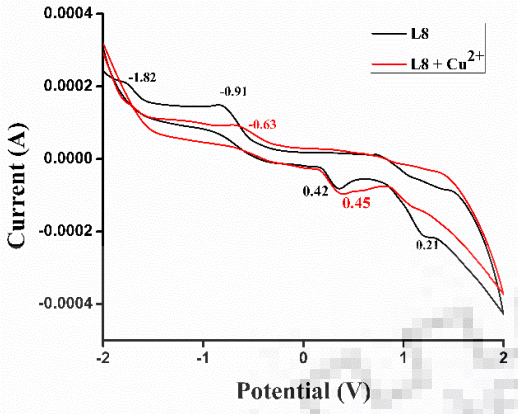


**Figure 5.16(a).** Electrochemical behavior of **L8** with copper ion.

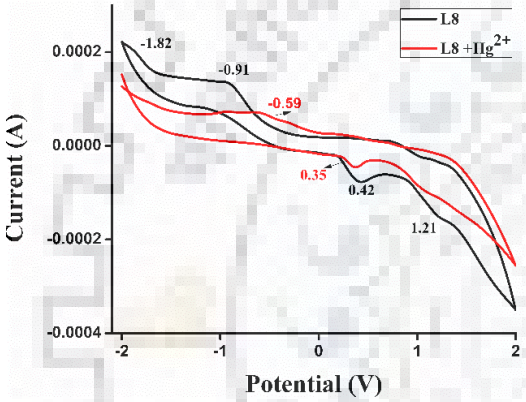


**Figure 5.16(b).** The electrochemical behavior of **L8** with mercury ion.

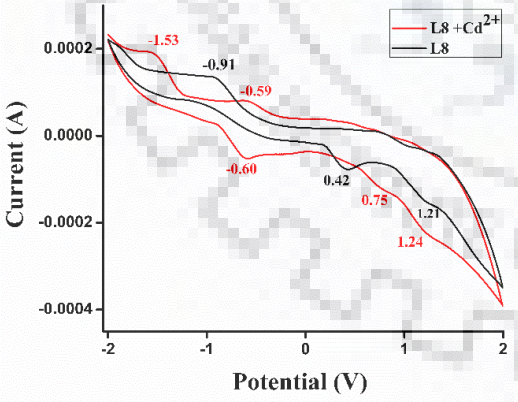


**Figure 5.16(c).** Electrochemical behavior of **L8** with cadmium ion.

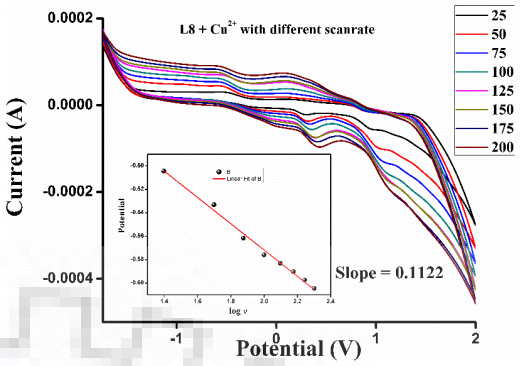


**Figure 5.17(a).** The cyclic voltammogram of **L8** with different scan rate plot of $Cu^{2+}$ and inset shows the plot between sweep rate and potential.

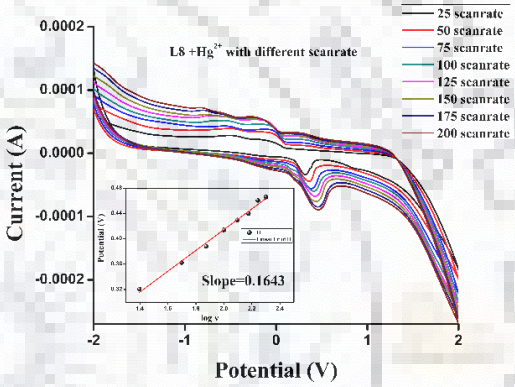


**Figure 5.17(b).** The cyclic voltammogram of **L8** with different scan rate plot of $Hg^{2+}$ and inset shows the plot between sweep rate and potential.

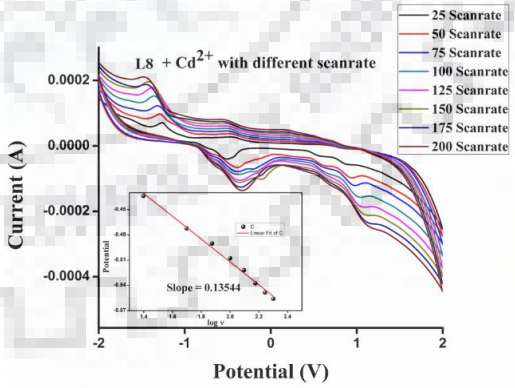


**Figure 5.17(c).** The cyclic voltammogram of **L8** with different scan rate plot of $Cd^{2+}$ and inset shows the plot between sweep rate and potential.

**Table 5.3:** Electrochemical behavior of ligand **L8** and their metal complexes.

| | **I Oxidation peak** | **II Oxidation peak** | **I Reduction peak** | **I Reduction peak** |
|---|---|---|---|---|
| **L8** | 1.21 | 0.42 | -0.91 | - |
| **$Cd_2$(L8)** | 1.24 | 0.75 | -0.59 | -1.53 |
| **$Cu_2$(L8)** | 0.45 | - | -0.63 | - |
| **$Hg_2$(L8)** | 0.35 | - | -0.59 | - |

### 5.3.5 *In-situ* experiment for anion sensing by L8 +metal ion ensemble

Further, the in-situ experiment was performed with different anions ($Cl^-$, $H_2PO_4^{2-}$, $HPO_4^{2-}$, $S^{2-}$, $SO_3^-$, $SO_4^-$, $NO_3^-$, $CN^-$, $NO_3^-$, $F^-$, $Br^-$, $SO_2^-$, $SO_4^{2-}$, $SCN^-$, $CO_3^{2-}$) in presence of metal ions ($Cu^{2+}$, $Hg^{2+}$ and $Cd^{2+}$) because some anions are good chelating binder with metal ions [35-36]. This could be indirect approach for anion sensing. On disclosure of different anions with **L8** in-situ presence of metal ions in water as result **L8** with $Cu^{2+}$ ion sense only $CN^-$ ion due to the strong binding behavior of $CN^-$ with $Cu^{2+}$ metal ion (strongly stable species $[Cu(CN)_x]^{n+}$) apart from other anions whereas **L8** with $Hg^{2+}$ and $Cd^{2+}$ ion was not sense any anion *via in-situ* experiment that shows no interference occurred by anion in the sensing of $Hg^{2+}$ and $Cd^{2+}$ ion. Figure 5.18 manifested the *in-situ* anion selectivity with ligand **L8** in presence of all three metal ions respectively. The study demonstrated that in case of $Cu^{2+}$ ion with **L8**, $CN^-$ ions confronted decomplexation of $Cu^{2+}$ ion with **L8** among the pool of anions that develop the ligand **L8** as previously whereas, in case of $Hg^{2+}$ and $Cd^{2+}$ ion the development of **L8** was not occurred with any anion which represented the strong binding between **L8** and both heavy metal ions. Figure 5.18 showed the sensing of anions with **L8** *in-situ* metal ions. After analyzation of selectivity of anion, the sensitivity of $CN^-$ ion was calculated by the changes in absorption spectra on consecutive addition of $CN^-$ ions with **L8**+$Cu^{2+}$ (Figure 5.19). The limit of detection of $CN^-$ ion was analyzed by plotting between log($CN^-$) and A-$A_{min}/A_{max}$-$A_{min}$ (Figure 5.20) and found 0.29 μM which was very less than the permissible limit given by WHO.

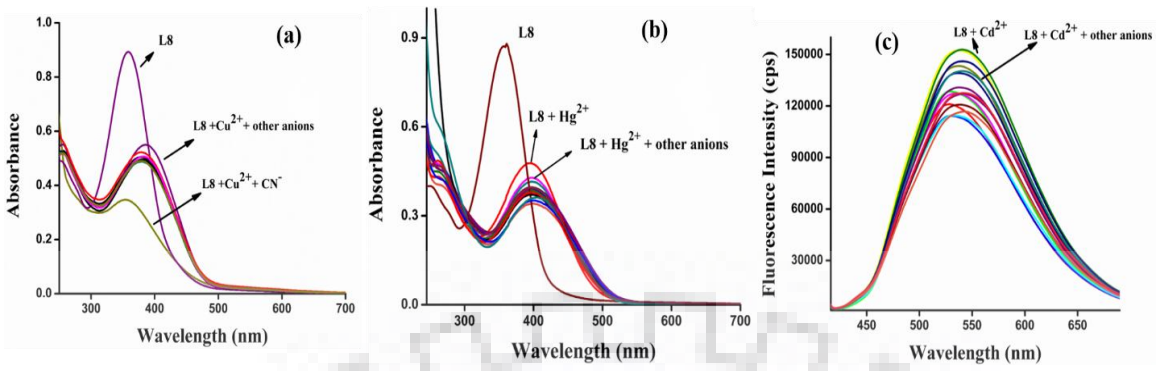


**Figure 5.18.** The selectivity of anions *in-situ* with metal ion in ligand **L8**, (a) represents the selectivity of different anions with **L8** in the presence of $Cu^{2+}$ ion, (b) shows the selectivity of anions with in presence of $Hg^{2+}$ ion whereas, (c) demonstrate the emission spectra of **L8**+$Cd^{2+}$ with different anions.

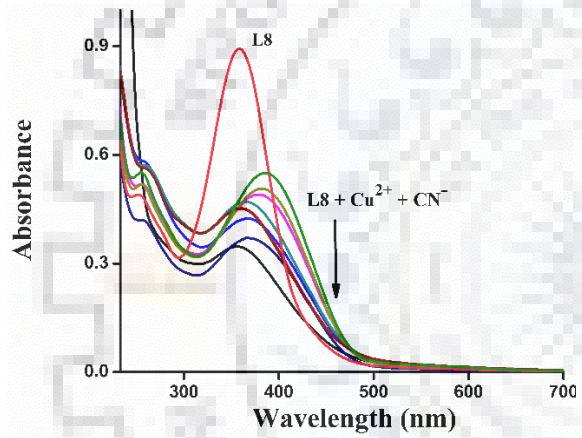


**Figure 5.19.** The titration experiment of in situ in presence of copper ion by Cyanide ion.

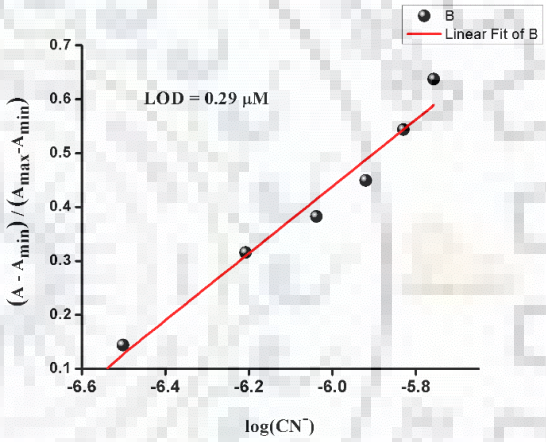


**Figure 5.20.** The limit of detection graph of **L8** + $Cu^{2+}$ with $CN^-$ ion.

## 5.4. APPLICATIONS

### 5.4.1 Real water analysis

Further to analyze the promising uses for presented ligand **L8**. The ligand was enforced in the investigation of diverse water samples. The tap water and ganga river water of Roorkee were used for the analysis, and these sample were spiked with known amount of $Cu^{2+}$, $Hg^{2+}$ and $Cd^{2+}$ ion. The estimation was analyzed by spiking of known amount of standard metal ions ($Cu^{2+}$, $Hg^{2+}$ and $Cd^{2+}$) solution followed by determining its recovery. The resulting recovery of diverse known amount of metal ions $Cu^{2+}$, $Hg^{2+}$ and $Cd^{2+}$ added was recognized to be 98% to 99.5% from tap water and 90% to 99% from

Ganga river water. These results show that this ligand is quite acceptable for the real water analysis. Table 5.4 contains the all finding of real water analysis.

**Table 5.4:** Represent the determination of $Cu^{2+}$, $Hg^{2+}$ and $Cd^{2+}$ ions in various water samples kit.

| | **Samples** | **Spiked $Cu^{2+}$ (M)** | **Found $^{a}Cu^{2+}$±SD (M)** | **Recovery (%)** |
|---|---|---|---|---|
| **L8** | Tap water | $10 \times 10^{-5}$ | $9.95 \pm 0.036 \times 10^{-5}$ | 99.5 % |
| | Ganga River water | $10 \times 10^{-5}$ | $9.00 \pm 0.037 \times 10^{-5}$ | 90 % |

[a]standard deviation with three measurement.

| | **Samples** | **Spiked $Hg^{2+}$ (M)** | **Found $^{a}Hg^{2+}$ ±SD (M)** | **Recovery (%)** |
|---|---|---|---|---|
| **L8** | Tap water | $10 \times 10^{-5}$ | $9.90 \pm 0.026 \times 10^{-5}$ | 99 % |
| | Ganga River water | $10 \times 10^{-5}$ | $9.50 \pm 0.14 \times 10^{-5}$ | 95 % |

[a]standard deviation with three measurement.

| | **Samples** | **Spiked $Cd^{2+}$ (M)** | **Found $^{a}Cd^{2+}$ ± SD (M)** | **Recovery** (%) |
|---|---|---|---|---|
| **L8** | Tap water | $10 \times 10^{-5}$ | $9.80 \pm 0.1 \times 10^{-5}$ | 98 % |
| | Ganga River water | $10 \times 10^{-5}$ | $9.90 \pm 0.1 \times 10^{-5}$ | 99 % |

[a]standard deviation with three measurement.

### 5.4.2 Mimicking of logic gate

The mimicking of logic gate was applied in case of copper ion with **L8**, due to the displacement occurred with $CN^-$ ion among other anions. The immediate changes were appeared in its emission intensity with $CN^-$ ion *in-situ* presence of $Cu^{2+}$ ion. Moreover, these variations were enforced as a molecular switch that uses Boolean logic operations [37]. Further the construction of the logic gate, 1 logic was designated to 'ON' state and 0 for 'OFF' state in representing input and output. The four conceivable input combos were (0 0), (1 0), (0 1) and (1 1) that represented by the figure 5.21 and it was recognized that in the presence and absence of $Cu^{2+}$ and $CN^-$ respectively given output signal 0 same as

with presence of $CN^-$ ion and absence of $Cu^{2+}$ shown the output signal 1 and when both are absent the output signal was 1, further presence of both ions shown the output signal 1. The truth table represented the two inputs $Cu^{2+}$ (In1) and $CN^-$ (In2) for Boolean logic circuit that demonstrated IMPLICATION job by emission output signal where AND gate act as an inverter to convert the input signal. Figure 5.21 manifested the emission spectra of both inputs and truth table also exhibited the inputs and outputs with represented the IMPLICATION logic gate.

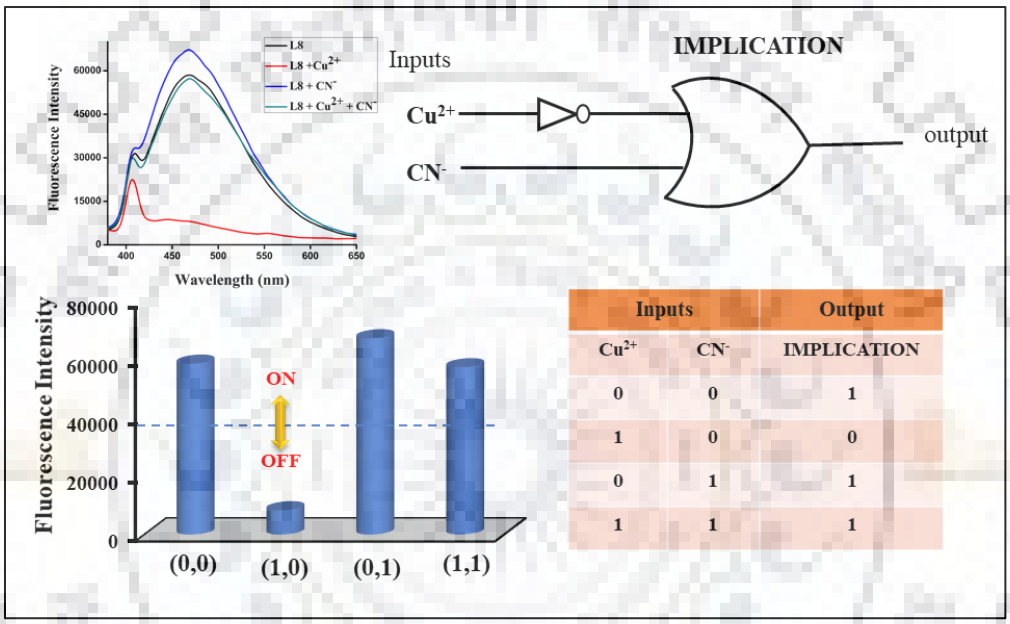


**Figure 5.21.** Fluorescence curve of "IMPLICATION" logic gate with different combination of inputs, column representation of fluorescence intensity, the blue dashed line shows the threshold value (40000 cps), truth table of "IMPLICATION" logic gate and electronical circuit representation of logic gate.

## 5.5 CONCLUSIONS

The oxalohydrazonamide based ligand was successfully synthesized and characterized by different technique such as NMR, FT-IR, mass spectrometry, crystal structure, elemental analysis and photophysical studies. This ligand shows high selectivity and sensitivity towards toxic heavy metal ions $Hg^{2+}$, $Cd^{2+}$ and $Cu^{2+}$ ions in 100% aqueous solution by visual and photophysical studies which supported different mechanism on complexation with metal ions. The stoichiometry 1:2 for all three metal

ions ($Hg^{2+}$, $Cd^{2+}$ and $Cu^{2+}$) supported through Job's plot. Further, the formation constant calculated using the S-V plot for $Cu^{2+}$ and $Hg^{2+}$ ion through PET and CHQF mechanisms respectively, whereas for $Cd^{2+}$ ion it was calculated by Hill plot *via* CHEF mechanism. The association constant ($K_a$) as $2.33 \times 10^6$, $7.35 \times 10^6$ and 11.612 ($log\ \beta$) for $Hg^{2+}$, $Cu^{2+}$ and $Cd^{2+}$ metal ions respectively. Furthermore, the LOD was calculated 0.33 μM, 0.16 μM and 0.11 μM for $Hg^{2+}$, $Cu^{2+}$ and $Cd^{2+}$ metal ions respectively. The complexation was successfully examined by NMR titration, mass spectrophotometry and electrochemical behavior. Moreover, the *in-situ* complexed ligand was used in practical applications such as real water analysis and mimicking of logic gate.

## References


1. H. N. Kim, W. X. Ren, J. S. Kim and J. Yoon, Fluorescent and colorimetric sensors for detection of lead, cadmium, and mercury ions, Chem. Soc. Rev. 41 (2012) 3210-3244.
2. B. Valeur, I. Leray, Design principles of fluorescent molecular sensors for cation recognition, Coord. Chem. Rev. 205 (2000) 3-40.
3. D. T. Quang and J. S. Kim, Fluoro- and chromogenic chemodosimeters for heavy metal ion detection in solution and biospecimens, Chem. Rev. 110 (2010) 6280–6301.
4. W. D. Vries, P. F. A. M. Romkens and G. Schutze, Critical soil concentrations of cadmium, lead, and mercury in view of health effects on humans and animals, Rev. Environ. Contam. Toxicol. 191 (2007) 91–130.
5. D. W. Domaille, E. L. Que and C. J. Chang, Synthetic fluorescent sensors for studying the cell biology of metals, Nature Chemical Biology 4 (2008) 168-175.
6. E. Gaggelli, H. Kozlowski, D. Valensin and G. Valensin, Copper homeostasis and neurodegenerative disorder's (Alzheimer's, Prion and Parkinson's diseases and Amyotrophic Lateral Sclerosis), Chem. Rev. 106 (2006) 1195-2044.
7. (a) I. Bertini and A. Rosato, Menkes disease, Cell. Mol. Life Sci. 65 (2008) 89-91. (b) Y. H. Hung, A. I. Bush, R. A. Cherny, Copper in the brain and Alzheimer's disease, J. Bol. Inorg. Chem. 15 (2010) 61-76.
8. S. Liu, Y.-M. Wang and J. Han, Fluorescent chemosensors for copper (II) ion: Structure, mechanism and application, J. Photoch. Photobio. C 32 (2017) 78-103.
9. R. R. Crichton, R. J. Ward and R. C. Hider, Metal chelation in medicine, Metal Toxicity, (2016) 1-23.
10. M. Wang, W.-Y. Feng, H. J Wang, Y. Zhang, J. Li, J. Li, B. Li, Y. L. Zhao and Z.-F. Chai, Analysis of mercury – Containing protein fractions in brain cytosol of the maternal and infant rats after exposure to a low-dose of methylmercury by SEC coupled to isotope dilution ICP-MS, J. Anal. At. Spectrom 23 (2008) 1112-1116.
11. W. F. Fitzgerald, C. H. Lamborg and C. R. Hammerschmidt, Marine biogeochemical cycling of mercury, Chem. Rev. 107 (2007) 641−662.

12. P. Mahato, S. Saha, P. Das, H. Agarwalla and A. Das, An overview of recent developments on $Hg^{2+}$ recognition, RSC Adv. 4 (2014) 36140-36174.
13. P. Grandjean, H. Satoh, K. Murata and K. Eto, Adverse effect of methylmercury: environmental health research implications, Environ Health Perspect. 118 (2010) 1137–1145. (b) M. Harada, Minamata disease: Methylmercury poisoning in Japan caused by environmental pollution, Critical Review in Toxicology 25 (1995) 1-25.
14. S. Goswami, K. Aich, S. Das, A. K. Das, A. Mannaa and S. Halder, A highly selective and sensitive probe for colorimetric and fluorogenic detection of $Cd^{2+}$ in aqueous media, Analyst 138 (2013) 1903 – 1907.
15. M. C. Aragoni, M. Arca, F. Demartin, F. A. Devillanova, F. Isaia, A. Garau, V. Lippolis, F. Jalali, U. Papke, M. Shamsipur, L. Tei, A. Yari and G. Verani, Fluorometric chemosensors. Interaction of toxic heavy metal ions $Pb^{II}$, $Cd^{II}$ and $Hg^{II}$ with novel mixed-donor phenanthroline-containing macrocycles: spectrofluorometric, conductometric, and crystallographic studies, Inorg. Chem. 41 (2002) 6623-6632.
16. A. Manna, D. Sarkar, S. Goswami, C. K. Quah and H.-K. Fun, Single excited state intramolecular proton transfer (ESIPT) chemodosimeter based on rhodol for both $Hg^{2+}$ and $OCl^{-}$: Ratiometric detection with live-cell imaging, RSC Adv. 6 (2016) 57417-57423.
17. J. J. Lee, Y. S. Kim, E. Nam, S. Y. Lee, M. H. Lim and C. Kim, A PET-based fluorometric chemosensor for the determination of mercury(II) and pH, and hydrolysis reaction-based colorimetric detection of hydrogen sulfide, Dalton Trans. 45 (2016) 5700-5712.
18. P. Venkatesan and S.-P. Wu, A turn-on fluorescent pyrene-based chemosensor for Cu(II) with live cell application, RSC Adv. 5 (2015) 42591-42596.
19. J. Wang, X. Qian and J. Cui, Detecting $Hg^{2+}$ ion with an ICT Fluorescent sensor molecule: Remarkable emission spectra shift and unique selectivity, J. Org. Chem. 71 (2006) 4308-4311.
20. S. Goswami, K. Aich, S. Das, C. D. Mukhopadhyay, D. Sarkar and T. K. Mondal, A new visible-light-excitable ICT-CHEF-mediated fluorescence ‘turn-on’ probe for

the selective detection of $Cd^{2+}$ in a mixed aqueous system with living cell imaging, Dalton Trans. 44 (2015) 5763-5770.

21. M. Li, H.-Y. Lu, R.-L. Liu, J.-D. Chen and C.-F. Chen, Turn-On fluorescent Sensor for selective detection of $Zn^{2+}$, $Cd^{2+}$ and $Hg^{2+}$ in water, J. Org. Chem. 77 (2012) 3670−3673.
22. F. W. Lewis, L. M. Harwood, M. J. Hudson, U. Müllich and A. Geist, Efficient masking of corrosion and fission products such as Ni(II) and Pd(II) in the presence of minor actinide Am(III) using hydrophilic anionic or cationic bis-triazines, Chem. Commun. 51 (2015) 9189-9192.
23. S. Goswami, A. K. Das and S. Maity, 'PET' *vs* 'Push-Pull' Induced ICT: A remarkable coumarinyl-appended pyrimidine based naked eye Colorimetric and fluorimetric sensor for the detection of $Hg^{2+}$ ions in aqueous media with test trips, Dalton Trans. 42 (2013) 16259-16263.
24. U. Fegade, A. Saini, S. K. Sahoo, N. Singh, R. Bendre and A. Kuwar, 2,2'-(hydrazine-1,2-diylidenedimethylylidene) bis(6-isopropyl-3-methylphenol) based selective dual – channel chemosensor for $Cu^{2+}$ in semi-aqueous media, RSC Adv. 4 (2014) 39639-39644.
25. H. He, Y. Song, F. Sun, Z. Bian, L. Gao and G. Zhu, A porous metal-organic framework formed by a V-shaped ligand and Zn(II) ion with highly selective sensing for nitroaromatic explosives, J. Mater. Chem. A 3 (2015) 16598-16603.
26. P. Kaewanan, P. Sricharoen, N. Limchoowong, T. Sripakdee, P. Nuengmatcha and S. Chanthai, A fluorescence switching sensor based on graphene quantom dots decorated with $Hg^{2+}$ and hydrolysed thioactamide for highly $Ag^{+}$- sensitive and selective detection, RSC Adv. 7 (2017) 48058-48067.
27. D. Singhal, N. Gupta and A. K. Singh, Chromogenic "naked eye" and fluorogenic 'turn-on' sensor for mercury metal ion using thiophene based Schiff base, RSC Adv. 5 (2015) 65731-65738.
28. (a) V. Tekuri and D. R. Trivedi, A new colorimetric chemosensors for $Cu^{2+}$ and $Cd^{+}$ ion detection application in environmental water samples and analytical method validation, Analytica Chimica Acta 972 (2017) 81-93. (b) N. Yadav and A. K.

Singh, Dicarbohydrazide based chemosensor for copper ion and cyanide ion *via* displacement approach, New J. Chem. 42 (2018) 6023-6033.

29. Y. M. Zhang, W. J. Qu, G. Y. Gao, B. B. Shi, G. Y. Wu, T. B. Wei, Q. Lin and H. Yao, A highly selective dual-channel chemosensor for mercury ions: utilization of the mechanism of intramolecular charge transfer blocking, New J. Chem. 38 (2014) 5075-5080.
30. S. B. Maity, S. Banerjee, K. Sunwoo, J. S. Kim and P. K. Bharadwaj, A fluorescent chemosensor for $Hg^{2+}$ and $Cd^{2+}$ ions in aqueous medium under physiological pH and its applications in imaging living cells, Inorg. Chem. 54 (2015) 3929-3936.
31. P. Gayathri and A. S. Kumar, Electrochemical behavior of the 1, 10-phenanthroline ligand on a multiwalled carbon nanotube surface and its relevant electrochemistry for selective recognition of copper ion and hydrogen peroxide sensing, Langmuir 30 (2014) 10513-10521.
32. A. N. Kursunlu, P. Deveci and E. Guler, Synthesis and spectroscopic-electrochemical properties of novel ratiometric Hg(II) chemosensor containing bodipy and the N-phenylaza-15-crown-5-moiety, J. Lumin. (2013) 430-436.
33. (a) D. S. Rajawat, N. Kumar and S. P. Satsangee, Trace determination of cadmium in water using anodic stripping voltammetry at a carbon paste electrode modified with coconut shell powder, J Anal. Sci. Technol. 5 (2014) 1-8. (b) A. B. Nepomnyashchii, M. A. Alpuche-Aviles, S. Pan, D. Zhan, F.-R. F. Fan and A. J. Bard, Cyclic voltammetry studies of $Cd^{2+}$ and $Zn^{2+}$ complexation with hydroxyl-terminated polyamidoamine generation 2 dendrimer at a mercury microelectrode, J. Electroanalytical Chemistry 621 (2008) 286-296.
34. E. Laviron, General expression of the linear potential sweep voltammogram in the case of diffusion less electrochemical systems, J. Electroanal. Chem. 101 (1979) 101, 19-28.
35. F. Wang, L. Wang, X. Chen and J. Yoon, Recent progress in the development of fluorometric and colorimetric chemosensors for detection of cyanide ions, Chem. Soc. Rev. 43 (2014) 4312-4324.

36. D. Udhayakumari, Chromogenic and fluorogenic chemosensors for lethal cyanide ion. A comprehensive review of the year 2016, Sens. Actuator B 259 (2018) 1022-1057.
37. R.-R. Gao, S. Shi, Y. Zhu, H.-L. Huang and T.-M. Yao, A RET-supported logic gate combinatorial library to enable modeling and implementation of Intelligent logic function, Chem. Sci. 7 (2016) 1853-1861.

# CHAPTER 6

## "CARBOHYDRAZIDE BASED CHEMOSENSORS FOR MAGNESIUM, MANGANESE AND COPPER ION"

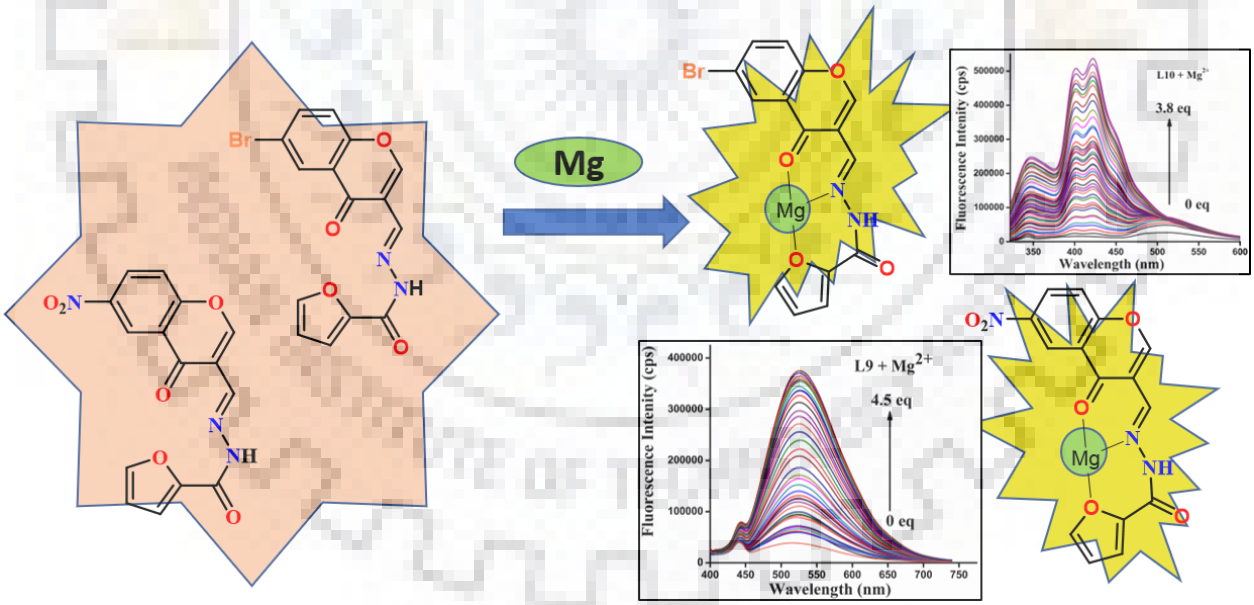

# CHAPTER 6

## 6.1 INTRODUCTION

The identification and sensing of metal ions have been a key research motif because of the paramount and essential roles of metal ion in the environment and biological field. Among the entire pool of metal ions magnesium possess the potential in the field of biologically activation [1]. Magnesium ions is the fourth most abundant element in the atmosphere [2]. It plays a vital role in DNA synthesis and protein phosphorylation [3,4]. It is very necessary for cardiovascular and neurological processes in human body. It's aberrant concentration in cytosol and subcellular regions generates many diseases such as Hypertension, Diabetes, Epilepsy and Alzheimer. Same as with copper ion it is essential for many biological processes such as neurotransmitter synthesis and metabolism [5], epigenetic modification, antioxidant defense and copper act as a catalytic cofactor in various cellular processes [6], but the abnormal concentration of copper ion is responsible for various diseases [7]. Similarly, in case of manganese, it is an essential metal ion *i.e.* demanding to metabolism because of its involvement in activation of enzymes; still in large concentration it is hazardous for environment [8]. Therefore, it is necessary to develop an easy method for detection of these ions rather than time consuming, sophisticated and expensive instruments. There are lots of conventional methods that are used in the detection of these metal ions [9].

In this context, this chapter deals with there were two coumarin based materials that have been synthesized and which was very important because of its desirable photophysical quality such as visible excitation and emission wavelength and large stoke shift [10,11]. Another one, coumarin family compounds has important quality is the tunability of photophysical properties [12,13]. In these ligands **L9** and **L10** has the fluorophore unit that have strong "push-pull" π-electron system [14]. **L9** ligand containing Nitro group, in which the fluorophore unit that generated more conjugation in the ligand and hampered the easy binding with metal ions. Rather than this **L9** also behave as a chemosensor for Mn ion *via* absorption spectra and it shows turn-ON behavior for magnesium metal ion by emission spectra among other metal ions. However, bromo group containing **L10** ligand has electron withdrawing group that shows less conjugation as compared to **L9** ligand and electron transfer occured from imine N-atom of the molecule. **L10** ligand also represent a turn-ON behavior in emission spectra with

magnesium ion among various metal ions, whereas it senses the copper ion in absorption spectra due to less hydrogen bonding generating with solvent than **L10**. These ligands show good selectivity towards magnesium ion in emission spectra and high selectivity and sensitivity towards manganese and copper ion. there was a smaller number of data present for sensing of magnesium and manganese ion. One of the ligands in both ligands sense manganese ions with good selectivity.

## 6.2 MATERIALS AND METHODS

### 6.2.1 Reagents and instruments

The experiments were performed in distilled or HPLC grade solvents. The chloride and nitrate metal salts were used of AR grade of Merck without further purification. Perkin Elmer-FT-IR-1000 spectrophotometer was used for the analysis of vibrational spectra. JEOL-400 MHz instrument was used for NMR (proton & carbon) spectra. The all absorption and emission studies were performed on Thermo-Scientific PC double beam spectrophotometer and Horiba RF-5301PC respectively with 3 cm path length quartz cell for absorption spectra, standard quartz cell for emission spectra. The elemental analysis (CHNS) was performed on Verio MICROV3.1.1 instrument. CHI760E Electro-Analyzer Instrument was used for electrochemical studies with three electrodes in which graphite electrode behave as counter electrode, Pt-wire electrode was performed as reference electrode and $Ag/AgCl_2$ electrode as working electrode with 0.1 M tetrabutylammonium hexafluorophosphate ($nBu_4NPF_6$) as supporting electrolyte. MTT (3-(4,5- Dimethylthiazol-2-yl)-2,5-diphenyltetrazolium bromide) was obtained from USA based Amresco life science. For cell-based assays, cervical cancer cells (HeLa cells) were pre-occupied from National Centre for Cell Science, Pune, India.

### 6.2.2 Cell Culture

All the cells were maintained in DMEM (Dulbecco's modified Eagle's medium) supplemented with 10% fetal bovine serum (FBS) and 1X Penicillin-streptomycin. Further, the cells were grown in aseptic condition inside a humidified chamber provided with 37°C along with 5% $CO_2$ and 95% air supply.

### 6.2.2.1 MTT based Cytotoxicity assay

The biocompatibility of synthesized imaging probes was estimated by MTT dye (3-(4,5-dimethylthiazol-2-yl)-2,5-diphenyltetrazolium bromide) [15]. Initially, HeLa cells in the log phase were seeded in 96 well plate following a seeding density of 6,000 cells/ well. The cells were left undisturbed overnight to adhere. This was followed with a concentration dependent treatment of **L9**, **L10** along with their Mg counterparts (**L9**+Mg, **L10**+Mg) (10μg/mL - 75μg/mL) for 24 hours. Onset of treatment, a brief PBS wash was done to remove samples in the wells. Fresh media along with 10 μL of MTT (5 mg/mL) was replaced with spent media to each well. After 3-4hs incubation of MTT, the insoluble purple formazan crystals were checked by microscopic observations. The latter was re-dissolved in dimethyl sulfoxide (DMSO) provided with gyratory shaking for 15-20 min. Finally, the absorbance readings of purple formazan (A570 nm) were determined by using a multimode microplate reader (Cytation 3, Biotek). The cell viability was then calculated with the following equation [mean (%) ± SEM, n=3].

Cell viability (%) = [(A570 − A690) of treated cells / (A570 − A690) of control cells] *100.

An $IC_{50}$ was calculated by nonlinear regression (curve fit model) adopted as standard methodology in dose-response analysis [16].

### 6.2.2.2 Bio Imaging

The fluorescent imaging property of the synthesized imaging probes were later validated in HeLa cells [17]. Initially, $3*10^5$ cells were seeded on each well of 6 well plate and allowed to attach until overnight. The cells were further treated with 75 μg/mL of all the four samples (**L9**, **L10**, **L9**+$Mg^{2+}$, **L10**+$Mg^{2+}$) in the growing well. After 24h incubation, cells were underwent PBS wash followed with PFA (3%) fixation. Lately, the cells were micrographed by inverted phase contrast fluorescent microscope (EVOS FL Color, AMEFC 4300) cell imaging system obtained from Life technologies, USA.

### 6.2.3 Synthesis of L9 and L10:

**Synthesis of L9 (6-nitro-4-oxo-4H-chromen-3-yl)methylene)furan-2-carbohydrazide:**

The ethanolic solution of furan-2-carbohydrazide (1mM, 0.6305 g) was added dropwise to the solution of 3-formyl-6-nitrochromone (1 mM, 0.2191 g) in THF with continuous

stirring. The immediate precipitate was observed in the reaction mixture, therefore reflux the reaction mixture for 3 hr and then check the TLC for reaction completion and found that reaction has been completed. The precipitate was washed with Methanol and dry it in the air. (Scheme 6.1)

**Yield. 70%,** Anal. Calculation for $C_{15}H_9N_3O_6$: C, 55.05; H, 2.77; N, 12.84; Found: C, 55.37; H, 2.292; N, 13.21; FT-IR data (KBr, $\nu_{max}/cm^{-1}$): -N-H: 3430, C-H: 3145, C=O: 1695, C=O: 1632, -C=N: 1592 and N-O (nitro): 1539, 1468. $^1$H NMR (400 MHz, ) δ 11.85 (s, 1H), 8.97 (s, 1H), 8.39 (s, 1H), 8.31 (dd, *J* = 9.0, 2.9 Hz, 1H), 8.28 (d, *J* = 2.8 Hz, 2H), 8.06 (d, *J* = 3.6 Hz, 1H), 7.16 (d, *J* = 9.0 Hz, 1H), 6.88 (dd, *J* = 3.7, 1.5 Hz, 1H). $^{13}$C NMR (100 MHz) δ 187.040, 162.91, 154.36, 151.11, 145.04, 143.97, 139.95, 135.207, 128.87, 126.81, 126.51, 126.48, 125.35, 118.11, 113.97. ESI-mass of **L9**: 350.0440.

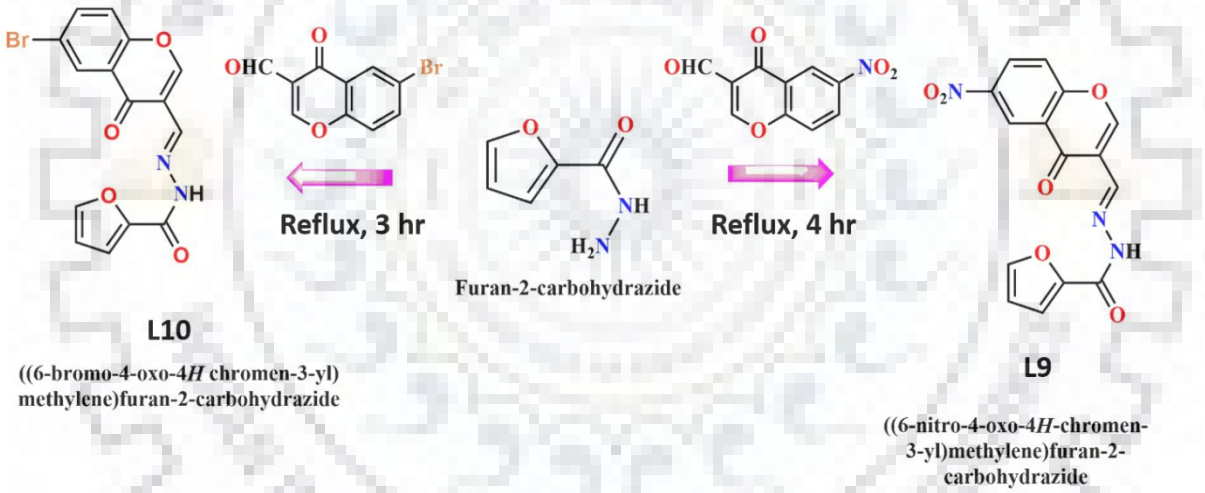


**Scheme 6.1.** Synthesis of **L9** and **L10**.

**Synthesis of L10 (6-Bromo-4-oxo-4H-chromen-3-yl)methylene)furan-2-carbohydrazide:**

The ethanolic solution of furan-2-carbohydrazide (1mM, 0.6305g) was added to the ethanolic solution of 3-formyl-6-Bromo-chromone (1.2mM, 0.1518g) with continuously stirring. After complete addition of chromone the reaction mixture was refluxed for 6hr and check the TLC for the confirmation of completion of reaction. The white precipitate was obtained on completion of reaction. This ligand was recrystallized

by ethanol: DMF (4:1) (Scheme 6.1). Further, the ligands were characterized by different techniques.

**Yield. 70%**, Ana. Calculation for $C_{15}H_9BrN_2O_4$: C, 49.89; H, 2.51; N, 7.76; Received: C, 49.97; H, 2.256; N, 6.77. FT-IR data (KBr, $\nu_{max}/cm^{-1}$): -N-H: 3420, -C-H (ar): 3028, -C=O: 1662, -C=O: 1630, and -C-Br: 609. $^1$H NMR (400 MHz) δ 11.96 (s, 1H), 8.80 (s, 1H), 8.53 (s, 1H), 8.13 (s, 1H), 7.96 (dd, *J* = 8.9, 2.5 Hz, 1H), 7.91 (s, 1H), 7.68 (d, *J* = 8.9 Hz, 1H), 7.28 (s, 1H), 6.66 (dd, *J* = 3.5, 1.7 Hz, 1H). $^{13}$C NMR (100 MHz) δ 174.43, 155.37, 155.24, 154.61, 146.85, 146.58, 140.46, 137.74, 127.82, 125.36, 121.95, 119.02, 118.97, 115.65, 112.65. ESI mass: 382.9735 $(M+Na)^+$.

## 6.3 RESULTS AND DISCUSSION

### 6.3.1 UV-Vis and emission studies of L9 and L10

The absorption and emission spectroscopy were recorded used for all photophysical properties of **L9** and **L10** in $CH_3CN$. **L9** showed one broad absorption band at 295 nm ($\lambda_{abs}$) due to n-π* transition of the N-atom to conjugated system in the ligand. Similarly, **L10** displayed two absorption band at 286 nm and 313 nm corresponding to π-π* and n-π* transition of conjugated system presents in the ligand. The binding of **L9** with the pool of various metal ions ($Ag^+$, $Na^+$, $Al^{3+}$, $Ba^{2+}$, $Ca^{2+}$, $Cd^{2+}$, $Co^{2+}$, $Cr^{3+}$, $Cs^+$, $Fe^{2+}$, $Hg^+$, $Hg^{2+}$, $K^+$, $Li^+$, $Mg^{2+}$, $Mn^{2+}$, $Pb^{2+}$, $Ni^{2+}$, $Zn^{2+}$) displayed the most significant binding with $Mg^{2+}$ and $Mn^{2+}$ ion *via* modulation of absorption and emission spectra and **L10** showed with $Cu^{2+}$ ion by absorption spectra whereas it demonstrate $Mg^{2+}$ ion sensing *via* plotting of emission spectra. **L9** has more conjugation and stable than **L10** due to the electron donating nitro group that become the ligand **L9** more stable than **L10**, therefore **L9** creates hydrogen bonding with solvent which inhibit the easy metal binding. Rather than this **L9** has high affinity towards $Mg^{2+}$ and $Mn^{2+}$ ion. However, **L10** has electron withdrawing bromo group in coumarin unit that creates less conjugation in the molecule, by which it was not hinder the easy metal binding with metal ions. It demonstrated high selectivity towards $Cu^{2+}$ and $Mg^{2+}$ ion through absorption and emission spectra respectively. In absorption spectra ($\lambda_{abs}$) of **L9** (20 μM), the significant change in absorption profile as a new broad band generated at 382 nm and 372 nm with on addition of $Mg^{2+}$ and $Mn^{2+}$ ion respectively with 87 nm & 77 nm bathochromic shift clearly indicates the interaction with $Mg^{2+}$ and $Mn^{2+}$ ion [18]. On the

other hand, **L10** demonstrate a broad band at 418 nm from 313 nm with large red shift (105 nm) in the presence of $Cu^{2+}$ ion by absorption spectra among other metal ions whereas emission spectra demonstrated an enhancement in the fluorescence intensity with $Mg^{2+}$ ion at excitation wavelength 340 nm among various metal ions that support the binding of $Mg^{2+}$ ion with **L10**. Figure 6.1 and figure 6.2 deals with the absorption and emission studies of **L9** and **L10** respectively with different metal ions and found that **L9** is highly selective or sensitive towards $Mn^{2+}$ and $Mg^{2+}$ ion among various metal ions and **L10** shown response towards $Mg^{2+}$ and $Cu^{2+}$ rather than other meal ions.

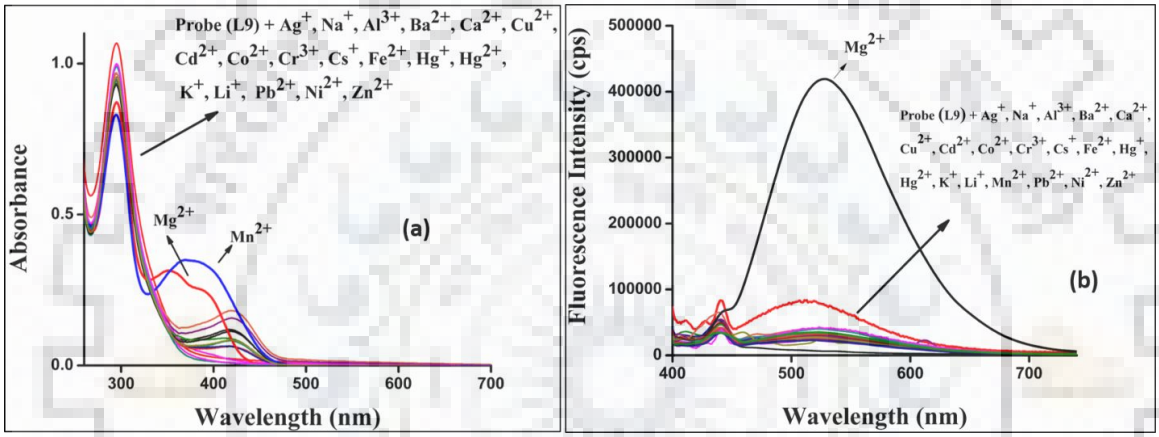


**Figure 6.1.** The absorption and emission studies of **L9** (20 μM) with different metal ions where, (a) represents absorption spectra and (b) shows emission studies.

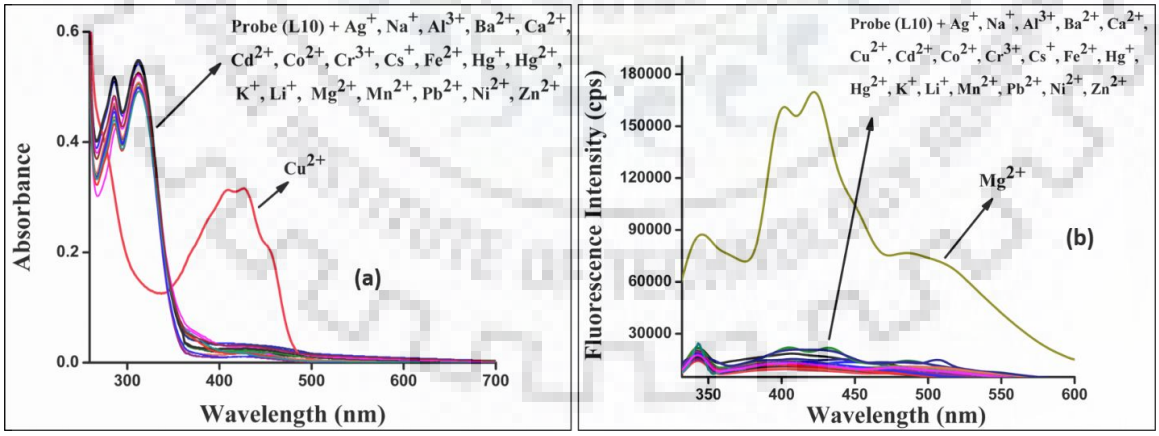


**Figure 6.2.** The absorption and emission studies of **L10** (20 μM) with different metal ions where (a) demonstrate absorption studies and (b) represents emission studies.

Further confirms the binding of both ligands with metal ions, such as **L9** with $Mg^{2+}$ & $Mn^{2+}$ metal ion and **L10** with $Cu^{2+}$ & $Mg^{2+}$ metal ion, the titration experiment

was executed. The consecutive addition of $Mg^{2+}$ and $Mn^{2+}$ to a fixed concentration of **L9** (20 μM) in $CH_3CN$ as well as absorption spectra was recorded after each addition and found that an increment occurred on gradual addition of $Mg^{2+}$ at 382 nm with one isosbestic point at 334 nm. Similarly, on gradual addition of $Mn^{2+}$ an increment was appeared at 372 nm in absorption spectra with one isosbestic point at 333 nm. Further, the emission spectra were recorded for the selectivity of metal ion with **L9** and found that there was no change with $Mn^{2+}$ ion but in case of $Mg^{2+}$ ion there was an enhancement in intensity occurred among other metal ions. Figure 6.3 manifested the titration of $Mg^{2+}$ and $Mn^{2+}$ with **L9** ligand [19].

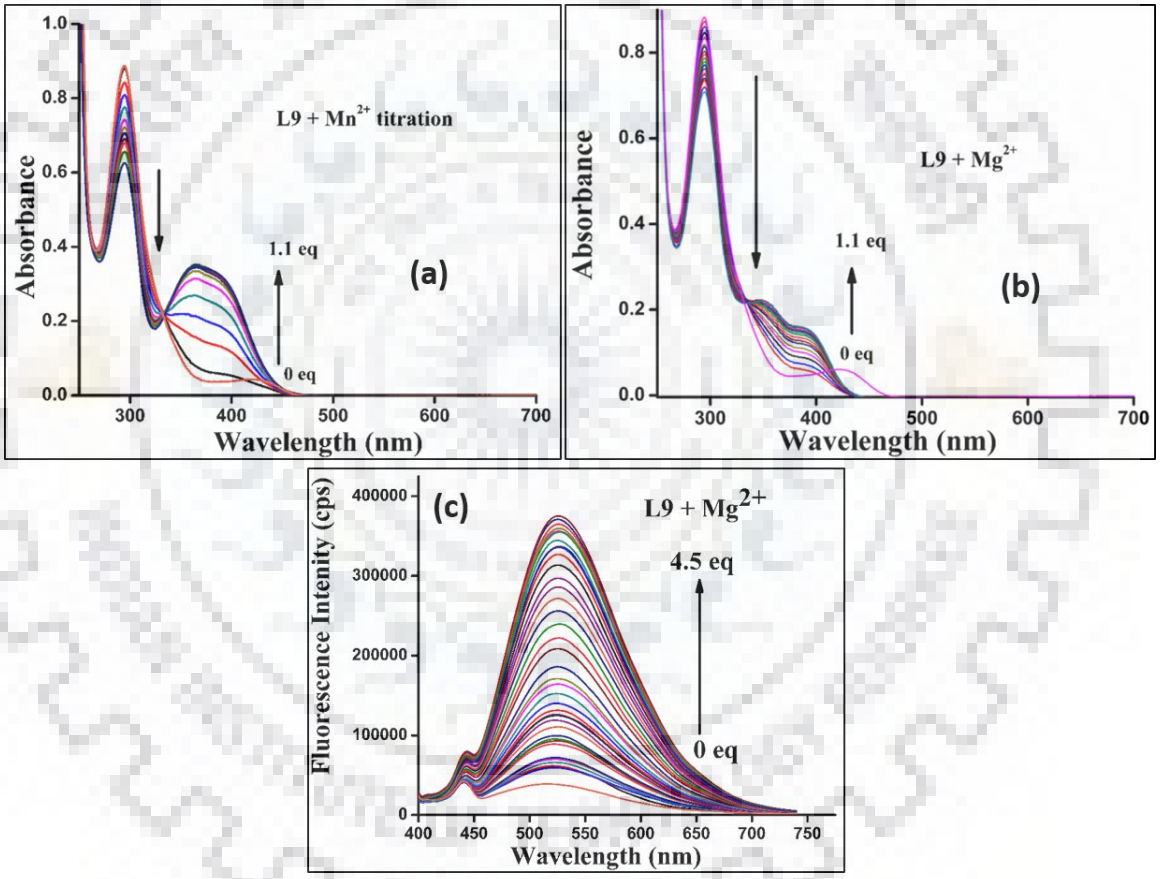


**Figure 6.3.** (a) and (b) represents the titration experiments of **L9** with $Mn^{2+}$ and $Mg^{2+}$ respectively by using UV-vis study and (c) shows the titration experiment with $Mg^{2+}$ ion by Fluorescence study.

In the titration experiment of **L10** with successive addition of $Cu^{2+}$ ion a band on 418 nm was continuously increased because of d-d transition with one isosbestic point at 346 nm but in emission spectra there was no change with $Cu^{2+}$ ion and **L10** also shows an

enhancement in fluorescence intensity with $Mg^{2+}$ ion due to LMCT (ligand to metal charge transfer) (figure 6.4) [20]. Further, the stoichiometry was supported by the Job's analysis, plotting between varied mole fraction of both ligand with metal ions and intensity or absorption of the ligands with metal ions. The Job's plot manifested that the 1:1 stoichiometry occurred with $Mg^{2+}$ and $Mn^{2+}$, same as with $L_b$ the 1:1 stoichiometry was received in case of $Cu^{2+}$ ion as well as $Mg^{2+}$ ion [21]. Figure 6.5 represented the Job's plot for ligands with metal ions.

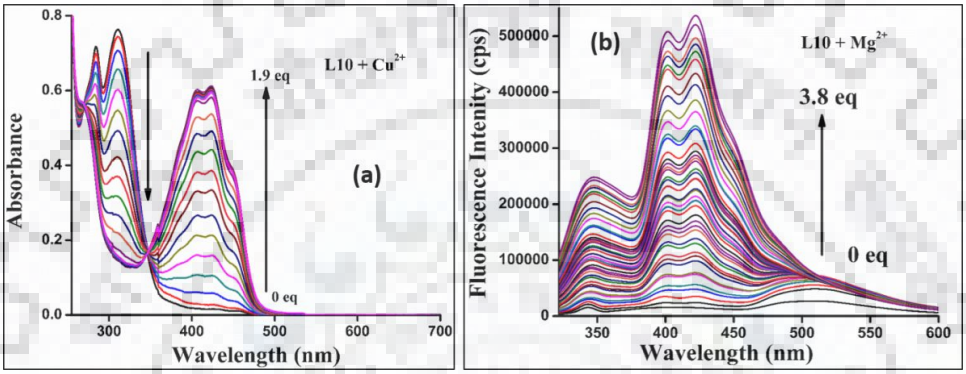


**Figure 6.4.** The absorption and emission titration of **L10** with $Cu^{2+}$ and $Mg^{2+}$ ion respectively by gradual addition of metal ion.

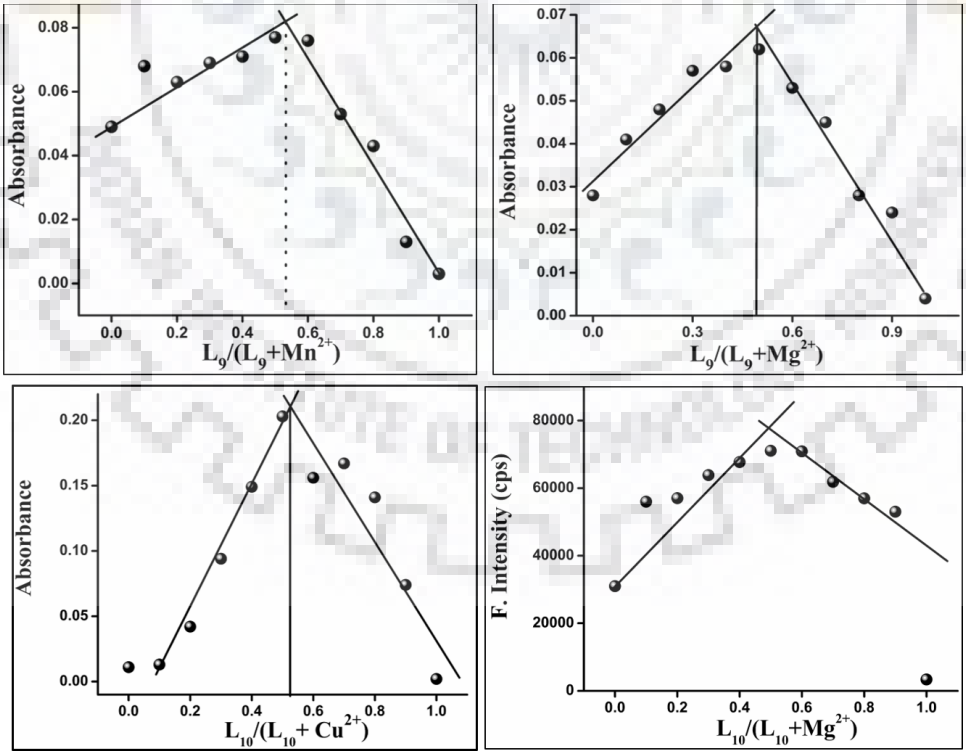


**Figure 6.5.** Job's plot of **L9** with $Mn^{2+}$ and $Mg^{2+}$ ion and **L10** with $Cu^{2+}$ and $Mg^{2+}$ ion and represents 1:1 stoichiometry with the metal ion.

Furthermore, the competitive experiment was also performed for the interference of other metal ions. The interference study reveals that there was not any metal ion interfere in the sensing of magnesium ion by emission studies. It is also clear in case $Mn^{2+}$ there was no interference occurred in sensing of $Mn^{2+}$ by absorption study. Figure 6.6 (a) & (b) demonstrated the competitive study of **L9** with $Mn^{2+}$ and $Mg^{2+}$ ion respectively. Whereas, the absorption study for $Cu^{2+}$ with **L10** ligand in the presence of other metal ions revealed that no interference was occurred in sensing of $Cu^{2+}$ ion and $Mg^{2+}$ with **L10** ligand there was also no interference by the other metal ion in the sensing of these ions. Figure 6.7 (a) & (b) displayed the competitive study of **L10** with $Cu^{2+}$ and $Mg^{2+}$ ion.

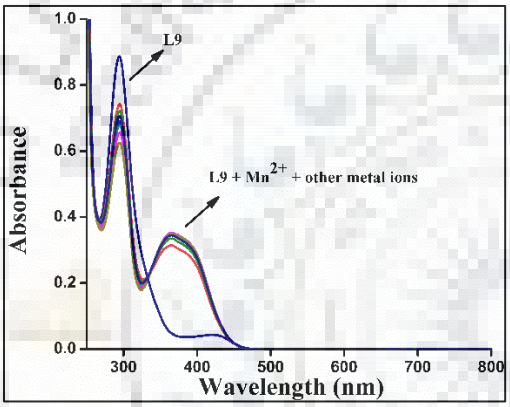


**Figure 6.6(a).** The interference study of **L9** with $Mn^{2+}$ in the presence of other metal ions.

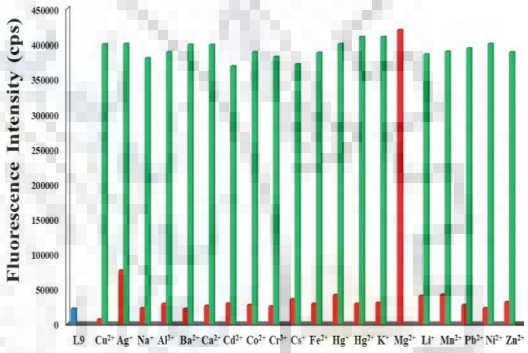


**Figure 6.6(b).** Competitive study of **L9** with $Mg^{2+}$ in the presence of foreign metal ions.

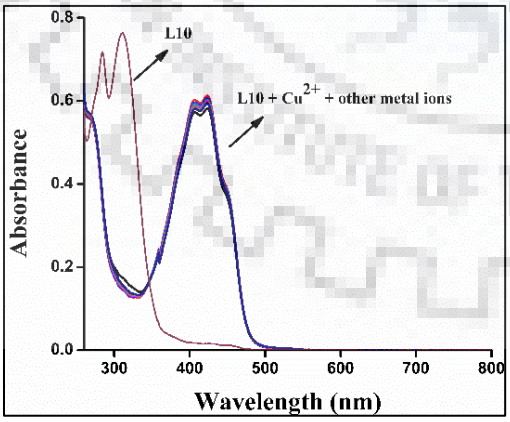


**Figure 6.7(a).** The interference study of **L10** with $Cu^{2+}$ ion with different metal ions.

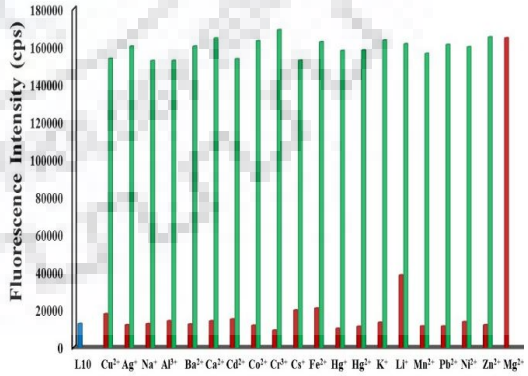


**Figure 6.7(b).** Competitive study of **L10** with $Mg^{2+}$ ion in presence of foreign metal ions.

Moreover, the association constants ($K_a$) of metal ions with ligands were calculated by plotting B-H plot between the concentration of metal ions, 1/($M^{2+}$) ion and 1/I-$I_0$ where I represents the intensity/absorption after consecutive addition of metal ion and $I_0$ shows the initial intensity/absorption of ligands (**L9** and **L10**) with-out addition of metal ions [22]. Figure 6.8 demonstrated the association constant of magnesium with **L9** *ca.* $1.2\times10^5$, for $Mn^{2+}$ ion with **L9** the formation constant is $1.6\times10^5$, similarly the binding constant of $Mg^{2+}$ and $Cu^{2+}$ with **L10** is $5.25\times10^4$ and $1.99\times10^5$ respectively. Same as, the limit of detection was calculated by the plotting between log ($M^{2+}$) and I-$I_0$/$I_{max}$-$I_0$ where $I_{max}$ shows maximum intensity/absorption after maximum addition of metal ion in the ligand. The findings of both ligands with metal ions are summarized in table 6.1 and LOD for $Mg^{2+}$ and $Mn^{2+}$ with **L9** showed 2.5 μM and 0.16 μM respectively. However, the LOD for $Mg^{2+}$ and $Cu^{2+}$ with **L10** represented as 1.2 μM and 0.37 μM respectively. Figure 6.9 showed the LOD plots.

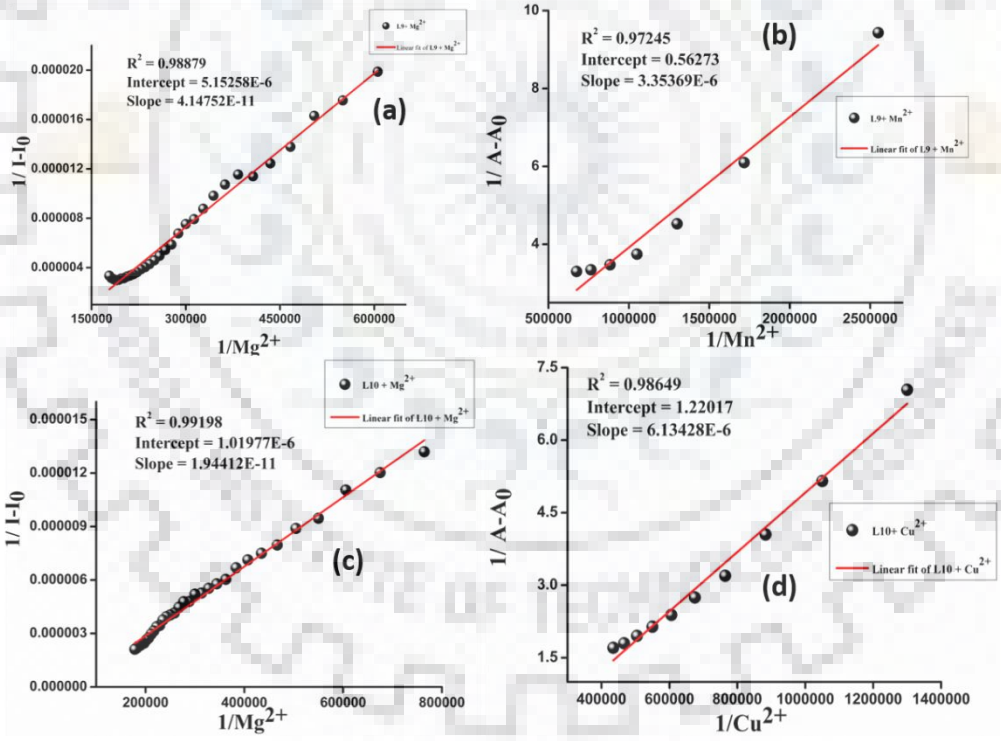


**Figure 6.8.** The B-H plot represent the association constant (a) shows B-H plot for $Mg^{2+}$ ion with **L9,** (b) represents binding constant of $Mn^{2+}$ ion with **L9**, (c) demonstrate the formation constant of $Mg^{2+}$ ion with **L10**, and (d) shows the B-H plot of $Cu^{2+}$ ion with **L10** ligand.

**Table 6.1:** All photophysical data of **L9** and **L10**.

| Ligands | Absorbance ($\lambda_{max}$) (nm) | Emission ($\lambda_{ex}$) (nm) | Stoichiometry | Binding constant | LOD |
|---|---|---|---|---|---|
| **L9** | 294 (n-π*) | | | - | |
| **L9 (Mg)** | 382 nm | Fluorescence enhancement at 526 nm | 1:1 | $1.2 \times 10^5$ | $2.56 \times 10^{-6}$ |
| **L9 (Mn)** | 372 nm | - | 1:1 | $1.68 \times 10^5$ | $1.63 \times 10^{-7}$ |
| **L10** | 286 (π-π*), 313 (n-π*) | | | - | |
| **L10 (Cu)** | 418 nm | - | 1:1 | $1.99 \times 10^5$ | $3.71 \times 10^{-7}$ |
| **L10 (Mg)** | - | Fluorescence enhancement at 422 nm | 1:1 | $5.25 \times 10^4$ | $1.28 \times 10^{-6}$ |

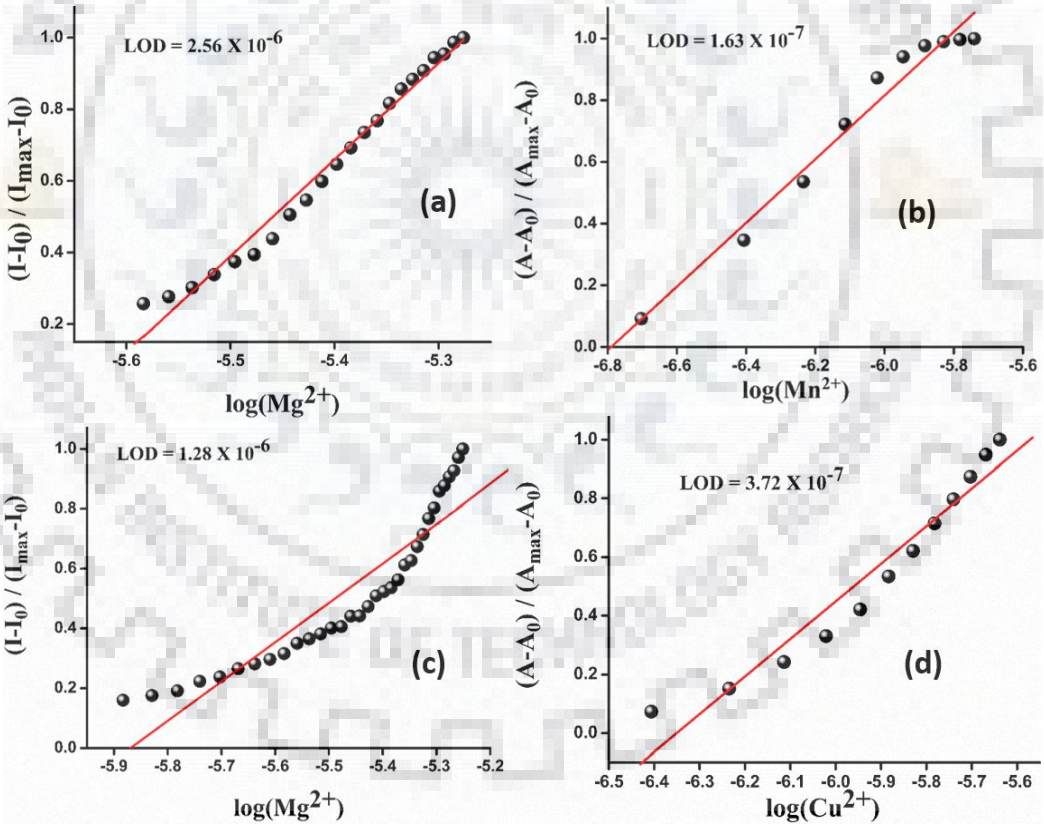


**Figure 6.9.** These plots represented Limit of Detection where (a) shows LOD plot for $Mg^{2+}$ ion with **L9**, (b) represented LOD of $Mn^{2+}$ ion with **L9**, (c) demonstrated the sensitivity of $Mg^{2+}$ ion with **L10**, and (d) showed the LOD plot of $Cu^{2+}$ ion with **L10** ligand.

### 6.3.2 $^{1}$H NMR titration of L9 and L10 with metal ions

Further, the coordination of magnesium ion to both ligands was approved by the $^{1}$H-titration with **L9** & **L10** ligands. The NMR titration revealed that the -NH proton in both ligands were downfield shifted with magnesium ion. In case of **L9** ligand the -NH proton is shifted from δ (ppm) 11.80 to 11.81 and with **L10** -NH proton is also deshielded from δ (ppm) 11.98 to 12.06 due to the strong conjugation between -NH and -C=O group that are adjacent to each other and solvent water peak was also shifted to downfield which reveals that the solvent water takes part in complexation. However, other aromatic and -imine protons of both ligands **L9** & **L10** were upfield shifted upon interaction with magnesium ion which suggested that the binding of magnesium ion is from -C=O of chromone moiety, imine nitrogen and oxygen of furan moiety and form a stable tridentate form (figure 6.10).

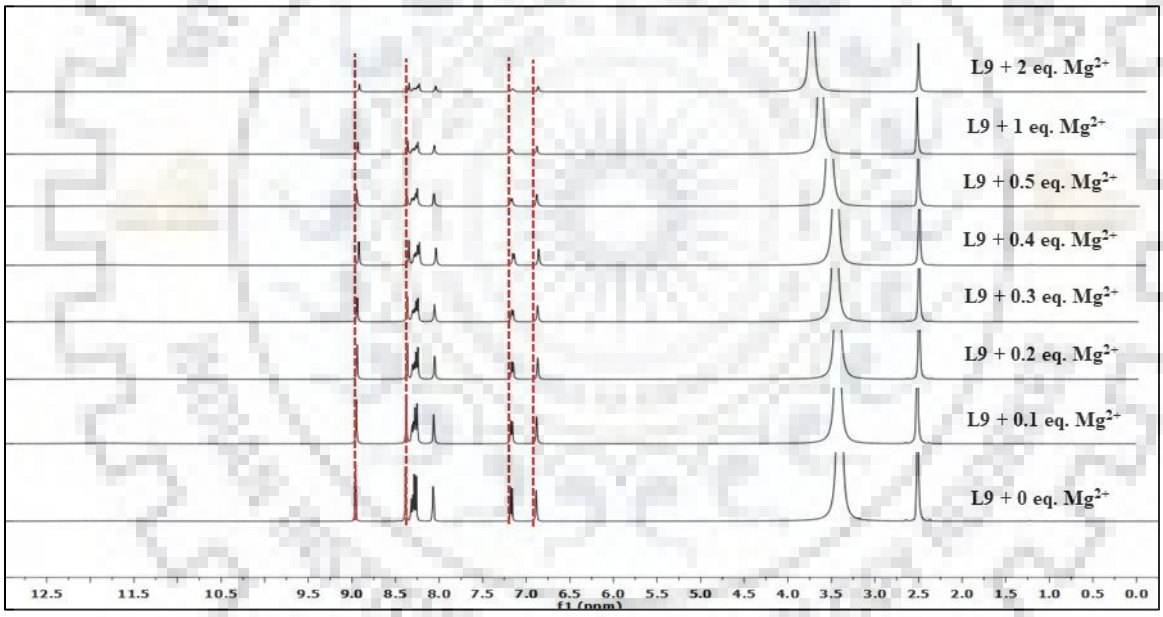


**Figure 6.10.** NMR titration of **L9** with magnesium ion.

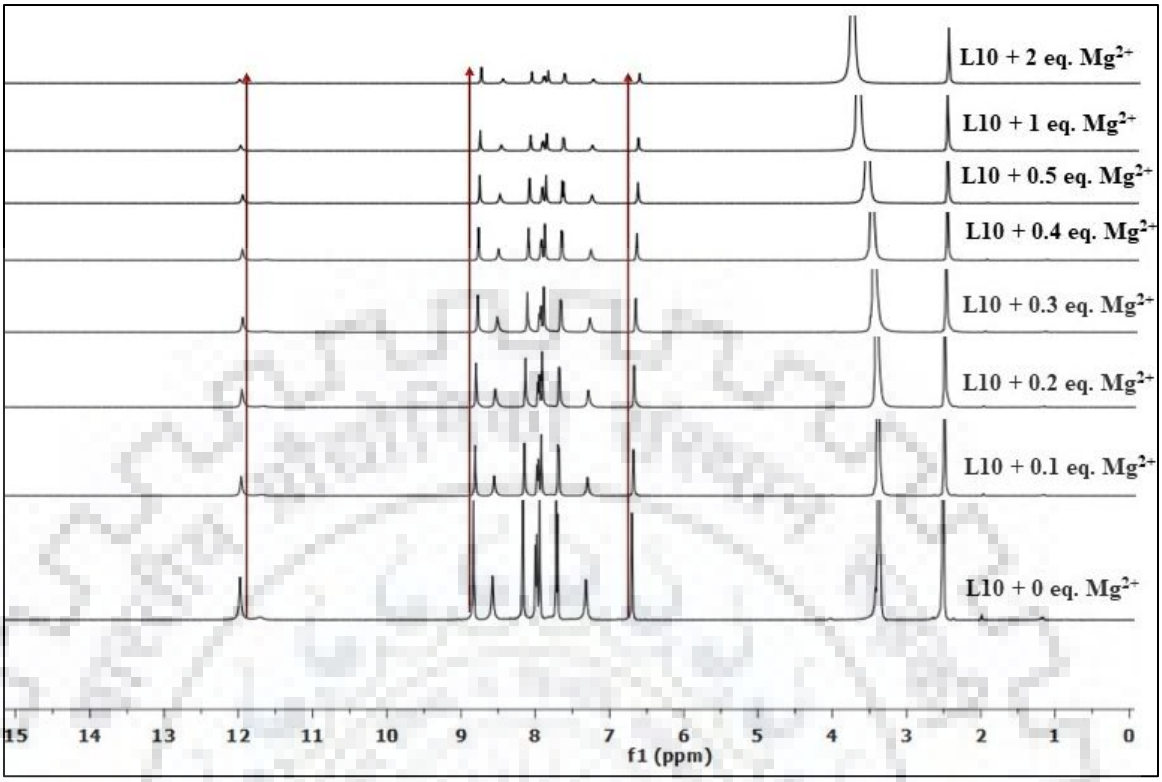


**Figure 6.11.** NMR titration of **L10** with magnesium ion.

With **L9** the -CH proton of imine is shifted Δδ (ppm) 0.03, similarly, in the presence of **L10** this proton shifted Δδ (ppm) 0.05. Other aromatic protons in both the cases were shifted to upfield shift by Δδ (ppm) 0.02, 0.03 and 0.05 that shows the coordination of magnesium ion to the ligands *via* inhibition of "push-pull" behavior of chromone and furan moiety in the molecules. Figure 6.10 & 6.11 represented the NMR titration of **L9** and **L10** with magnesium ion respectively [23].

Similarly, the binding of manganese ion to the **L9** ligand also supported by the $^{1}H$ NMR titration. The study demonstrated that upon interaction of $Mn^{2+}$ ion with **L9** ligand, the all aromatic protons was shifted to upfield Δδ (ppm) 0.01 and the -NH proton was completely disappeared upon complexation with manganese ion whereas the intensity of imine proton was decreased that supported the interaction was occurred with -C=O of chromone moiety, imine nitrogen, -NH proton of ligand and furan oxygen. The NMR (proton) titration was supported the binding of $Mg^{2+}$ with **L9**, **L10** ligands and $Mn^{2+}$ with **L9** ligand (Figure 6.12). Figure 6.13 represents the binding mode of **L (L9 & L10)** with $Mg^{2+}$ ion.

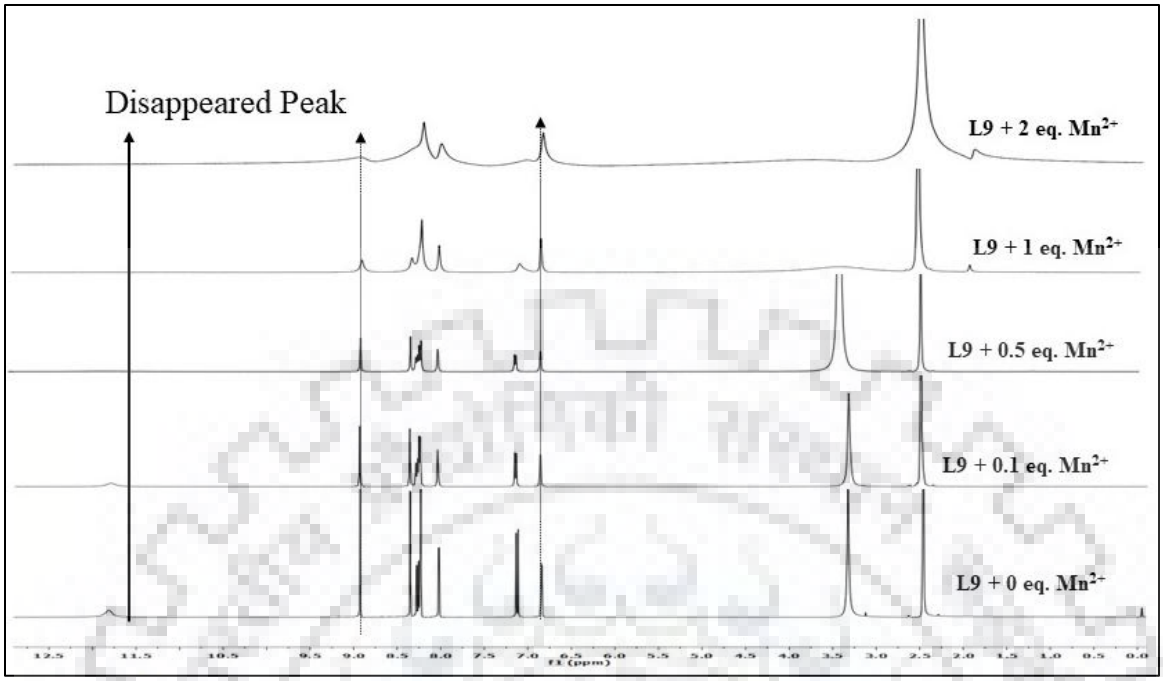


**Figure 6.12.** The NMR titration of **L9** with manganese ion.

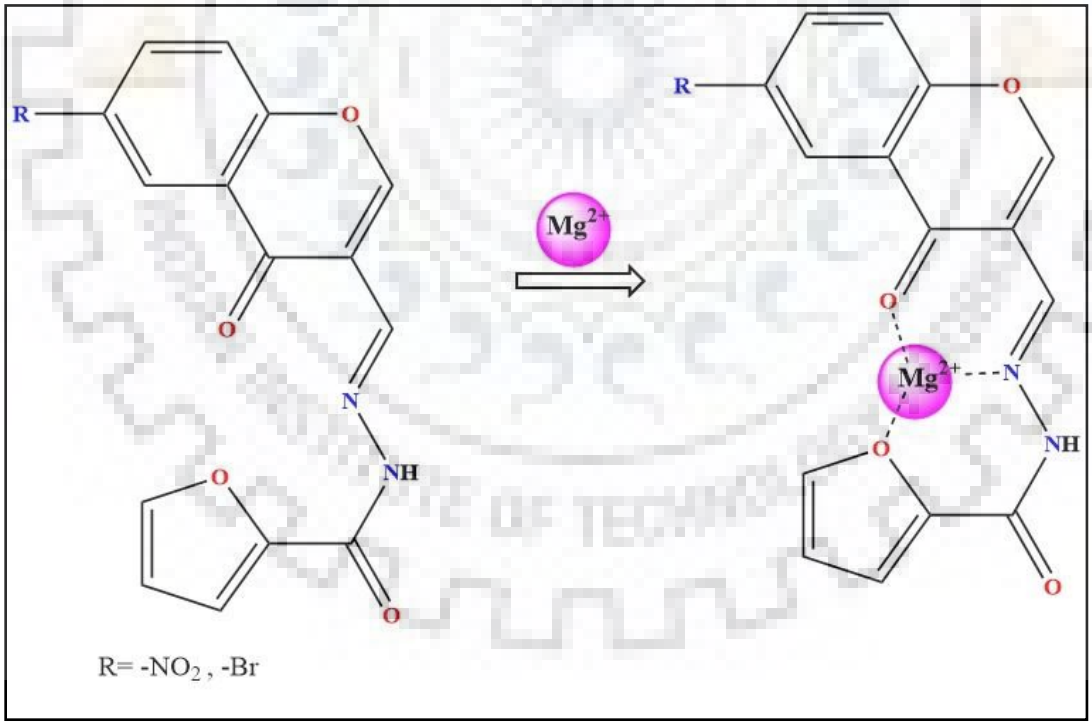


**Figure 6.13.** The Binding mode of **L (L9 & L10)** with manganese ion.

### 6.3.3 Electrochemical studies

The binding proximity was also supported by the electrochemical behavior of both ligands with magnesium ion, **L9** with $Mn^{2+}$ ion and **L10** with $Cu^{2+}$ ion. the redox properties of **L9**, **L9** with $Mg^{2+}$, $Mn^{2+}$ and **L10**, **L10** with $Mg^{2+}$, $Cu^{2+}$ ion was analyzed in the potential range -2 V to +2 V in $CH_3CN$ medium for **L9** and **L10** in MeOH medium. The cyclic voltammetry of **L9** was shown two irreversible reduction peaks at -0.77 V and -0.52 V and one oxidation peak at 1.411 V (table 6.2). After the addition of $Mn^{2+}$ to **L9**, the reduction peak was shifted to -0.74 towards cathodic shift, oxidation peak was shifted to anodic shift at 1.465 V and there were two new peaks was appeared -0.09 and 0.35 V due to the electron transfer from ligand to metal ion [24]. Similarly, when **L9** interact with $Mg^{2+}$ ion the reduction peaks were shifted to -0.76 V and -0.50 V whereas the oxidation peak at 1.411 V was diminished completely as well as current slightly decreased and two new peaks was appeared at -0.12 and 0.17 V which support the interaction between $Mg^{2+}$ ion with **L9** ligand. Further, the same study was performed with **L10** ligand in presence or absence of metal ions ($Mg^{2+}$ and $Cu^{2+}$ ion). **L10** was represented one irreversible reduction peak at -0.85 V and three oxidation peaks at 0.48 V, 1.48 V, 1.64 V, which was shown sifting upon the interaction between **L10** and $Mg^{2+}$. The reduction peak was shifted anodic shift at 0.91 V and some oxidation peaks were disappeared upon interaction with $Mg^{2+}$ ion. one oxidation peak was shifted to 0.44 V and a new peak was found at 0.68 V due to the inhibition of push-pull behavior in the ligands. However, in the presence of $Cu^{2+}$ ion the cyclic voltammogram showed there are two new oxidation peaks at 0.62 V and 1.14 V, besides this the irreversible reduction peak at -0.91 was shifted to anodic shift upto -0.87 V and peaks at 1.48 V, 1.64 V were diminished, and new peaks was appeared at 0.62 V, 1.14 V [25-27]. These electrochemical studies were strongly supported the interaction between **L9**, **L10** with metals ions ($Mg^{2+}$, $Mn^{2+}$ and $Cu^{2+}$). The all cyclic voltammogram were given in figure 6.14 (a), (b), (c) & (d) and all oxidation and reduction peaks were summarized in table 6.2.

**Table 6.2:** The all Cyclic voltammogram data.

| | Oxidation peaks | | Reduction peaks | |
|---|---|---|---|---|
| **L9** | 1.41 | - | -0.77 | -0.52 |
| **L9 + $Mg^{2+}$** | - | - | -0.76 | -0.50 |
| **L9 + $Mn^{2+}$** | 1.47 | 0.35 | -0.74 | -0.51 |
| **L10** | 1.48 | 1.64 | -0.91 | - |
| **L10 + $Mg^{2+}$** | - | - | -0.89 | - |
| **L10 + $Cu^{2+}$** | 0.62 | 1.14 | -0.87 | -0.38 |

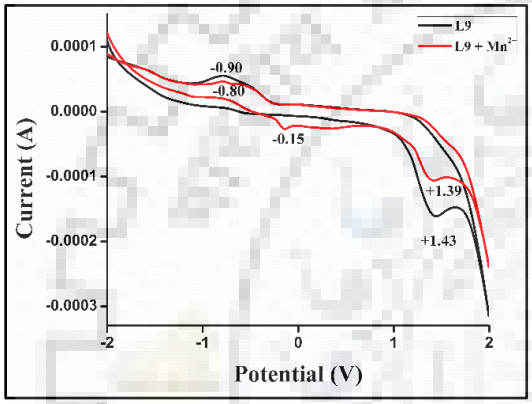


**Figure 6.14(a).** The Cyclic Voltammogram of **L9** in the presence and absence of $Mn^{2+}$ ion.

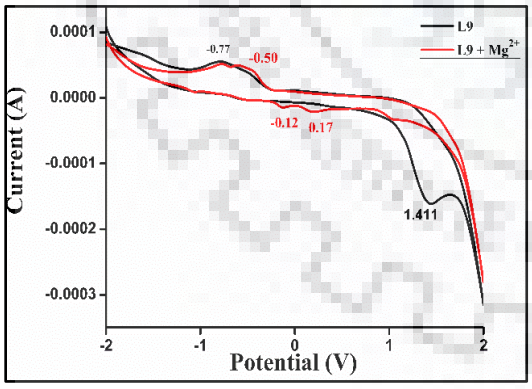


**Figure 6.14(b).** The Cyclic Voltammogram of **L9** in the presence and absence of $Mg^{2+}$ ion.

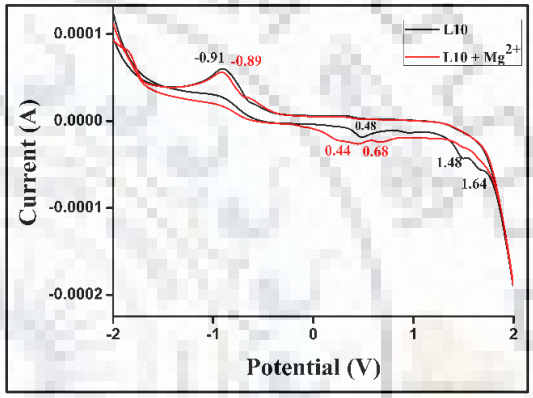


**Figure 6.14(c).** The Cyclic Voltammogram of **L10** in the presence and absence of $Mg^{2+}$ ion.

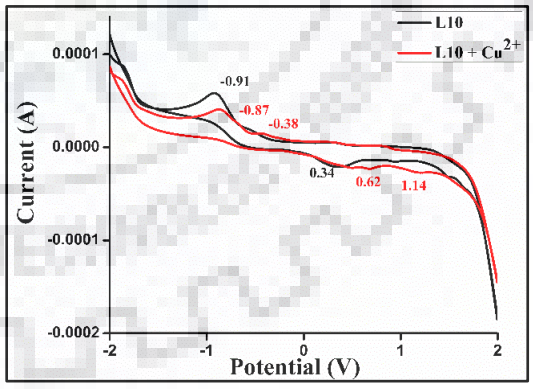


**Figure 6.14(d).** The Cyclic Voltammogram of **L10** in the presence and absence of $Cu^{2+}$ ion.

## 6.4 APPLICATIONS

### 6.4.1 Cytotoxicity assay

The biocompatibility of the synthesized imaging probe (**L9**, **L10**, **L9**+Mg, **L10**+Mg) is a limiting factor for the influential usage of the same in the bio-imaging field. To confer this, all the samples were tested their cytotoxicity assay in a dose dependent manner in HeLa cancer cell lines [28]. In HeLa cells, only **L9**+Mg was found little toxicity of 27.8% at maximum concentration of 75μg/mL (Figure 6.15). On the contrary, **L9**, **L10** and **L9**+Mg shows better bio-compatibility than **L10**+Mg. The ligand alone (**L9** and **L10**) showed negligible toxicity towards the cells used. The possible reason behind the differences in the cytotoxicity might be due to the magnesium complexes (positive charged) can effectively interact with of negatively charged biomolecules like cell membrane, DNA, Protein *etc*. [29,30]. A close examination into the result obtained from the assay entrust the knowledge better and facilitated improvisation of imaging agents can be possible with synthesized metal complexes.

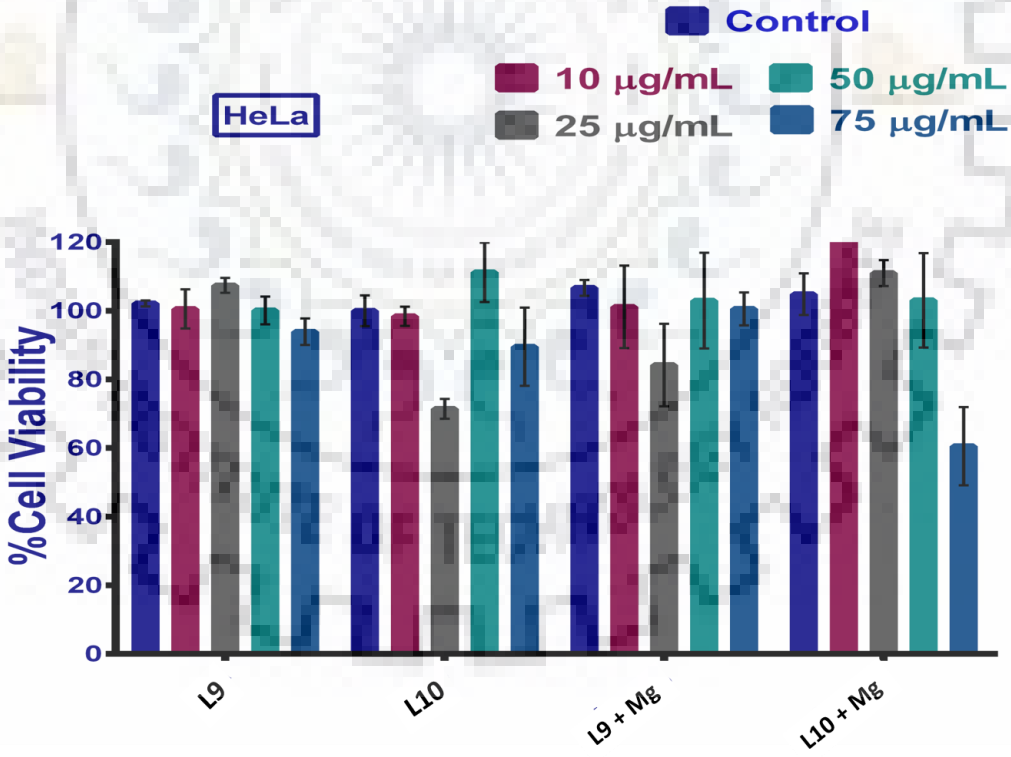


**Figure 6.15.** MTT based cytotoxic assessment of **L9**, **L10**, **L9**+$Mg^{2+}$ and **L10**+$Mg^{2+}$ on HeLa cells for 24h.

### 6.4.2 Bioimaging

As the synthesized metal complexes possess an intrinsic fluorescent activity, this can be applied in the bioimaging field. So, we performed bioimaging in cancer cells. A multiple color scheme in the GFP (Green Fluorescent Protein) and Qdot (Quantum Dot) filters. The HeLa cells were screened for bioimaging provided with **L9** + $Mg^{2+}$ with maximum and better resolution than any of the others (**L9**, **L10** and **L9** + $Mg^{2+}$) (Figure 6.16). The increased interaction of **L10** + $Mg^{2+}$ with cells and biomolecules as described in the cytotoxic assay was later confirmed with the micrograph obtained after the treatment. A wideband pass of Qdot was having a fluorescent excitation of 445 nm provided with an emission maxima of 525-800 nm (wide bandpass) resulted with pale yellow fluorescence of the complexes [31]. Furthermore, the fluorescence was observed throughout the cell shows the ubiquitous distribution and interaction of the biomolecule present inside the cells [32]. Figure 6.16 represented bioimaging of HeLa cells treated with **L9**, **L10**, **L9** + $Mg^{2+}$ and **L10** + $Mg^{2+}$.

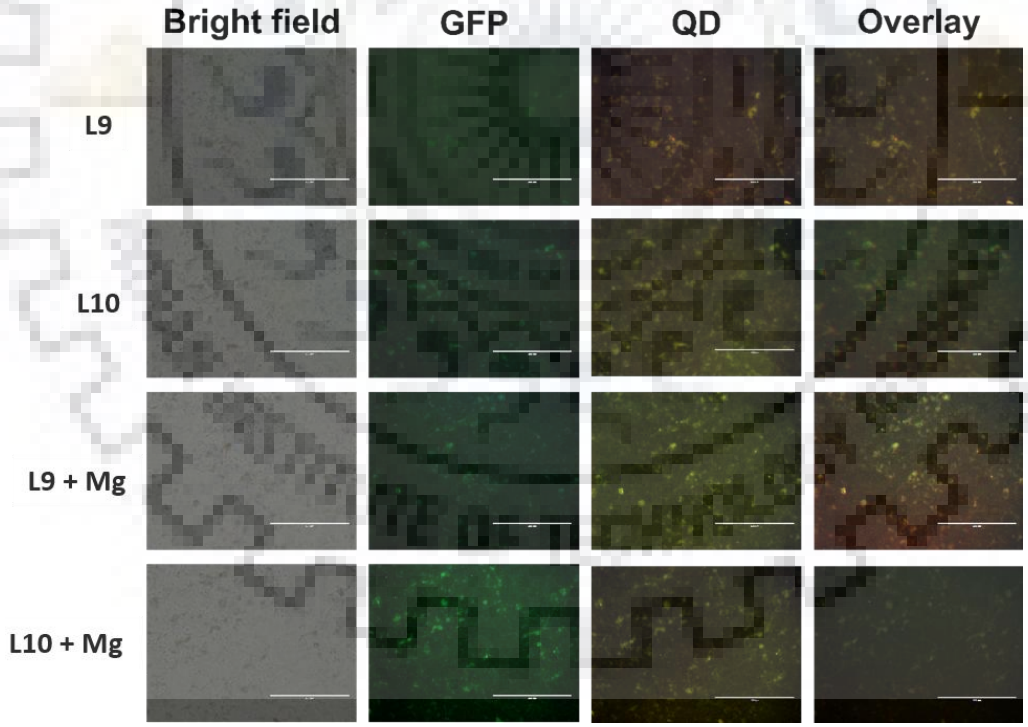


**Figure 6.16.** Bioimaging of HeLa cells treated with **L9**, **L10**, **L9**+$Mg^{2+}$ and **L10**+$Mg^{2+}$ for 24h.

## 6.5 CONCLUSIONS

In summary, carbohydrazide based novel chemosensors (**L9** & **L10**) were successfully synthesized by simple path and characterized by different analytical techniques. Both chemosensor is highly sensitive towards magnesium ion and **L9** was also analyzed $Mn^{2+}$ ion *via* absorption studies. Whereas, **L10** sense the $Cu^{2+}$ ion through absorption studies and it also sense $Mg^{2+}$ ion *via* fluorescence studies. These all findings were supported by the UV-vis, emission spectra, NMR studies and electrochemical studies. The binding affinity for $Mg^{2+}$ and $Cu^{2+}$ ion with **L9** *ca.* $1.2 \times 10^5$ and $1.68 \times 10^5$ respectively. Similarly, the association constant of $Mg^{2+}$ and $Cu^{2+}$ ion with **L10** determined as $5.25 \times 10^4$ and $1.99 \times 10^5$ respectively. Both chemosensors shown high sensitivity with magnesium ion as the LOD was calculated for $Mg^{2+}$ ion with **L9** and **L10** *viz.* 2.5 μM and 1.2 μM respectively. The LOD for $Mn^{2+}$ ion with **L9** was 0.16 μM and LOD for $Cu^{2+}$ ion with **L10** was 0.37 μM. Further, these ligands were used to check cytotoxicity and found that the ligands **L9**, **L10** and **L9** + $Mg^{2+}$ demonstrate excellent biocompatibility than **L10** + $Mg^{2+}$ ion. These ligands with magnesium ion were successfully used in bioimaging of HeLa cancer cells.

**References**


1. L. Ma, T. Lang, K. Wang, C. Wang, Y. Shen and W. Zhu, A coumarin-based fluorescent and colorimetric chemosensor for rapid detection of fluoride ion, Tetrahedron 73 (2017) 1306-1310.
2. R. Santos, S. A. Yamini and S. X. Dou, Recent progress in magnesium-based thermoelectric materials, J. Mater. Chem. A 6 (2018) 3328-3341.
3. M. S. Afzal, J.-P. Pitteloud and D. Buccella, Enhanced ratiometric fluorescent indicates for magnesium based on azoles of the heavier chalcogens, Chem. Commun. 50 (2014) 11358-11361.
4. J. J. DiNicolantonio, J. H. O'Keefe and W. Wilson, Subclinical magnesium deficiency: A principal driver of cardiovascular disease and a public health crisis, Open Heart 5 (2018) e000668.
5. S. Ferguson-Miller and G. T. Babcock, Heme/ Copper terminal Oxidases, Chem. Rev. 96 (1996) 2889-2908.
6. (a) N. J. Robinson and D. R. Winge, Copper metallochaperones, Annu. Rev. Biochem, 79 (2010) 537-562. (b) K. J. Waldron and N. J. Robinson, How do bacterial cells ensure that metalloprotein gets the correct metal? Nat. Rev. Microbiol. 7 (2009) 25-35.
7. H. Diao, W. Niu, W. Liu, L. Feng and J. Xie, Design, Properties and application of a facile fluorescence switch for Cu(II), Spectrochim. Acta A 170 (2017) 65-68.
8. A. Sargenti, G. Farruggia, E. Malucelli, C. Cappadone, L. Merolle, C. Marraccini, G. Andreani, L. Prodi, N. Zaccheroni, M. Sgrazi, C. Trobini, M. Lombardo and S. Lotti, A novel fluorescent chemosensor allows the assessment of intracellular total magnesium in small samples, Analyst 139 (2014) 1201-1207.
9. L. Lvova, C. G. Goncalves, L. Prodi, M. Sgarzi, N. Zaccheroni, M. Lombardo, A. Legin, C. D. Natale and R. Paolesse, Systematic approach in $Mg^{2+}$ ions analysis with a combination of tailored fluorophore design, Anal. Chimica Acta 988 (2017) 96-103.
10. S. R. Trenor, A. R. Shultz, B. J. Love and T. E. Long, Coumarins in polymers: From light harvesting to photo-cross-linkable tissue scaffolds, Chem. Rev. 104 (2004) 3059-3078.

11. N. C. Lim, J. V. Schuster, M. C. Porto, M. A. Tanudra, L. Yao, H. C. Freake and C. Bruckner, Coumarin-based chemosensors for Zinc(II) ; Towards the determination of the design algorithm for CHEF-type and ratiometric probes, Inorg. Chem. 44 (2005) 2018-2030.
12. D. Vashisht, K. Kaur, R. Jukaria, A. Vashisht, S. Sharma and S. K. Mehta, Colorimetric chemosensor based on coumarin skeleton for selective naked eye detection of cobalt (II) ion in near aqueous medium, Sens. Actuator B 280 (2019) 219-226.
13. Y. Dong, J. Li, X. Jiang, F. Song, Y. Cheng and C. Zhu, $Na^{+}$ triggered fluorescence sensors for $Mg^{2+}$ detection based on a coumarin salen moiety, Org. Lett. 13 (2011) 2252-2255.
14. D. Ray and P. K. Bharadwaj, A coumarin-derived fluorescence probe selective for magnesium ion, Inorg. Chem. 47 (2008) 2252-2254.
15. S. Naqvi, S. Mohiyuddin and P. Gopinath, Niclosamide loaded biodegradable chitosan nanocargoes: An in vitro study for potential application in cancer therapy, R. Soc. Open Sci. 4 (2017) 1-18.
16. A. Dutt, A. H. Ramos, P. S. Hammerman, C. Mermel, J. Cho, T. Sharifnia, A. Chande, K. E. Tanaka, N. Stransky, H. Greulich, N. S. Gray, M. Meyerson, Inhibitor-sensitive FGFR1 amplification in human non-small cell lung cancer, PLoS One. 6 (2011) 1-10, e20351.
17. R. Alam, T. Mistri, A. Katarkar, K. Chaudhari, S. K. Mandal, A. R. Khudu-Bukhsh, K. K. Das and M. Ali, A novel chromo- and fluorogenic dual sensor for $Mg^{2+}$ and $Zn^{2+}$ with cell imaging possibilities and DFT studies, Analyst 139 (2014) 4022-4030.
18. P. Saluja, H. Sharma, N. Kaur, N. Singh and D. O. Jang, Benzimidazole-based imine-linked chemosensor: Chromogenic sensor for $Mg^{2+}$ and fluorescent sensor for $Cr^{3+}$, Tetrahedron 68 (2012) 2289-2293.
19. H. Zhang, C. Yin, T. Liu, J. Chao, Y. Zhang and F. Huo, Selective "off-on" detection of magnesium (II) ions using a naphthalimide-derived fluorescent probe, Dyes and Pigments 146 (2017) 344-351.

20. S. B. Maity and P. K. Bharadwaj, A molecular dual fluorescence-ON probe for $Mg^{2+}$ and $Zn^{2+}$: Higher selectivity towards $Mg^{2+}$ over $Zn^{2+}$ in a mixture, J. Lumin. 155 (2014) 21-26.
21. Z. Liu, H. Xu, S. Chen, L. Sheng, H. Zhang, F. Hao, P. Su and W. Wang, Solvent-dependent "turn-on" fluorescence chemosensor for $Mg^{2+}$ based on combination of C=N isomerization and inhibition of ESIPT mechanisms, Spectrochim. Acta A 149 (2015) 83-89.
22. X. Dong, J. H. Han, C. H. Heo, H. M. Kim, Z. Liu and B. R. Cho, Dual-color imaging of magnesium/calcium ion activities with two-photon fluorescent probes, Anal. Chem. 84 (2014) 8110-8113.
23. A. Nehra, V. K. Hinge and C. P. Rao, Phenylene-diimine-capped conjugated of lower rim 1,3-calix[4]arene as molecular receptor for $Mg^{2+}$ *via* arm conformational changes followed by aggregation and mimicking the species by molecular mechanics, J. Org. Chem. 79 (2014) 5763-5770.
24. S. Rodrigues, N. Munichandraiah and A. K. Shukla, A cyclic voltammetric study of the kinetics and mechanism of electrodeposition of manganese dioxide, J. Appl. Electrochem. 28 (1998) 1235-1241.
25. K. Chen, S. Song, K. Li and D. Xue, Water-soluble inorganic salts with ultrahigh specific capacitance: Crystallization transformation investigation of $CuCl_2$ electrodes, Cryst. Eng. Comm. 15 (2013) 10367-10373.
26. L. M. Abrantes, L. V. Araujo and M. D. Levi, Voltammetric studies on copper deposition/dissolution reactions in aqueous chloride solutions, Mineral Engineerings 8 (1995) 1467-1475.
27. I. Valov and W. D. Lu, Nanoscale electrochemistry using dielectric thin films as solid electrolytes, Nanoscale 8 (2016) 13828-13837.
28. H. M. Kim, C. Jung, B. R. Kim, S.-Y. Jung, J. H. Hong, Y.-G. Yo, K. J. Lee and B. R. Cho, Environment-sensitive two-photon probe for intracellular free magnesium ions in live tissue, Angew. Chem. Int. Ed. 46 (2007) 3460-3463.
29. P. Raj, A. Singh, A. Singh, N. Singh, Syntheses and photophysical properties of Schiff base Ni (II) complexes: Application for sustainable antibacterial activity and cytotoxicity, ACS Sustainable Chem. Engineer. 5 (2017) 6070-6080.

30. L. Luo, G. Li, D. Luan, Q. Yuan, Y. Wei and X. Wang, Antibacterial adhesion of borneol-based polymer *via* surface chiral stereochemistry, ACS Appl. Mater. Interfaces 6 (2014) 19371-19377.
31. T. Yu, P. Sun, Y. Hu, Y. Ji, H. Zhou, B. Zhang, Y. Tian and J. Wu, A novel and simple fluorescence probe for detecting main group magnesium ion in HeLa cells and Arabidopsis, Biosens. Bioelectron. 86 (2016) 677-682.
32. S. Lohar, K. Dhara, P. Roy, S. P. S. Babu, P. Chattopadhyay, Highly sensitive ratiometric chemosensor and biomarker for cyanide ions in the aqueous medium, ACS Omega 3 (2018) 10145-10153.

**Spectrum No. 1**: FTIR spectra of probe **L1.**

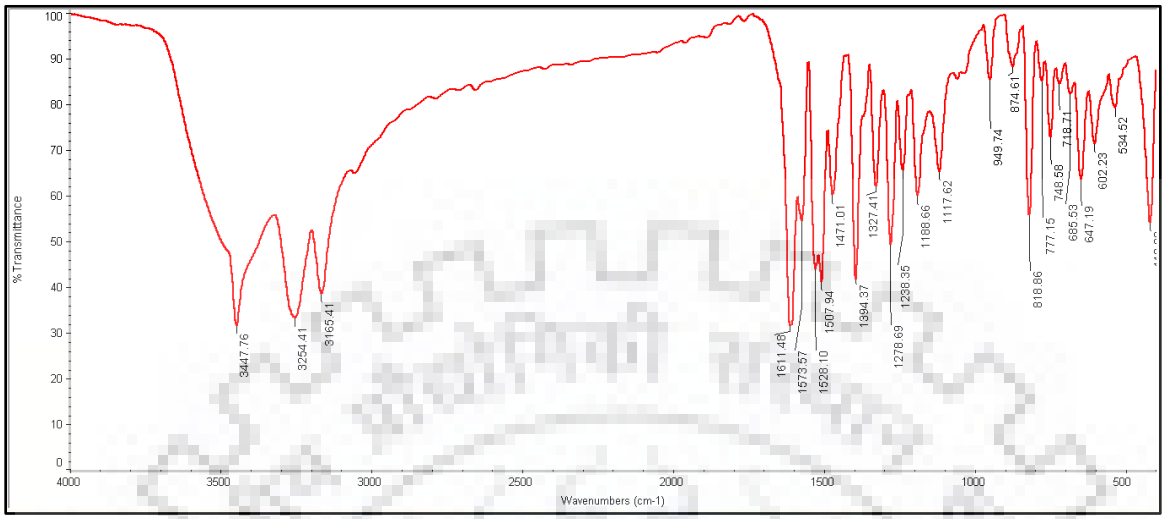


**Spectrum No. 2.** UV-Visible spectra of probe **L1.**

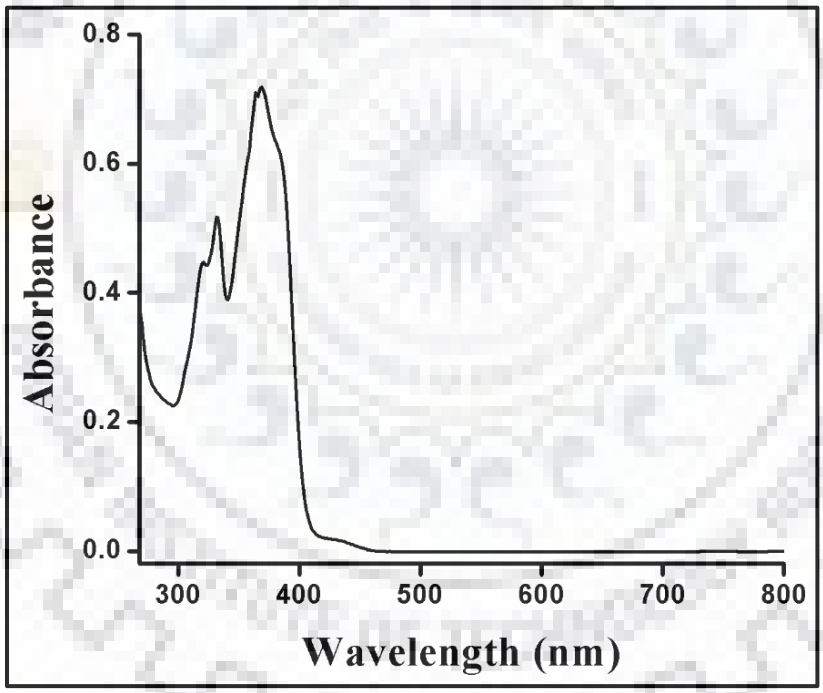

**Spectrum No. 3**. $^{1}$H NMR spectra of probe **L1.**

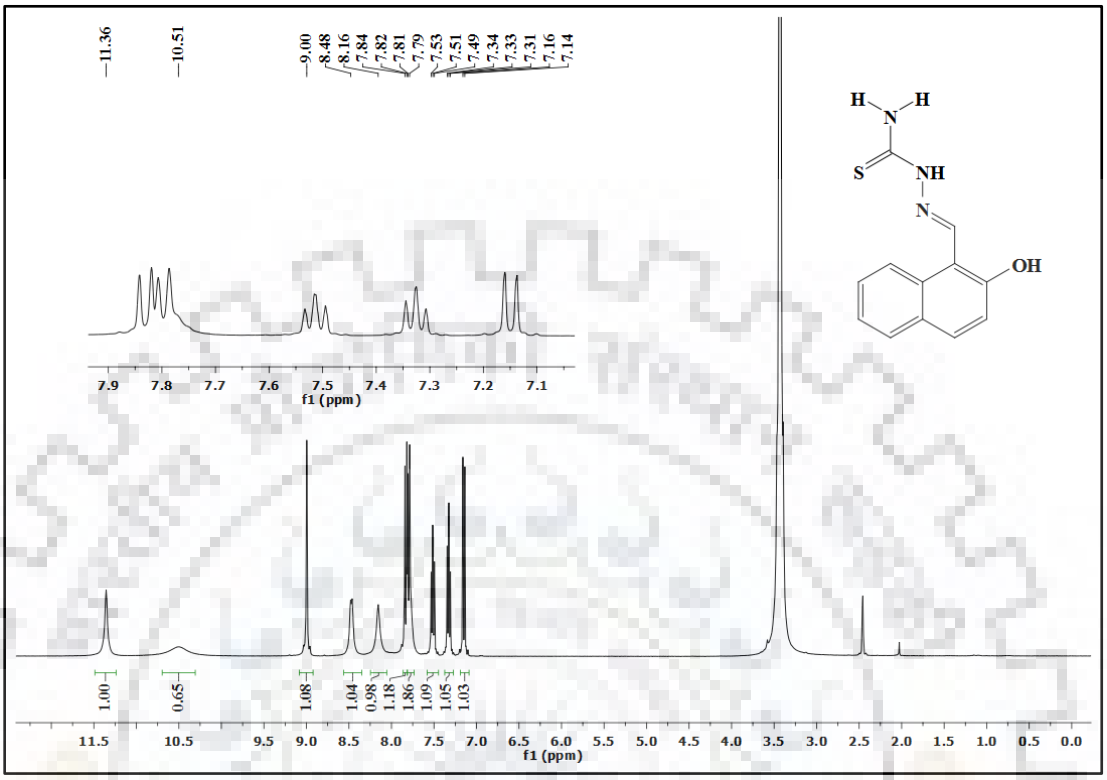


**Spectrum No. 4.** $^{13}$C NMR spectra of probe **L1.**

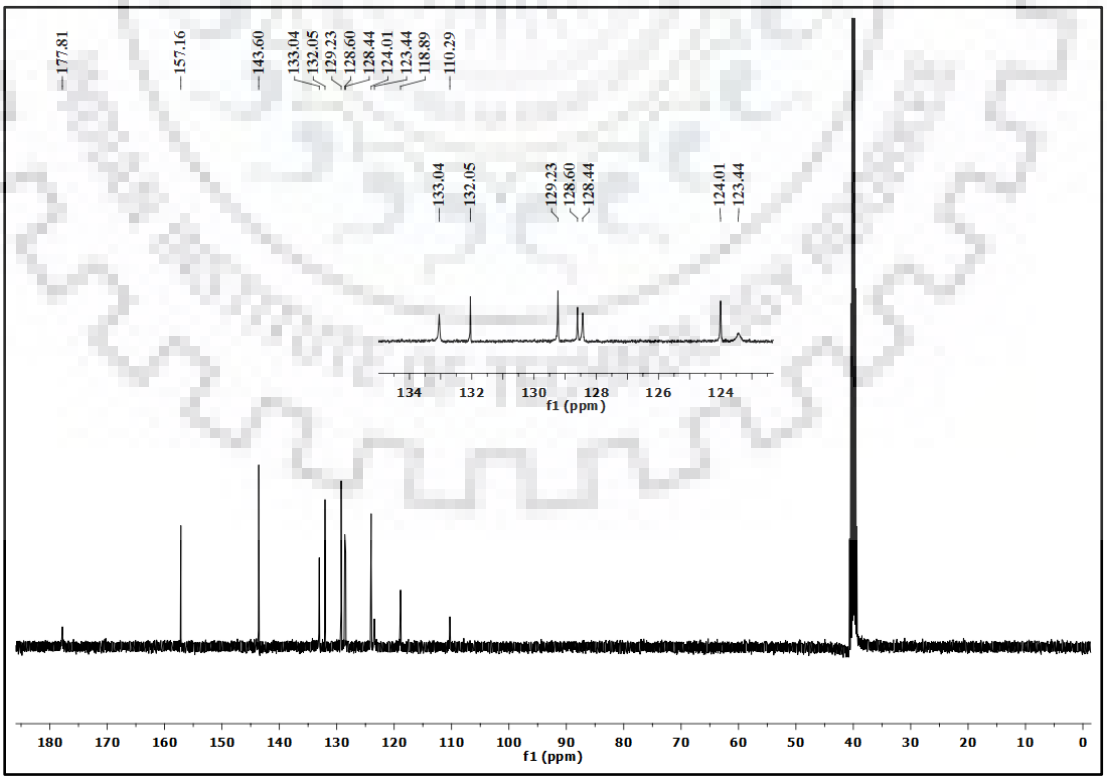

**Spectrum No. 5.** ESI-MS spectra of **L1**.

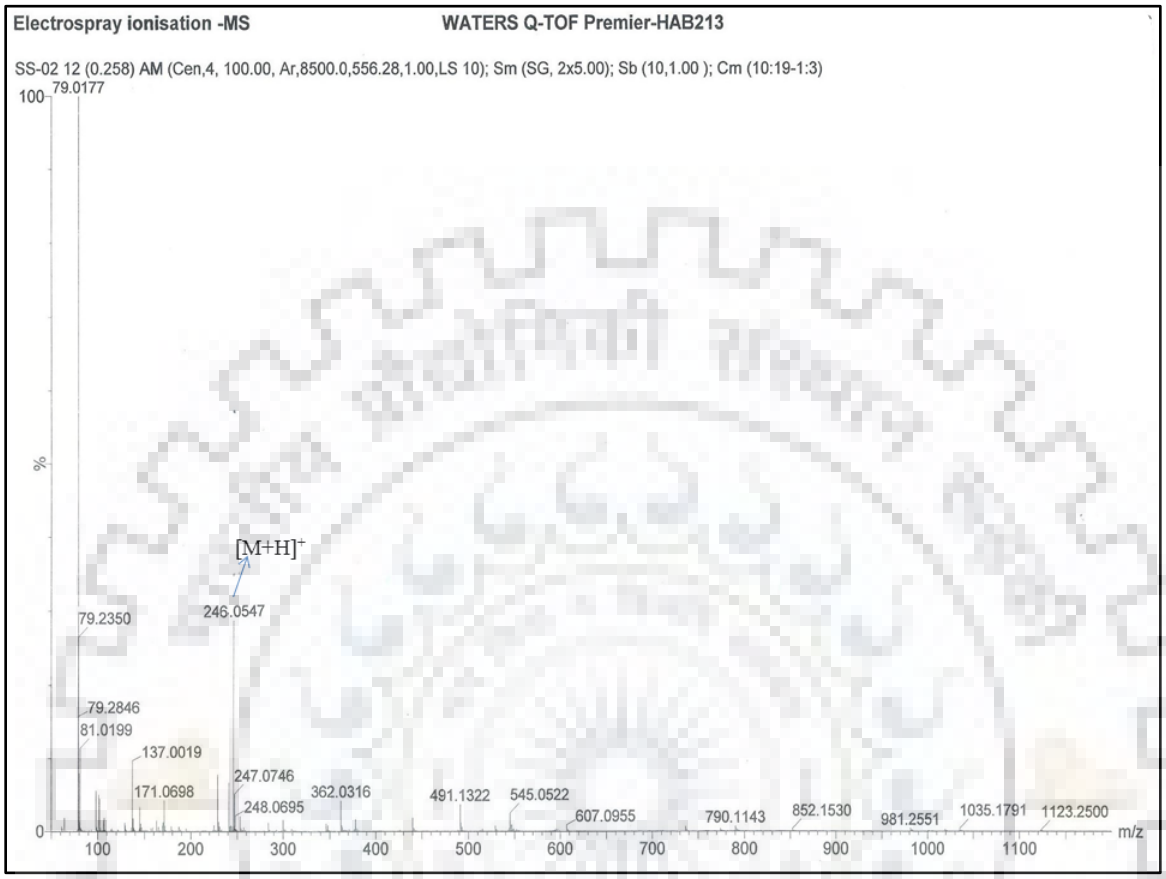


**Spectrum No. 6.** FT-IR spectrum of pyridine-2,6-dicarbohydrazide **(1).**

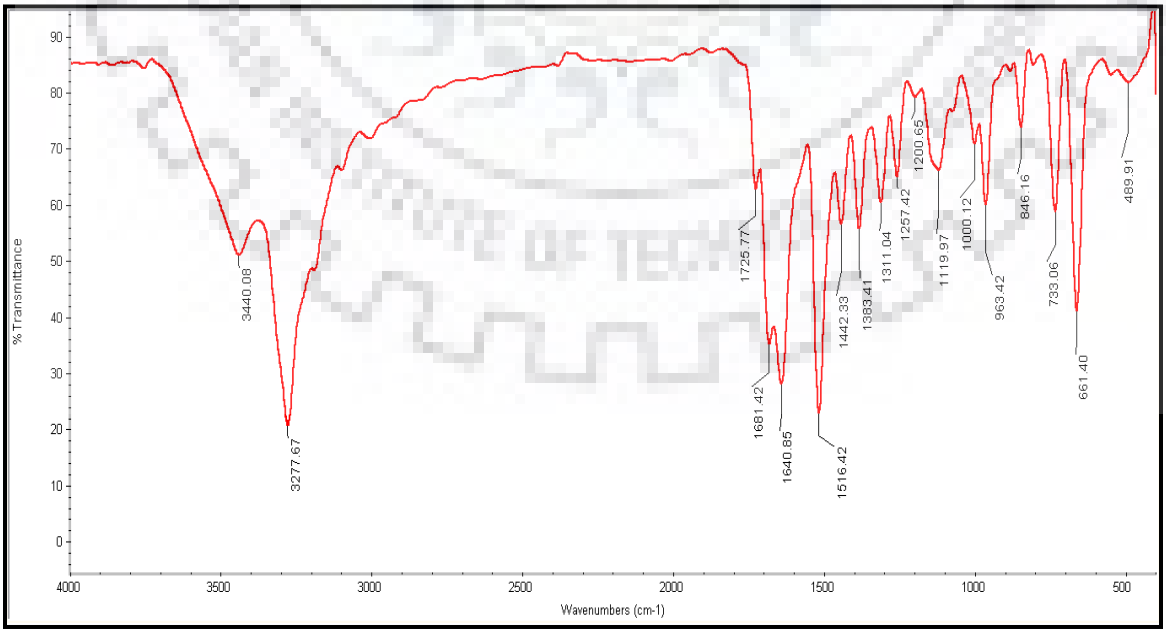

**Spectrum No. 7.** FT-IR Spectrum of ligand **L2.**

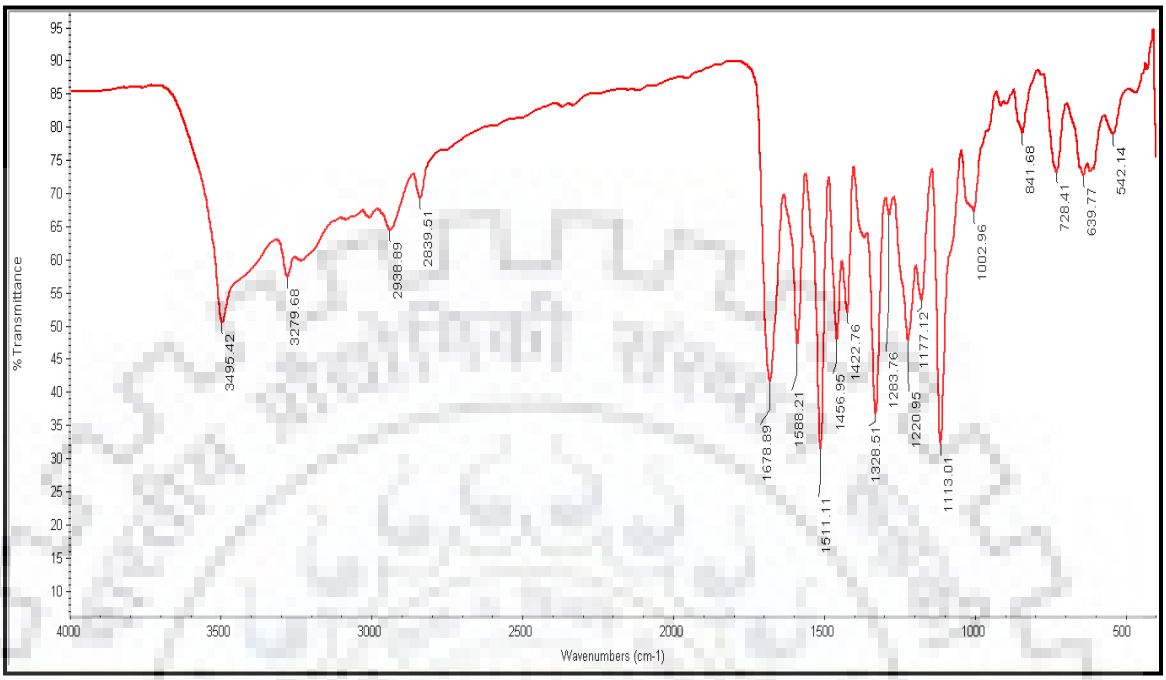


**Spectrum No. 8.** FT-IR Spectrum of ligand **L3.**

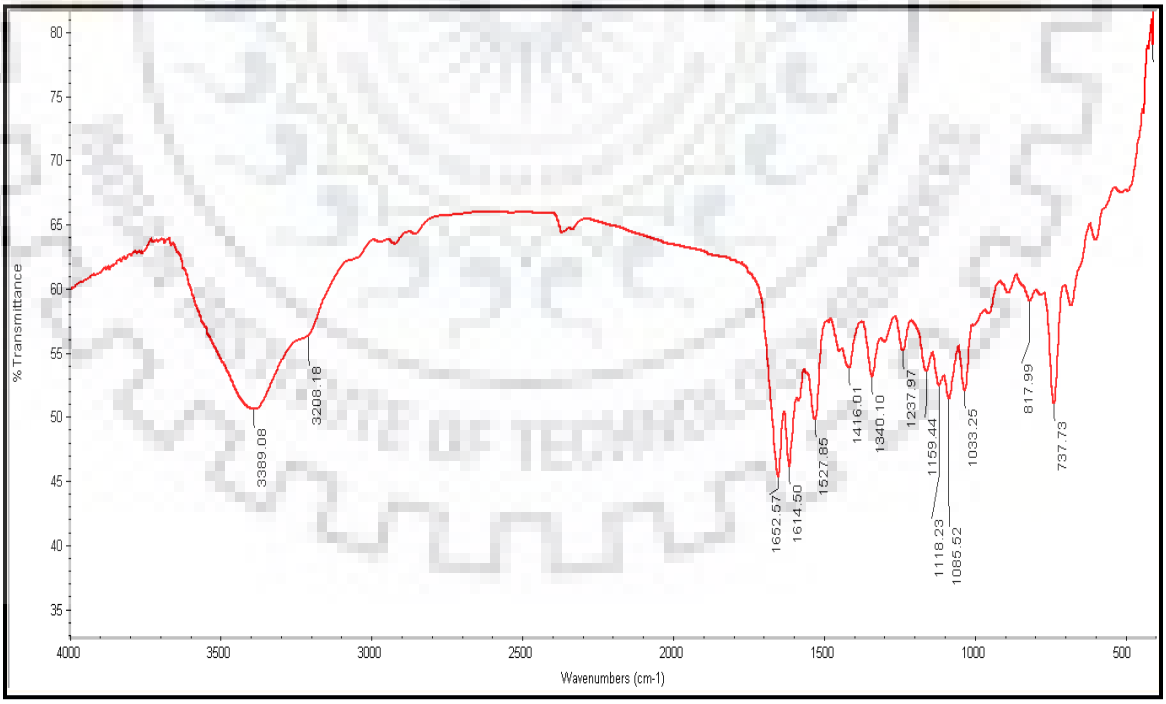

**Spectrum No. 9.** FT-IR Spectrum of ligand **L4.**

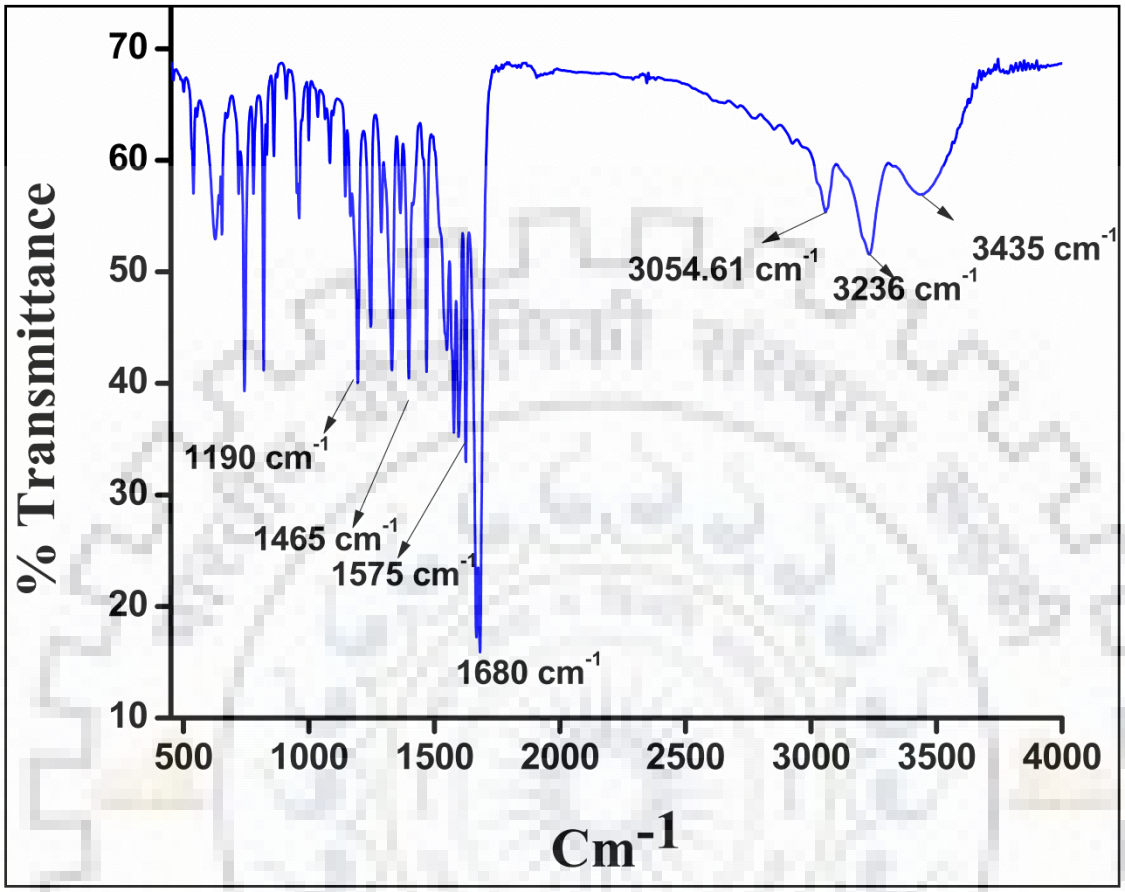


**Spectrum No. 10.** FT-IR Spectrum of ligand **L5.**

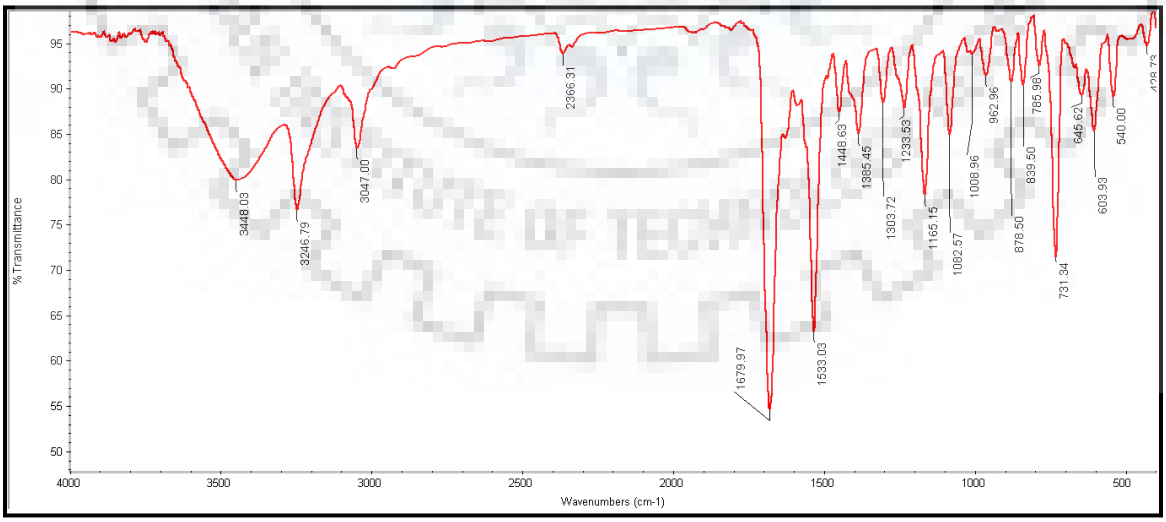

**Spectrum No. 11.** UV Spectrum of ligand **L2.**

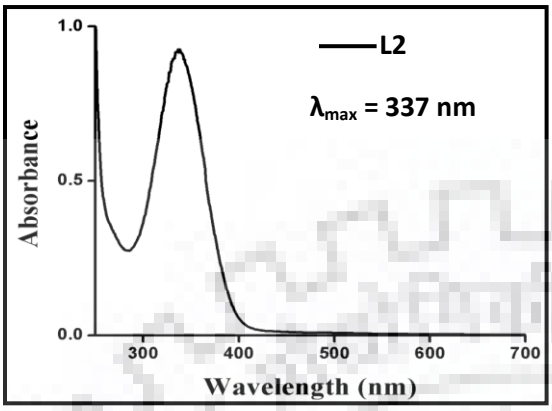


**Spectrum No. 12.** UV Spectrum of ligand **L3.**

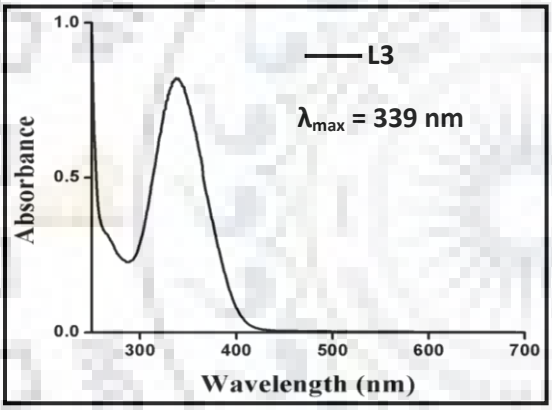


**Spectrum No. 13.** UV Spectrum of ligand **L4.**

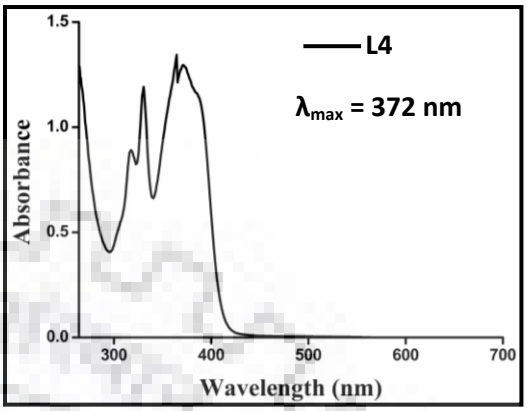


**Spectrum No. 14.** UV Spectrum of ligand **L5.**

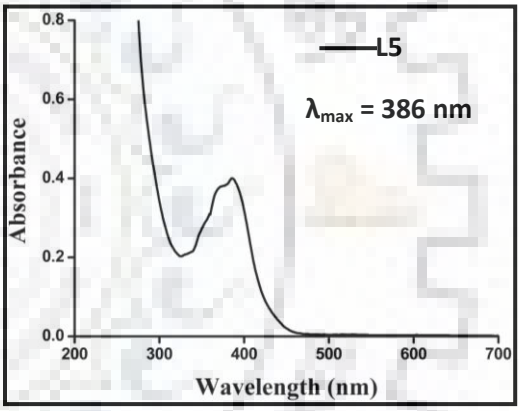

**Spectrum No. 15.** $^{1}$H NMR Spectrum of precursor **(1).**

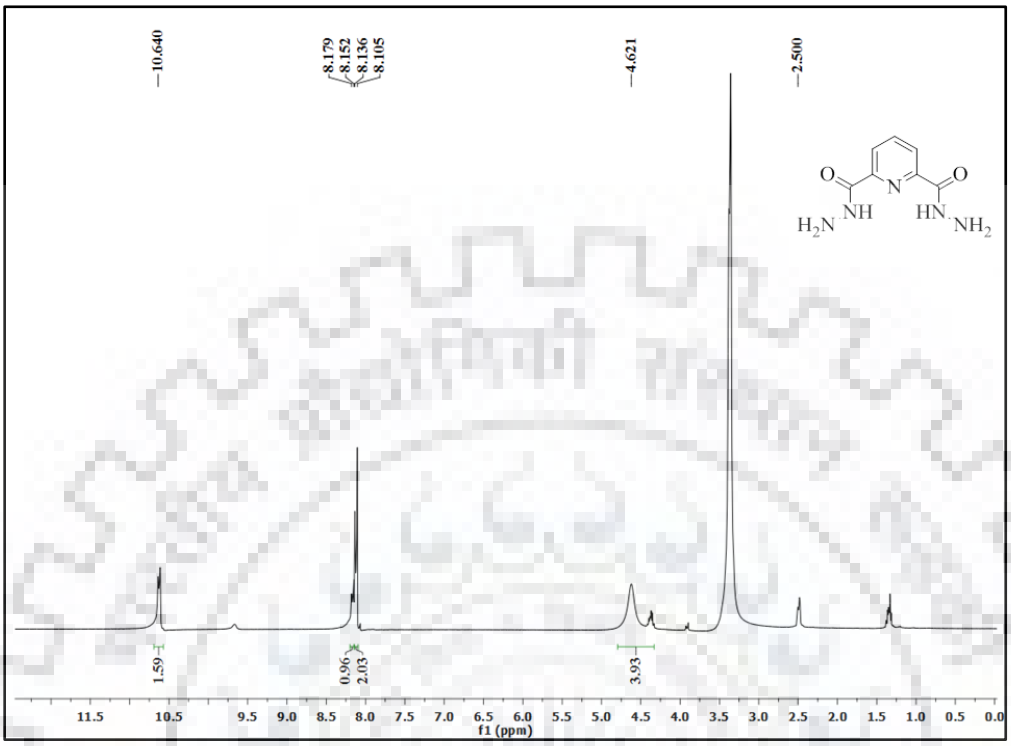


**Spectrum No. 16.** $^{13}$C NMR spectrum of precursor **(1).**

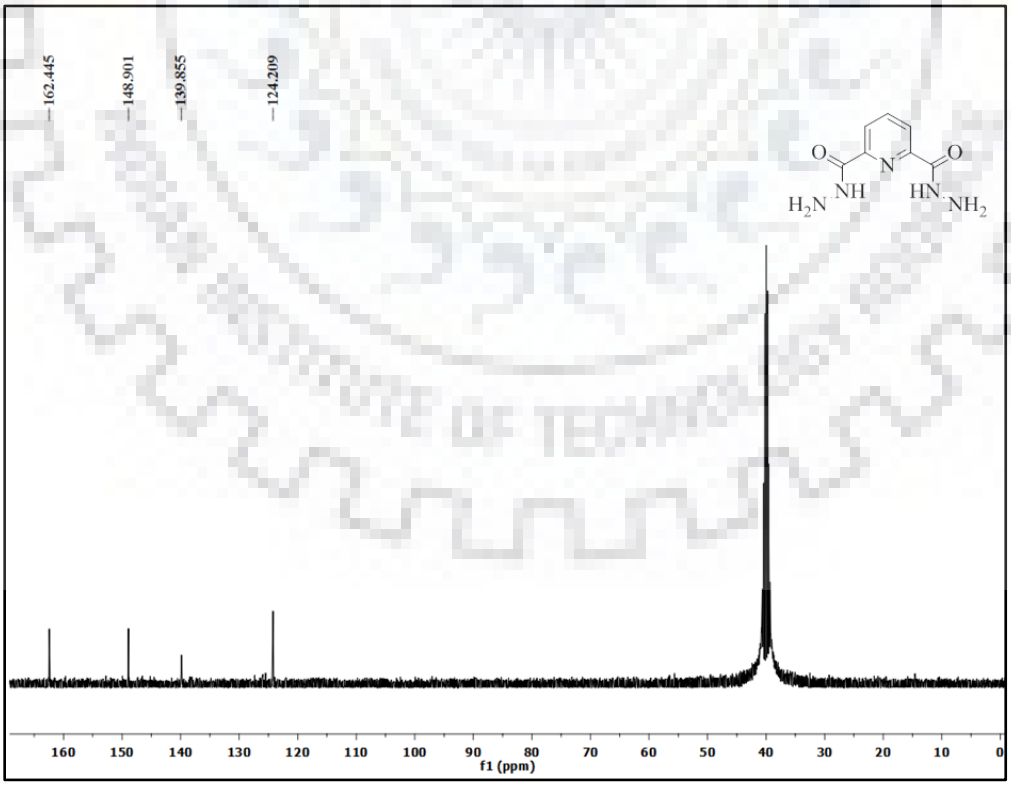

**Spectrum No. 17.** $^{1}$H NMR spectrum of Ligand **L2.**

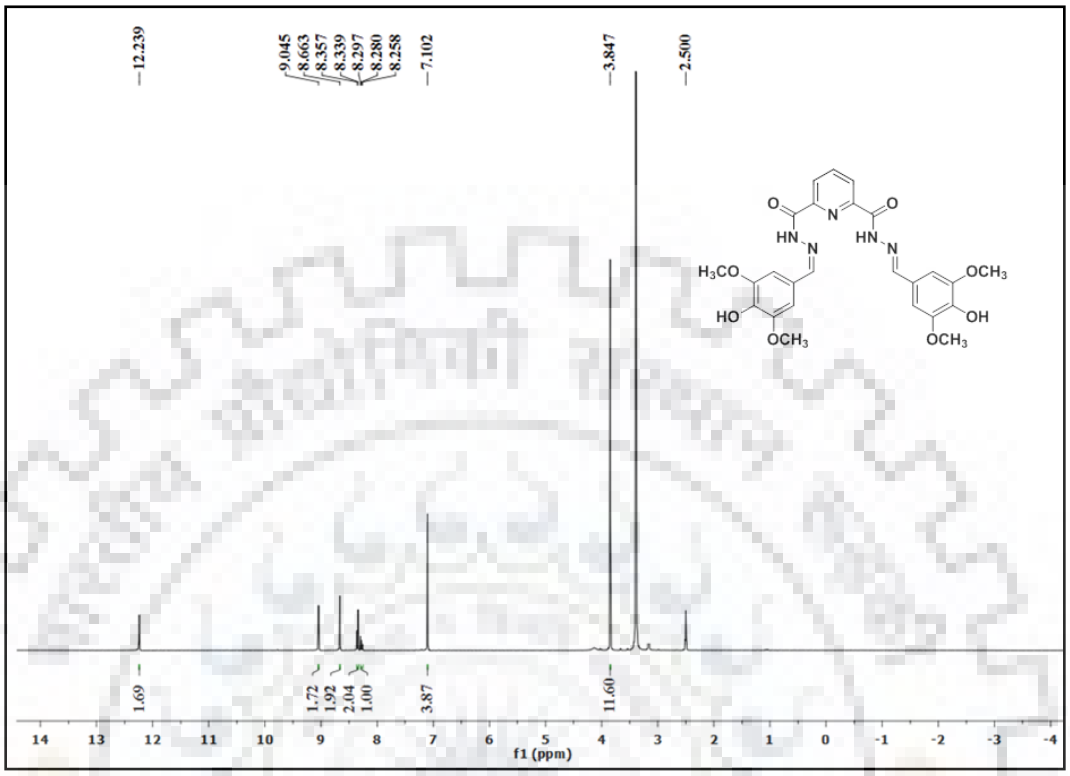


**Spectrum No. 18.** $^{13}$C NMR spectrum of Ligand **L2.**

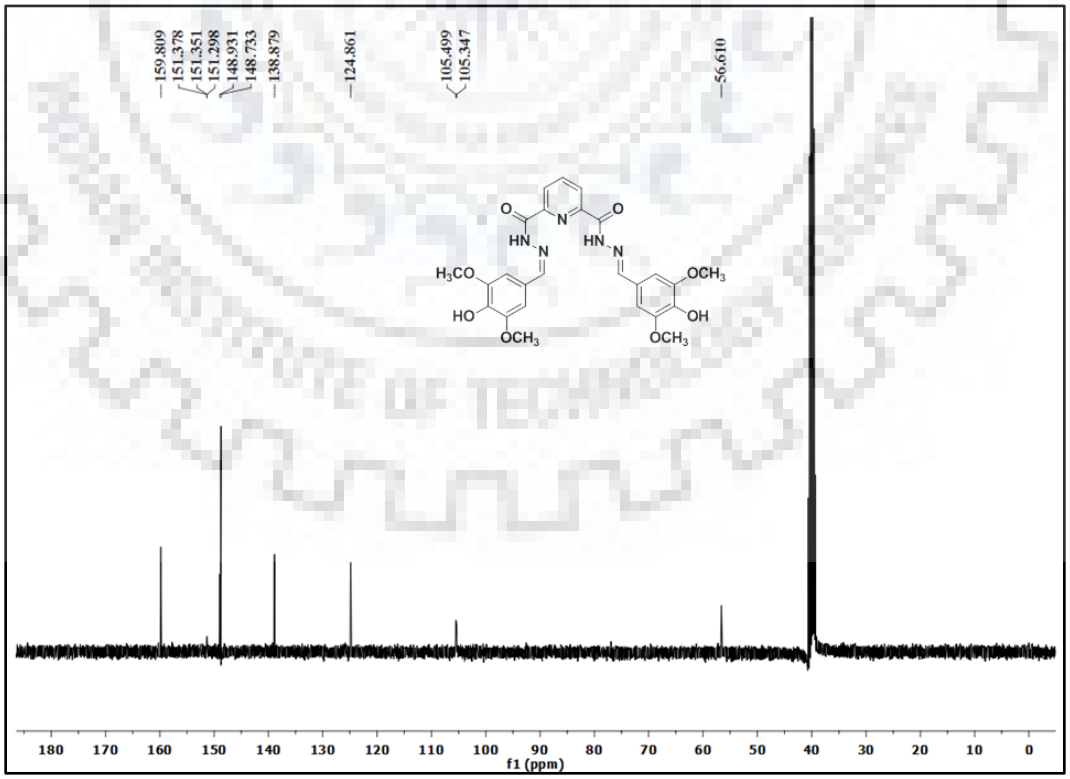

**Spectrum No. 19.** $^{1}$H NMR Spectrum of Compound **L3.**

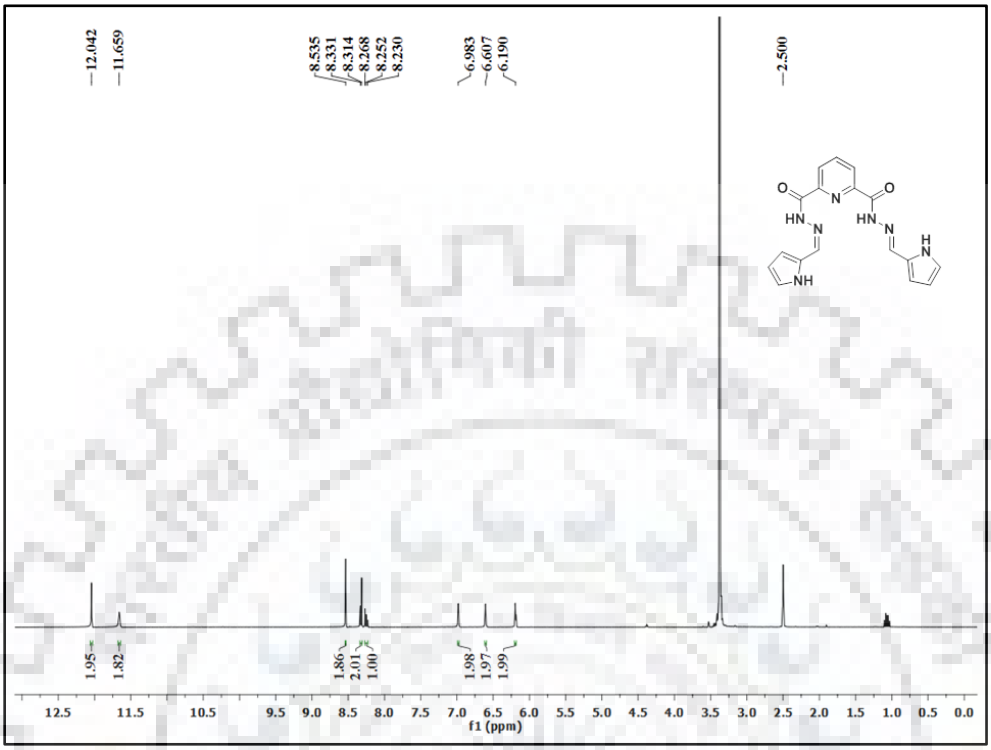


**Spectrum No. 20.** $^{13}$C NMR spectrum of ligand **L3.**

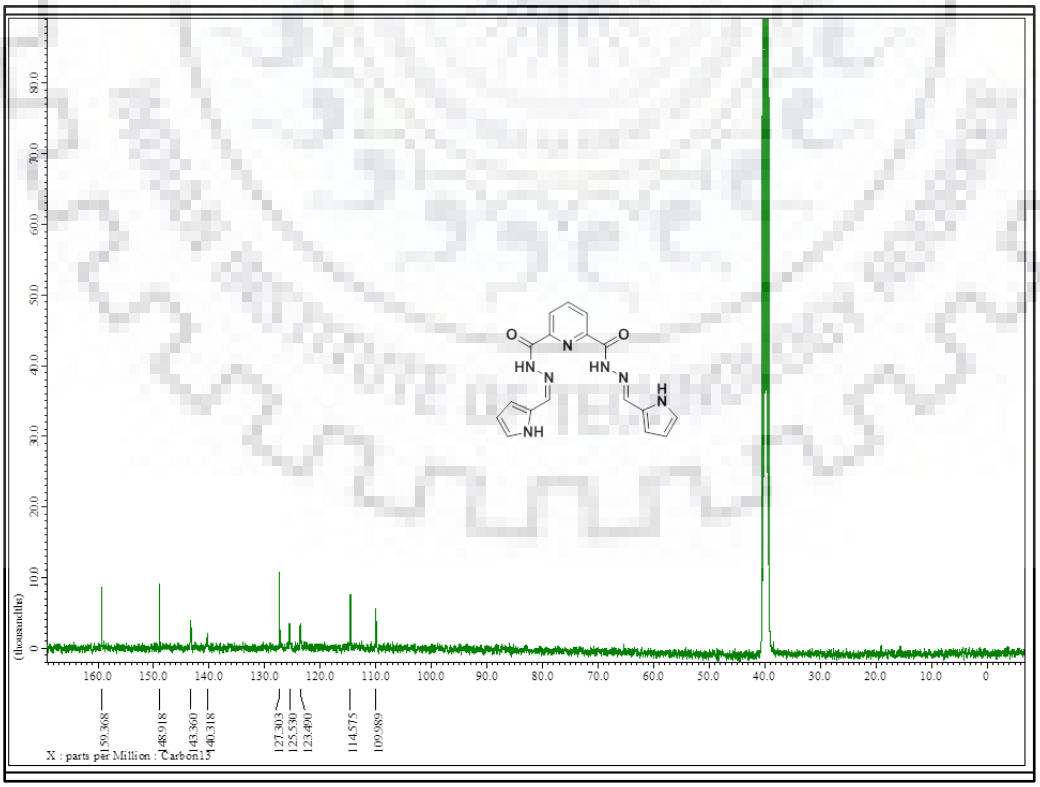

**Spectrum No. 21.** $^{1}$H NMR Spectrum of Compound **L4.**

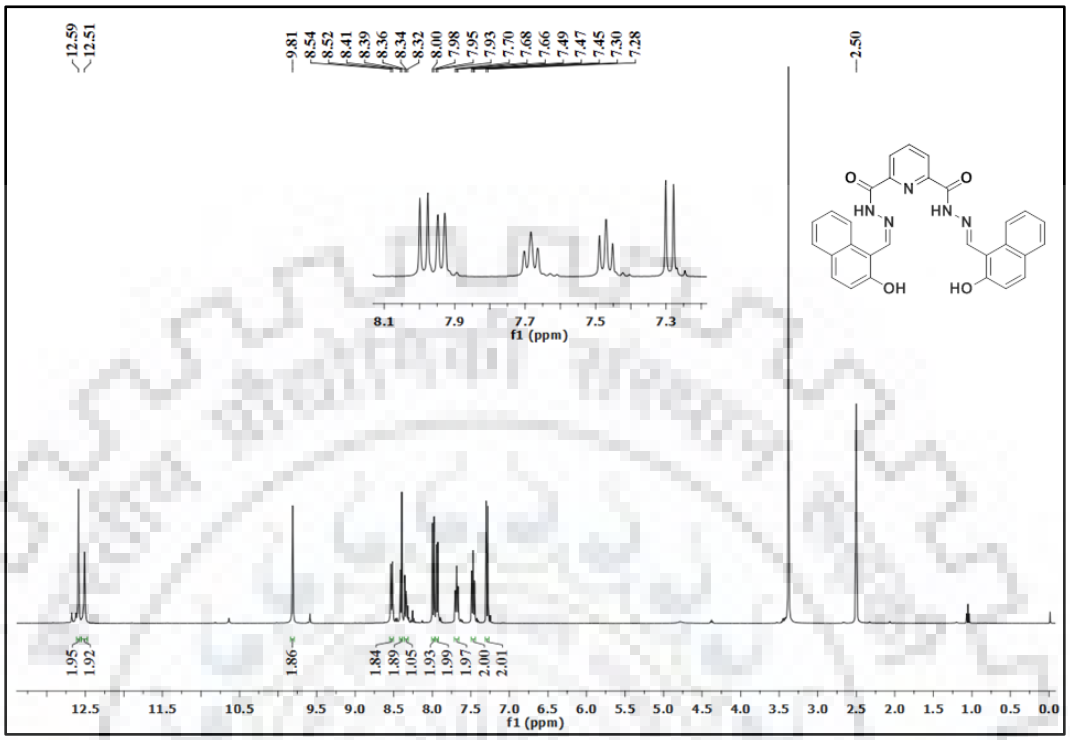


**Spectrum No. 22.** $^{13}$C NMR spectrum of ligand **L4.**

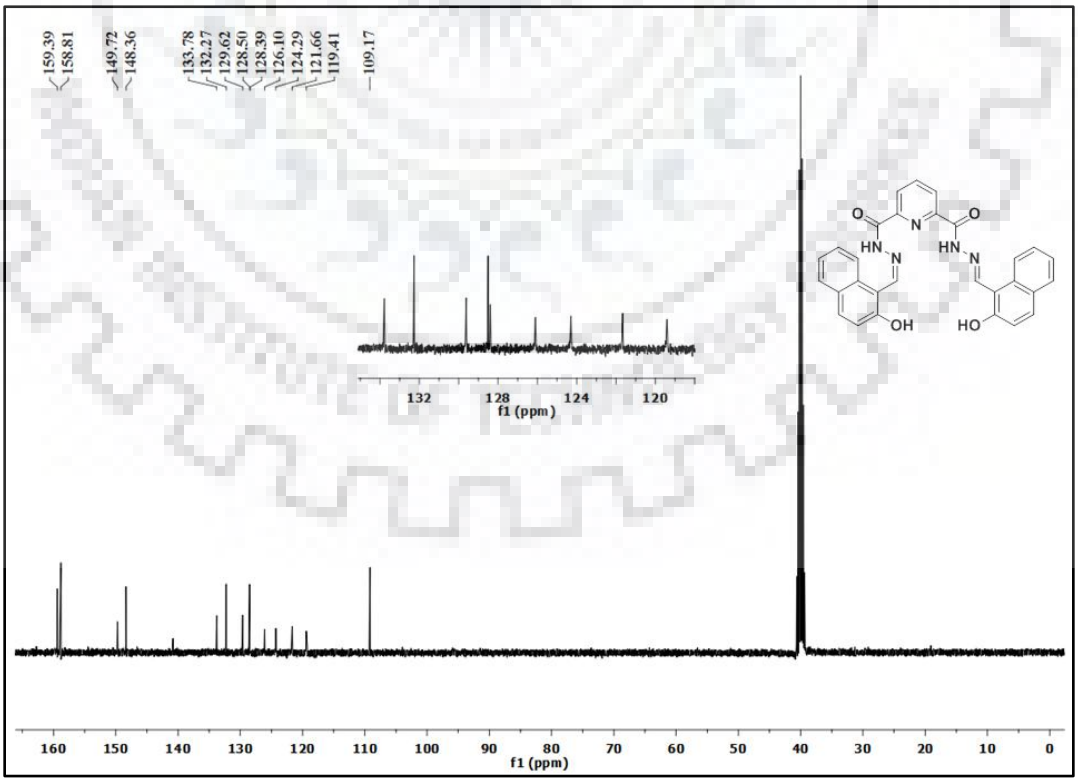

**Spectrum No. 23.** $^{1}$H NMR spectrum of ligand **L5.**

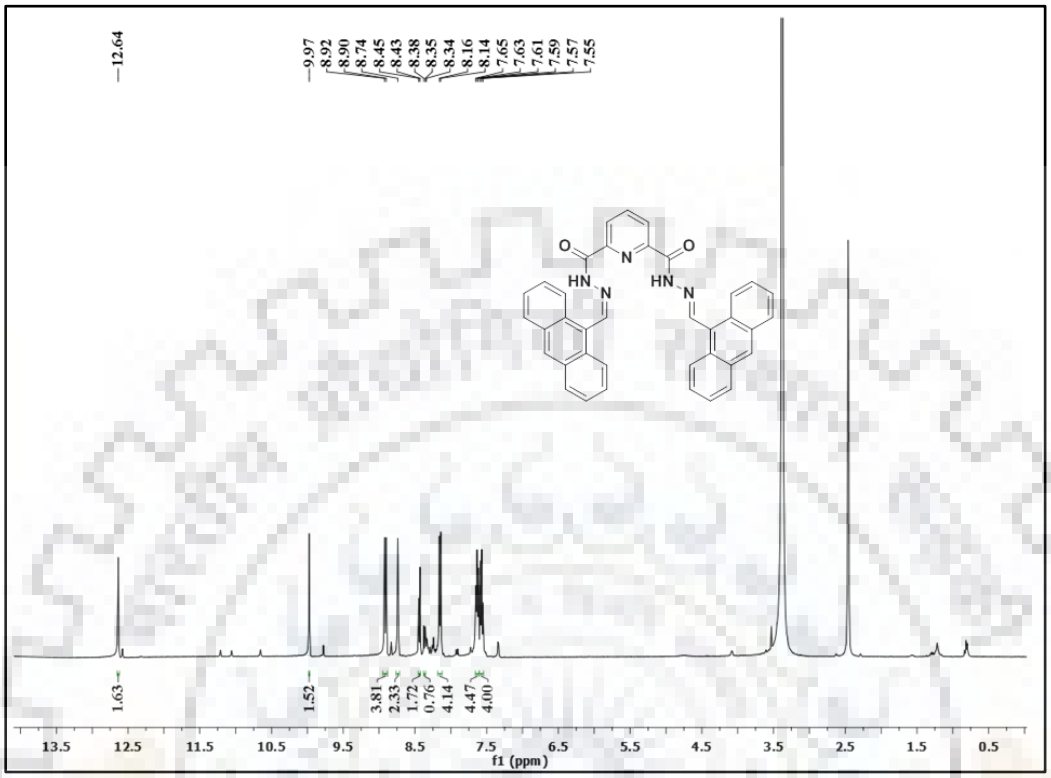


**Spectrum No. 24.** $^{13}$C NMR spectrum of ligand **L5.**

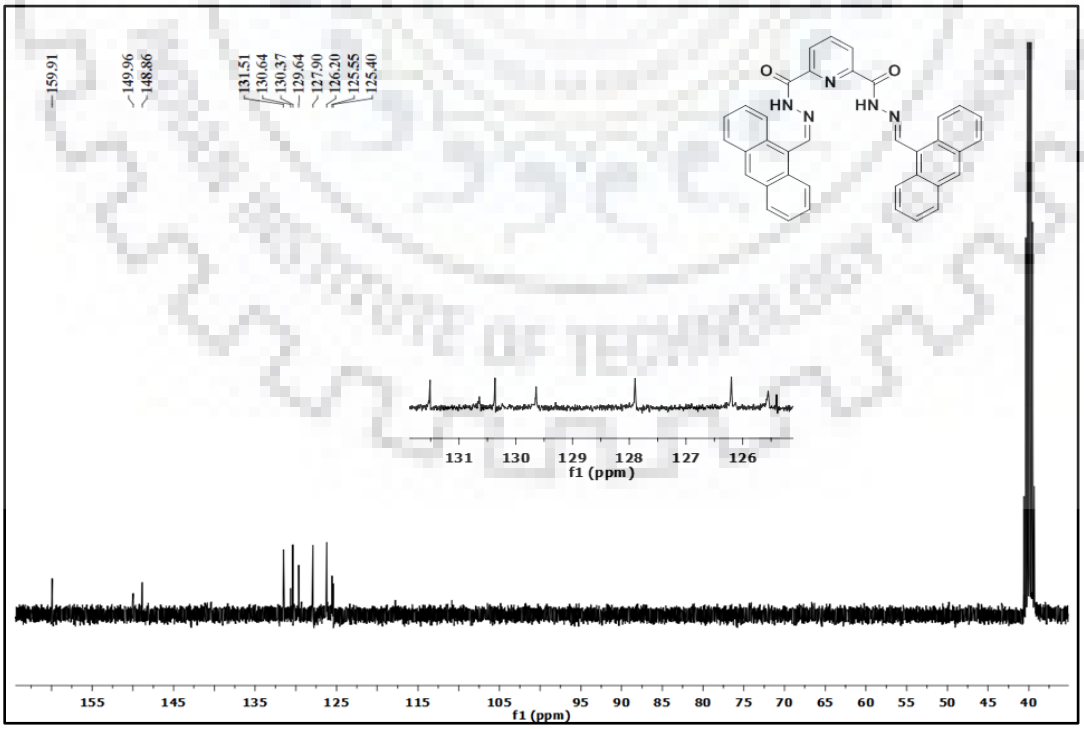

**Spectrum No. 25.** Mass Spectrum of ligand **L2.**

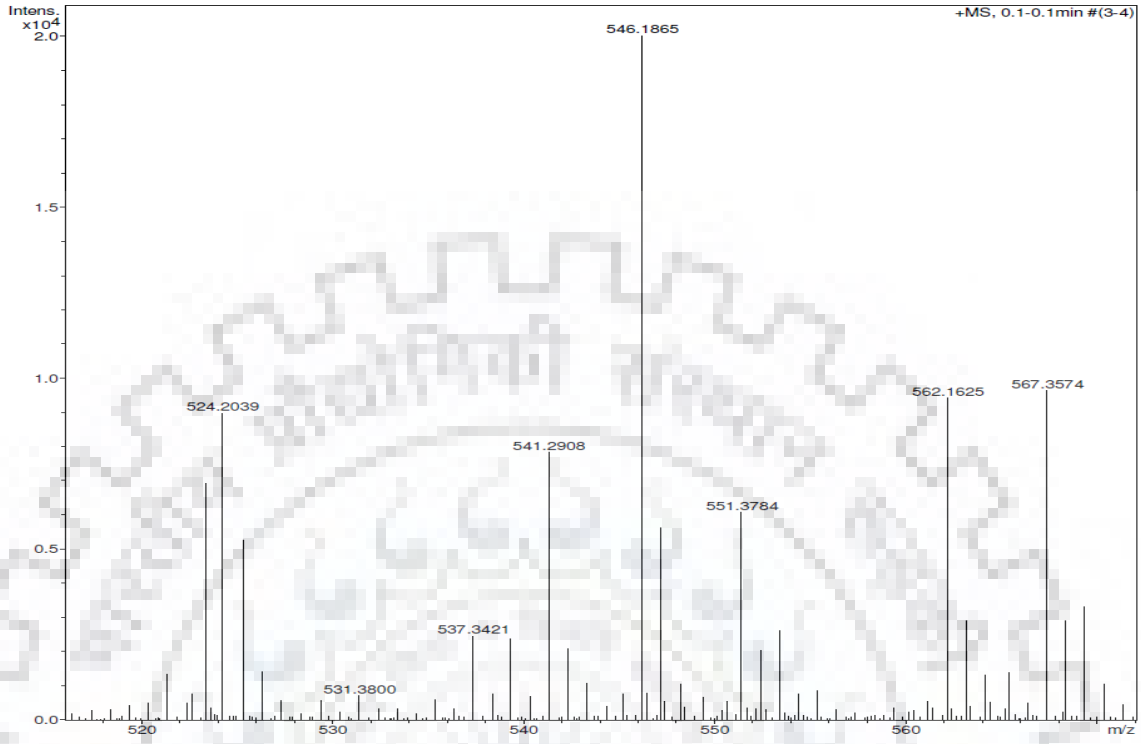


**Spectrum No. 26.** Mass Spectrum of ligand **L3.**

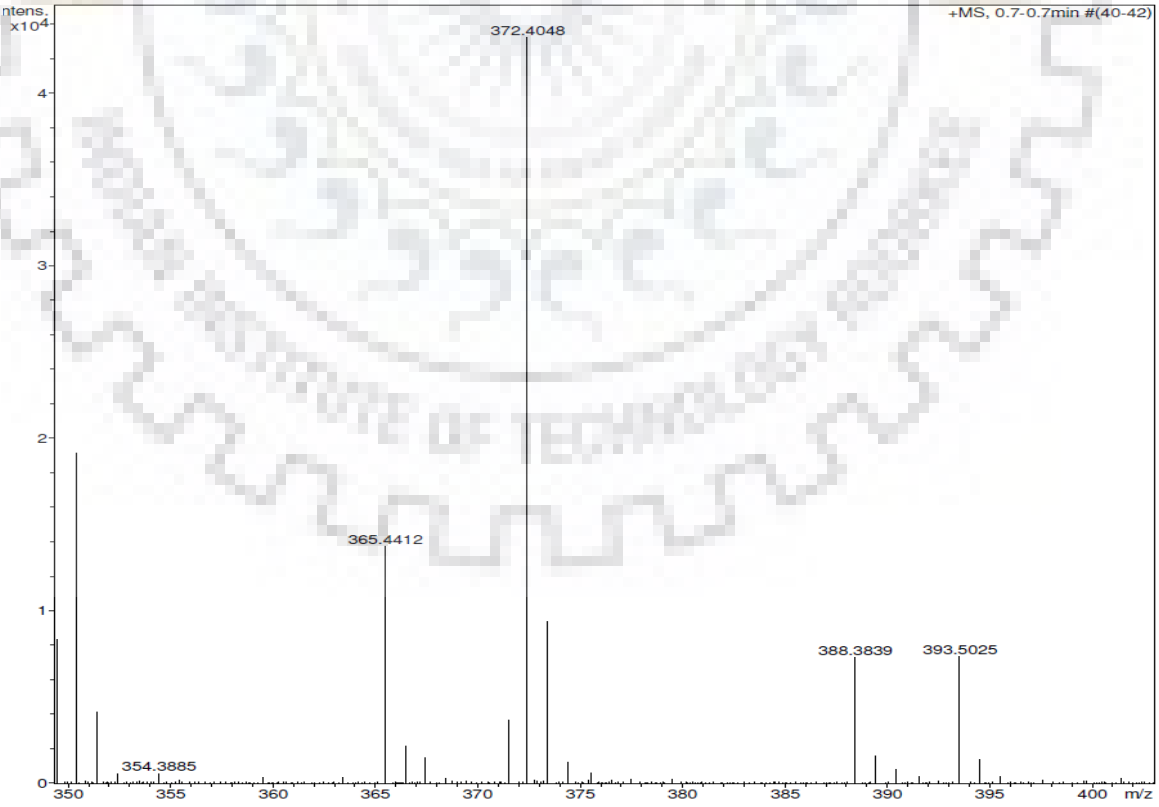

**Spectrum No. 27.** Mass Spectrum of ligand **L4.**

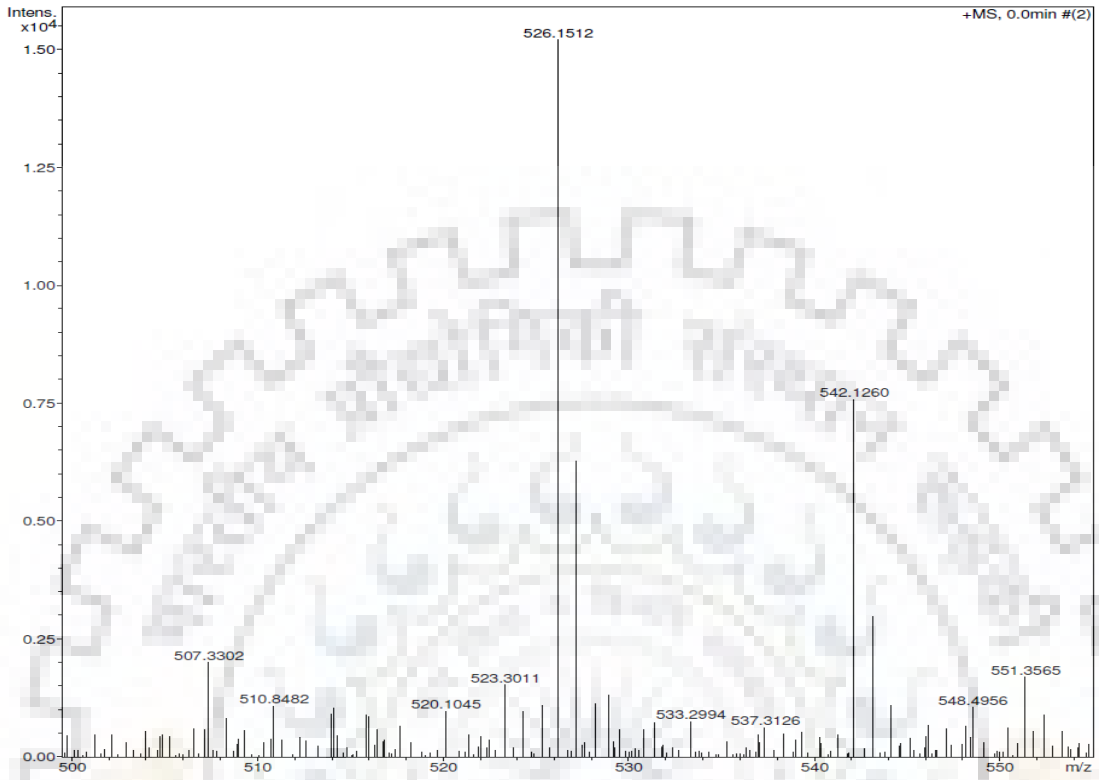


**Spectrum No. 28.** Mass Spectrum of ligand **L5.**

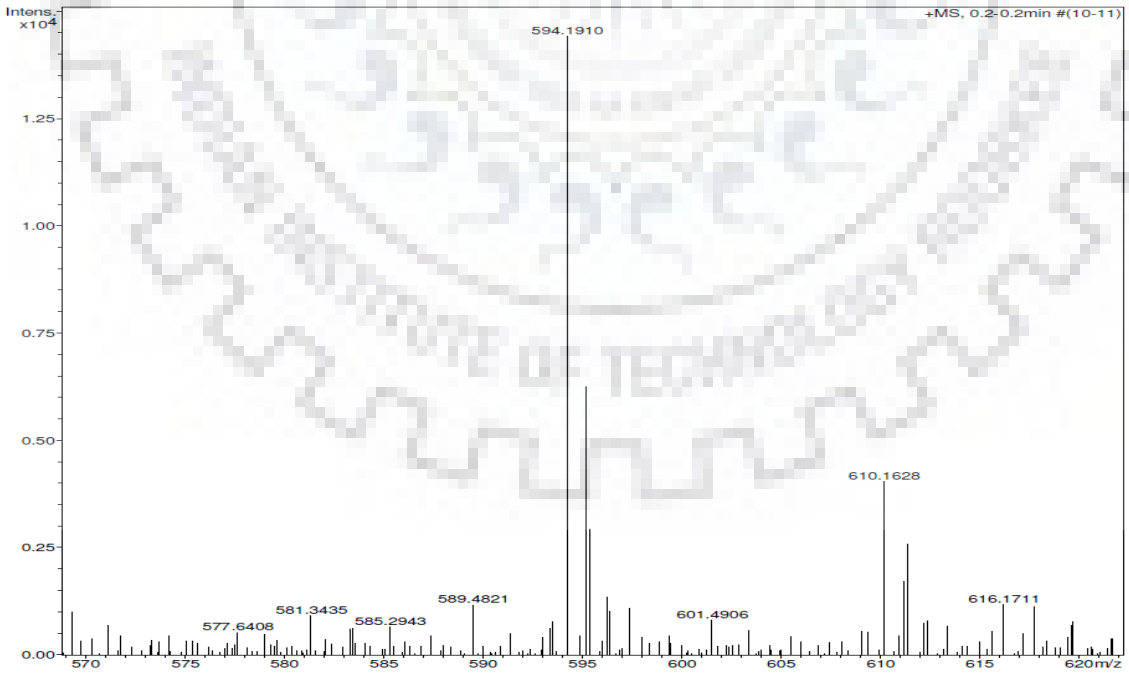

**Spectrum No. 29.** FT-IR of **L6**.

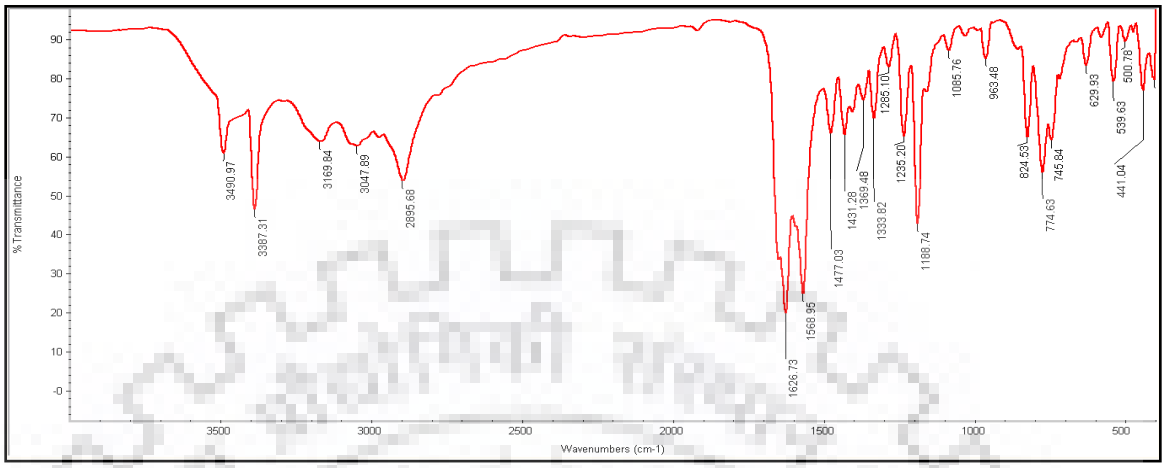


**Spectrum No. 30.** FT-IR of **L7**.

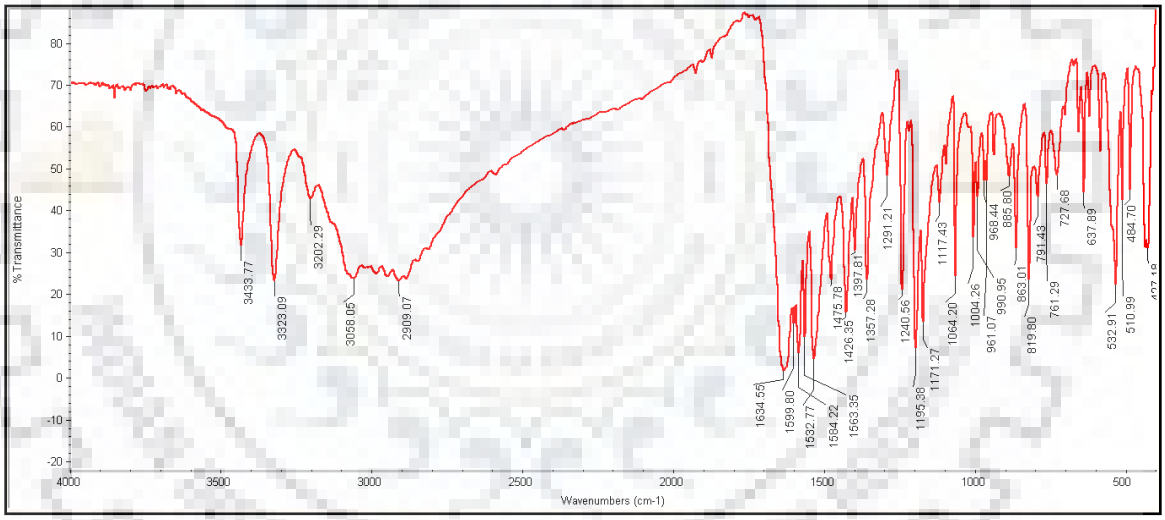

**Spectrum No. 31.** $^{1}$H NMR spectra of **L6** in DMSO-$d_6$.

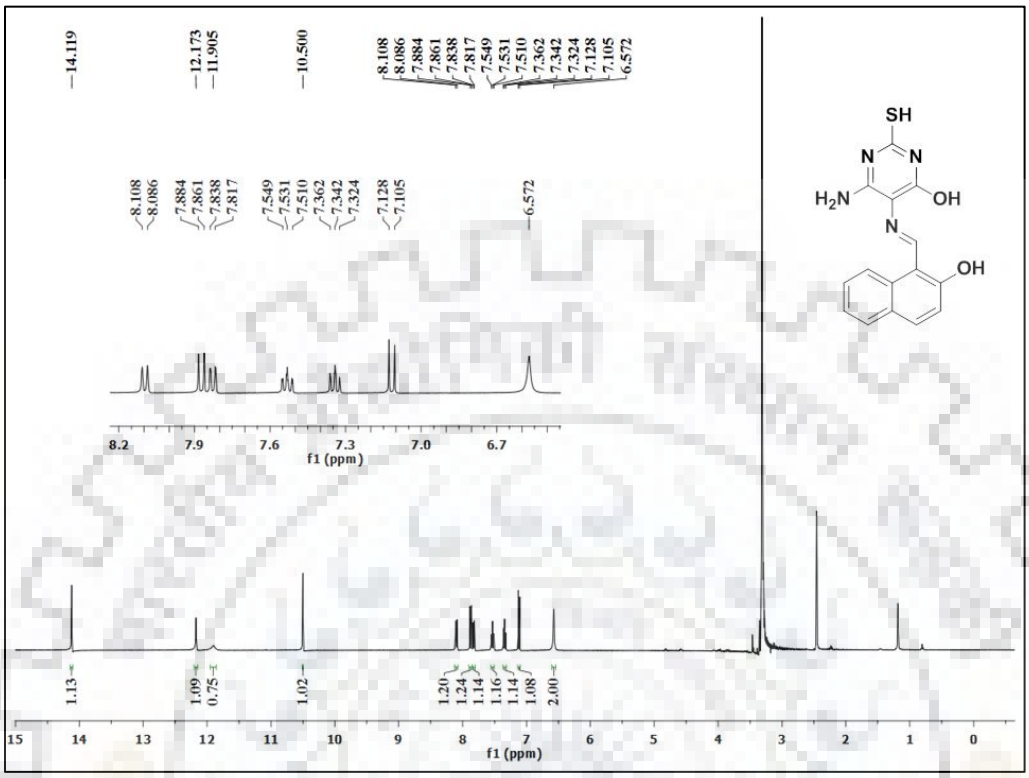


**Spectrum No. 32.** $^{1}$H NMR spectra of **L7** in DMSO-$d_6$.

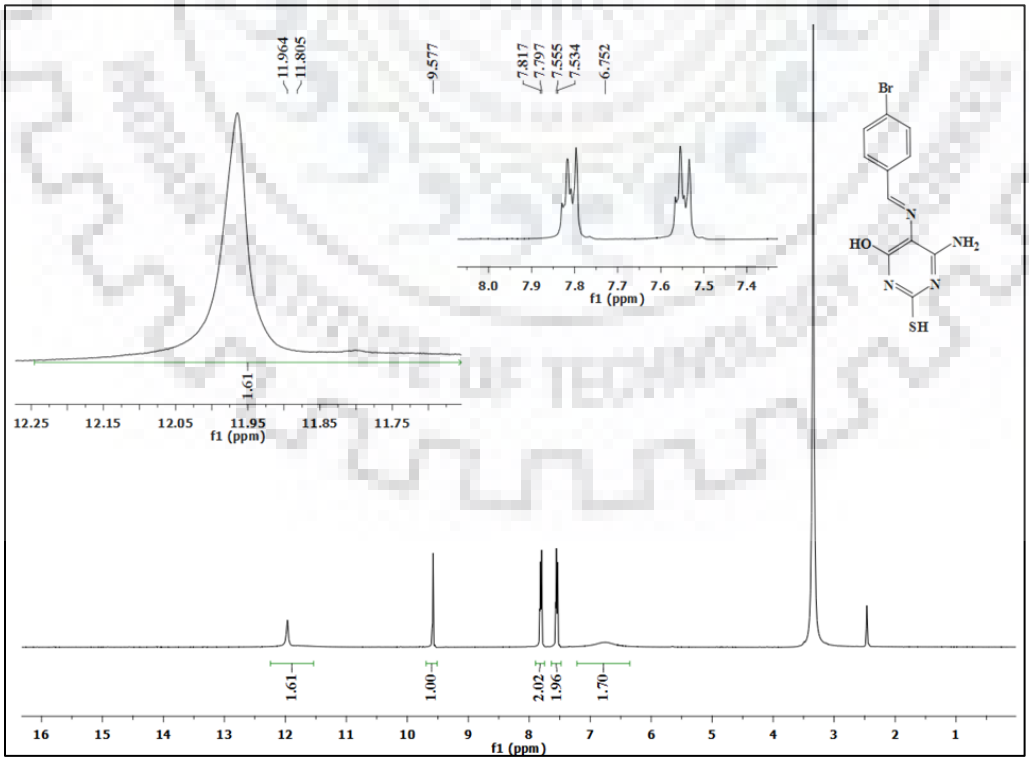

**Spectrum No. 33.** $^{13}$C NMR spectra of **L6** in DMSO-$d_6$.

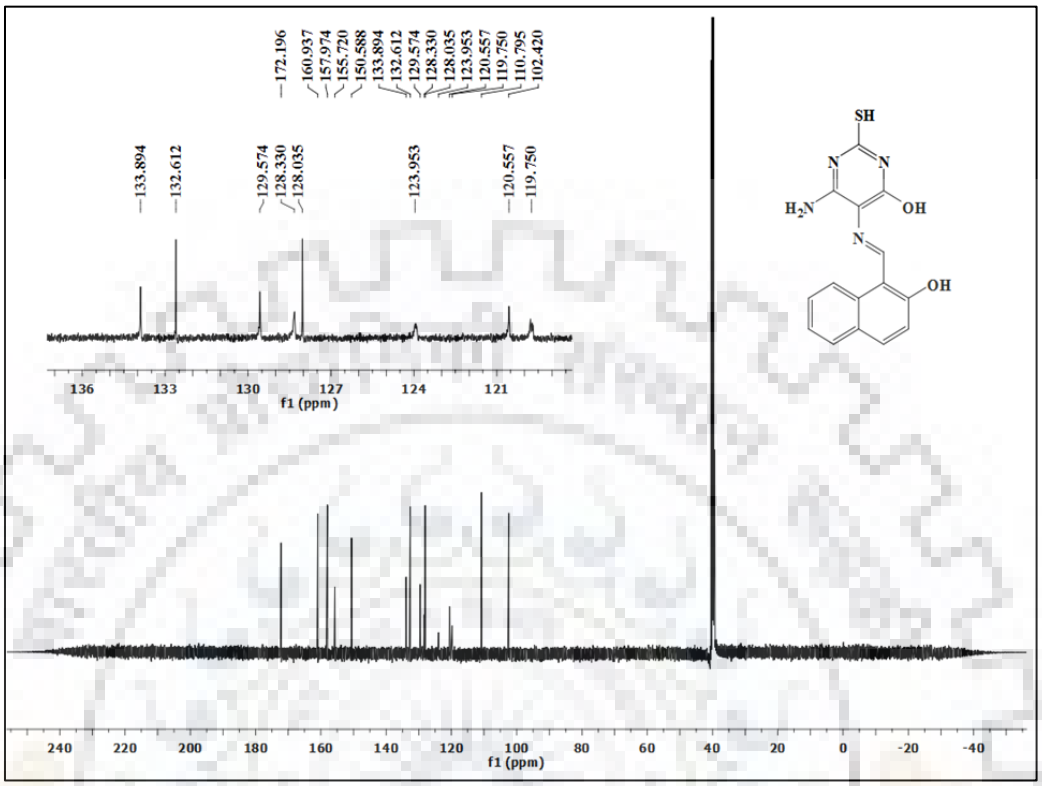


**Spectrum No. 34.** $^{13}$C NMR spectra of **L7** in DMSO-$d_6$.

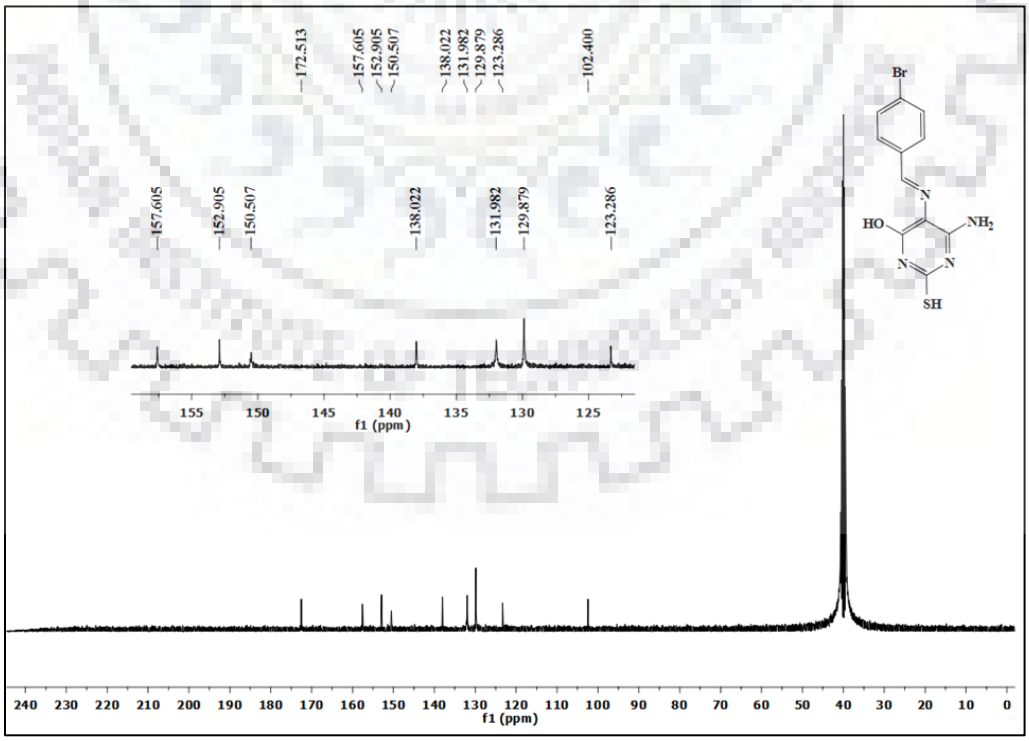

**Spectrum No. 35.** UV-vis spectra of **L6**.

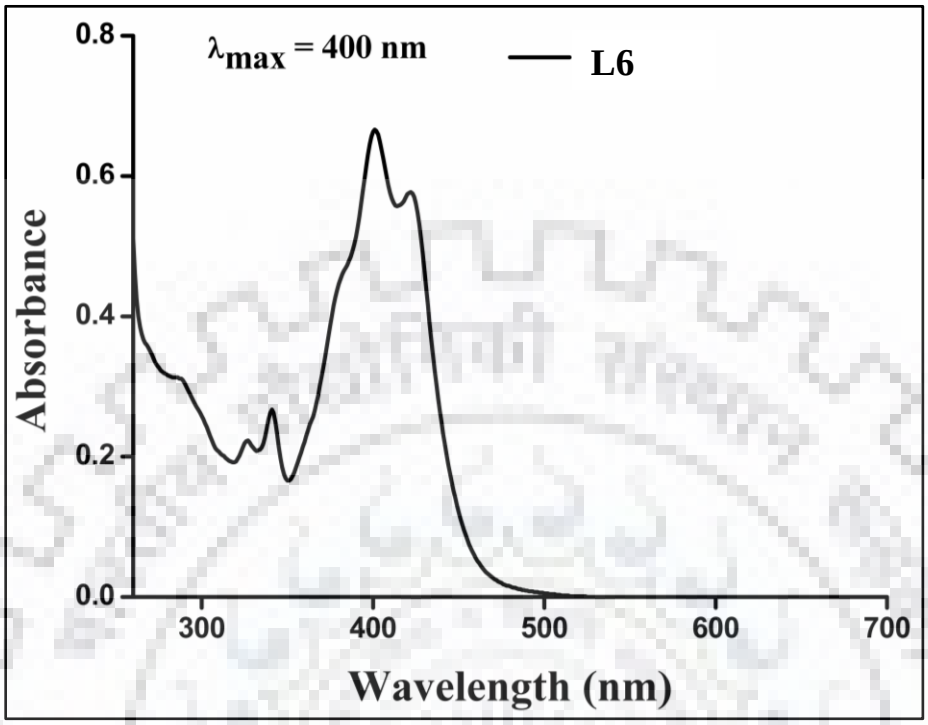


**Spectrum No. 36.** UV-vis spectra of **L7**.

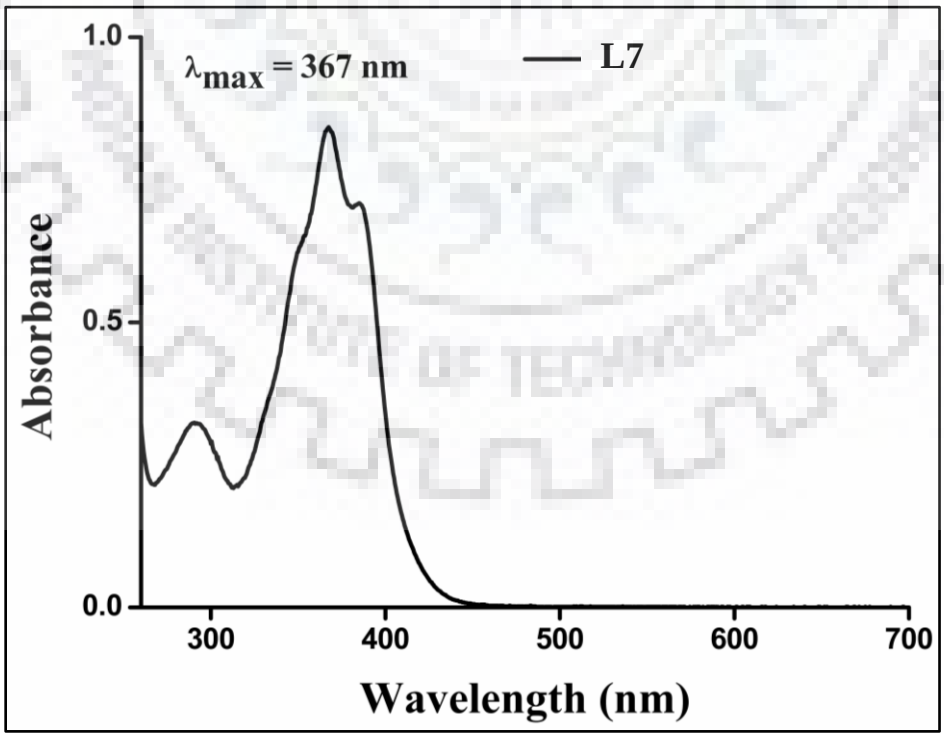

**Spectrum No. 37.** ESI-MS of **L6**.

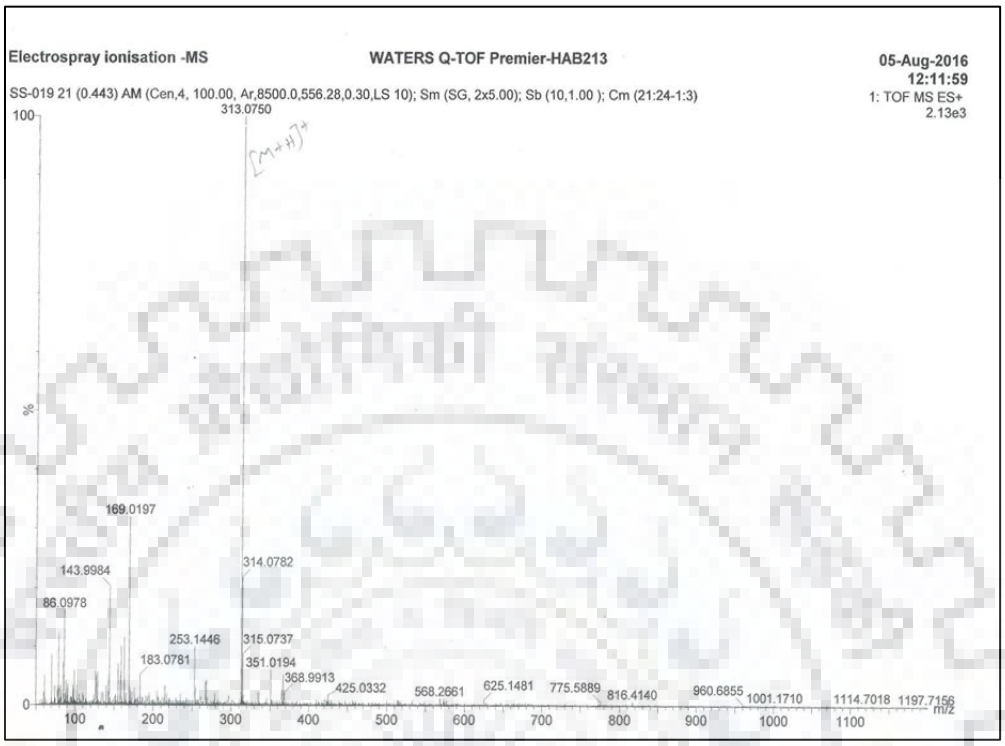


**Spectrum No. 38.** ESI-MS of **L7**.

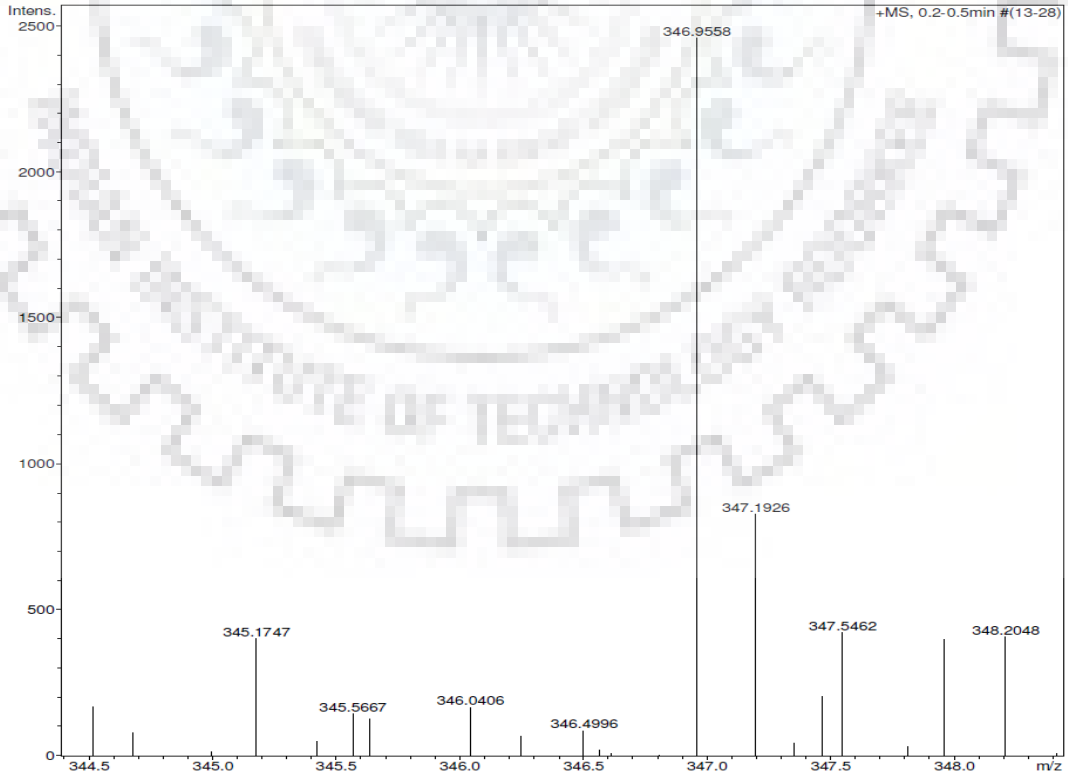

**Spectrum No. 39.** FT-IR spectra of **L8.**

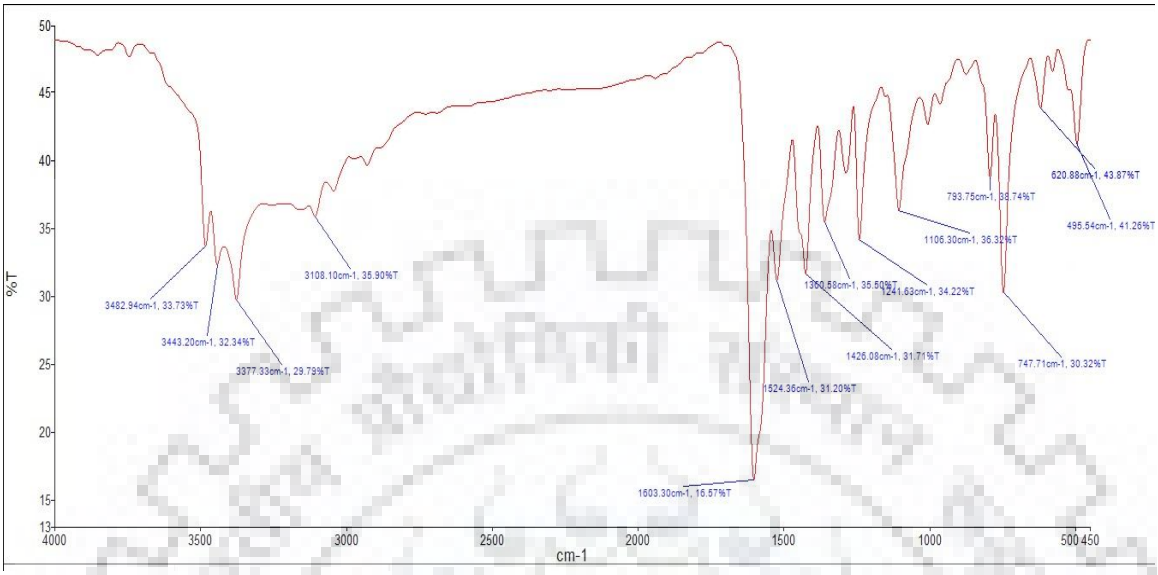


**Spectrum No. 40.** UV-Vis spectra of **L8**.

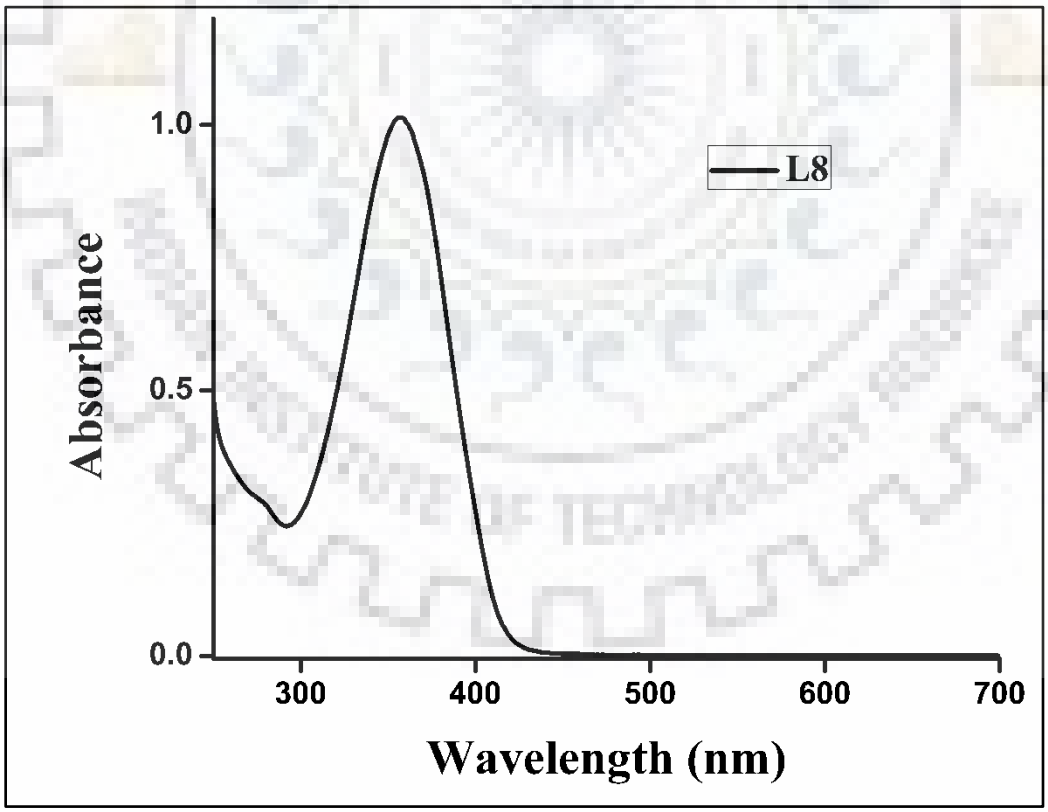

**Spectrum No. 41.** $^{1}$H NMR of **L8**.

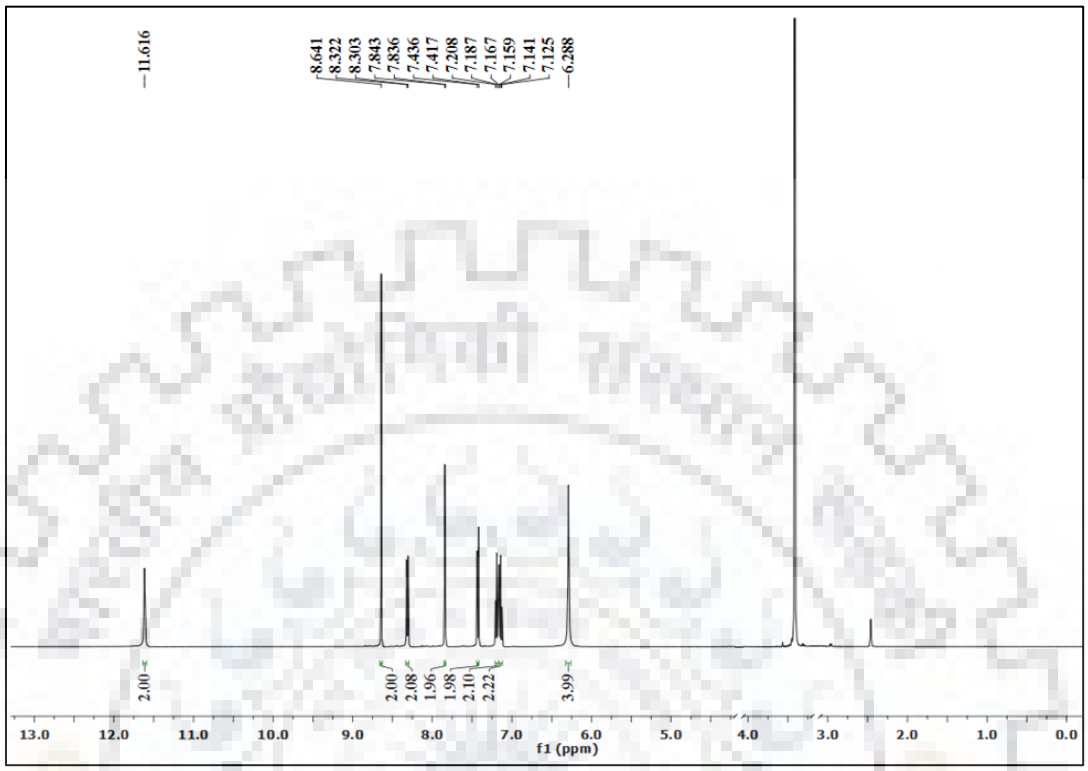


**Spectrum No. 42.** $^{13}$C NMR of **L8**.

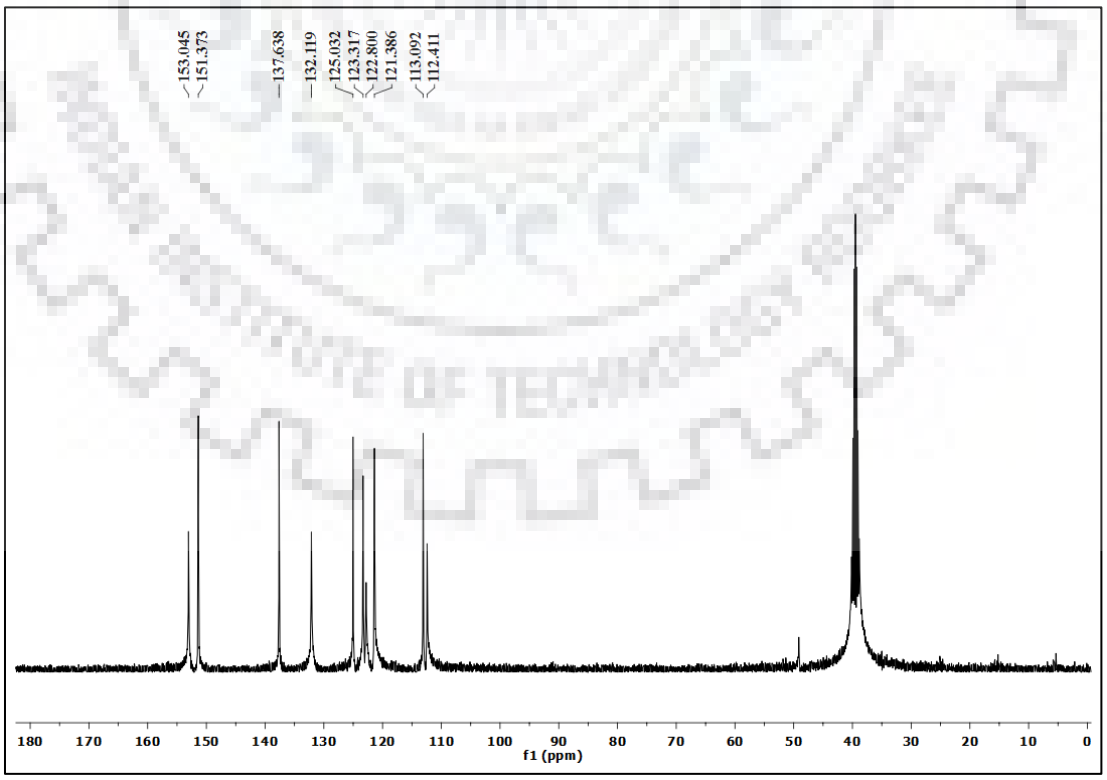

**Spectrum No. 43.** ESI-MS of **L8**.

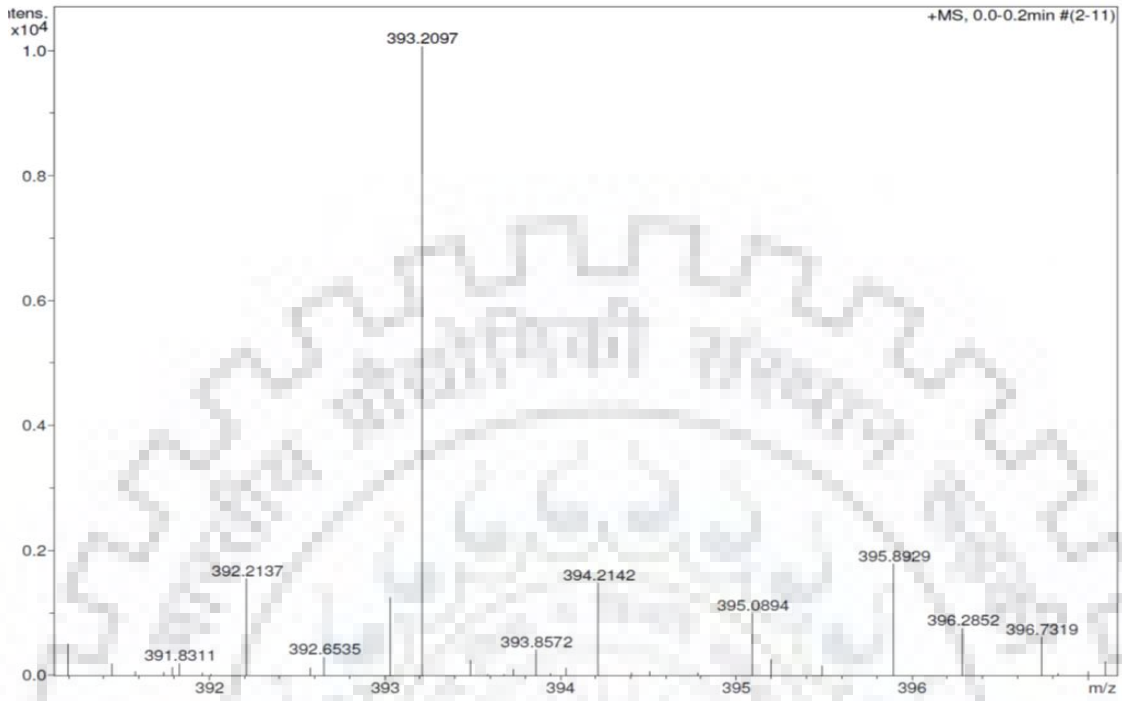


**Spectrum No. 44.** FT-IR spectra of **L9**.

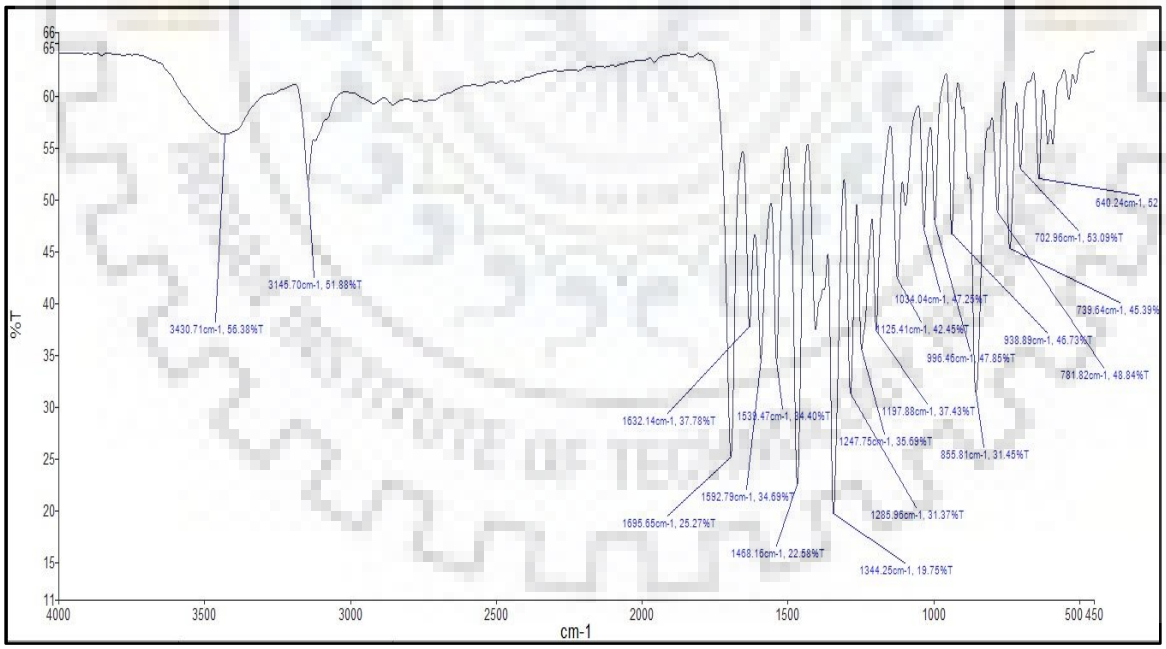

**Spectrum No. 45.** FT-IR spectra of **L10**.

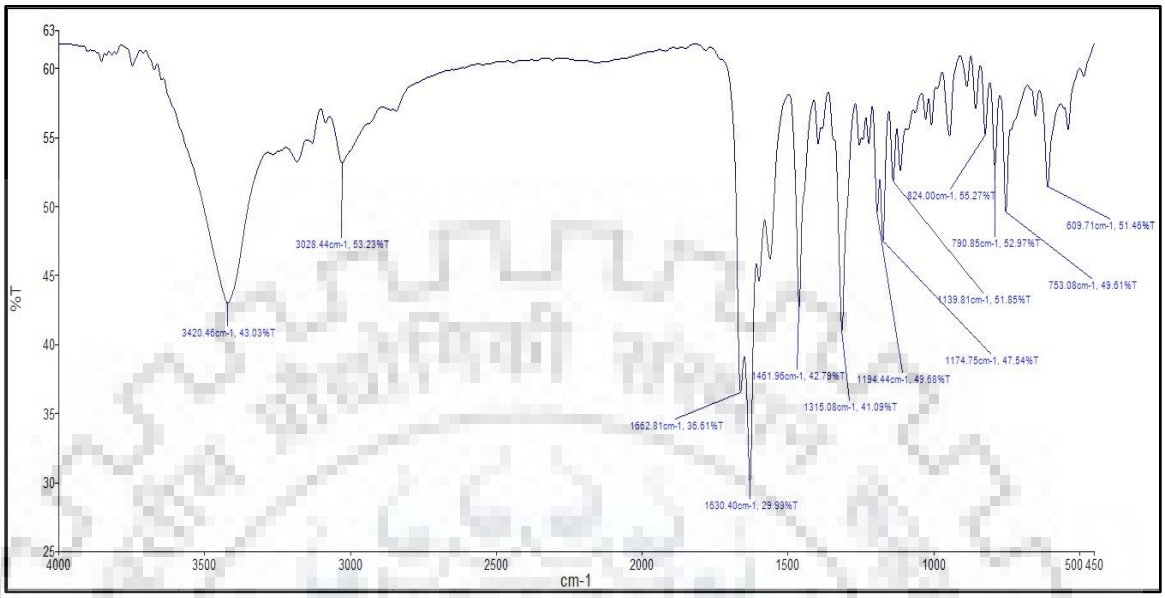


**Spectrum No. 46.** UV-Vis spectra of **L9**.

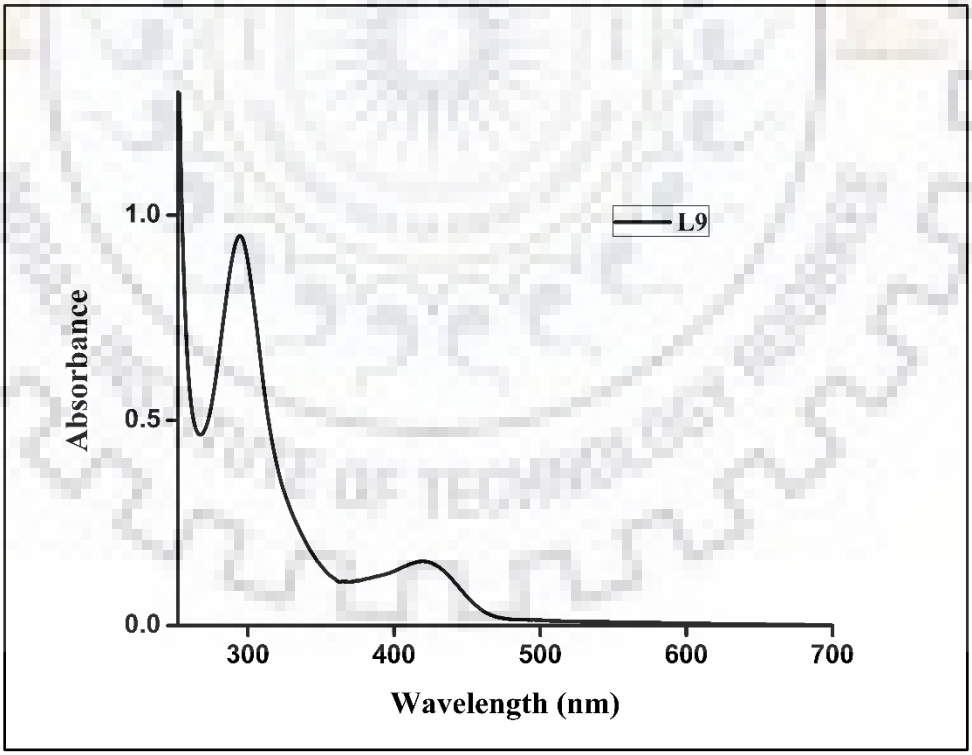

**Spectrum No. 47.** UV-Vis spectra of **L10.**

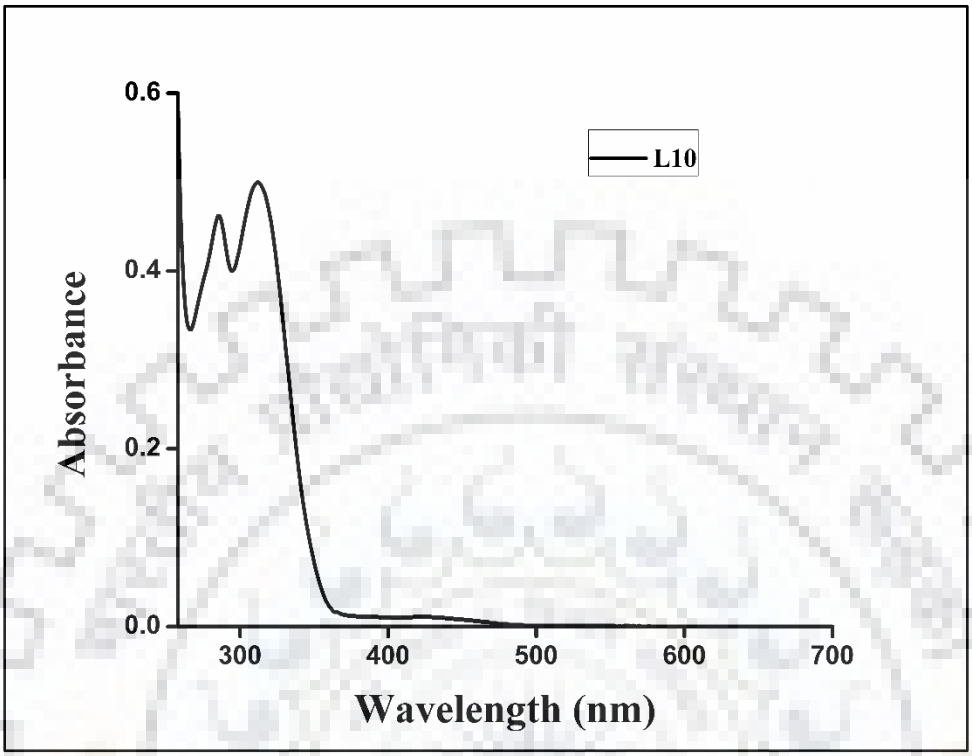


**Spectrum No. 48.** $^{1}$H-NMR spectra of **L9**.

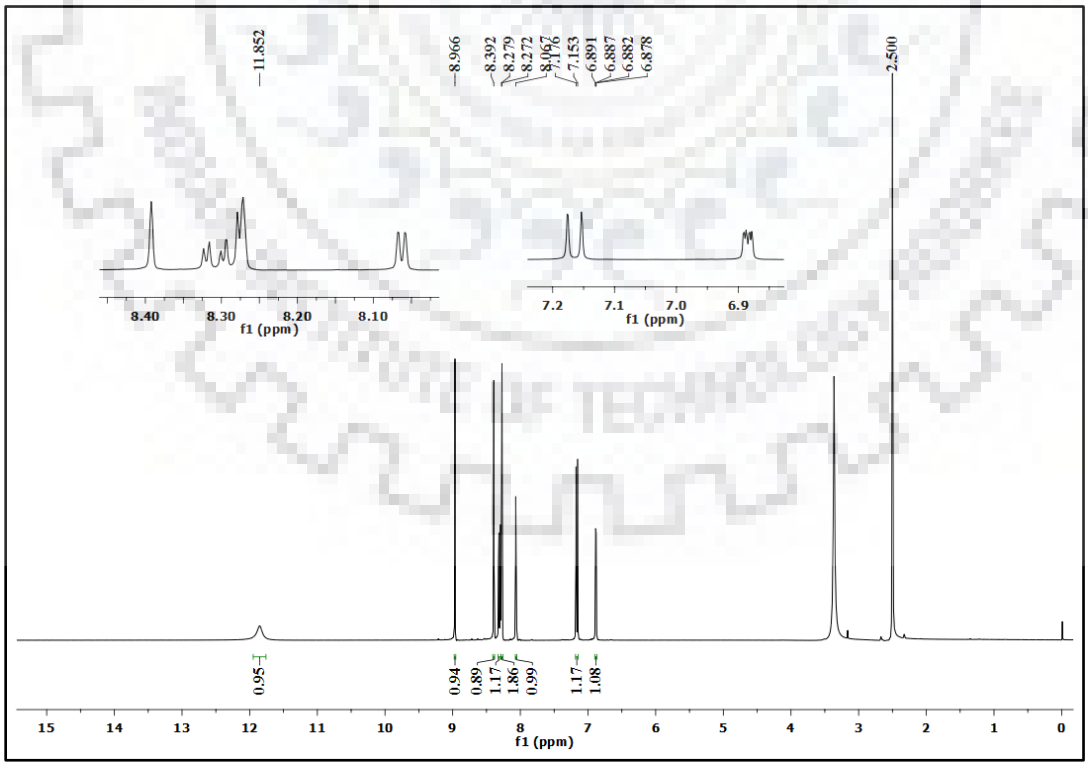

**Spectrum No. 49.** $^{13}$C-NMR spectra of **L9**.

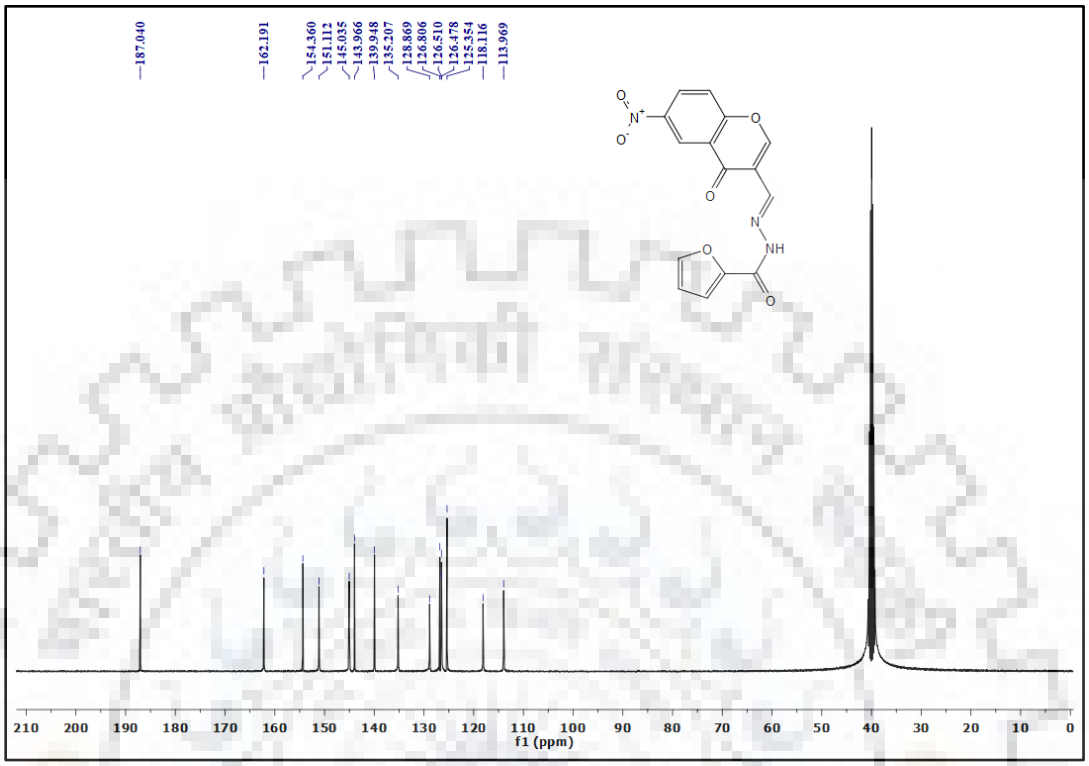


**Spectrum No. 50.** $^{1}$H-NMR spectra of **L10**.

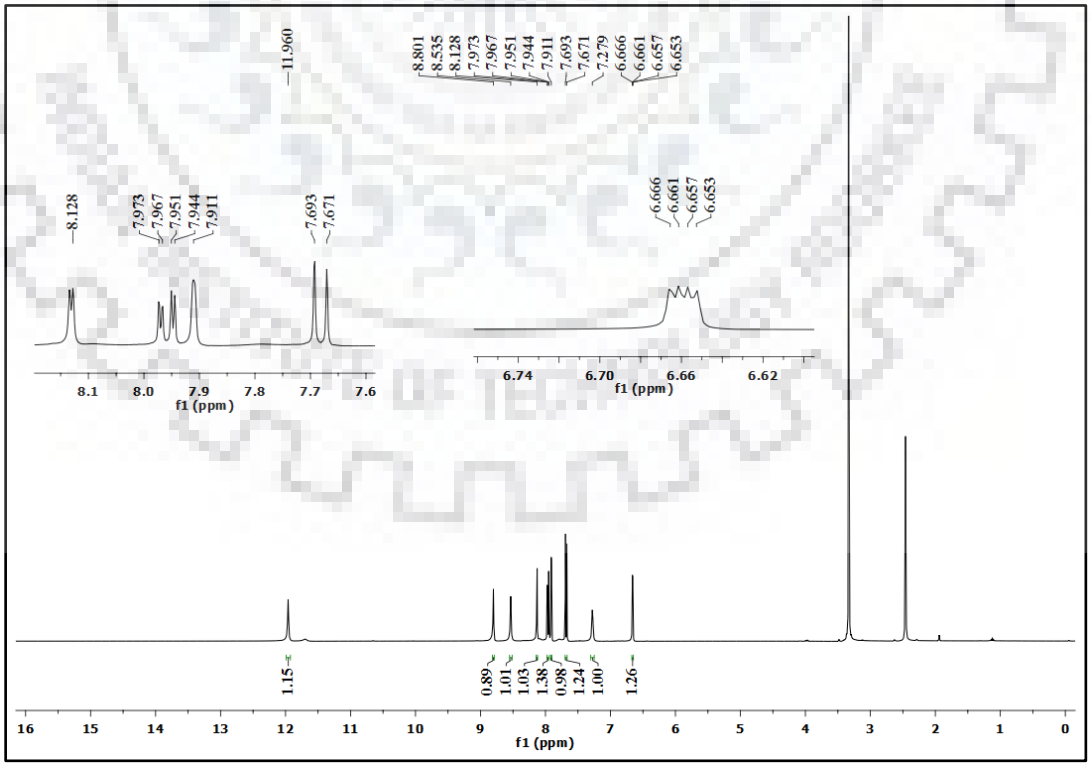

**Spectrum No. 51.** $^{13}$C-NMR spectra of **L10**.

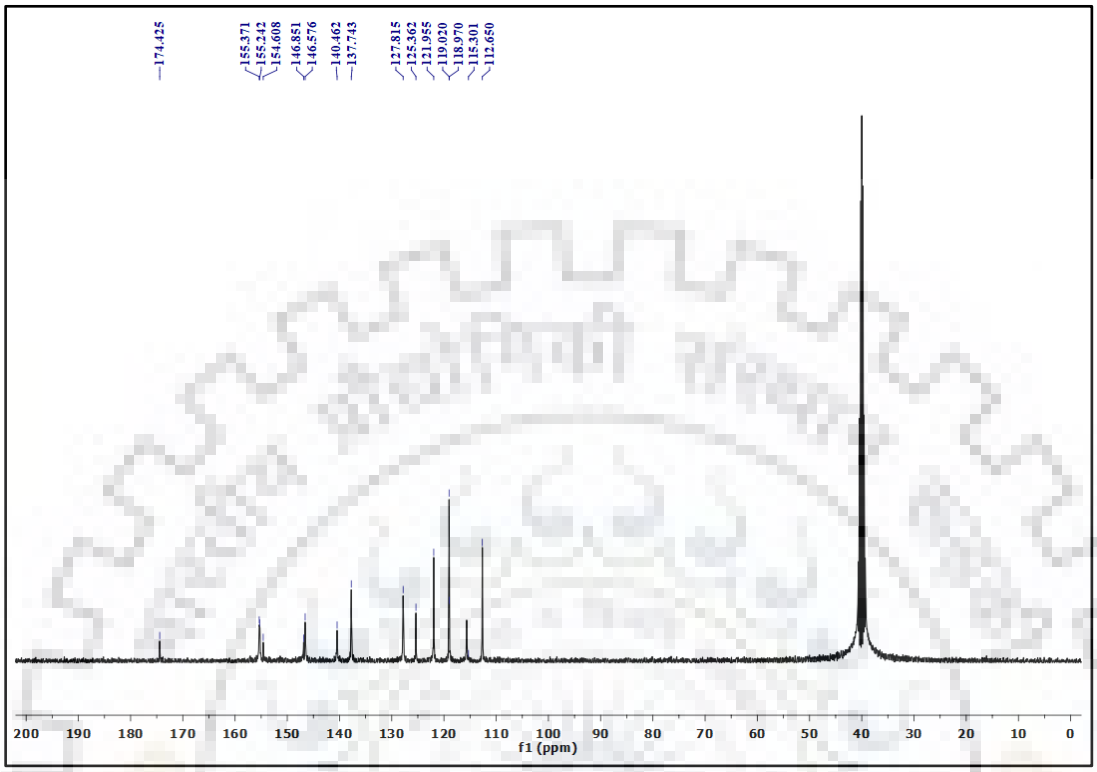


**Spectrum No. 52.** Mass spectrum of **L9**.

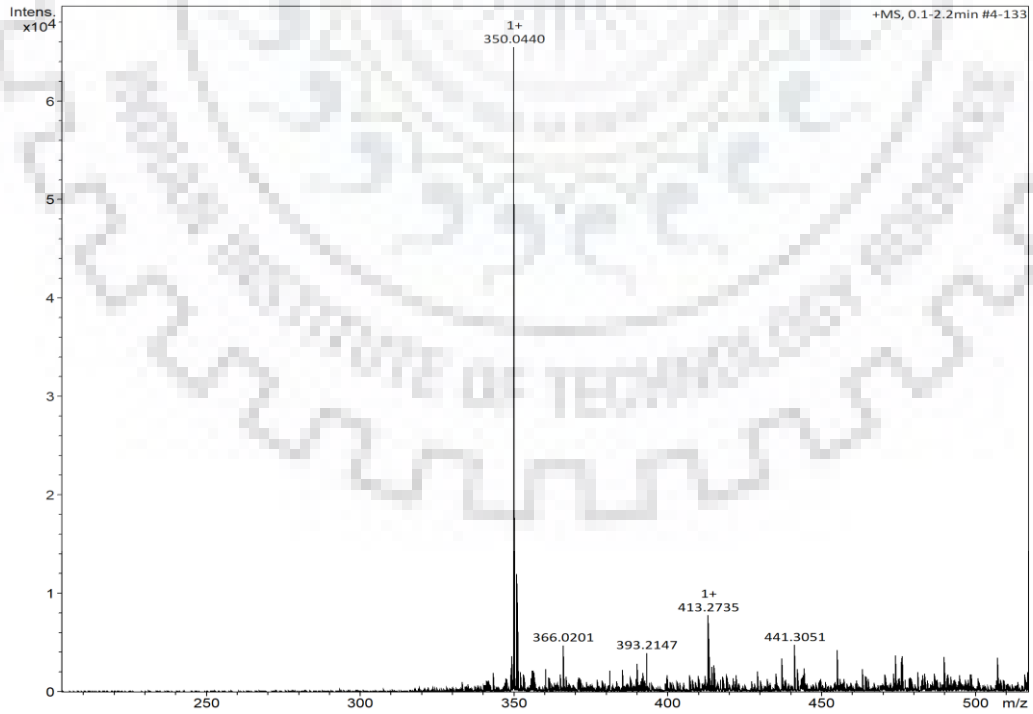

**Spectrum No. 53.** Mass spectrum of **L10**.

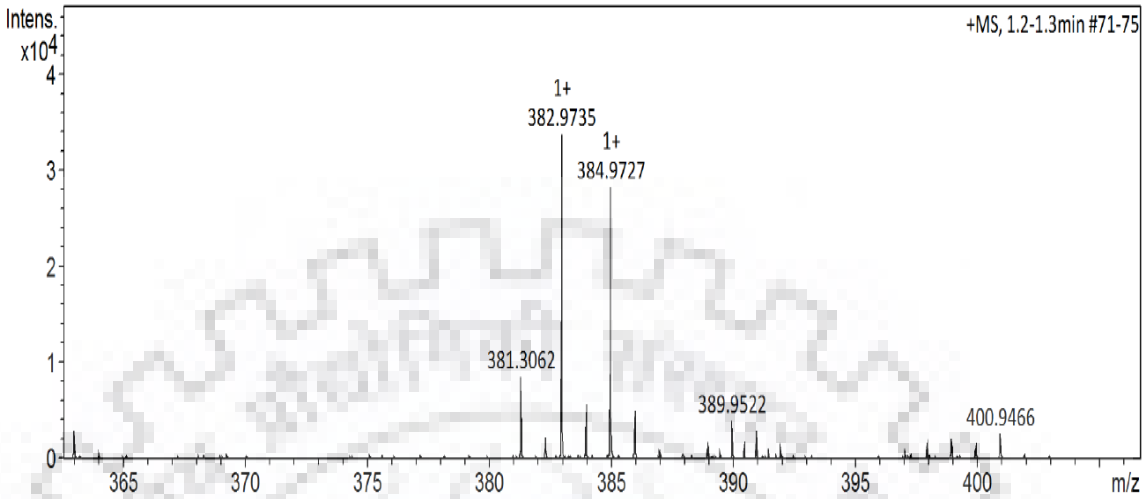

RSC Advances

PAPER

View Article Online
View Journal | View Issue



CrossMark click for updates

Cite this: *RSC Adv.*, 2016, **6**, 100136

# Dual anion colorimetric and fluorometric sensing of arsenite and cyanide ions†

Neetu Yadav and Ashok Kumar Singh*

Received 4th August 2016
Accepted 28th September 2016

DOI: 10.1039/c6ra19781g

www.rsc.org/advances

A naphthalene appended probe, 2-((2-hydroxynaphthalen-1-yl)methylene)hydrazine carbothioamide, was synthesized and found to recognize $AsO_2^-$ and $CN^-$ ions with turn-on emission fluorescence over different anions in a DMF : $H_2O$ (HEPES buffer, pH = 7.2) (9 : 1, v/v solution) medium. The probe was characterized using different techniques including NMR, IR, CHNS, UV-visible and ESI mass spectroscopy. This probe shows colorimetric change and an enhancement in the fluorescence emission with arsenite and cyanide ions among the other anions. The 1 : 1 and 1 : 2 stoichiometries of the probe with arsenite and cyanide ions, respectively, were calculated from the Job's plots based on the UV-visible spectra. The binding constant was established using the B–H (Benesi–Hildebrand) plots for both anions arsenite and cyanide as $3.1 \times 10^5$ and $1.9 \times 10^6$, respectively. The limit of detection (LOD) of arsenite and cyanide ions was 66 nM and 77 nM, respectively, using the emission spectra. The binding affinity of probe L with both anions was determined using NMR, DFT optimization, ESI-mass spectroscopy, electrochemical behavior and optical studies. The probe is the first chemical sensor that detects both major toxic anions with significantly high detection limits.

## 1. Introduction

Anions demonstrate their necessity in a broad range of chemical and biological processes. Various efforts have been devoted to generate numerous receptors for anionic species over the last two decades.[1] Among all the anions, it is well known that arsenic (in the form of anions) and cyanide ions are extremely toxic and lethal to living organisms. Arsenic is the 20$^{th}$ most abundant element in the earth's crust. It mainly exists in the four oxidation states, As(v), As(iii), As(0) and As(−3), in the environment.[2] Inorganic arsenic, *viz.* arsenite As(iii) and arsenate As(v) is more toxic than organic arsenic, *viz.* monomethylarsonic acid and dimethylarsonic acid.[3] Arsenite [As(iii)] is more toxic than arsenate [As(v)] due to its binding with the sulfhydryl unit of proteins, which can intervene with the reactions of other enzymes and proteins.[4] The binding of trivalent arsenic with specific proteins can convert the conformation and functionality of the protein as well as hamper their reaction with other proteins. As(v) can also interrupt the conversion of ATP to ADP *via* the permanent replacement of phosphate groups due to its resemblance to phosphite ions.[5] The main source of arsenic exposure in the environment is from ground water or drinking water.[6,7] The chronic toxicity of arsenic has adverse effects on human health, such as skin cancer, skin lesions, neurotoxicity, cardiovascular diseases and diabetes.[8]

Similarly, cyanide anions are also detrimental to biological systems and the environment. Its acute poisoning can damage the body's central respiratory system because it can easily bind with heme-proteins to block cytochrome c oxidase, which hinders the electron transfer chain in the mitochondria.[9] It is released in the environment by ammonia manufacturing, electroplating, steel production and extraction of gold.[10] Inhalation of toxic cyanide can occur from absorption by the lungs and exposure *via* the skin, polluted drinking water and contaminated food.[11] As per as the guidelines of the World Health Organization (WHO) and U.S. Environment Protection Agency (USEPA), the permissible limits of arsenic and cyanide in drinking water are 0.01 ppm (or 10 ppb) and 0.2 ppm, respectively.[12] There have been many methods developed for the detection of arsenite and cyanide ions. Electrochemical analysis and ion chromatography are the traditional methods, which require time consuming procedures and the use of sophisticated instrumental techniques,[13] whereas chemical sensors are another approach, which are simple, affordable and expeditious in real time monitoring. The sensing process frequently uses absorption and emission spectroscopy, which precisely monitor and sometimes detect using the naked eye.[14] Chemical sensors for arsenite anions are rarely available with fluorescence intensity enhancement. Cyanide ions are analysed by their Lewis basicity, nucleophilicity[15] and quality of making hydrogen bonds in a solution.[16] There are numerous mechanisms, including internal charge transfer,[17] single electron transfer,[18] fluorescence resonance energy transfer[19] and plated electrode,[20–22] which support the fluorescence behaviour for anions.

*Department of Chemistry, Indian Institute of Technology-Roorkee, Roorkee-247667, India. E-mail: akscyfcy@iitr.ernet.in*

† Electronic supplementary information (ESI) available. See DOI: 10.1039/c6ra19781g

NJC

PAPER

View Article Online
View Journal | View Issue





Cite this: *New J. Chem.*, 2018, **42**, 6023

# Dicarbohydrazide based chemosensors for copper and cyanide ions *via* a displacement approach†

Neetu Yadav and Ashok Kumar Singh *

Received 14th January 2018,
Accepted 7th March 2018

DOI: 10.1039/c8nj00230d

rsc.li/njc

Ligands attached to pyridine dicarbohydrazide were synthesized and characterized by NMR, FT-IR, elemental analysis, UV-visible spectroscopy, mass spectrophotometry, emission spectra and single crystal X-ray diffraction. These ligands were found to recognize copper ions over other metal ions and cyanide ions by a copper complex performing an *in situ* experiment with turn on–off–on behaviour over different anions in a $CH_3OH : H_2O$ (9 : 1, v/v solution) medium. These ligands displayed a red shift in their absorption spectra and quenching in their emission spectra when exposed to copper ions *via* a PET mechanism and a further copper complex was applied for cyanide detection among the other anions. The 1 : 2, 1 : 3, 1 : 2 and 1 : 2 stoichiometric ratios of the ligands ($L_1$–$L_4$, respectively) with copper ions were calculated from a Job plot based on the UV-visible spectra. The S–V plot represents the linearity of the ligands with copper ions. The limits of detection (LOD) of copper ions along with the ligands ($L_1$–$L_4$) were calculated to be 0.12, 0.10, 0.097 and 0.098 μM using emission spectra, respectively. The binding affinities of the ligands with copper ions were determined by various characterization techniques such as FTIR, mass spectrophotometry and electrochemical and optical studies. Furthermore, an *in situ* experiment was performed for cyanide detection *via* a metal displacement approach. $L_1$ and $L_4$ with $Cu^{2+}$ ions showed an affinity towards cyanide ions, with detection limits of 0.31 and 0.53 μM.

## 1. Introduction

Transition metals, such as iron, zinc, magnesium and copper, play an important role in living systems. Of all transition metals, copper is the third most essential trace metal and performs a foremost role in the human nervous system as the cofactor of many metalloenzymes.[1,2] It is essential for a wide range of physiological processes, such as in bone growth, haemoglobin biosynthesis, dopamine production, nerve function regulation, the functional and structural augmentation of proteins and enzymatic functions. Copper also generates cellular energy, induces signal transduction and diminishes molecular oxygen.[3] However, the presence of unregulated copper and disrupted copper ion homeostasis[4] can lead to numerous neurogenerative diseases such as Menkes syndrome, Alzheimer's disease, Wilson's syndrome,[5] Amyotrophic lateral sclerosis, Parkinson's disease and Prion diseases.[6,7] Menkes syndrome[8] is due to copper deficiency, while Wilson's syndrome is due to copper toxicosis, and both are human genetic disorders.[9–12] Cyanide ions are more toxic compared to other anions, although cyanide is a very vital reagent for many industrial processes in different areas, such as mining, synthetic fibre production and electroplating.[13–16] The "excessive" utilization of cyanide[17] in these factories and its fundamental transportation, expands the likelihood of human exposure. Its acute toxicity destroys the central respiratory system of the body and blocks the electron transfer chain in mitochondria.[18,19] The extensive use of copper within daily life is the prime reason for copper pollution in the environment, and although copper is an essential metal ion, it is harmful for living systems when found in concentrations higher than required. This is similar with cyanide ions, as its frequent use in industries is the reason that it makes environments polluted. According to the World Health Organization (WHO), the permissible limits of copper ions and cyanide ions in drinking water are 2 ppm (30 μM) and 0.2 ppm,[20,21] respectively. In blood, the maximum concentration of copper ions should not be greater than 100–150 μg $dL^{-1}$.[22,23] The Environmental Protection Agency has advised that the safe maximum limit of copper in drinking water should be 1.3 ppm (*ca.* 20 μM).[24]

There are many sensors which can sense copper ions, using different mechanisms. Aside from this, some multidentate chemosensors also have the ability to sense other specific metal ions. In this study, multidentate ligands have been synthesized and applied as chemosensors. The presented work shows that the ligands, which have a large number of donor atoms and a

*Department of Chemistry, Indian Institute of Technology Roorkee, Uttarakhand, India. E-mail: akscyfcy@iitr.ernet.in*

† Electronic supplementary information (ESI) available. CCDC 1577825 and 1552443. For ESI and crystallographic data in CIF or other electronic format see DOI: 10.1039/c8nj00230d

Materials Science & Engineering C 90 (2018) 468–475

Contents lists available at ScienceDirect

Materials Science & Engineering C

journal homepage: www.elsevier.com/locate/msec

# A turn-on ESIPT based fluorescent sensor for detection of aluminum ion with bacterial cell imaging and logic gate applications

Neetu Yadav, Ashok Kumar Singh*

*Department of Chemistry, Indian Institute of Technology, Roorkee 247667, India*

ARTICLE INFO

*Keywords:*
Aluminum sensor
OFF-ON type
Fluorometric sensor
Logic gate
Cell imaging

ABSTRACT

6-amino-5-(((2-hydroxynaphthalen-1-yl)methylene)amino)-2-mercaptopyrimidin-4-ol (L1) and 6-amino-5-((4-bromobenzylidene)amino)-2-mercaptopyrimidin-4-ol (L2) have been designed and characterized by various techniques such as UV–Vis, fluorescence, FT-IR, mass spectrometry and NMR spectroscopy. L1 was successfully applied for selective recognition of aluminum ion and showed "OFF-ON type" mode in the presence of $Al^{3+}$ ion. The sensor was recommended for the selective detection of $Al^{3+}$ with 1:1 stoichiometry by Job's plot in ACN medium. The high sensitivity of host L1 supports the high detection limit, 99 nM with good association constant. It was also used for bacterial cell imaging (E.coli DHα) and logic gate applications which was manifested the green and red fluorescent images with $Al^{3+}$ ion and represents INHIBIT logic gate in switching behavior.

## 1. Introduction

Aluminum is the 3rd generous element in the earth's crust. Acid rain is one of the main sources of leaching of free aluminum ion in the environment and surface water. It's uses have been increased drastically in day-to-day activities from last few years *i.e.* cooking utensils, aluminum foil which raises the amount of aluminum metal ion in daily food and drinking water [1,2] as well as pervasive use in diverse field like automotive and aeronautic transport, food additive, space industries, construction, packaging and aluminum-based pharmaceuticals which creates adverse effect on the environment. Its toxicity causes many deceases such as Alzheimer's disease [3,4], Amyotrophic lateral sclerosis, Parkinson's disease *i.e.* damages the human nervous system as well as it also deadly hindered the plants growth [5,6] *etc.* According to FAO/WHO the tolerable limit of aluminum ion is 7.0 mg/Kg body weight in a week which was suggested based on short term toxicity [7,8]. Therefore, to prevent the direct impact on the human being and biosphere by $Al^{3+}$, it is needed to control the concentration levels of $Al^{3+}$ in the environment. Due to poor coordination ability and insufficient spectroscopic characteristics, it is difficult to detect the aluminum ion concentration in the environment and surface water. Therefore, it is required to promote $Al^{3+}$ sensors, which possess easy synthetic route, and sensitive, selective mechanisms.

Some tedious, time consuming and sophisticated techniques such as graphite furnace atomic absorption spectroscopy and inductively coupled plasma atomic emission spectroscopy are used in the detection of aluminum ion. Due to the drawbacks of these techniques, in recent years, fluorescent sensing has great attraction by virtue of its high efficiency to sense numerous biological and chemical species. Therefore, many fluorescent sensors have been synthesized and used them in the detection of different metal ions with different mechanism [9–17]. ESIPT mechanism (excited state intramolecular proton transfer) has unique properties in practical application because of its attractive photophysical properties such as large Stokes shift that avoided the self-absorption of molecule or inner filter effect, which improve the fluorescence analysis with this type of molecule. Another property is keto tautomer or transient character of molecule in the ground state. Those molecules that has H-bond donor group such as phenolic or amino group also established photo-tautomer by transferring the proton to an adjoining atom in electronically excited state. Similarly, here C=N isomerization is also occurred.

On the basis, of these properties present article demonstrates the sensor that has –OH group adjacent to the imine nitrogen which exemplifies intramolecular proton transfer from –OH to imine nitrogen *i.e.* represents ESIPT mechanism. Here the C=N isomerization is also inhibited after addition of aluminum ion and showed high fluorescent properties. Presented sensor depicts specific affinity towards $Al^{3+}$ ion unlike other metal ions with large spectral shift (58 nm) due to the presence of polar groups such as hydroxyl groups, amine group. This trivalent form of these groups has high affinity with $Al^{3+}$ ion. As result the interaction between hosts with $Al^{3+}$ ion leads to hinder ESIPT mechanism and C=N isomerization of host. Introduced sensor reveals low detection limit in nano-molar range (99 nM) for $Al^{3+}$ ion in ACN. Photoluminescence of host with $Al^{3+}$ ion emits green and red

* Corresponding author.
*E-mail address:* akscyfcy@iitr.ernet.in (A.K. Singh).

https://doi.org/10.1016/j.msec.2018.04.087
Received 16 August 2017; Received in revised form 15 March 2018; Accepted 28 April 2018
Available online 30 April 2018
0928-4931/ 

*Journal of The Electrochemical Society*, **166** (8) B644-B653 (2019)
0013-4651/2019/166(8)/B644/10/$38.00 © The Electrochemical Society

# Colorimetric and Fluorometric Detection of Heavy Metal Ions in Pure Aqueous Medium with Logic Gate Application

**Neetu Yadav and Ashok Kumar Singh** [z]

*Department of Chemistry, Indian Institute of Technology-Roorkee, Roorkee-247667, India*

The new Ligand was developed and characterized by different spectroscopic techniques such as NMR, mass spectrometry, single crystal XRD and photophysical studies. The ligand was shown colorimetric and turn-OFF behavior for $Hg^{2+}$ and $Cu^{2+}$ ions via PET and CHQF mechanisms respectively, whereas it shows turn-ON demeanor for $Cd^{2+}$ metal ions among other metal ions through CHEF mechanism. It demonstrated good sensitivity toward $Hg^{2+}$, $Cu^{2+}$, and $Cd^{2+}$ ions ca. 0.33 μM, 0.16 μM and 0.11 μM respectively, with a good binding constant in 100% aqueous medium. The binding of these metal ions with ligand was supported through NMR titration, mass spectrometry, electrochemical studies, and FT-IR spectroscopy. In-situ experiment appended with copper ion was supported for selective detection of cyanide ion among other anions and given 0.29 μM limit of detection for cyanide ion. The practical applications such as real water analysis and logic gate were successfully demonstrated with it.
 [DOI: 10.1149/2.1341906jes]

Manuscript submitted January 31, 2019; revised manuscript received March 29, 2019. Published May 8, 2019.

The exposure and assessment of low contamination of transition and heavy metal ions are exclusively essential because these metal ions played a vital role in living systems and their high concentration showed an extremely toxic impact on the environment.[1,2] This toxic effect of these metal ions attracts not only the scientific community, especially chemist and biologist, but also the general population who have knowledge of some disadvantages of these metal ions.[3] Among various metal ions mercury and cadmium are very toxic in nature due to their less solubility, nonbiodegradable behavior, and thence can accumulate in the environment, that contaminate food and water.[4] Apart from this, the slightly large concentration of copper ion also has the property to be an ecological pollutant and probably toxic to living cells.[5] Thus, this metal ion has been involved in many diseases such as neurodegenerative diseases (Menkes, Alzheimer's and Wilson diseases) that related to the high concentration of copper ion.[6–9] Same as Hg(II) ion is highly toxic ion that can coordinate to biological ligands like DNA, Enzyme and proteins, which increases the toxic level of mercury ion that causes significant damage of kidney, brain[10] and central nervous system,[11] accretion of Hg(II) in human body can supremacy of cognitive disorders and Minamata disease.[12–14] Cadmium is also an immensely toxic and carcinogenic metal ion whose higher level can associate with cardiovascular diseases, cancer mortality and damage to kidneys and liver.[15] So, WHO (world health organization) and EPA (environmental protection agency) had rigidly determined the permissible limit of the concentration of these metal ions that allowed in the drinking water. Therefore, it is necessary to develop an easy way to detect these ions in the environment. In this context, there are lots of instruments are available such as AAS, IES, ICP but these are very sophisticated and time-consuming. Moreover, the development of the chemosensor is the best way to analyze these ions instantly. Despite, there are many sensors were designed for Copper, Mercury or Cadmium[16] via numerous mechanism such as ESIPT (excited state intramolecular proton transfer),[17] PET (photoinduced electron transfer),[18] ICT (intramolecular charge transfer).[19] In all these mechanisms, the CHEF mechanism has some different quality such as large stock shift which established enhancement in the fluorescence intensity with large shifting. On the next hand still, there are some flaws among the noted chemosensors. The detection of cations by the various fluorophores are limited and usually, organic solvent was used as media for the detection of cations that limited practical applications for many sensors.

Therefore, designed new chemosensor is highly sensitive toward the detection of $Cu^{2+}$, $Hg^{2+}$, and $Cd^{2+}$ ion simultaneously under pure aqueous conditions without using an organic solvent. Whereas, a smaller number of chemosensors that could analyze three cations simultaneously via PET and CHEF mechanism in pure aqueous media. Moreover, the detection of these toxic metal ions in pure aqueous condition is still practical and challenging. In this context, this chemosensor detected copper, mercury, and cadmium metal ion in aqueous media with good sensitivity. The present chemosensor has the multi-donor atom i.e. the main reason to detect these ions. This chemosensor detects all three metal ions via PET and CHEF mechanism with good selectivity.

## Materials and Methods

The distilled solvents were used throughout the whole experiments. The metal salts were used of analytical grade without further purification purchased from Merck. The FT-IR spectra were produced from Perkin Elmer FT-IR 1000 spectrophotometer. The NMR ($^1H$ and $^{13}C$) was received by JEOL 400 MHz spectrometer. All absorption spectra were gleaned by using Specord 600 Thermo Scientific PC double beam spectrophotometer with 3 cm path length quartz cell. Horiba RF-5301PC instrument was used for all emission spectra with standard quartz cell. The Verio MICROV3.1.1 instrument was used to perform elemental analysis (CHNS). The electrochemical studies executed on CHI760E Electro-Analyser instrument with three electrodes as, graphite electrode as working electrode, Pt wire had used as counter electrode and $Ag/AgCl_2$ electrode as reference electrode with 0.1 M tetrabutylammonium hexafluorophosphate ($nBu_4NPF_6$) supporting electrolyte. The mass spectra were received by using Brukar micrOTOF-QII mass spectrometry.

***Synthesis of starting materials.***—*Synthesis of oxalohdrazonamide (1).*—The ethanolic solution of dithiooxamide (1 mmol) and dropwise addition of 3 mmol hydrazine in the solution. After that this reaction mixture was reflux for overnight. The dark brown precipitate was obtained after completion of the reaction by reported method.[20]

***Synthesis of Bis((indol-3-yl)methylene)oxalohydrazonamide (2).***—The ethanolic solution of **1** (1 mmol, 0.116g) was added dropwise to the ethanolic solution of indole 3-carboxaldehyde (2 mmol, 0.290g) with continuous stirring. The reaction mixture was refluxed for 6 hr. TLC was continuously checked up to completion of the reaction. A yellow colored solution was acquired which was placed for crystallization for 7–8 days, after 7–8 days there were yellow colored crystals appeared in block shaped. These crystals were separated from the solution and washed with ethanol and used for further studies (Figures 1 and 2). Crystallographic data of **2** has been deposited in Cambridge Crystallographic Data Centre with **CCDC 1835002**.

Yield: 70%, Calculated for C20 H18 N8; C: 68.28, H: 5.18, N: 26.54, and Found; C: 68.48, H: 5.099, N: 32.27, FTIR data (KBr, $\upsilon_{max}$ $Cm^{-1}$): $NH_2$: 3377, imidazole N-H: 3443, aromatic C-H: 3108, C = N: 1603, C-N: 1524, N = N: 1426 (ESI fig. S2). UV-Visible (water, $\lambda_{max}$ nm): 358 nm. $^1H$ NMR (400 MHz) δ 11.62 (s, 2H), 8.64 (s, 2H), 8.31 (d, $J = 7.5$ Hz, 2H), 7.84 (d, $J = 2.8$ Hz, 2H), 7.43 (d, $J = 7.6$ Hz, 2H),

[z]E-mail: akscyfcy@iitr.ernet.in